5-8-2020

The Synthesis and Characterization of Gold Nanoparticles Prepared with Novel Thioether-Ionic Liquids

Joie Games
game9049@bears.unco.edu

UNIVERSITY OF NORTHERN COLORADO

Greeley, Colorado

The Graduate School

THE SYNTHESIS AND CHARACTERIZATION OF GOLD NANOPARTICLES PREPARED WITH NOVEL THIOETHER-IONIC LIQUIDS

A Thesis Submitted in Partial Fulfillment
of the Requirement for the Degree of
Master of Science

Joie A. Games

College of Natural and Health Sciences
Department of Chemistry and Biochemistry

May 2020

This Thesis by: Joie A. Games

Entitled: *The Synthesis and Characterization of Gold Nanoparticles Prepared with Novel Thioether-Ionic Liquids*

has been approved as meeting the requirement for the Master of Science in the College of Natural and Health Sciences in the Department of Chemistry and Biochemistry

Accepted by the Thesis Committee:

_____

Murielle Watzky, Ph.D., Research Advisor

_____

Hua Zhao, Ph.D., Co-Research Advisor

_____

Aaron Apawu, Ph.D., Committee Member

Accepted by the Graduate School

_____

Cindy Wesley, Ph.D.
Interim Associate Provost and Dean
Graduate School and International Admissions
Research and Sponsored Project

ABSTRACT

Games, Joie. *The Synthesis and Characterization of Gold Nanoparticles Prepared with Novel Thioether-Ionic Liquids.* Unpublished Master of Science thesis, University of Northern Colorado, 2020.

Gold nanoparticles have found a broad range of applications in the biomedical field including in drug delivery and biosensor development.[1] The latter applications take advantage of a unique optical property called surface plasmon resonance.[2] Easily accessible "bottom-up" synthesis methods are commonly used for the preparation of metal nanoparticles, in which a metal precursor is reduced in the presence of a stabilizing agent to prevent aggregation.[3] Ionic liquids have been used in "bottom up" metal nanoparticle syntheses as stabilizing agents and as a means to functionalize metal nanoparticles' surface.[4] Due to the strength of gold-sulfur interactions, thiol-stabilized gold nanostructures are of great interest.[5] This project focused on the development of gold nanoparticle syntheses with a series of novel thioether-functionalized ionic liquids. The effect of ionic liquid structure and composition, ionic liquid concentration, and ionic liquid solubility on the synthetic reproducibility, elemental composition, and size of the gold nanoparticles were evaluated. The gold nanostructures were characterized by UV-visible spectroscopy, atomic force microscopy, and scanning electron microscopy with electron dispersive x-ray spectroscopy. Possible interactions between the ionic liquid and $HAuCl_4$ in aqueous solution were studied using fast scan cyclic voltammetry and UV-visible spectroscopy.

TABLE OF CONTENTS

LIST OF FIGURES

LIST OF TABLES

LIST OF SCHEMES

CHAPTER I

INTRODUCTION

Gold has been used in many forms throughout history, including in jewelry and coinage, mostly due to its chemical inertness as bulk metal. Gold nanostructures have existed at least since the 4th century Roman Lycurgus cup—even if not identified at the time.[6] More recently, gold nanostructures have found an array of applications in materials, sensing, and catalysis, thanks to advances in gold nanostructure research over the past several decades.

Gold nanostructures exhibit plasmonic properties not present in their bulk counterpart that depend on the nanostructure size and composition.[7] Gold nanostructures have thus drawn great interest from researchers, with wide applications in the area of biosensing. Many uses of metal nanostructures in biosensing have been in the form of large ensembles of nanoparticles, although each nanoparticle in the ensemble can act as a single sensor and improve detection limits.[8] These nanostructures have promising applications for measurements inside the cell or tissue where fixed arrays cannot penetrate.[9] Nanoparticle size must be taken into account towards ensuring enough signal intensity, as nanoparticle absorbance and scattering both depend on the size of the nanoparticle. Using nanoparticles as surface plasmon resonance sensors has shown promise for measuring molecular concentrations, binding kinetics, and conformational changes.[10]

Synthesis of gold nanostructures through ‘greener’ alternatives could produce these structures in a more sustainable way, leading to the design of more biocompatible nanostructures.[11] Ionic liquids are considered ‘greener’ alternatives to organic solvents; they can also be functionalized to act as nanoparticle stabilizers, providing the opportunity to tune the nanostructures’ synthesis and/or properties. Thioether-functionalized ionic liquids can take advantage of strong Au-S interactions to provide nanoparticle stabilization akin to thioalkanes,[12] but in aqueous solutions.

The goal of this project was to synthesize and characterize gold nanoparticles prepared in an aqueous bottom-up method and stabilized with novel thioether-ionic liquids . Research was performed towards the optimization of (i) the gold nanoparticles synthesis, and (ii) nanoparticle isolation and purification. The gold nanoparticles were characterized with Ultraviolet-visible spectroscopy (UV-Vis), scanning electron microscopy with energy dispersive X-ray (SEM/EDX), and atomic force microscopy (AFM). The gold and thioether ionic liquid aqueous mixtures were analyzed before addition of the reducing agent using fast scan cyclic voltammetry (FSCV) and UV-Vis spectroscopy.

CHAPTER II

LITERATURE REVIEW

2.1 Nanostructures

2.1.1 Definition

A nanostructure must have a dimensional range of less than 100 nm in at least one-dimension of space.[13] There are three types of nanostructures, defined by their dimension on the macroscale: zero dimensional (quantum dots and nanoparticles), one-dimensional (nanorods, tubes, and fibers), and two-dimensional (film coatings and single layers). Examples are shown in Figure 2-1.

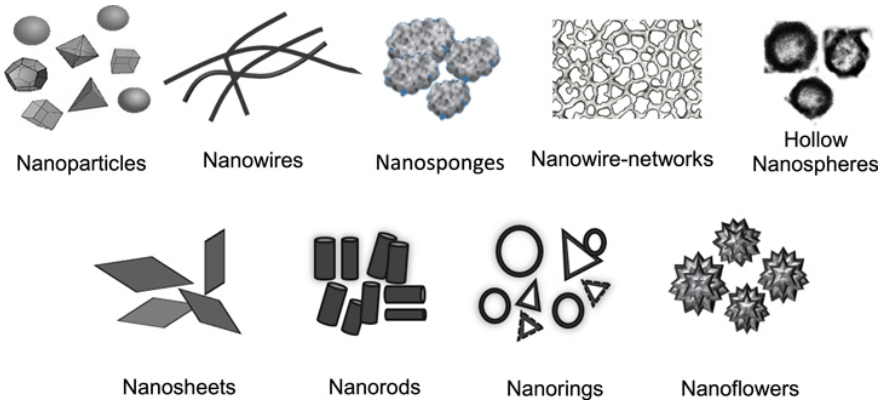

Figure 2-1. Representations of various types of nanostructures.[14]

2.1.2 Applications

Nanostructures have found a wide variety of applications in organic catalysis[15], photodetection[16], biomedicine[17], and solar technology.[18]

2.2 Gold Nanoparticles

2.2.1 Surface Plasmon Resonance

Gold and various other metals exhibit unique optical properties at the nanoscale with applied electromagnetic radiation. This phenomenon has been coined surface plasmon resonance (SPR), and corresponds to the oscillation of electrons on the surface on a thin film by electromagnetic enhancement.[19] SPR results in strong extinction of light in the visible domain of the electromagnetic spectrum for noble metals such as gold. This extinction is produced when the wavelength of incoming light is in resonance with the oscillating electrons. In the case of nanoparticles, a so-called localized surface plasmon resonance occurs (LSPR), illustrated in Figure 2-2, in which the electrons oscillate locally around the nanoparticle instead of oscillating on the surface of a thin film.[20]

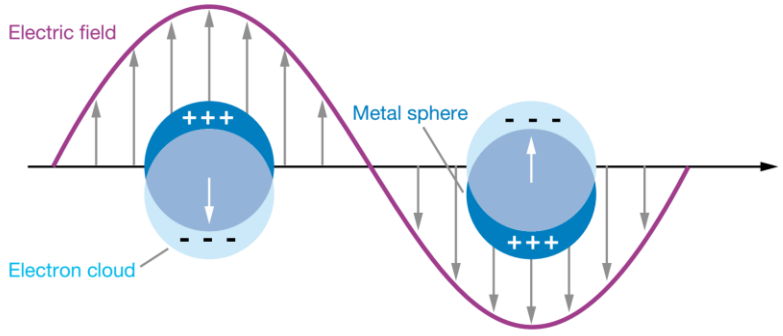

Figure 2-2. Schematic illustrating localized surface plasmon resonance.[2] Coherent oscillations in the electrons on the surface of the metal nanoparticle are induced by electromagnetic radiation. The induced oscillating electric dipole greatly increases the scattering and absorption at the resonant wavelength at the surface of the nanoparticle.

The strong absorption band given by gold nanoparticles is typically in the range of 500 – 600 nm. The LSPR peak maximum is dependent on the size, shape, and dielectric environment of the nanoparticle,[21,22] and the peak maximum wavelength typically increases with particle diameter.[23]

The extinction spectrum represents both the absorption and the scattering of the electromagnetic radiation. The extinction cross-section of a small concentric sphere embedded in a medium is given by Equation 2.1 ,[24]

$$C_{ext} = \frac{24\pi^2 R^3 \varepsilon_m^{2/3}}{\lambda} \frac{\varepsilon_2}{(\varepsilon_1+2\varepsilon_m)^2+\varepsilon_2^2} \quad (2.1)$$

where *R* represents the particle volume, λ the extinction wavelength, ε_m the medium dielectric function, and ε_1 and ε_2 the real and imaginary parts of the material dielectric function ($\varepsilon = \varepsilon_1 + i\varepsilon_2$). For a core-shell nanoparticle, the extinction cross-section is given by Equation 2.2,

$$C_{ext} = 4\pi R^2 k^* \times Im\left\{\frac{(\epsilon_{shell}-\epsilon_m)(\epsilon_{core}-2\epsilon_{shell})+(1-g)(\epsilon_{core}-\epsilon_{shell})(\epsilon_m+2\epsilon_{shell})}{(\epsilon_{shell}+2\epsilon_m)(\epsilon_{core}+2\epsilon_{shell})+(1-g)(2\epsilon_{shell}-2\epsilon_m)(\epsilon_{core}-\varepsilon_{shell})}\right\} \quad (2.2)$$

where *R* is the radius of the core-shell particle, $k = 2\pi\sqrt{\varepsilon_m/\lambda}$, *Im* represents the imaginary part, ε_{core} is the complex dielectric function of the core material, ε_{shell} is that of the shell, ε_m is the complex dielectric function of the surrounding medium, and *g* is the volume of the shell layer.[25] Experimental variables that contribute to the shift in LSPR extinction maximum include the change in refractive index upon adsorption on a nanoparticle surface, as illustrated by Equation 2.3,

$$\Delta\lambda = m(n_{adsorbate} - n_{medium})\left(1 - e^{\frac{-2d}{I_d}}\right) \quad (2.3)$$

where $\Delta\lambda$ represents the LSPR spectral shift, *m* the sensitivity factor, $n_{absorbate}$ and n_{medium} the refractive indices of the adsorbate and medium surrounding the nanoparticle, respectively, *d* the effective thickness of the adsorbate layer (in nm), and I_d the electromagnetic field decay length (in nm).[2] The shifts can be maximized by adjusting and optimizing for *m* and I_d, which results in improving the detection limit and sensitivity

in analyte sensing applications. The change in refractive index shifts the LSPR extinction maximum by modifying the dielectric environment.[26]

2.2.2 Applications

Gold metal nanoparticles have been used in the areas of biomedicine and biopharmacy for a variety of applications such as drug delivery[27], cancer therapy[28,29], and chemical or biochemical sensing[10,30–33]. The relative chemical inertness of gold metal has been advantageous for biological applications, while the strong optical properties (via surface plasmon resonance) of nanoparticles has been useful for chemical and biochemical sensing.[34,35]

Surface plasmon resonance properties have been used towards the design and application of sensors for monitoring biomolecules in clinical samples. Graphene oxide-gold nanoparticle hybrids can be employed as biosensors to selectively detect for MicroRNA,[36] whose increased levels are associated with many genetic diseases and cancer.[37] SPR sensors are also versatile tools to monitor Alzheimer's disease via the Tau protein[38] or fibrinogen;[39] diabetes mellitus via insulin,[40] putative kidney markers via transferrin,[41] rheumatoid arthritis through cathepsin G,[42] and many more. The biofluids analyzed with these sensors range from serum, plasma, urine, tissue, and blood.[1]

2.3 Synthetic Methods for Gold Nanoparticles

2.3.1 Bottom-Up Syntheses

The bottom-up approach is widely used in nanoparticle synthesis, because of its simplicity and accessibility. In a bottom-up approach, nanostructures are synthesized by stacking atoms onto each other, giving rise to crystal planes; these further stack onto each

other, resulting in nanostructures.[3] Figure 2-3 below shows a schematic of the bottom-up and top-down approaches.

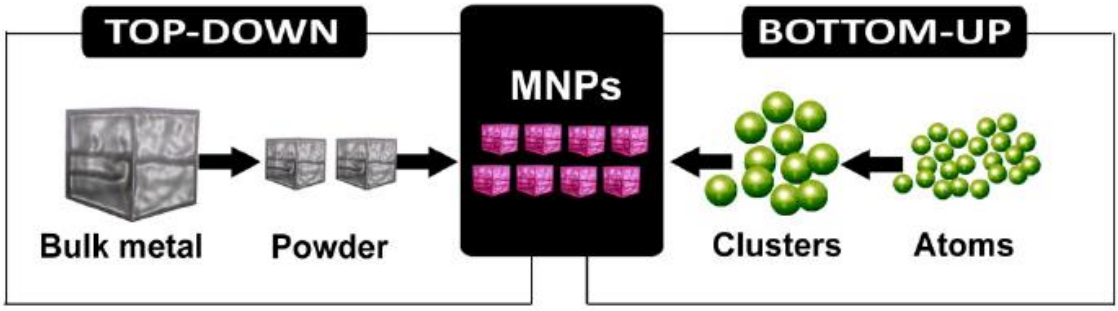

Figure 2-3. Schematic of top-down and bottom-up approach.[43] The top-down approach forms nanoparticles from bulk metal. The bottom-up approach builds from atoms that form into clusters, then grow into nanoparticles.

A conventional bottom-up method is known as chemical vapor deposition (CVD), a gas phase process where reactive constituents react over a pre-made surface to form the nanostructured materials. This method is useful for 1D nanostructures and 2D thin film production. Industrially, CVD is an economical way to produce carbon nanotubes.[44]

Liquid phase bottom-up methods are more commonly used for preparing nanoparticles and other nanostructures. They allow for possible size and shape control at lower temperatures with shorter synthesis times, are more affordable than other methods, are relatively simple while producing a high yield of product and allow for surface functionalization that can be performed *in situ*.[45] There are multiple components to a bottom-up synthesis, including capping or stabilizing agents, potentially dispersing agents, and reducing agents if a metal ion reduction is involved.[46] Some reagents can play all three of these roles. Capping or stabilizing agents are used in colloidal synthesis to inhibit nanoparticle overgrowth and aggregation.[47] Dispersing agents can also be used to prevent aggregation. When working with a metal ion precursor, the reducing agent is necessary, for example to reduce Au(III) to Au(0). Strong reducing agents such as $NaBH_4$

can reduce gold from Au(III) to Au(0) quickly.[48] Weaker reducing agents such as ascorbic acid or citrate reduce Au(III) to Au(I) which then disproportionates to Au(0).[49]

Bottom-up synthesis in solution involves nucleation and growth from a metal precursor, as shown in Figure 2-4. Nucleation is the process by which metal atoms arrange themselves according to their crystalline structure to form a nucleation site (or building block), on which more metal atoms can be added for the nanoparticle to undergo subsequent growth.[50] In the absence of Ostwald ripening, the metal atoms will nucleate and grow until they form a stable nanostructure. Without a stabilizing agent, the aggregation of nanostructures cannot be overcome, and bulk metal, the thermodynamic minimum, will form instead. In gold nanoparticles synthesis, the most famous and deceivingly simple bottom-up liquid phase synthesis method is the so-called Turkevich method.[51]

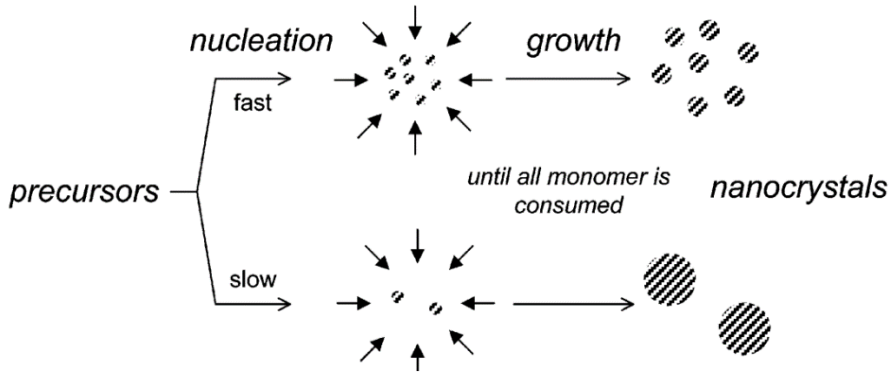

Figure 2-4. Schematic representation of nanocrystal synthesis in the absence of Ostwald ripening.[52] The metal precursor is reduced; the monomers nucleate and grow from these nuclei until all the metal precursor is consumed.

2.3.2 Turkevich Method

The Turkevich method, based on a 1951 publication by Turkevich et. al. on the synthesis of colloidal gold,[53] is one the most commonly used methods for gold nanoparticle synthesis. This method uses citrate as the reducing and stabilizing agent and

produces spherical-like particles over tunable size ranges. Here, sodium citrate is added to an aqueous tetrachloroauric acid solution and heated under stirring; over time, the solution turns from a greyish-pink then greyish-blue tone to a deep wine red, indicating that the reaction is complete. The greyish-blue tone in the early stages of the reaction could be attributed to the inclusion of gold ions in the electric double layer that forms on the surface of the nanoparticle, changing its electric properties.[54] Sodium citrate reduces gold from Au(III) to Au(I), which then disproportionates to the desired Au(0). Figure 2-5 depicts the formation of an $Au(0)_n$ nucleus after addition of the reducing agent.

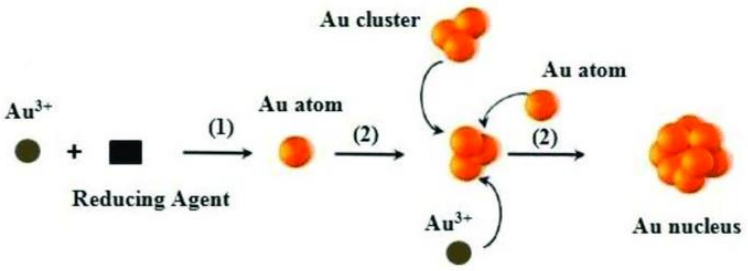

Figure 2-5. Depiction of the process of nucleation of gold nanoparticles in solution.[55] The reducing agent (citrate) reduces Au^{3+} to Au^0. The atoms nucleate to form n Au_n nucleus.

The authors studied the effect of temperature and found that a 10 ˚C decrease resulted in a decrease in mean particle size and root-mean-square deviation. They also studied the effect of citrate concentration, and found that a decrease in sodium citrate concentration resulted in a decrease in mean particle size.[53] These studies demonstrated that nanoparticles could be tuned through adjustments to experimental conditions.[53] While the Turkevich method presents a simple procedure, it does involve complex chemistry.[56]

A recently proposed mechanism for the Turkevich synthesis is shown in Figure 2-6.[56] Figure 2-6a depicts the oxidation of citrate that leads to the formation of acetonedicarboxylate (ADC), and the reduction of Au(III) precursor that yields Au(I) ions. Figure 2-6b illustrates how ADC may bind to Au(I), which precedes the disproportionation of Au(I) to Au(0) and Au(III), as shown in Figure 2-6c. Figure 2-6d shows the ensuing nucleation and growth to form $Au(0)_n$ nanoparticles.

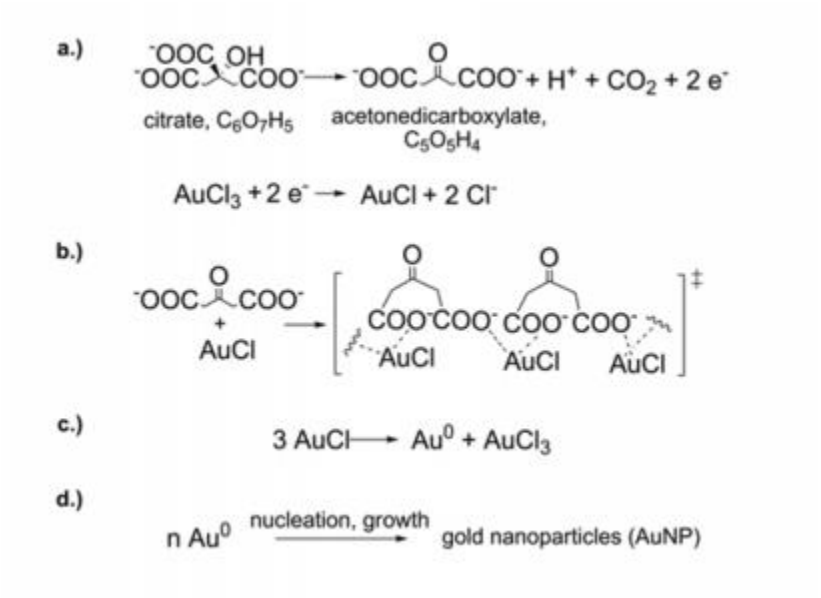

Figure 2-6. Proposed mechanism for the Turkevich synthesis.[56]

2.3.3 Thiol-Stabilized Gold Nanoparticles

Gold metal nanoparticles stabilized by alkanethiols have been prepared via one-phase and two-phase syntheses in organic solvents. In one instance, unfractionated dodecanethiolated-protected Au clusters with an average core diameter size from 1.5 – 5.2 nm were prepared via a two-phase synthesis with toluene as the organic phase.[57] Here the two-phase synthesis involves the phase transfer of $Au^{III}Cl_4^-$ from the aqueous solution to the organic solution, after which it is reduced by $NaBH_4$ in the presence of thiols.[58]

Spherical particles with a 4 nm average size have been synthesized via one-phase synthesis using THF as the solvent and lithium triethylborohydride as the reducing agent.[59] Here THF was chosen because both *n*-octadecanethiol and the reducing agent, lithium triethylborohydride, are soluble. These synthesis methods have been found to be reproducible and have the ability to be upscaled; however; the organic solvents used are volatile and can be harmful to the environment and human health.

2.3.4 Ionic Liquids

Ionic liquids (ILs) are organic salts with an organic cation and inorganic/organic anion that exist as a liquid at <100 ºC.[60] Imidazolium-based ILs are most commonly used because of their stability in air and water.[4] This solvent system is intrinsically conductive and is stable over a wide range of electropotentials.[61] The physical properties of an IL depend on the length of the alkyl groups on the heterocyclic rings. ILs can be perceived as green solvents, due to their low volatility; they are thus seen as a more environmentally friendly alternative to many organic solvents.[11] ILs have been used for a number of organic reactions such as cyclic carbonate synthesis[62], aldol reaction[63], and cross coupling reactions[64].They are limited in their "green" chemistry context by the inorganic anion; for example BF_4^- and SF_6^- are believed to evolve into hydrofluoric acid over time. The unique physiochemical properties and potential green chemistry benefits of ILs have brought researchers to use them for metal nanostructures syntheses.

The bottom-up approach is commonly used in metal nanoparticle synthesis with ILs, which are generally performed using imidazolium derivatives with various counterions. Kim reported the synthesis of gold nanoparticles by $NaBH_4$ reduction of $HAuCl_4$ in the presence of a thiolated IL.[4] This yielded nanoparticles with diameters of

2.0-3.5nm. There are also examples of using ILs as stabilizing agents in gold nanoparticle synthesis without the presence of sulfur in the IL.[65]

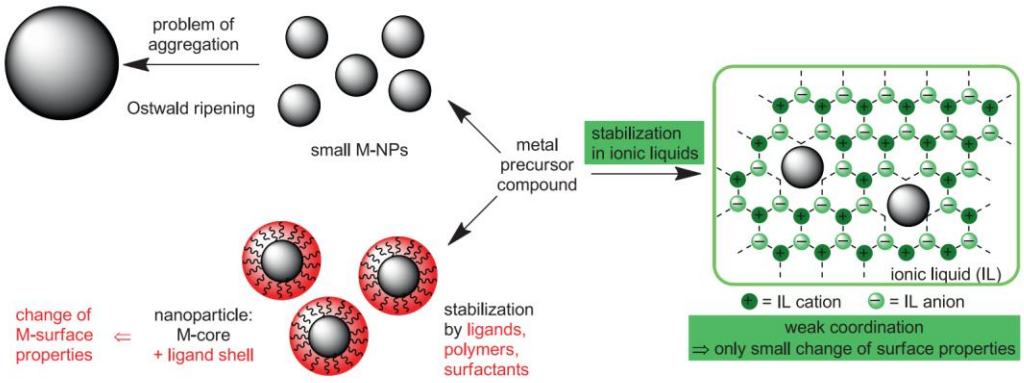

Figure 2-7. Schematic representation of the stabilization of metal nanoparticles through stabilizers or in ionic liquids to prevent aggregation.[66] The metal precursor is reduced and grown into metal nanoparticles. To form small nanoparticles, Ostwald ripening needs to be prevented. Stabilization through ligands, polymers, and surfactants can prevent aggregation, but changes the metal surface properties. Ionic liquids provide stabilization while only making small changes to the metal surface properties.

ILs can stabilize metal nanoparticles through their electrostatic and steric properties, without the use of stabilizing or capping agents. Without a stabilizing agent, small nanoparticles will aggregate to thermodynamically more stable larger particles, for example through Ostwald ripening,[67] see Figure 2-7. Functionalized ILs can further stabilize metal nanoparticles (a functionalized IL has an added functional group for example on the imidazolium cation).

ILs are not without their disadvantages. They tend to be hygroscopic and readily absorb water from air. When used as a solvent, the presence of water and impurities in the solvent system can affect the size and shape of the intended nanostructure. ILs are also more viscous than common organic solvents. The solvent viscosity is mostly dependent on the cation's size and the structure of the anion. For example, viscosity is an

issue for hydrogenation reactions using ruthenium nanoparticles because it causes a slow mass transfer in the multiphase system.[68]

Thioether-based ILs could provide both stabilization and functionalization in a bottom-up synthesis of gold nanoparticles, which is still in need of investigation. Strong gold-sulfur interactions[5] have been employed in a variety of fields such as physics, pharmaceuticals, and material science.[69] Many self-assembled monolayers and biomedical devices also use gold-sulfur interactions.[70]

2.3.5 Deep Eutectic Solvents

Deep Eutectic Solvents (DES) were first published in 2003 by the Abbott research group as an alternative to ionic liquids.[71] DES and IL are both ionic solvents with similar properties. The Abbott group showed that substituted quaternary ammonium salts could form complexes with hydrogen bond donors. In doing this, they produced eutectics that are liquid at room temperature with unusual solvent properties.[72] Figure 2-8 shows two examples of DESs: Reline, a 1:2 choline chloride-to-urea molar ratio and, Ethaline, a eutectic mixture of 1:2 choline chloride-to-ethylene glycol molar ratio.

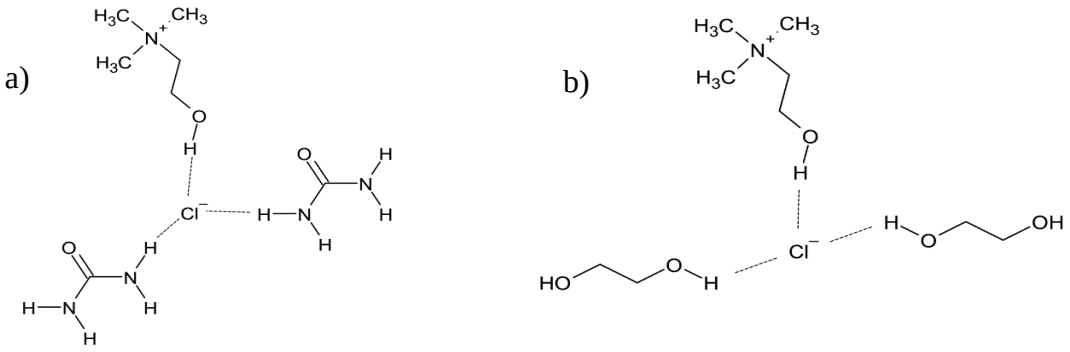

Figure 2-8. Examples of Deep Eutectic Solvents a) Reline b) Ethaline.

There are many characteristics of DES that differentiate them from ILs. They are easy to prepare as a mixture; they have well characterized toxicological effects, and many are biodegradable. They have a potential as green solvents as they can be prepared in mixtures of natural compounds that interact through hydrogen bonding;[73] these are termed natural deep eutectic solvents (NADESs). DES are cheaper than ILs and their preparation is simple. However, there are disadvantages of using DES over ILs in metal nanoparticles syntheses. Both ILs and DES are viscous, but the viscosity of the DESs cannot be tuned, as these are exact mixtures that cannot be modified. ILs, on the other hand, can be functionalized to make them more or less viscous. ILs are thus more controllable and can be modified to meet the synthesis needs.

2.4 Characterization Methods for Gold Nanoparticles

In addition to the use of UV-Vis spectroscopy to monitor surface plasmon resonance, atomic force microscopy and scanning electron microscopy with electron dispersive x-ray spectroscopy were used to characterize the size, morphology, and elemental composition of the gold nanoparticles prepared with the novel thioether ionic liquids. The tetrachloroaurate and ionic liquid aqueous mixture present before the addition of a reducing agent was analyzed using UV-Vis spectroscopy and fast scan cyclic voltammetry.

2.4.1 Atomic Force Microscopy

Atomic force microscopy (AFM) works by having a probe (a cantilever) that is brought into proximity to the sample surface and scanned across the surface to monitor the interaction between the tip and the surface, see Figure 2-9. AFM is useful to material and nanostructure[74] studies, as well as studies of biological systems[75] and polymers.[76] Its

resolution can reach the nanometer range. It also has topographical applications in which forces are measured as a function of distance.[77] Where scanning electron microscopes (SEM) may only be limited to observing metal nanoparticles, AFM can be used to observe the various anisotropies in nanostructures. It is capable of producing a three-dimensional topography in a single scan, whereas SEM has difficulty resolving subtle changes in a smooth surface and gives images only in x and y directions. AFM also has the benefit of working in different environments, including air, liquid, and under vacuum. AFM utilizes a piezoelectric scanner that works by moving the sample in three dimensions by a sub-nanometer amount under applied voltage.[78] A commonly used set-up is the beam deflection method, in which a laser beam is emitted from a laser diode and focused on the backside of the cantilever. The cantilever is brought close to the sample by the laser beam, causing the cantilever to be deflected over the sample due to the electric charge generated by the mechanical stress. The laser beam is reflected to the photodiode.[79] This deflection results in a line-by-line image.[80]

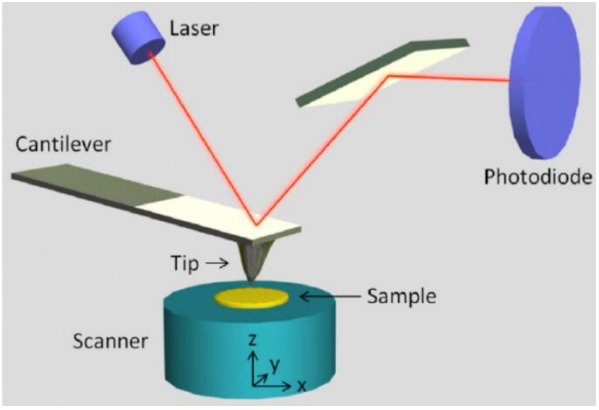

Figure 2-9. Depiction of the principles of AFM.[81]

Careful sample preparation is important for producing quality AFM images. Gold nanostructures must be dispersed on flat surfaces for the measurements; the roughness of

the surface should be small enough that it is of nominal size to the nanoparticles. This provides a consistent baseline for the height (z-axis) measurements. Suitable substrates include high quality mica, gold coated mica, or single crystal silicon.[82] These substrates have minimal surface roughness, making them optimal for use in nanostructure measurements. The nanostructures, once thoroughly washed, are dispersed onto these substrates and are fixed to the substrate by weak physical forces. Once the plate is slid under the cantilever, adjustments are made to calibrate the z- displacement by bringing the cantilever closer to the sample. For measuring nanostructures, the cantilever tips should have a radius of less than 10 nm while being 10° to 20° relative to the surface of the sample.[83] The scan size should be adjusted depending on the size of the nanostructures. Once calibrated, the nanostructures can be imaged. A large scan should be used at first to identify a region in which there is homogeneous nanoparticle distribution. When the region has been identified, measurements can be collected. After obtaining images, various analyses can be done to visualize and determine the physical properties of the imaged nanostructures. These analyses can be used to make horizontal, vertical, and angular measurements, allowing to find the average particle height of a batch of synthesized nanoparticles.[84]

2.4.2 Scanning Electron Microscopy with Electron Dispersive X-Ray Spectroscopy

Scanning electron microscopy with electron dispersive X-ray spectroscopy (SEM/EDX) is a useful instrumentation for elemental analysis, and beneficial for metal nanostructure characterization. SEM utilizes electrons to take high resolution imaging of surfaces, see Figure 2-10. The SEM generates a beam of incident electrons (from thermal

emission source) in an electron column. The electrons are focused by a series of electromagnetic lenses in the column. Scanning coils position near the end of the column direct and position the focused electron beam onto the sample. The emitted electrons will be registered by a detector and an image will be produced.[85] EDX works by producing diffraction and reflection of emitted radiation from single particle surfaces.[86] It is used in conjunction with SEM by detecting the X-Ray that are emitted from the sample to characterize its elemental composition. There is a bias towards heavy metals with SEM, which is beneficial for gold analysis. Size resolution is not as high as with AFM, but SEM/EDX can help confirm the elemental nature of the nanostructures.

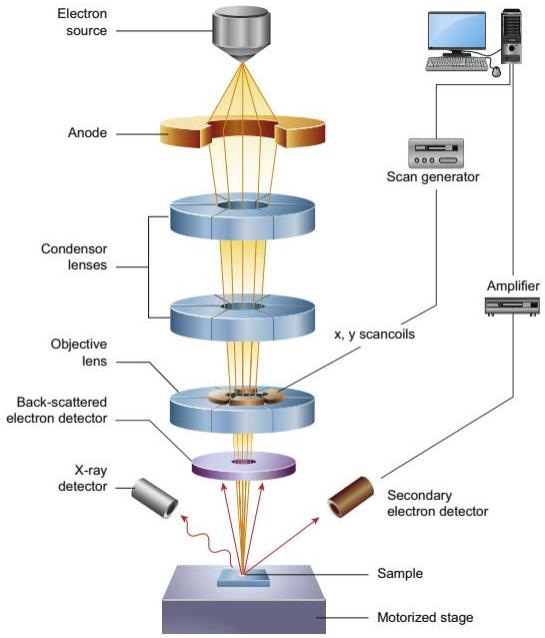

Figure 2-10. Schematic diagram of the core components of an SEM Microscope.[87]

2.4.3 Cyclic Voltammetry

Cyclic voltammetry (CV) is an electrochemical technique commonly employed to observe the reduction and oxidation processes of molecular species and to study electron transfer-initiated chemical reactions.[88,] CV has been used to study the catalytic activity of

metal surfaces.[89, 90, 91] CV was also used to monitor the change in redox potential between a “bare” gold surface and one modified with grafted thioalkanes.[92] CV is commonly used to monitor changes in redox potential at the metal center in a coordination complex upon changes in the ligand environment .

CHAPTER III

METHODOLOGY

3.1 Materials and Instrumentation

The materials purchased for this study were used without further purification. Hydrogen tetrachloroaurate (III) hydrate (99.8% Au) was purchased from Strem Chemicals; sodium borohydride (99%) was purchased from Acros Organics; Millipore (18 MΩ) nanopure water was used as the solvent in all gold nanoparticle syntheses. The ionic liquids 2-(phenylmercapto)ethyl-tributyl phosphonium, 2-(phenylmercapto)ethyl-methylimidazolium chloride and 2-(ethylmercapto)ethyl-tributyl phosphonium chloride were prepared using 2-chloroethylphenyl sulfide (98%) purchased from Tokyo Chemical Industry, CO (TCI), 2-chloroethyl ethyl sulfide (98%) purchased from TCI, tributyl phosphine (95%) purchased from Beantown Chemical (BTC), and 1-methylimidazole (>99.0%) from TCI. Acetonitrile was purchased from Millipore Corporation, hexane from VWR, dichloromethane from Pharmco-Aaper, and the activated charcoal from J.T. Baker. The attempted synthesis of 1,8-bis(tri(n-butyl)phosphonium bromide)-3,6-dithiaoctane was performed with 3,6-dithia-1,8-octanediol (97%) purchased from Sigma Aldrich, triphenyl phosphine (95%) purchased from TCI, and tetrabromomethane (98%) purchased from Acros Organics. Silver nitrate tests were performed with $AgNO_3$ (0.1N) purchased from VWR. Ethanol (100%) was purchased from Pharmco-Aaper, and acetone (99.5%) from Fischer Science Education. All glassware was cleaned with 8 M nitric acid

(certified ACS Plus) purchased from Fisher Chemical and rinsed with Millipore (18 MΩ) nanopure water before use.

An Olis HP 8452 Diode Array UV-visible spectrometer was used for surface plasmon resonance (SPR) analysis. An Eppendorf 5418 centrifuge and a Branson 2800 sonicator were used for nanoparticle isolation and SEM/EDX, AFM sample preparation. A JEOL JSM-6610LV scanning electron microscope (SEM) with energy dispersive spectroscopy (EDX) was used to observe gold nanoparticles and perform elemental composition analyses. A Nanosurf Mobile S all-in-one atomic force microscope (AFM) was used to obtain preliminary imaging and size data of the nanoparticles. NMR Analysis was conducted using a Bruker Advance II 400MHz NMR spectrometer. A dual-channel WaveNeuro Fast Scan Cyclic Voltammetry (FSCV) Potentiostat System was used for cyclic voltammetry analysis of the Au-IL mixtures. A Thermo Scientific Nicolet IS5 spectrometer with iD1 Transmission attachment was used for FTIR analysis of the synthesized gold nanoparticles.

3.2 Ionic Liquids Synthesis

3.2.1 Synthesis of 2-(Phenylmercapto) Ethyl-Tributylphosphonium Chloride

10.626 g of 2-chloroethylphenyl sulfide were transferred to a 500 mL round bottom flask; 50 mL of acetonitrile was then added to prevent ignition upon the subsequent addition of tributylphosphine. 13.785 g of tributyl phosphine were added in 10% molar excess, and 100 mL of acetonitrile was added to the reaction mixture. The reaction mixture was then refluxed for 24 hours under stirring. Excess acetonitrile was removed by rotary evaporation under vacuum (50 $^{\circ}$C, 100 mbar). The product was rinsed with hexane to remove the excess tributyl phosphine, and vacuum filtration was used to

isolate the product. Any remaining hexane in the product was further removed by rotary evaporation. Drops of the ionic liquid product were added to a solution of $AgNO_3$ to confirm the presence of chloride counterion(s) through AgCl precipitate formation. Product formation was confirmed via ^{1}H-NMR and ^{13}C-NMR.

3.2.2 Synthesis of 2-(Phenylmercapto) Ethyl-Methylimidazolium Chloride

12.121g of 2-chloroethylphenyl sulfide were transferred to a 500 mL round bottom flask, and 6.34 g of 1-methyl imidazole were added in 10% molar excess. 100 mL of acetonitrile was then added to the reaction mixture, which was then refluxed for 24 hours under stirring. Excess acetonitrile was removed by rotary evaporation under vacuum (50 $^{\circ}$C, 100 mbar). The product was purified via ether extraction and hexane extraction, and further purified with 3 scoops of activated charcoal in 100 mL of dichloromethane. Drops of the ionic liquid product were added to a solution of $AgNO_3$ to confirm the presence of chloride counterion(s) through AgCl precipitate formation. Product formation was confirmed via ^{1}H-NMR and ^{13}C-NMR.

3.2.3 Synthesis of 2-(Ethylmercapto) Ethyl-Tributylphosphonium Chloride

12.6 g of 2-chloroethyl ethyl sulfide were transferred to a 500 mL round bottom flask; 50 mL of acetonitrile was then added to prevent ignition upon the subsequent addition of tributylphosphine. 18.6 g of tributyl phosphine were added in 10% molar excess, and 100 mL of acetonitrile was added to the reaction mixture. The reaction mixture was then refluxed for 24 hours under stirring. Excess acetonitrile was removed by a rotary evaporation under vacuum (50 $^{\circ}$C, 100 mbar). The product was rinsed with hexane to remove the excess tributyl phosphine, and vacuum filtration was used to isolate

the product. Any remaining hexane in the product was further removed by rotary evaporation. Drops of the product were added to a solution of $AgNO_3$ to confirm the presence of chloride counterion(s) through AgCl precipitate formation. Product formation was confirmed via ^{1}H-NMR and ^{13}C-NMR.

3.2.4 Synthesis Attempt of 1,8-Bis (Tri(n-butyl)phosphonium Bromide) -3,6-Dithiaoctane

15.271 g of 3,6-dithia-1,8-octanediol were transferred to a round bottom flask, and 61.095 g of tetrabromethane were added in 120% molar excess. The resulting mixture was dissolved in 100 mL of acetonitrile. Once the mixture was dissolved, 48 g of triphenyl phosphide were added, batchwise over 40 minutes, in a 120% molar ratio. After the addition of triphenyl phosphide, the reaction mixture was left to stir for 24 hrs. Excess acetonitrile was removed by rotary evaporation under vacuum (50 ºC, 100 mbar), and the product was extracted with hexane. ^{1}H-NMR and ^{13}C-NMR were used to confirm the formation of 1-bromo-2-({2-[(2-bromoethyl)sulfanyl]ethyl}sulfanyl)ethane product. 4.62 g of tributyl phosphine were added to 3.228 g of the 1-bromo-2-({2-[(2-bromoethyl)sulfanyl]ethyl}sulfanyl)ethane product, and 100 mL of acetonitrile was added to the reaction mixture. The reaction mixture was refluxed for 24 hours under stirring. Excess acetonitrile was removed by rotary evaporation under vacuum (50 $^{\circ}$C, 100 mbar). The semi-solid product was rinsed with hexane, and the remaining hexane was then removed by rotary evaporation. The product was left to dry overnight. Product confirmation was attempted with ^{1}H-NMR, but the intended product could not be confirmed.

3.3 Gold Nanoparticle Syntheses

3.3.1 Gold Nanoparticles Synthesis with 2-(Phenylmercapto)Ethyl-Tributylphosphonium Chloride

10 mL of 0.762 mM $HAuCl_4$ aqueous solution was placed in a 50 ml beaker, upon which 10 mL of 2-(phenylmercapto)ethyl-tributylphosphonium chloride (IL-1A) aqueous solution (0.762, 3.81 mM, and 7.62 mM) was added dropwise. Reactions were run with 1:1, 5:1, and 10:1 IL:$HAuCl_4$ molar ratios. The reaction mixture was then heated and stirred at 200 rpm until clear and colorless (30 minutes at 47 $^{\circ}$C for 1:1 IL-1A:Au, 37 minutes at 45 $^{\circ}$C for 5:1 IL-1A:Au, 41 minutes at 48 $^{\circ}$C for 10:1 IL-1A:Au). The reaction mixture was then cooled to 21 $^{\circ}$C, upon which 10 mL of 0.381 mM of $NaBH_4$ aqueous solution was added dropwise over 1.5 minutes, with stirring set at 200 rpm. Bubbling in the reaction mixture ceased after ~14 minutes; the reaction mixture was then stirred for another 7 minutes.

3.3.2 Gold Nanoparticles Synthesis with 2-(Phenylmercapto)Ethyl-Methylimidazolium Chloride

10 mL of 0.762 mM $HAuCl_4$ aqueous solution was placed in a 50 ml beaker, upon which 10 mL of 2-(phenylmercapto)ethyl-methylimidazolium chloride (IL-1B) aqueous solution (0.762, 3.81 mM, and 7.62 mM) was added dropwise. Reactions were run with 1:1, 5:1, and 10:1 IL:$HAuCl_4$ molar ratios. 10 ml of 0.381 mM $NaBH_4$ aqueous solution was added dropwise over 1.5 minutes, with stirring set at 200 rpm. Bubbling in the reaction mixture ceased after ~15 minutes; the reaction was then stirred for another 10 minutes.

3.3.3 Gold Nanoparticles Synthesis with 2-(Ethylmercapto)Ethyl-Tributylphosphonium Chloride

10 mL of 0.762 mM $HAuCl_4$ aqueous solution was placed in a 50 mL beaker, upon which 10 mL of 2-(ethylmercapto)ethyl-tributylphosphonium chloride (IL-2) aqueous solution (0.762, 3.81 mM, and 7.62 mM) was added dropwise. Reactions were run with 1:1, 5:1, and 10:1 IL-2:$HAuCl_4$ molar ratios. 10 ml of 0.381 mM $NaBH_4$ aqueous solution was added dropwise over 1.5 minutes, with stirring set at 200 rpm. Bubbling in the reaction mixture ceased after ~15 minutes; the reaction was then stirred for another 10 minutes.

3.4 Nanoparticles Isolation

One milliliter (1 mL) aliquots of the reaction mixture were transferred into 1.5 mL centrifuges tubes. A set of 8 tubes was centrifuged for one hour (checking the pellet at 30-minute intervals) at 12700 rcf (relative centrifugal force). After centrifugation, the supernatant was removed from each tube, and 0.300 mL of ethanol was added to each tube. To consolidate the nanoparticles, two tubes were combined into one for a total of 4 tubes containing 0.600 mL of solution each. 0.400 mL of ethanol was then added to each of the 4 tubes for a total of 1 mL. Sonification was used to help disperse the nanoparticles into the ethanol solvent. The tubes were then centrifuged for another 30 minutes (checking the pellet at 10-minute intervals) at 10000 rcf (relative centrifugal force). The supernatant was then removed and 1.0 mL of ethanol was added. The tubes were then centrifuged for another 30 minutes (checking the pellet at 10-minute intervals) at 10000 rcf. The supernatant was removed, and the nanoparticles were used for further analysis.

3.5 Nanoparticles Purification Study

Preparation of gold nanoparticles using a 5:1 IL:$HAuCl_4$ molar ratio were conducted with each IL, and UV-Vis spectra of the reaction mixtures were collected. 1 mL aliquots of each reaction mixture were transferred into 1.5 mL centrifuges tubes. A set of 18 tubes was centrifuged for one hour (checking the pellet at 30-minute intervals) at 12700 rcf (relative centrifugal force). After centrifugation, the supernatant was removed from each tube, and a UV-Vis spectrum of the supernatant was collected. To consolidate the nanoparticles, the pellets from two tubes were combined into one, for a total of 9 tubes. 500 µL of solvent (ethanol, acetone, or nanopure water) was added to a total of 3 centrifuge tubes for each solvent. The nanoparticles were then redispersed by sonification, and the samples were centrifuged at 8000 rpm for 12 minutes. UV-Vis spectra of the supernatant and of the nanoparticles redispersed in nanopure water were taken for each solvent. The procedure was repeated for two more cycles.

3.6 Ultraviolet-Visible Spectroscopy

UV-Vis spectra of the reaction mixture were collected using a 1:2 (v/v) dilution with Millipore (18 MΩ) nanopure water. UV-Vis spectra of the isolated nanoparticles redispersed in Millipore (18 MΩ) nanopure water were also collected; There, nanoparticles collected from 3 centrifuge tubes after the wash(es) were redispersed in 1.000 mL of nanopure water to give a 3 mL sample for UV-Vis analysis.

3.7 Scanning Electron Microscopy with Electron Dispersive Microscopy

3.7.1 Sample Preparation

A sample holder was first prepared by attaching a carbon sticky to an aluminum support. Isolated nanoparticles from one centrifuge tube (which had been previously consolidated from two centrifuge tubes, see Section 3.4) were redispersed in 1.000 mL of ethanol with sonification. 3 drops of the redispersed nanoparticles were then placed onto the carbon sticky, and the sample was left to dry for at least 24 hrs.

3.7.2 Analysis

The option selected for analysis was “Inorganic”. To find a good area to observe, a “Scan 1” setting was first used; this setting quickly measures the surface but doesn’t give the highest resolution. Once an area of interest was found, one could zoom into the area. Upon zooming, a “coarse focus” adjustment was used, upon which a “fine focus” adjustment could be used to further put the structures into focus. A “Scan 3” setting could then be used to get a more high-quality image. Auto-contrast and brightness settings were also used. Using the EDX software, the detector was first cooled; a selected area in the SEM image was then chosen for EDX analysis.

3.8 Atomic Force Microscopy

3.8.1 Sample Preparation

A mica disk was first prepared by punching a hole out of a mica sheet, then using tape to remove the top two layers in order to ensure a smooth surface. Isolated

nanoparticles from one centrifuge tube (which had been previously consolidated from two centrifuge tubes, see Section 3.4) were redispersed in 1.0 mL of ethanol with sonification. 3 drops of the redispersed nanoparticles were then placed onto the prepared clean mica disk, and the disk was left to dry for at least 24 hours.

3.8.2 Analysis

The sample was first placed onto the plate under the cantilever. The sample was then moved to the area of interest, usually starting with the middle of the sample then going around to the sides. Using the AFM software, the side camera was turned on in the positioning window to observe the cantilever and sample surface. The operating mode chosen was “static force” and “Sicona”. In the “z-controller” mode, the set point was set to 18 nN and the loop gain to 5000. In the positioning window, the cantilever was brought closer to the sample surface, see Figure 3-1 below. Once the cantilever was close enough, the “approach” button was pressed, and the cantilever was automatically brought to the mica surface. If the approach wasn’t rejected, the instrument would start creating an image of the area line by line.

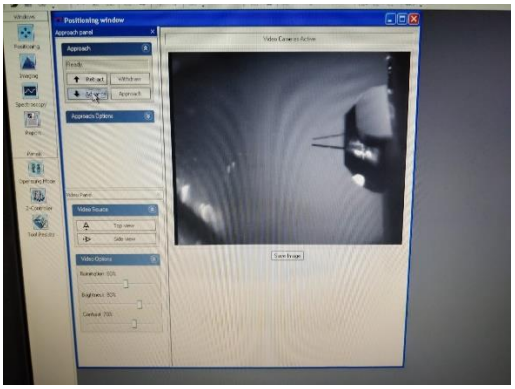

Figure 3-1. Picture showing an example of how close in proximity the probe needs to be to the surface of the mica before approaching.

3.9 Nuclear Magnetic Resonance

3.9.1 Sample Preparation

50 µL of ionic liquid product was added to 700 µL of $CDCl_3$ solvent in a 1-mL centrifuge tube. The centrifuge tube was then shaken thoroughly to mix the sample, after which it was transferred to an NMR tube.

3.9.2 Analysis

^{1}H-NMR and proton decoupled ^{13}C-NMR spectra were collected for the sample. The ^{1}H-NMR peaks were integrated to assist with counting protons associated with the intended product.

3.10 Fast Scan Cyclic Voltammetry

3.10.1 Sample Preparation

A 5:1 IL-1A:$HAuCl_4$ molar ratio mixture was prepared by adding 10 mL of a 3.81 mM IL-1A aqueous solution to 10 mL of a 0.762 mM $HAuCl_4$ aqueous solution, dropwise. A 5-mL sample of the cloudy, yellow Au-IL mixture was collected. The remainder of the mixture was heated at a hot plate setting of 103 ºC until it was homogenous but still colorless. Another 5-mL sample was collected from the colorless, homogenous mixture. The temperature of the hot plate was raised to 150 ºC and the remaining homogeneous mixture was heated until it became pinkish-brown. The remainder of the mixture was then collected. FSCV analysis was conducted on all of the individual samples.

3.10.2 Analysis

A carbon fiber microelectrode was used as the working electrode, with Ag/AgCl as the reference electrode. In the first set of experiments, the buffer used was a 150 mM

trizma hydrochloride,1.4 M NaCl, 32.5 mM KCl, 12 mM $CaCl_2$, NaH_2PO_4, 12 mM $MgCl_2$ and 20 mM Na_2SO_4 solution, with a scan rate of 400 V/s. In the second set of experiments, the buffer used was a 50 mM Na_3PO_4 and 4 mM NaCl solution, with a scan rate of 100 V/s used. Here the working electrode was conditioned between scans at 60 Hz for 2-3 minutes. The potential range scanned for the experiments was -1.5 to 1.5 V.

CHAPTER IV

RESULTS AND DISCUSSION

4.1. Ionic Liquids Synthesis and Characterization

Ionic liquid structures were confirmed by ^{1}H NMR. The ^{1}H NMR peaks were integrated to verify the correct ratio of protons. Additional ^{13}C NMR spectra of ionic liquids can be found in Appendix A.

4.1.1. 2-(Phenylmercapto)Ethyl-Tributylphosphonium Chloride

The synthesis of 2-(phenylmercapto)ethyl-tributylphosphonium chloride (**IL-1A**) was performed according to Scheme 4.1. below and as described in Section 3.2.1 of the Methods chapter.

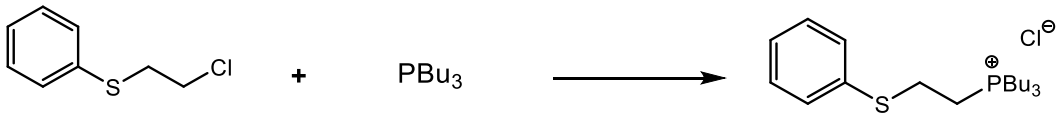

Scheme 4-1. Reaction of 2-chloro phenyl ethyl sulfide with tributlyphosphine to produce 2-(phenylmercapto)ethyl-tributylphosphonium chloride.

The product of the reaction shown in Scheme 4.1. was characterized with ^{1}H-NMR as shown in Figure 4-1.

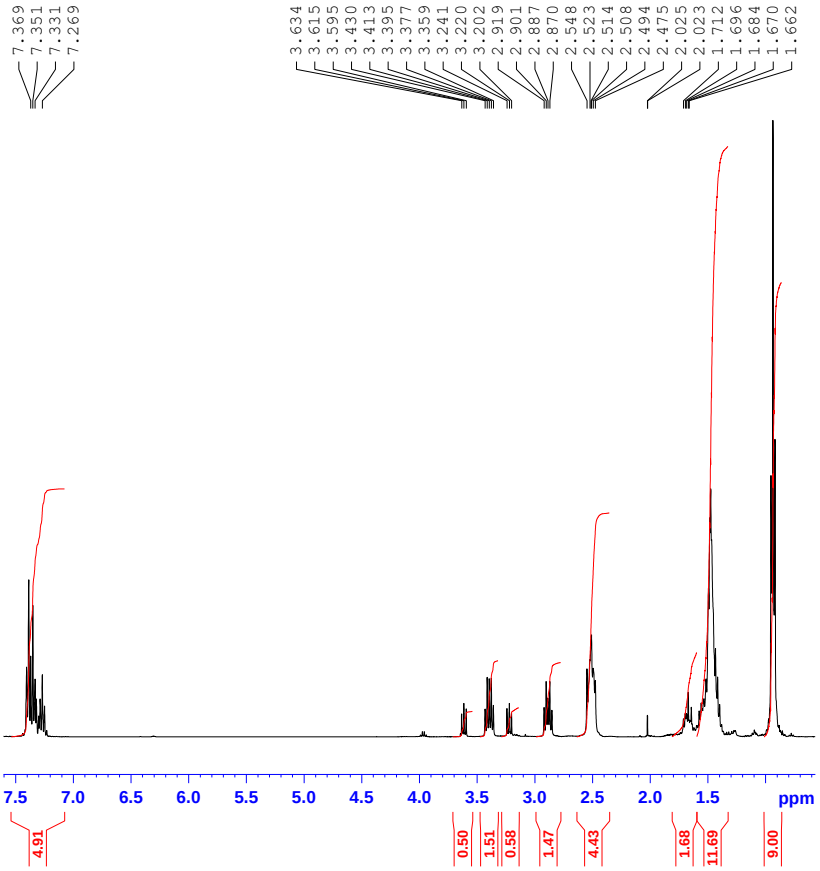

Figure 4-1. ^{1}H NMR of 2-(phenylmercapto)ethyl-tributylphosphonium chloride in $CDCl_3$.

(400 MHz, $CDCl_3$, [ppm]) δ = 0.94 (9H, m, 3CH_3CH$_2$CH$_2$CH$_2$-), 1.48 (12H, m, 3CH$_3$CH_2CH_2CH$_2$-), 2.51 (6H, m, 3CH$_3$CH$_2$CH$_2$CH_2), 2.89 (2H, m, -SCH$_2$CH_2-P), 3.39 (2H, m, -SCH_2CH$_2$-P), 7.27–7.37 (5H, m, C$_6H_5$S-).

4.1.2. 2-(Ethylmercapto)Ethyl-Tributylphosphonium Chloride

The synthesis of 2-(ethylmercapto)ethyl-tributylphosphonium chloride (**IL-2**) was performed according to Scheme 4.2. below and as described in Section 3.2.2 in the Methods chapter.

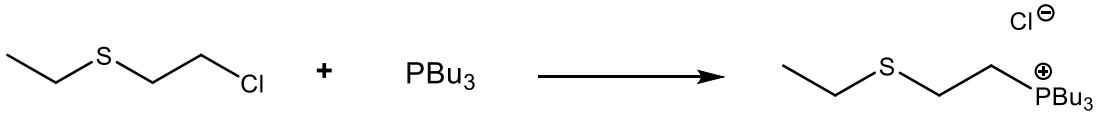

Scheme 4-2. Reaction of 2-chloro ethyl ethyl sulfide with tributlyphosphine to produce 2-(ethylmercapto)ethyl-tributylphosphonium chloride.

The product of the reaction shown in Scheme 4.2. was characterized with ^{1}H-NMR as shown in Figure 4-2.

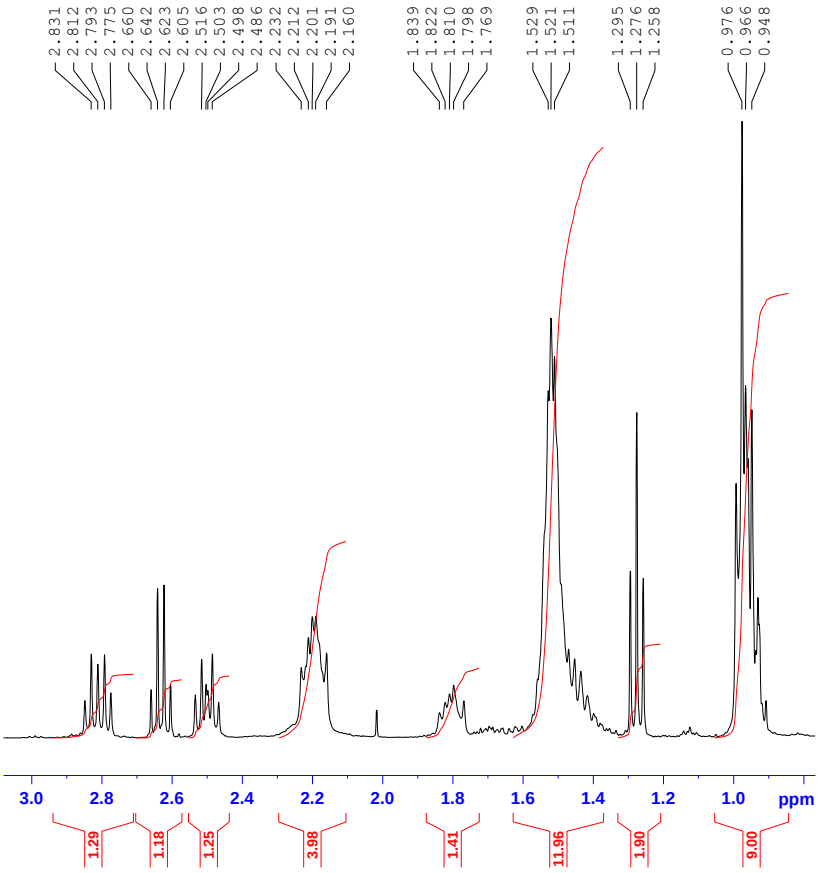

Figure 4-2. ^{1}H NMR of 2-(ethylmercapto)ethyl-tributylphosphonium chloride in $CDCl_3$.

^{1}H-NMR (400 MHz, $CDCl_3$, [ppm]) δ = 0.96 (9H, m, 3C*H*$_3$CH$_2$CH$_2$CH$_2$-), 1.28 (3H, t, C*H*$_3$CH$_2$S-), 1.52 (12H, m, 3CH$_3$C*H*$_2$C*H*$_2$CH$_2$-), 2.20 (6H, m, 3CH$_3$CH$_2$CH$_2$C*H*$_2$), 2.50 (2H, m, -SCH$_2$C*H*$_2$-P), 2.63 (2H, m, CH$_3$C*H*$_2$S-), 2.63 (2H, m, -SC*H*$_2$CH$_2$-P).

4.1.3. 2-(Phenylmercapto)Ethyl-Methylimidazolium Chloride

The synthesis of 2-(phenylmercapto)ethyl-methylimidazolium chloride (**IL-1B**) was performed according to Scheme 4.3. below and as described in Section 3.2.3 in the Methods chapter.

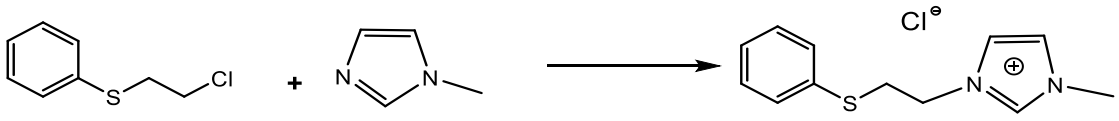

Scheme 4-3. Reaction of 2-chloro phenyl ethyl sulfide with methylimidazolium to produce 2-(phenylmercapto)ethyl-methylimidazolium chloride.

The product of the reaction shown in Scheme 4.3. was characterized with ^{1}H-NMR as shown in Figure 4-3.

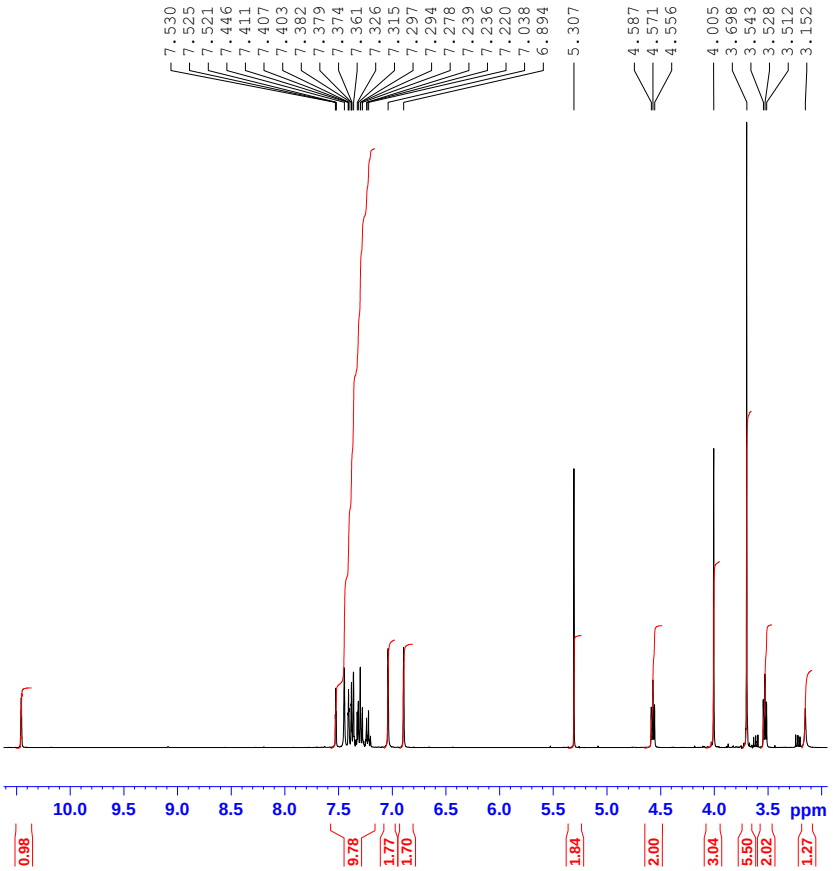

Figure 4.3. ^{1}H NMR of 2-(phenylmercapto)ethyl-methylimidazolium chloride in $CDCl_3$.

^{1}H-NMR (400 MHz, $CDCl_3$, [ppm]) δ = 4.01 (3H, s, -N-CH_3), 4.95 (2H, m, -SCH_2CH_2N-), 5.31 (2H, m, -SCH_2CH_2N), 6.90 (1H, m, -NC*H*CHN), 7.04 (1H, m, -NCHC*H*N), 7.27–7.57 (5H, m, C_6H_5S-).

4.1.4. Attempted Synthesis of 1,8-Bis (Tri(n-butyl)phosphonium Bromide)-3,6-Dithiaoctane

An attempt of the synthesis of 1,8-bis(tri(*n*-butyl)phosphonium bromide)-3,6-dithiaoctane was performed according to Scheme 4.4. below and as described in section 3.2.4 in the Methods chapter.

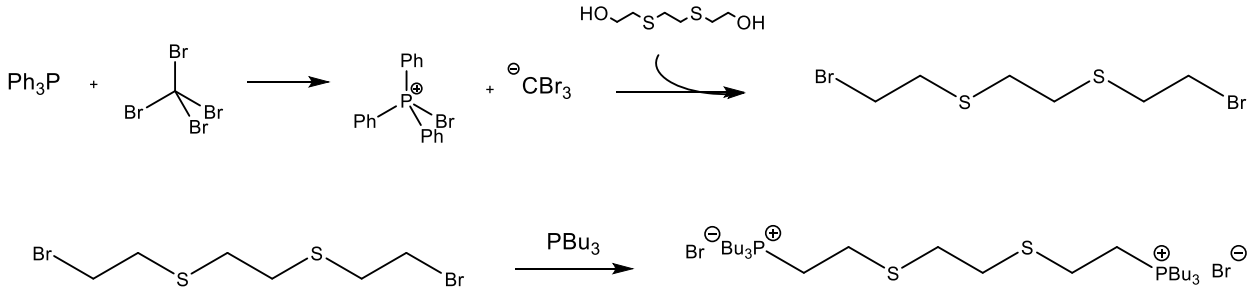

Scheme 4-4. Proposed reaction scheme for synthesis of 1,8-bis(tri(*n*-butyl)phosphonium bromide)-3,6-dithiaoctane.

The product of the reaction shown in Scheme 4.4. was characterized with ^{1}H-NMR as shown in Figure 4-4.

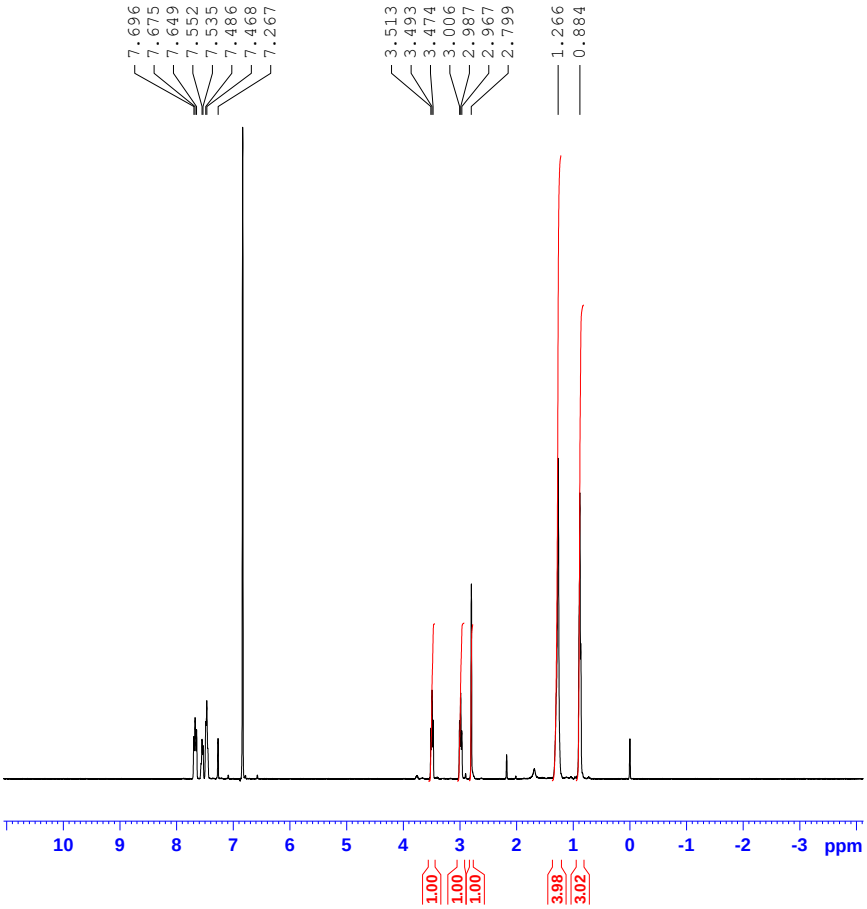

Figure 4-4. ^{1}H NMR of failed 1,8-bis(tri(*n*-butyl)phosphonium bromide)-3,6-dithiaoctane synthesis in $CDCl_3$.

The proposed ionic liquid, 1,8-bis(tri(*n*-butyl)phosphonium bromide)-3,6-dithiaoctane, wasn't successfully synthesized. The ^{1}H-NMR did not correlate with the intended structure. There are peaks in the aromatic region, but there aren't any aromatic hydrogens present in the intended product. Peaks around 2.9 and 2.4 ppm support the possibility of original dithiaoctanediol reactant. The presence of other impurities are seen as well.

4.2 Optimization of Gold Nanoparticles Synthesis with 2-(Phenylmercapto)Ethyl-Tributylphosphonium Chloride

4.2.1. Preliminary Synthesis

Preliminary syntheses were conducted as described in Chapter III, but without heating the aqueous $HAuCl_4$ and IL mixture prior to the addition of $NaBH_4$. The syntheses were performed with 10:1, 5:1 , and 1:1 IL-1A:$HAuCl_4$ molar ratios, and with a 1:1 $NaBH_4$:$HAuCl_4$ molar ratio. The $HAuCl_4$ and ionic liquid aqueous mixture was cloudy and yellow before addition of reducing agent. UV-Vis spectra of the reaction mixture were collected after reaction completion. The surface plasmon resonance (SPR) absorbance maxima of the reaction mixtures for the different syntheses are shown below in Figures 4-5 to 4-7 and in Table 4.1.

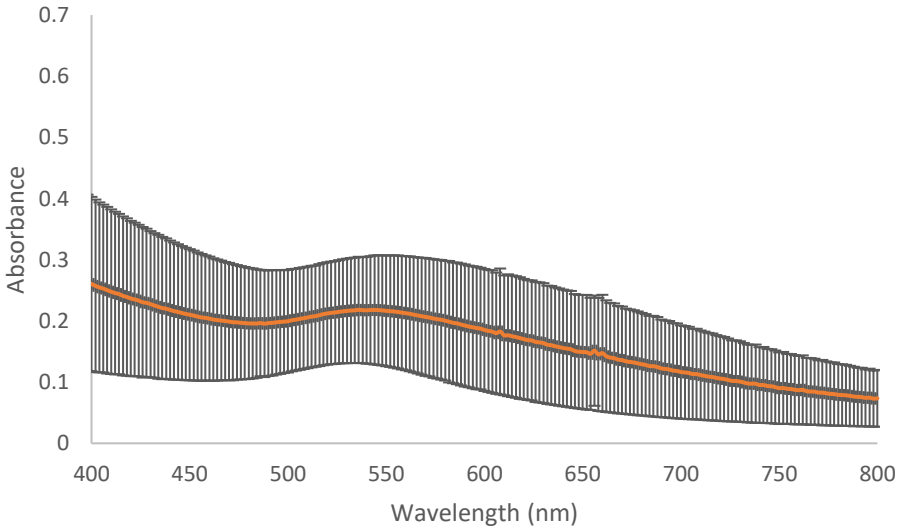

Figure 4-5. UV-Vis spectra of 10:1 IL-1A:$HAuCl_4$ molar ratio duplicates. The concentrations used were 5.867 mM IL-1A, 0.5867 mM $HAuCl_4$, and 0.5867 mM $NaBH_4$.

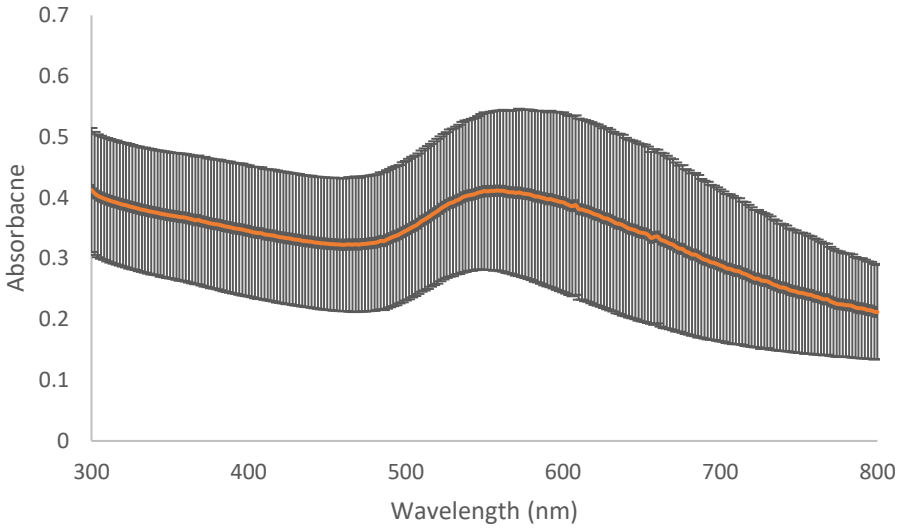

Figure 4-6. UV-Vis spectra of 5:1 IL-1A:$HAuCl_4$ molar ratio duplicates. The concentrations used were 5.00 mM IL-1A, 1.00 mM $HAuCl_4$, and 1.00 mM $NaBH_4$.

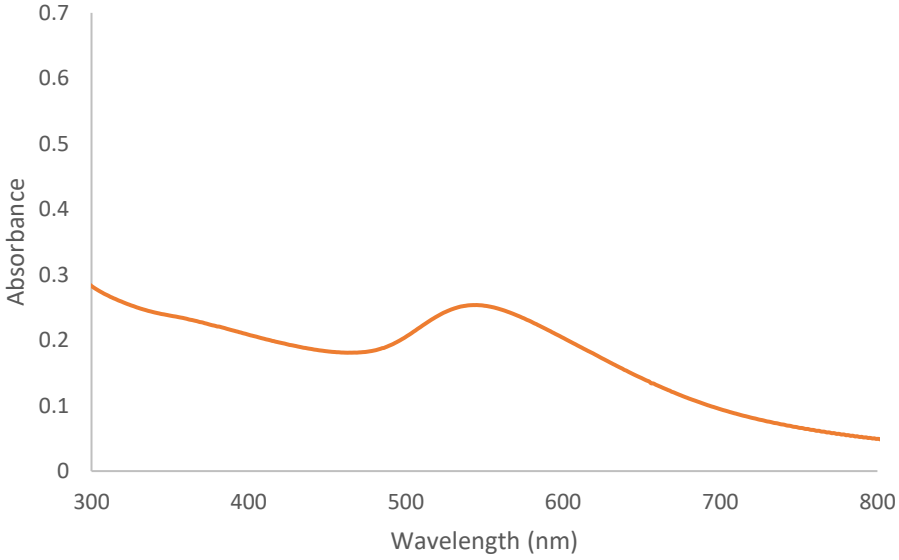

Figure 4-7. UV-Vis spectra of 1:1 IL-1A:$HAuCl_4$ molar ratio synthesis. The concentrations used were 0.762 mM IL-1A, 0.762 mM $HAuCl_4$, and 0.762 mM $NaBH_4$.

Table 4-1. Absorbance maxima of the reaction mixtures for preliminary syntheses with 2-(phenylmercapto)ethyl-tributylphosphonium chloride

Concentration (IL-1A:$HAuCl_4$ molar ratio)	***Absorbance Max (λ_{max})***
10:1	535 nm
10:1	546 nm
5:1	572 nm
5:1	550 nm
1:1	543 nm

The absorbance maxima varied significantly (10-20 nm) between replicates within the same IL:Au concentration ratios, indicating a lack of reproducibility in the syntheses. This irreproducibility is most likely due to the heterogeneity of the gold-ionic liquid mixture. The syntheses products were still observed using microscopy techniques before the reproducibility issues could be investigated and improved.

4.2.2. Scanning Electron Microscopy with Electron Dispersive X-Ray Spectroscopy Characterization

Scanning electron microscopy/electron dispersive x-ray spectroscopy (SEM/EDX) was performed on gold nanoparticles samples for each gold:IL molar ratio; all samples were isolated as described in Section 3.4. Additional SEM images and EDX measurements were taken for each IL:Au molar ratio and are shown in Appendix C. The images shown below in Figures 4-8 to 4-10 were chosen as representative SEM/EDX data.

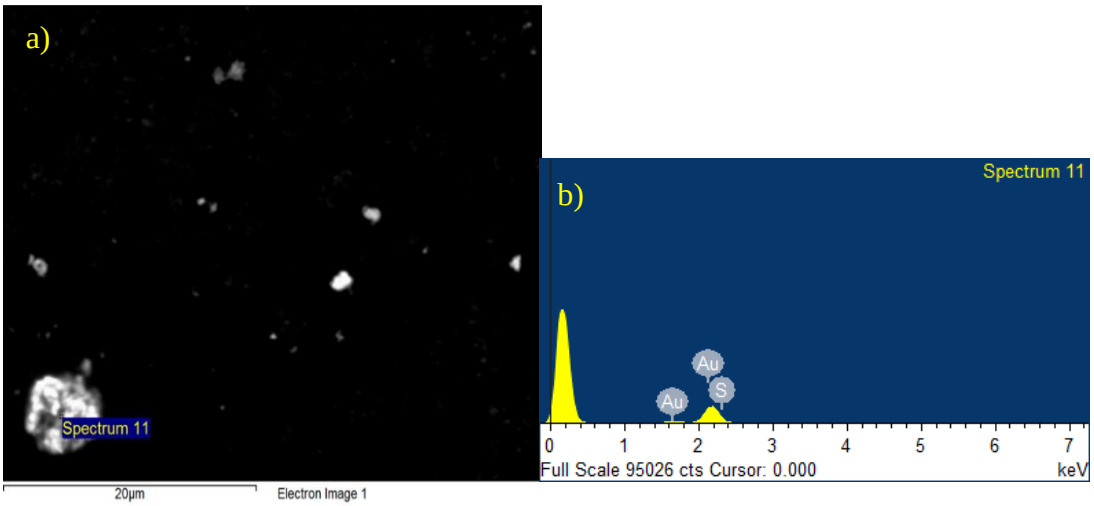

Figure 4-8. SEM-EDX of 10:1 2-(phenylmercapto)ethyl-tributylphosphonium chloride:$HAuCl_4$ molar ratio synthesis. The concentrations used in this reaction are 5.867 mM IL-1A, 0.5867 mM $HAuCl_4$, and 0.5867 mM $NaBH_4$. A) SEM b) EDX

The 10:1 IL-1A:Au molar ratio gold nanoparticle synthesis samples showed the formation of large aggregates, as seen in the SEM in Figure 4-8(a). Nanoparticles sizes under 100 nm and aggregates were observed throughout the sample. The elemental analysis showed 95.57(w)% gold and 4.43 sulfur (w)%.

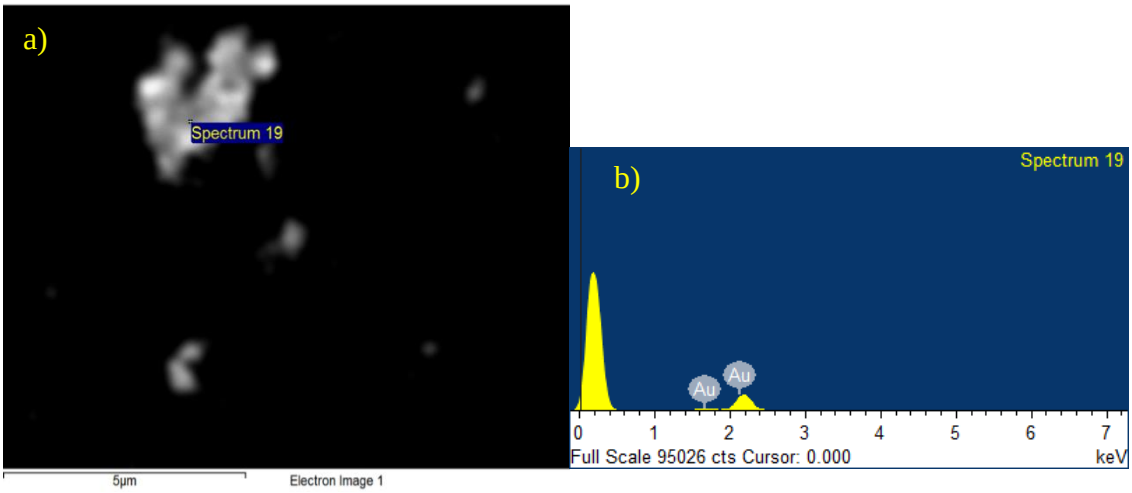

Figure 4-9. SEM-EDX data for 5:1 2-(phenylmercapto)ethyl-tributylphosphonium chloride:$HAuCl_4$ molar ratio synthesis. The concentrations used in this reaction were 3.81 mM IL-1A, 0.762 mM $HAuCl_4$, and 0.762 mM $NaBH_4$.a) SEM b) EDX

The 5:1 IL-1A:Au molar ratio gold nanoparticle synthesis samples showed the formation of large aggregates, as seen in Figure 4-9(a). The elemental analysis gave 100(w)% gold, as seen in Figure 4-9(b). Nanoparticles and particles over 100 nm were observed throughout the sample.

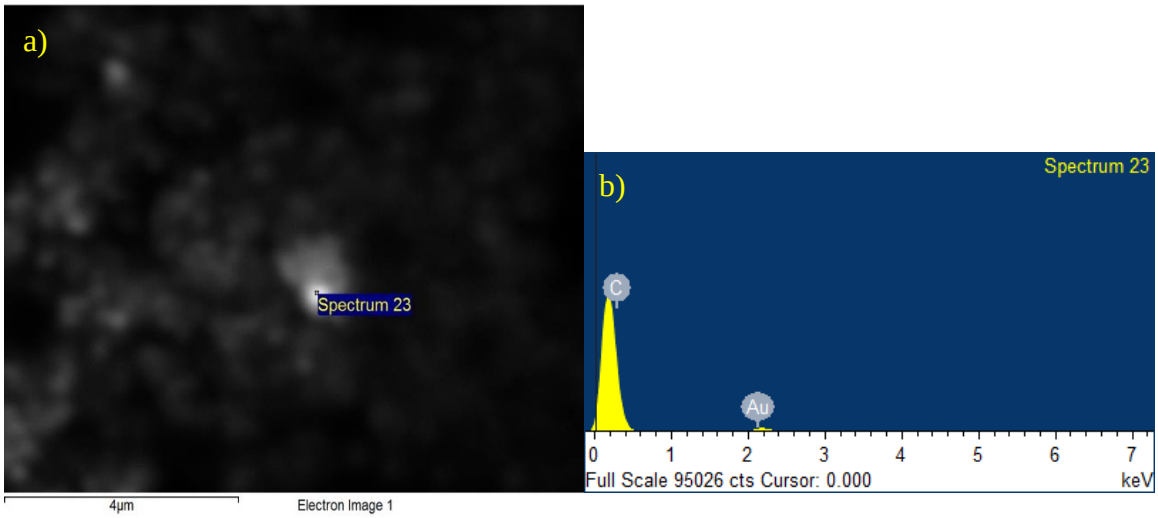

Figure 4-10. SEM-EDX of 1:1 2-(phenylmercapto)ethyl-tributylphosphonium chloride:$HAuCl_4$ molar ratio synthesis. The concentrations used in this reaction were 0.762 mM IL-1A, 0.762 mM $HAuCl_4$, and 0.762 mM $NaBH_4$. a) SEM b) EDX

Aggregates were mostly observed in 1:1 IL-1A:Au molar ratio gold nanoparticle synthesis samples, as seen in Figure 4-10(a). The elemental analysis gave 6.47(w)% gold and 93.53(w)% carbon. Here the carbon sticky signal was stronger than the gold signal, see Figure 4-10(b).

4.2.3. Atomic Force Microscopy Characterization

Atomic force microscopy (AFM) was used to obtain preliminary size data for each gold nanoparticle sample. Multiple images (or areas) were observed. The images below are representative of each IL-1A:Au molar ratio.

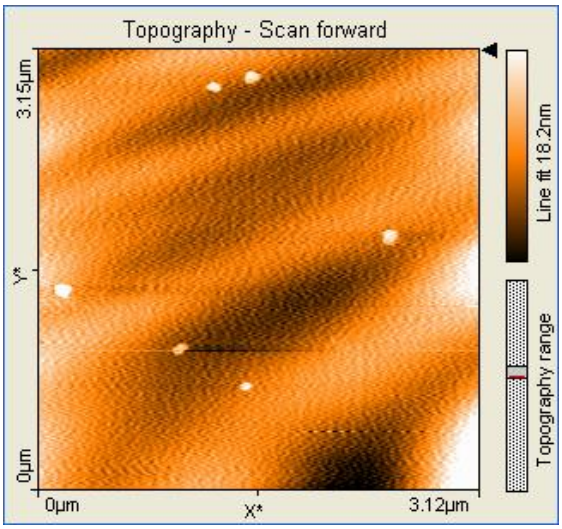

Figure 4-11. AFM of 10:1 2-(phenylmercapto)ethyl-tributylphosphonium chloride:$HAuCl_4$ molar ratio synthesis. The concentrations used in this reaction were 5.867 mM IL-1A, 0.5867 mM $HAuCl_4$, and 0.5867 mM $NaBH_4$.

The area represented in Figure 4-11 shows larger nanoparticles between 50 – 100 nm within the 10:1 IL-1A:$HAuCl_4$ molar ratio gold nanoparticle synthesis sample.

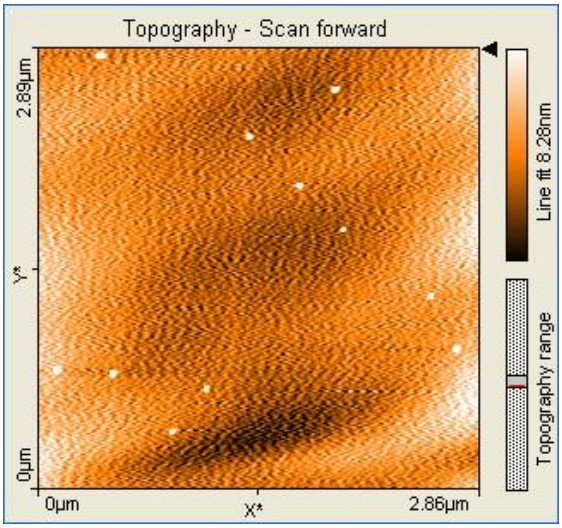

Figure 4-12. AFM of 5:1 2-(phenylmercapto)ethyl-tributylphosphonium chloride:$HAuCl_4$ molar ratio synthesis. The concentrations used in this reaction were 3.81 mM IL-1A, 0.762 mM $HAuCl_4$, and 0.762 mM $NaBH_4$.

The area represented in Figure 4-12 shows nanoparticles under 50 nm across within the 5:1 IL-1A:$HAuCl_4$ molar ratio gold nanoparticle synthesis sample.

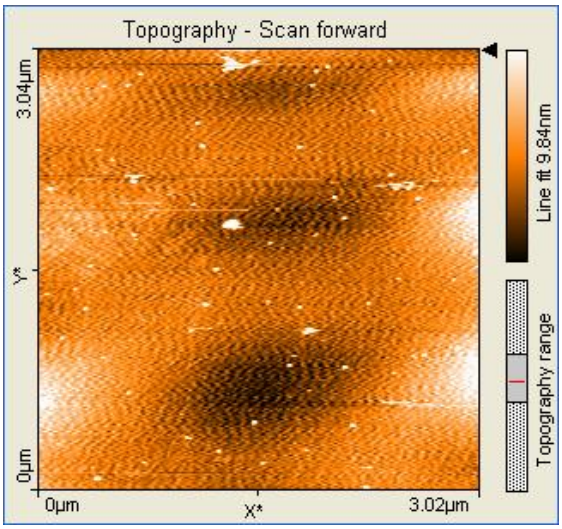

Figure 4-13. AFM of 1:1 2-(phenylmercapto)ethyl-tributylphosphonium chloride:$HAuCl_4$ molar ratio synthesis. The concentrations used in this reaction were 0.762 mM IL-1A, 0.762 mM $HAuCl_4$, and 0.762 mM $NaBH_4$.

The area represented in Figure 4-13 is heavily populated with nanoparticles from 30 – 100 nm observed in the 1:1 IL-1A:$HAuCl_4$ molar ratio gold nanoparticle synthesis sample. Aggregates over 100 nm are observed as well.

From AFM data obtained, nanoparticles around the same size were observed within each IL-1A:Au concentration ratio. While the 1:1 IL:Au molar ratio seemed to produce a higher concentration of nanoparticles than the other IL:Au molar ratios, the image shown represents only one area of the mica disc. The areas of interest are manually chosen, not scanned, so areas like this in other samples could have been missed.

4.2.4. Investigation of the Effect of Ionic Liquid Solubility on Gold Nanoparticle Syntheses and Possible Formation of a Gold-Ionic Liquid Intermediate

As detailed in Section 4.2. above, the reaction mixture did not form a homogenous solution upon the addition of aqueous IL-1A to the aqueous $HAuCl_4$

solution, likely preventing the reproducible formation of gold nanoparticles, as shown by the SPR maxima in Table 4.1. The IL-1A and $HAuCl_4$ aqueous mixture was thus heated to try to obtain a more homogeneous reaction mixture before the addition of $NaBH_4$.

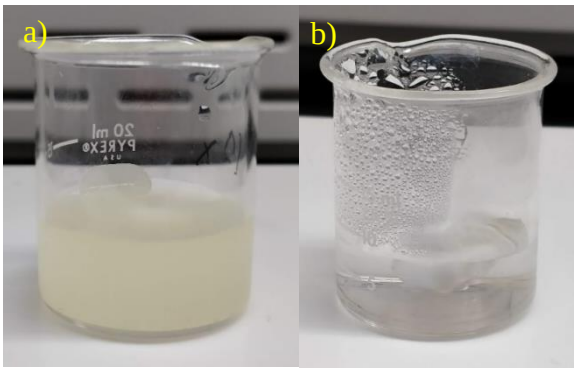

Figure 4-14. 10:1 molar ratio mixture of IL-1A:$HAuCl_4$: a) before heating; b) after heating to colorless, clear solution.

Figure 4-14(a) shows the formation of a cloudy, yellow 10:1 IL1A:Au reaction mixture before heating. After 30 minutes of heating the solution to 47 ºC, the 10:1 IL1A:$HAuCl_4$ mixture became colorless and homogenous, see Figure 4-12(b). It was observed that after increasing the temperature of solution to 56 ºC, the mixture went from colorless to a lightly brownish color; this color change occurred at 54 minutes and was completed at 78 minutes, with a solution temperature of 59 ºC. This change is illustrated in Figure 4-15. A peak appearing in the 500 – 600 nm region (see 46 minutes spectrum) grows over time into a shoulder (see 72 minutes spectrum).

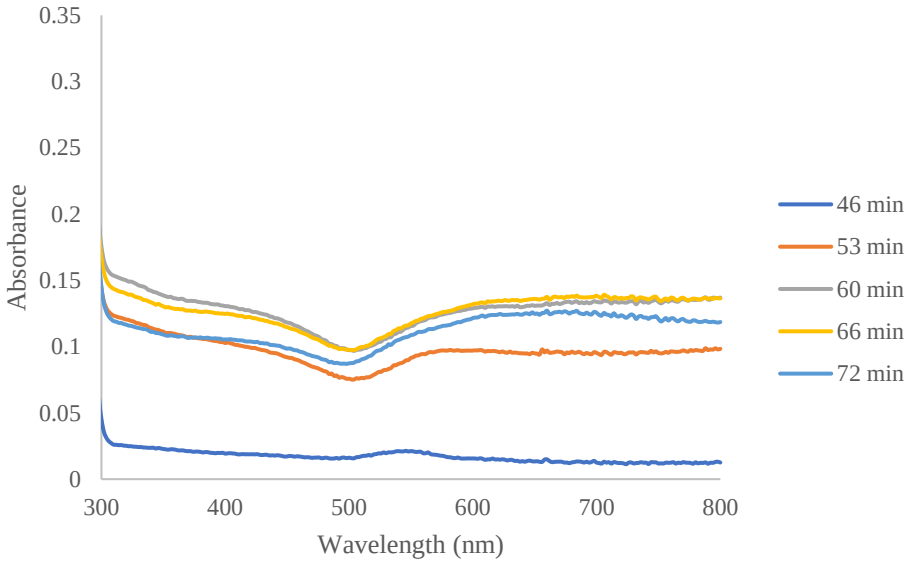

Figure 4-15. UV-Vis spectra of 10:1 IL-1A:$HAuCl_4$ mixture monitored over time during heating.

Other IL-1A and $HAuCl_4$ reaction mixtures (in 5:1 and 1:1 IL1A:Au molar ratios) also showed a color change upon heating and without the addition of $NaBH_4$, albeit to different colors, see Figure 4-16. This color change was monitored using UV-Vis over time.

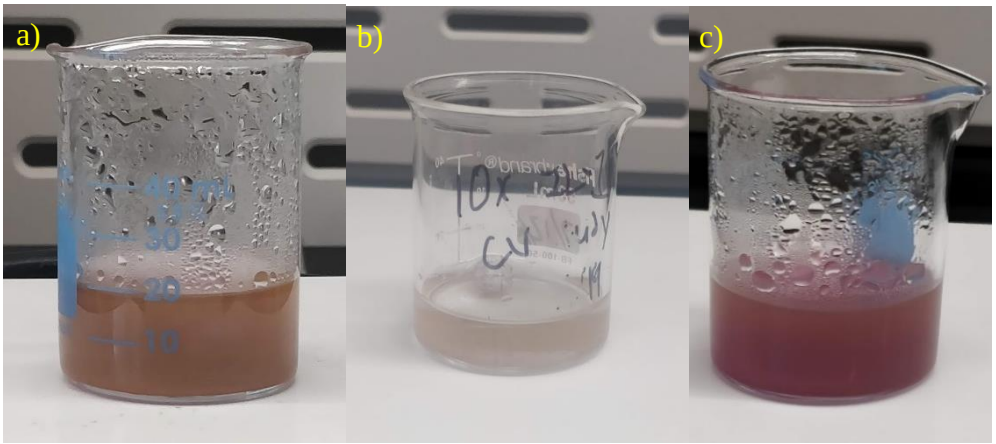

Figure 4-16 Heated IL-1A:$HAuCl_4$ mixtures: a) 10:1 molar ratio; b) 5:1 molar ratio; c) 1:1 molar ratio

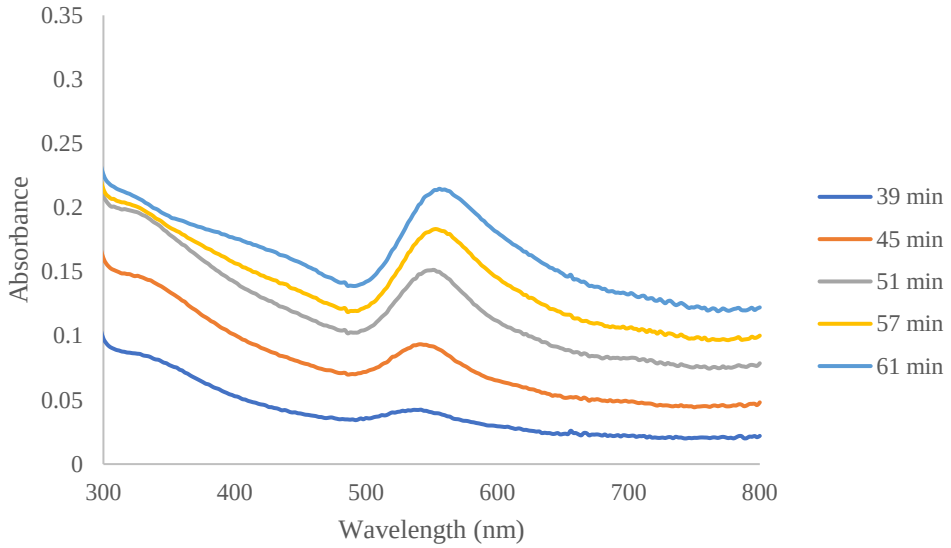

Figure 4-17. UV-Vis spectra of 5:1 IL-1A:$HAuCl_4$ mixture monitored over time during heating.

As seen in Figure 4-17 for the 5:1 IL-1A:$HAuCl_4$ molar ratio solution, a peak begins to form in the 500 – 600 nm range and continues to grow over time. The 5:1 IL-1A:$HAuCl_4$ molar ratio solution became homogeneous after 32 minutes at a solution temperature of 45 ^{0}C. After continuous heating, a color change occurred at 39 minutes; the solution reached its final color at 61 minutes and a 49 ºC solution temperature. The absorbance maximum of the final solution was 562 nm.

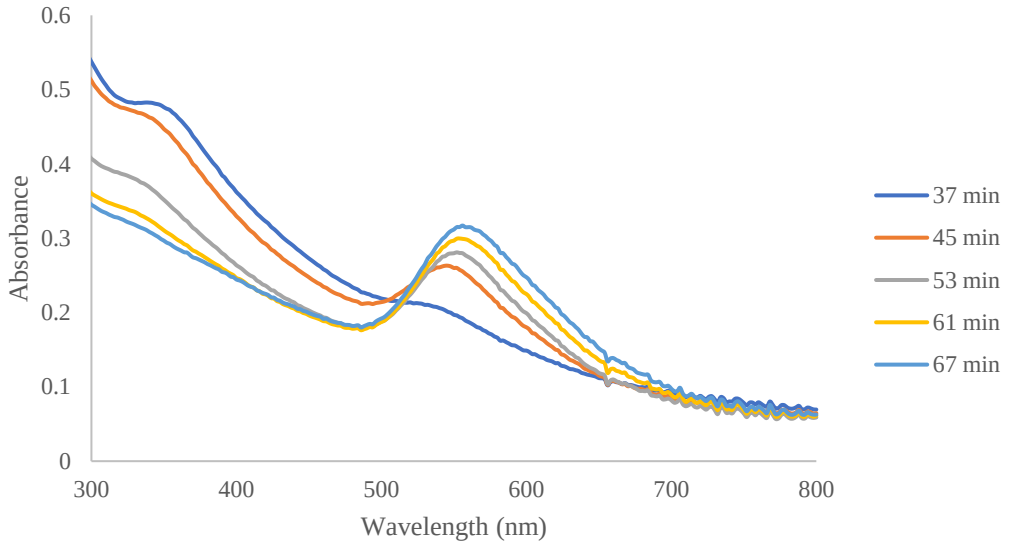

Figure 4-18. UV-Vis spectra of 1:1 IL-1A:$HAuCl_4$ mixture monitored over time during heating.

As seen Figure 4-18 for the 1:1 IL-1A:$HAuCl_4$ molar ratio solution, a shoulder appears in the 500 – 600 nm range and grows over time into a more well-defined peak. The 1:1 IL-1A:$HAuCl_4$ molar ratio solution didn't become completely homogenous before the color change; instead, it transitioned from the cloudy, yellow mixture to a whitish mixture and quickly began its color change. The color change occurred after 37 minutes and a solution temperature of 38 ºC. The solution was heated continuously until it reached its final color after 67 minutes and a 41ºC solution temperature. The maximum absorbance peak of the final solution was 564 nm.

The cooled homogenous, colorless 10:1 and 5:1 IL-1A:$HAuCl_4$ molar ratio solutions were used in the optimized synthesis of the gold nanoparticles reported in Section 4.2.7. For the 1:1 IL-1A:$HAuCl_4$ gold nanoparticle synthesis, the solution obtained right before the color change was used.

4.2.5. Fast Scan Cyclic Voltammetry of Possible Au-IL Intermediate Study

Fast scan cyclic voltammetry (FSCV) was employed to further investigate the possible formation of an Au-IL complex intermediate upon heating the IL-1A and $HAuCl_4$ reaction mixture, as the redox potential of Au is expected to vary with the ligand environment. Three samples were prepared: (i) the initial cloudy yellow mixture, (ii) the homogenous colorless mixture, and (iii) the homogeneous mixture after the color change. The 10:1 IL-1A:Au molar ratio mixture was used in a preliminary study; the resulting voltammograms are shown below in Figure 4-19.

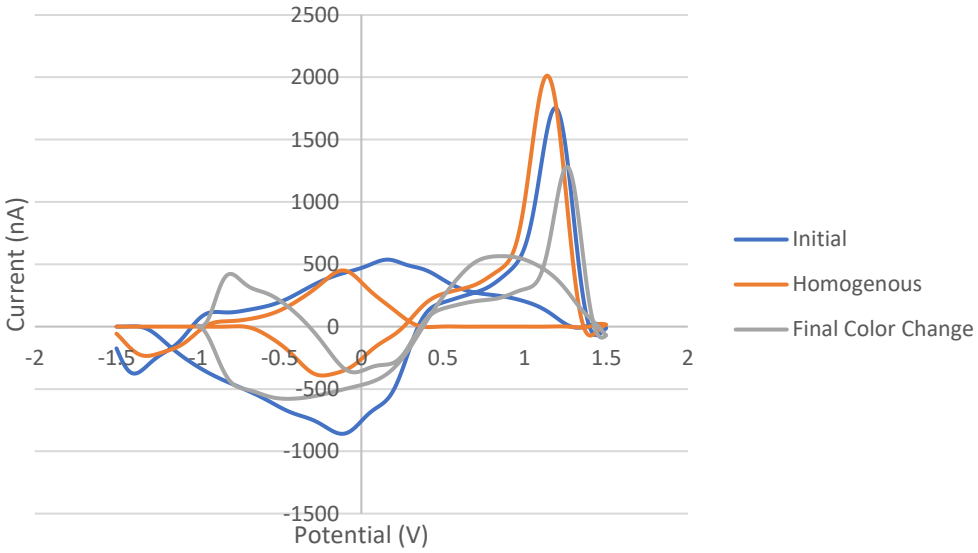

Figure 4-19. FSCV study of 10:1 IL-1A:Au mixture under different heating conditions. The scan rate used was 400 V/s, the working electrode was a carbon fiber microelectrode, the reference electrode was Ag/AgCl, and the buffer used was an electrolyte buffer containing NaCl, KCl, and Na_2CO_3.

The voltammograms in Figure 4-19 were collected in a $NaCl/KCl/Na_2CO_3$ electrolyte solution with a 400 V/s scan rate. Fouling of the carbon fiber working electrode was found to occur, so that the Au oxidation peaks (1.1-1.3 V) could not be consistently obtained between scans. In an optimized FSCV study, the electrolyte

solution was changed to a less concentrated phosphate buffer, the scan rate was decreased to 100 V/s, and the working electrode was conditioned between scans (at 60 Hz for 2-3 minutes). Here the 5:1 IL-1A:Au molar ratio mixture was used because of its more distinct absorption peak upon heating, see Figure 4-17. The resulting voltammograms are shown in Figure 4-20. While the Au oxidation peaks appear to be more aligned between samples, there are inconsistencies in reversibility between these samples. The fine structure observed with some of the Au oxidation peaks likely corresponds to different redox couples (Au(III)/Au(I)/Au).

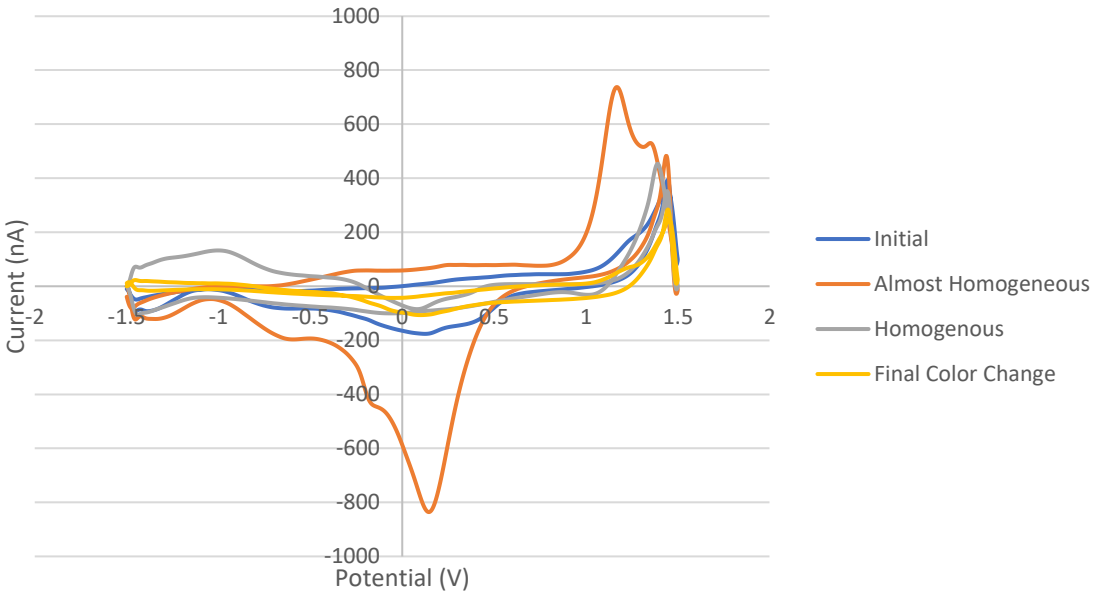

Figure 4-20. FSCV study of 5:1 IL-1A:Au mixture under different heating conditions. The scan rate used was 100 V/s, the working electrode was a carbon fiber microelectrode, the reference electrode was Ag/AgCl, and the buffer used was a phosphate electrolyte buffer.

4.2.6. Preliminary $NaBH_4$ Concentration Study

Several $NaBH_4$:$HAuCl_4$ molar ratios were studied to find an optimal reducing agent concentration. Here syntheses were performed with a10:1 IL-1A:$HAuCl_4$ molar

ratio and conducted with 2:1, 1:1, and 1:2 $NaBH_4$:$HAuCl_4$ molar ratios, in duplicates. The resulting UV-Vis spectra for the reaction mixtures are shown below in Figures 4-21 to 4-23 ("1" and "2" in the legend represent the replicates).

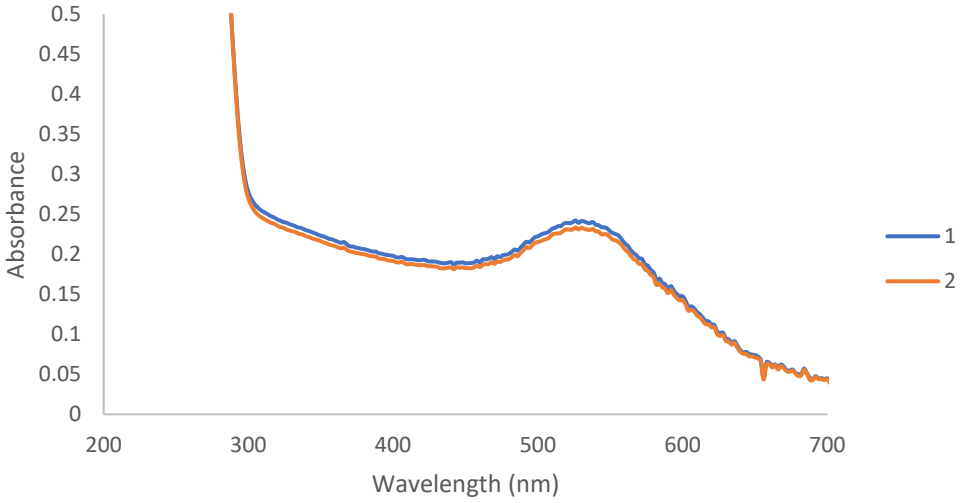

Figure 4-21. Gold nanoparticles syntheses with 2:1 $NaBH_4$:Au molar ratio and 10:1 IL-1A:Au molar ratio. The concentrations used were 7.62 mM IL-1, 0.762 mM $HAuCl_4$, and 1.524 mM $NaBH_4$.

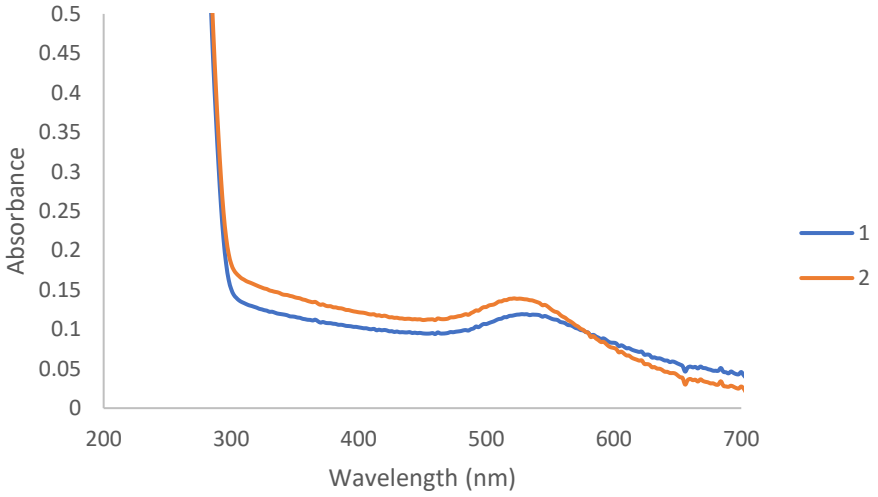

Figure 4-22. Gold nanoparticles syntheses with 1:1 $NaBH_4$:Au molar ratio and 10:1 IL-1A:Au molar ratio. The concentrations used were 7.62 mM IL-1, 0.762 mM $HAuCl_4$, and 0.762 mM $NaBH_4$.

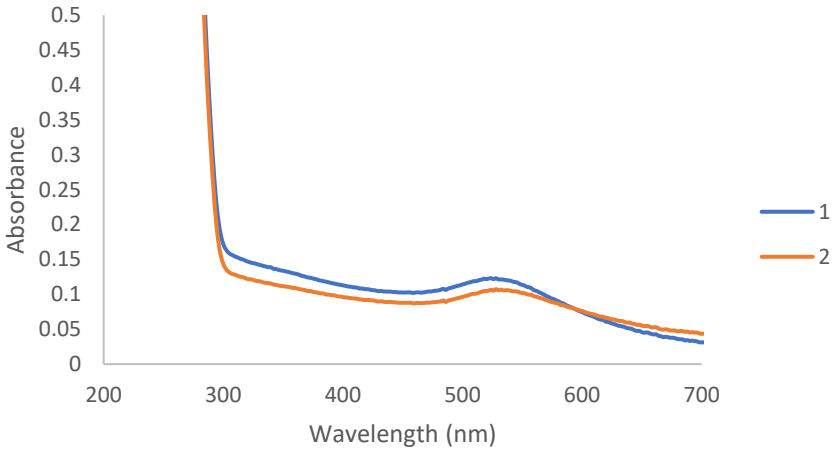

Figure 4-23. Gold nanoparticles syntheses with 1:2 $NaBH_4$:Au molar ratio and 10:1 IL-1:Au molar ratio. The concentrations used were 7.62 mM IL-1, 0.762 mM $HAuCl_4$, and 0.381 mM $NaBH_4$.

The 2:1 $NaBH_4$:$HAuCl_4$ molar ratio gave a larger SPR absorbance for the gold nanoparticles, see Figure 4-21, while the 1:1 and 1:2 $NaBH_4$:Au molar ratios gave comparable SPR absorbances for the gold nanoparticles, see Figures 4-22 and 4-23. Because of concern over the larger IL shoulder with a 2:1 $NaBH_4$:$HAuCl_4$ molar ratio, and because of the comparable results between the 1:1 and 1:2 $NaBH_4$:$HAuCl_4$ molar ratio, the 1:2 $NaBH_4$:$HAuCl_4$ molar ratio was chosen for the optimized syntheses. However, the $NaBH_4$:$HAuCl_4$ molar ratio was later changed to 2:1 in the final syntheses, see Section 4.6.

4.2.7. Optimized Gold Nanoparticles Syntheses

The gold nanoparticles syntheses were performed using the homogeneous and colorless IL-1AA and $HAuCl_4$ reaction mixtures after cooling to room temperature (in 10:1, 5:1, and 1:1 molar ratios), with a 1:2 $NaBH_4$:Au molar ratio. The syntheses were performed in triplicates, and UV-Vis spectra of the reaction mixture were recorded after reaction completion for each synthesis. Within each IL1A:Au molar ratio, the spectra

were averaged, and the reproducibility was assessed for each triplicate synthesis, see Figures 4-24 to 4-26 below.

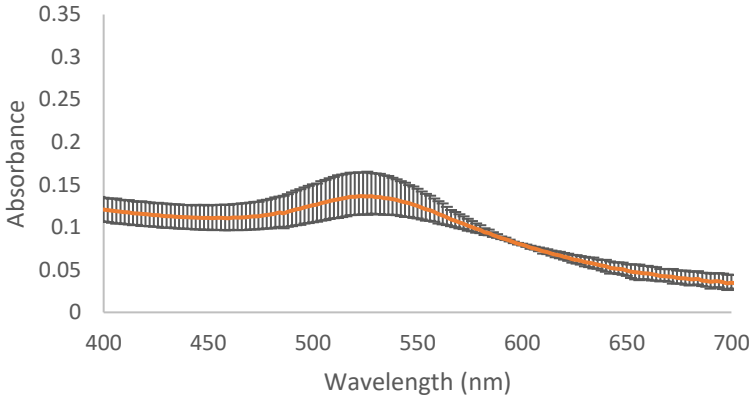

Figure 4-24. UV-Vis spectra of the reaction mixture triplicates for the 10:1 IL-1A:$HAuCl_4$ syntheses. The concentrations used were 7.62 mM IL-1A, 0.762 mM $HAuCl_4$, 0.381 mM $NaBH_4$.

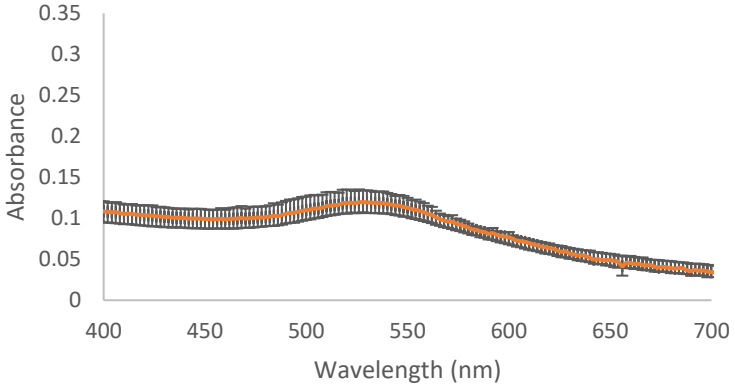

Figure 4-25. UV-Vis spectra of the reaction mixture triplicates for the 5:1 IL-1A:$HAuCl_4$ syntheses. The concentrations used were 3.81 mM IL-1A, 0.762 mM $HAuCl_4$, 0.381 mM $NaBH_4$.

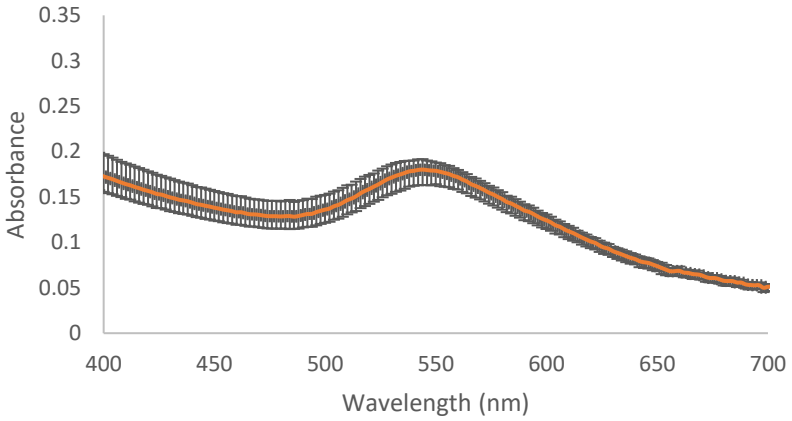

Figure 4-26. UV-Vis spectra of the reaction mixture triplicates for the 1:1 IL-1A:$HAuCl_4$ syntheses. The concentrations used were 0.762 mM IL-1A, 0.762 mM $HAuCl_4$, 0.381 mM $NaBH_4$.

The average absorbance maxima at the gold nanoparticles SPR peak for all the IL-1A:Au molar ratios are shown below in Table 4-2.

Table 4-2. Absorbance maxima of the reaction mixture triplicates for optimized syntheses with 2-(phenylmercapto)ethyl-tributylphosphonium chloride

	1	***2***	***3***	***Average λ_{max}***
10:1	524 nm	526 nm	528 nm	526(±2) nm
5:1	528 nm	526 nm	528 nm	527(±1) nm
1:1	544 nm	546 nm	550 nm	547(±3) nm

The reproducibility in gold nanoparticles SPR absorbance was significantly increased between replicates with heating the IL-1A and $HAuCl_4$ mixtures prior to $NaBH_4$ addition (see Figures 4-22 and 4-5). However, a larger variation in SPR absorbance between replicates was found for the higher 10:1 IL-1A:Au molar ratio, possibly due to a reduced solubility.

4.2.8. Scanning Electron Microscopy Characterization of Optimized Gold Nanoparticles Syntheses with IL-1A

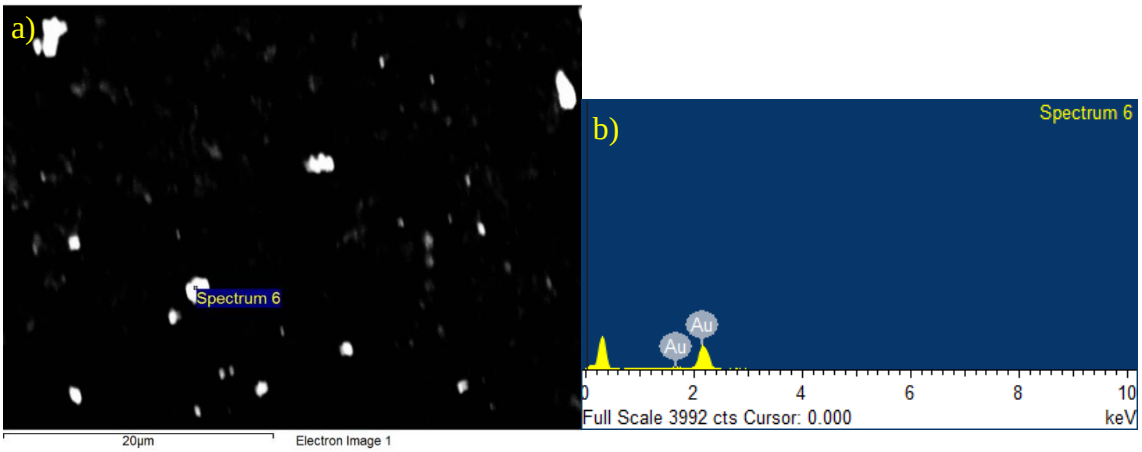

Figure 4-27. SEM-EDX of optimized 10:1 IL-1A:Au molar ratio synthesis. The concentrations used in these syntheses were 7.62 mM IL-1A, 0.762 mM $HAuCl_4$, 0.381 mM $NaBH_4$. a) SEM image b) EDX

Nanoparticles of various sizes between 50 – 100 nm were found in the 10:1 IL-1A:$HAuCl_4$ gold nanoparticle synthesis sample, along with some aggregates, see Figure 4.27(a). Elemental analysis gave 100 (w) % gold, see Figure 4-27(b).

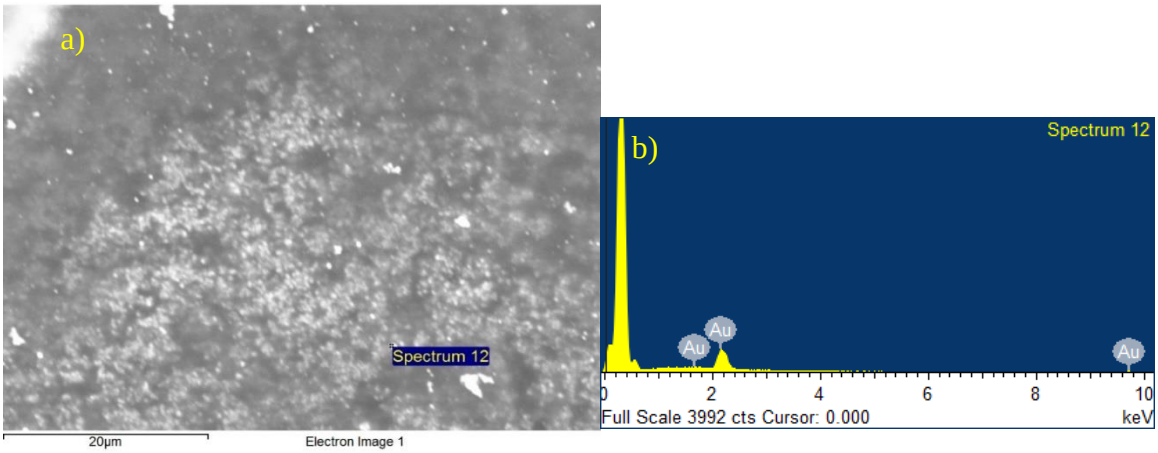

Figure 4-28. SEM-EDX of optimized 5:1 IL-1A:$HAuCl_4$ molar ratio synthesis. The concentrations used in these syntheses were 3.81 mM IL-1A, 0.762 mM $HAuCl_4$, 0.381 mM $NaBH_4$. a) SEM image b) EDX

Nanoparticles of various sizes under 100 nm were found in the 5:1 IL-1A:$HAuCl_4$ molar ratio gold nanoparticle synthesis sample, see Figure 4-28(a). The sample area

showed good dispersion of the nanoparticles. Elemental analysis gave 100 (w)% gold, see Figure 4-28(b).

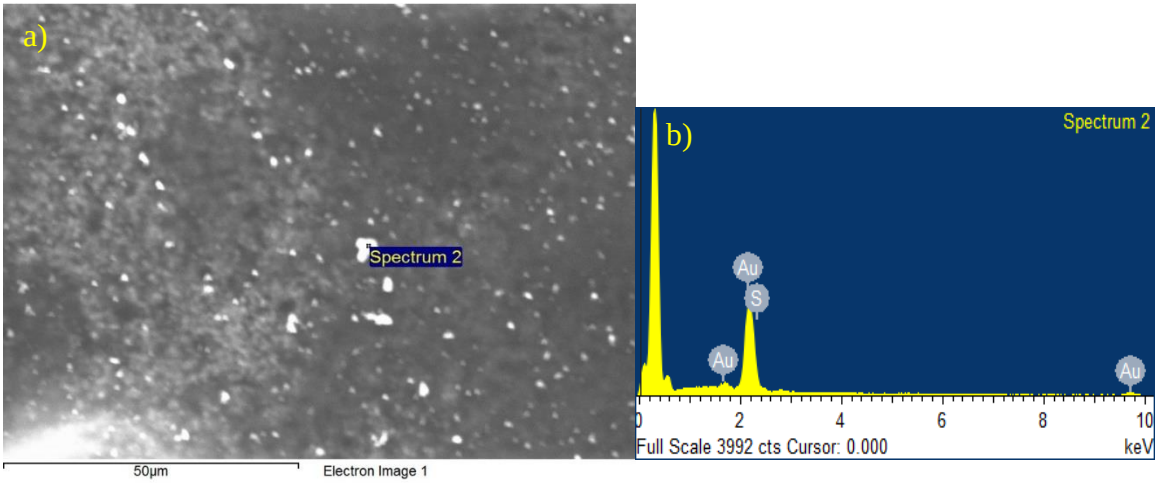

Figure 4-29. SEM-EDX of optimized 1:1 IL-1A:Au molar ratio synthesis. The concentrations used in these syntheses were 0.762 mM IL-1A, 0.762 mM $HAuCl_4$, 0.381 mM $NaBH_4$. a) SEM image b) EDX

Aggregates between 100 – 500 nm were found in the 1:1 IL-1A:$HAuCl_4$ molar ratio gold nanoparticle synthesis sample, see Figure 4-29(a). The sample area showed good dispersion of the particles. Elemental gave 99.9 (w)% gold and 0.1 (w)% sulfur, see Figure 4-29(b). The sulfur is likely due to ionic liquid residue contamination. The high population of aggregates shown are limited to the resolution of the SEM. The AFM, see 4-31, shows nanoparticles between 50-100 nm.

4.2.9. Atomic Force Microscopy Characterization of Optimized Gold Nanoparticles Syntheses with IL-1A

AFM images were taken of the optimized 5:1 and 1:1 IL-1A:$HAuCl_4$ molar ratio gold nanoparticles syntheses. AFM has a better resolution than SEM, allowing for preliminary size data of the nanoparticles.

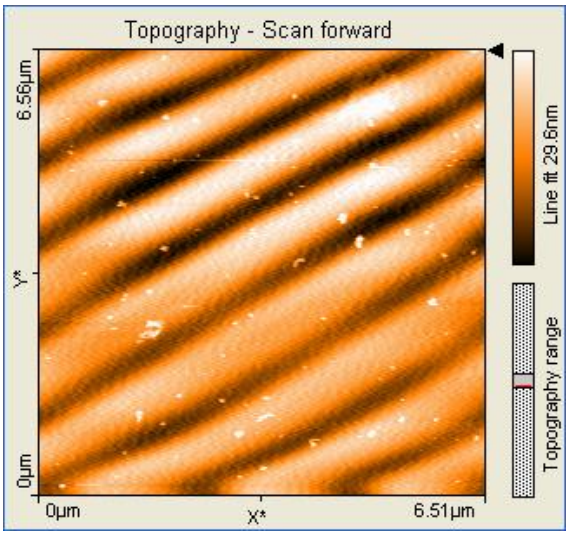

Figure 4-30. AFM image of the optimized 5:1 IL-1A:$HAuCl_4$ molar ratio synthesis. The concentrations used were 3.81 mM IL-1A, 0.762 mM $HAuCl_4$, and 0.381 mM $NaBH_4$.

The 5:1 IL-1A:$HAuCl_4$ molar ratio gold nanoparticle synthesis sample showed good dispersion of the nanoparticles, see Figure 4-30. Nanoparticle sizes ranged from approximately 30 to 100 nm. Aggregates ranging from 100 nm to 500 nm could be observed as well.

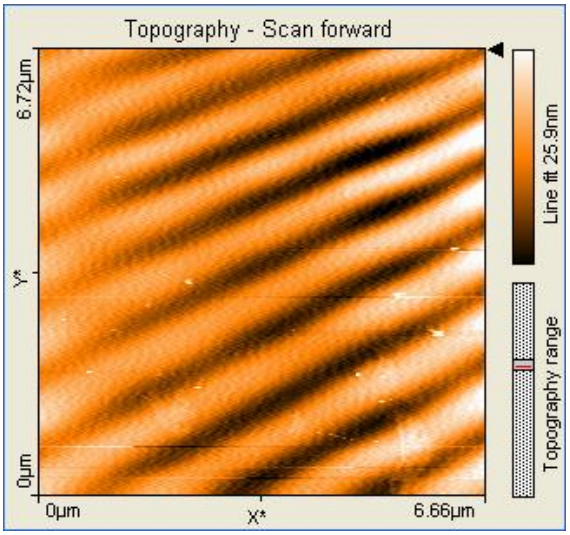

Figure 4-31. AFM image of the optimized 1:1 IL-1A:$HAuCl_4$ molar ratio synthesis. The concentrations used were 0.762 mM IL-1A, 0.762 mM $HAuCl_4$, and 0.381 mM $NaBH_4$.

The 1:1 IL-1A:$HAuCl_4$ molar ratio gold nanoparticle synthesis sample showed a higher dispersion and a less dense population of nanoparticles, see Figure 4-31. In this selected area, nanoparticles ranging from 50 - 100 nm were mostly seen, with a few aggregates over 100 nm present.

4.3 Gold Nanoparticles Synthesis with 2-(Phenylmercapto) Ethyl-Methylimidazolium Chloride

The ionic liquid solubility could possibly be improved by changing the organic cation. Here, the tributylphosphonium group of IL-1A was replaced with a methylimidazolium in IL-1B. The Au-IL-1B reaction mixture was homogenous without heating prior to the addition of $NaBH_4$. The gold nanoparticles syntheses were completed in triplicate with 10:1, 5:1, and 1:1 IL-1B:$HAuCl_4$ molar ratios and 1:2 $NaBH_4$:$HAuCl_4$. UV-Vis spectra of the reaction mixture were taken at the completion of each synthesis. The triplicates were averaged, and the reproducibility was assessed. The resulting spectra are shown below in Figures 4-32 to 4-34.

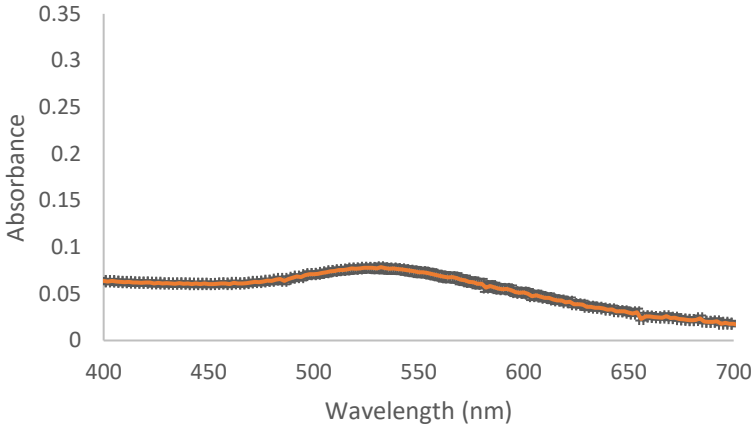

Figure 4-32. UV-Vis spectra of the reaction mixture triplicates for the 10:1 IL-1B:$HAuCl_4$ syntheses. The concentrations used were 7.62 mM IL-2, 0.762 mM $HAuCl_4$, 0.381 mM $NaBH_4$.

The 10:1 IL-1B:$HAuCl_4$ molar ratio gold nanoparticle syntheses showed a good reproducibility between replicates, but without a well-defined SPR absorbance maximum for the gold nanoparticles, see Figure 4-32 (compare to Figure 4-24).

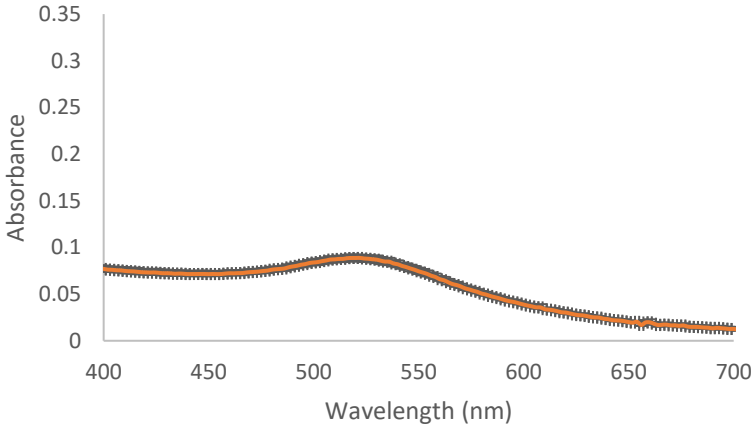

Figure 4-33. UV-Vis spectra of the reaction mixture triplicates for the 5:1 IL-1B:$HAuCl_4$ syntheses. The concentrations used were 3.81 mM IL-2, 0.762 mM $HAuCl_4$, 0.381 mM $NaBH_4$.

The 5:1 IL-1B:Au molar ratio gold nanoparticle syntheses showed a good reproducibility between replicates and an average SPR absorbance maximum at 522 nm, see Figure 4-33 (compare to Figure 4-25).

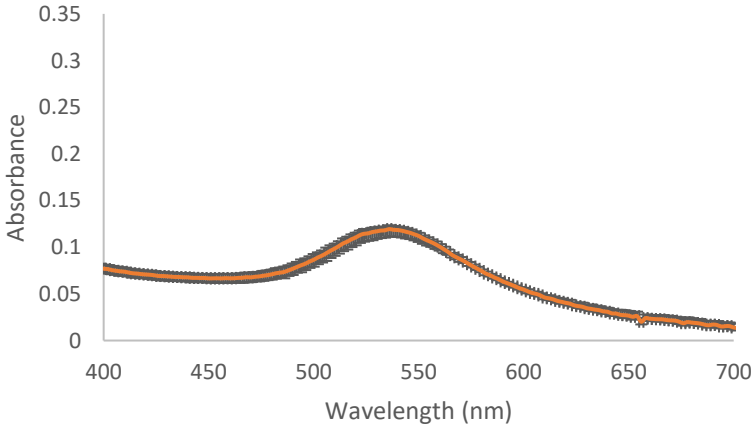

Figure 4-34. UV-Vis spectra of the reaction mixture triplicates for the 1:1 IL-1B:$HAuCl_4$ syntheses. The concentrations used were 0.762 mM IL-2, 0.762 mM $HAuCl_4$, 0.381 mM $NaBH_4$.

The 1:1 IL-1B:Au molar ratio gold nanoparticle syntheses showed a good reproducibility between replicates and an average SPR absorbance maximum at 536 nm, see Figure 4-34 (compare to Figure 4-26).The SPR absorbance maxima for the gold nanoparticles are shown in Table 4-3.

Table 4-3. Absorbance maxima of the reaction mixture triplicates for optimized syntheses with 2-(phenylmercapto)ethyl-methylimidazolium chloride

	1	***2***	***3***	***Average λ_{max}***
5:1	518 nm	522 nm	522 nm	521(±2) nm
1:1	544 nm	536 nm	536 nm	539(±5) nm

4.3.1. Scanning Electron Microscopy Characterization of Gold Nanoparticles Syntheses with IL-1B

SEM images were taken for each molar ratio. These images are shown in Figures 4-35 to 4-37.

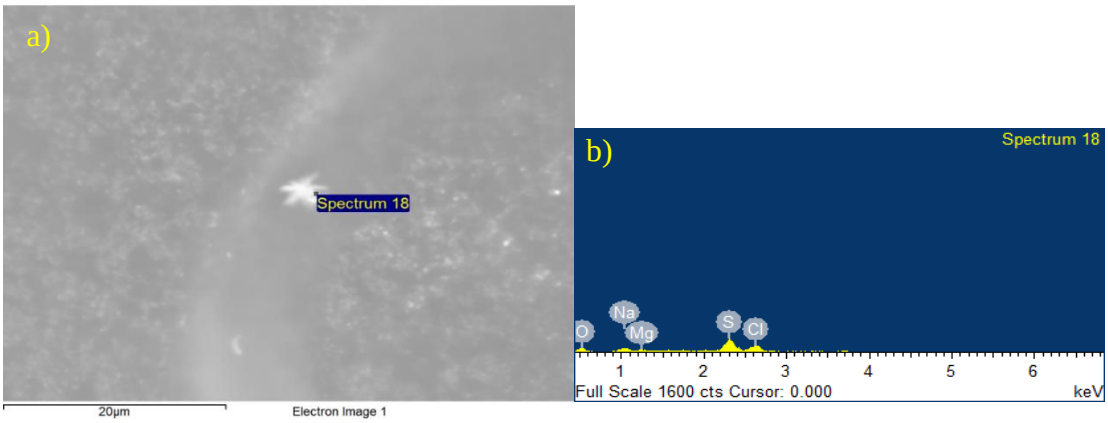

Figure 4-35. SEM-EDX of optimized 10:1 IL-1B:Au molar ratio synthesis. The concentrations used in these syntheses were 7.62 mM IL-1B, 0.762 mM $HAuCl_4$, 0.381 mM $NaBH_4$. a) SEM image b) EDX

For the gold nanoparticles synthesis with a 10:1 IL-1B:$HAuCl_4$ molar ratio, the nanoparticles could be isolated by centrifugation from the reaction mixture; however, they could not be isolated from the first ethanol wash. The SEM/EDX sample was thus prepared from the first ethanol wash, see Figure 4-35. The salt-like structure seen in Figure 4-35(a) most likely corresponds to dried-out ionic liquid. Elemental analysis of the salt-like structure gave 76.49 (w)% carbon, 10.27 (w)% oxygen, 1.86 (w)% sodium, 0.69 (w)% magnesium, 6.51 (w)% sulfur, and 4.19 (w)% chlorine, see Figure 4-35(b). The salt-like structure is about 4 µm; there are some smaller particles present that are about 300 nm.

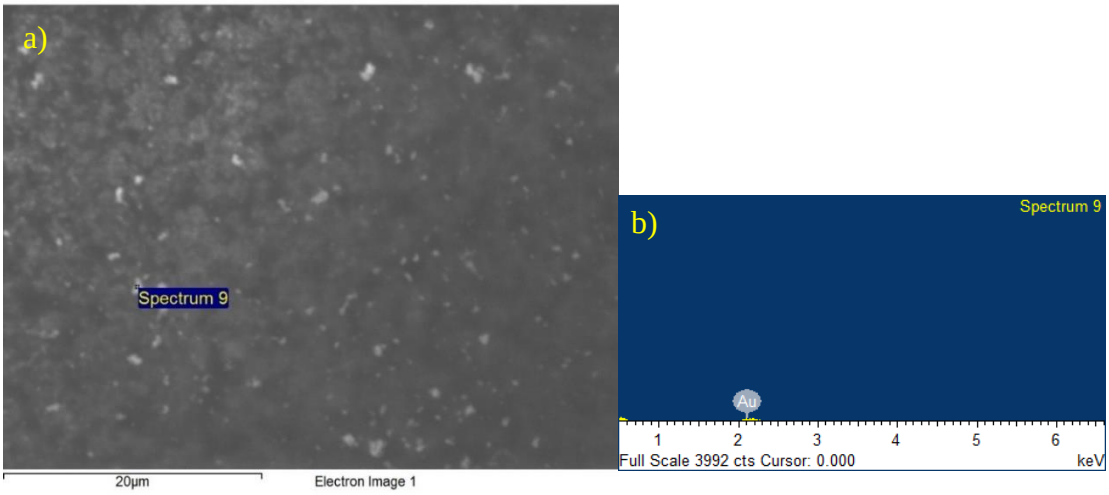

Figure 4-36. SEM-EDX of optimized 5:1 IL-1B:Au molar ratio synthesis. The concentrations used in these syntheses were 3.81 mM IL-1B, 0.762 mM $HAuCl_4$, 0.381 mM $NaBH_4$. a) SEM image b) EDX

The gold nanoparticles synthesis with a 5:1 IL-1B:$HAuCl_4$ molar ratio showed good nanoparticle dispersion, see Figure 4-36(a). There were both aggregates and nanoparticles present, with aggregates as large as 1.66 µm, smaller aggregates around 100 -200 nm, and nanoparticles under 100 nm. Elemental analysis gave 100 (w)% gold, see Figure 4-36(b).

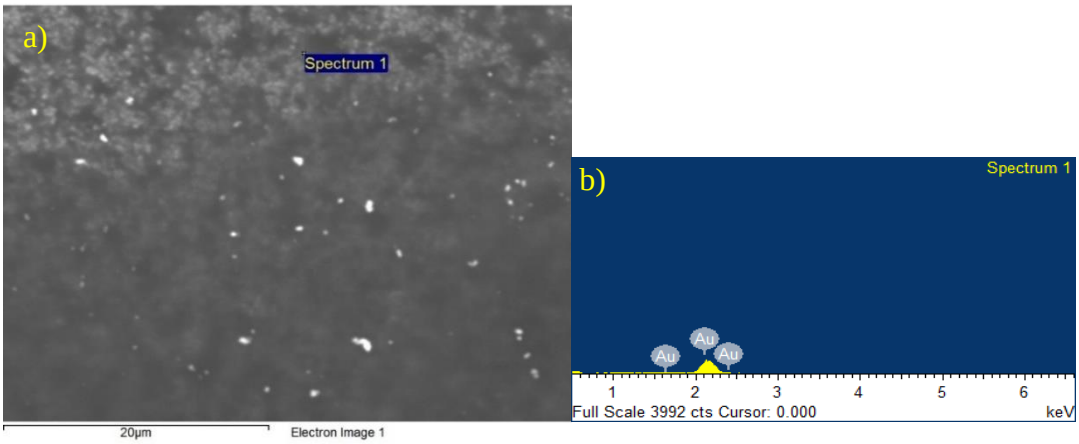

Figure 4-37. SEM-EDX of optimized 1:1 IL-1B:Au molar ratio synthesis. The concentrations used in these syntheses were 0.762 mM IL-1B, 0.762 mM $HAuCl_4$, 0.381 mM $NaBH_4$. a) SEM image b) EDX

The gold nanoparticles synthesis with a 1:1IL-1B:$HAuCl_4$ molar ratio showed reasonable nanoparticle dispersion, see Figure 4-37(a). This area showed both nanoparticles and aggregates, with aggregates ranging from 100 nm – 2 µm. Nanoparticles in this area were on the larger side, with a size range between 90-100 nm. Elemental analysis gave 100 (w)% gold, see Figure 4-37(b).

4.3.2. Heating Studies of 2-(Phenylmercapto) Ethyl-Methylimidazolium Chloride

Gold nanoparticles syntheses with IL-1B did show improved reproducibility compared with IL-1A, most likely due to a better solubility of IL-1B. However, heating studies of the Au-IL-1B mixture prior to addition of $NaBH_4$ were conducted with IL-1B as well. Here the Au-IL-1B mixture was heated for 35 minutes at a hot plate temperature of 103 ºC, then cooled before addition of the $NaBH_4$ reducing agent. The syntheses were completed in triplicates and UV-Vis spectra of the reaction mixture were taken at the completion of each synthesis. These results are shown below in Figures 4-38 to 4-40.

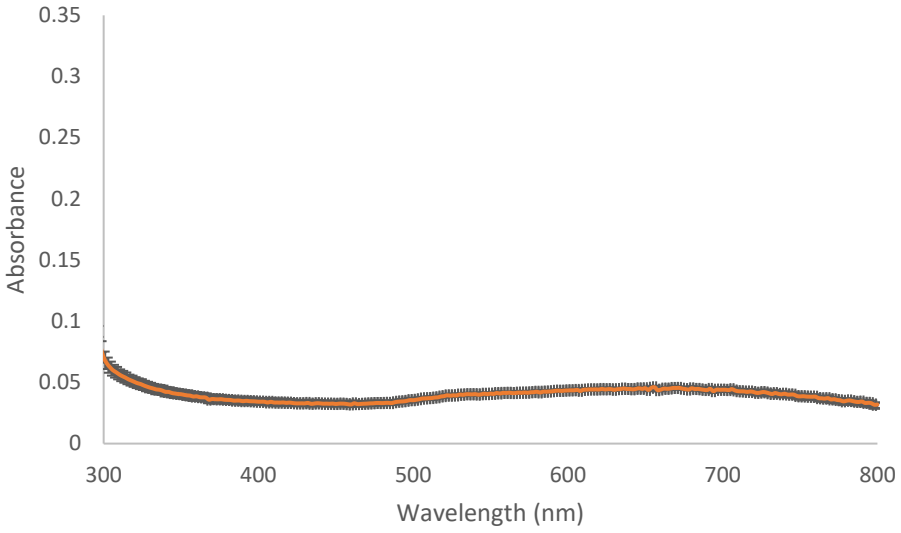

Figure 4-38. UV-Vis spectra of the reaction mixture triplicates for the 10:1 IL-1B:$HAuCl_4$ heated study syntheses. The concentrations used were 7.62 mM IL-1B, 0.762 mM $HAuCl_4$, 0.381 mM $NaBH_4$.

Although the UV-Vis spectra of the triplicate gold nanoparticle syntheses with a 10:1 IL-B:Au molar ratio with prior heating were found to be reproducible, see Figure 4-38, the spectra themselves were much different from those of syntheses without prior heating, and did not show an SPR peak (see Figures 4-38 and 4-32). This could indicate that a change in the Au-IL-1B mixture occurred upon heating.

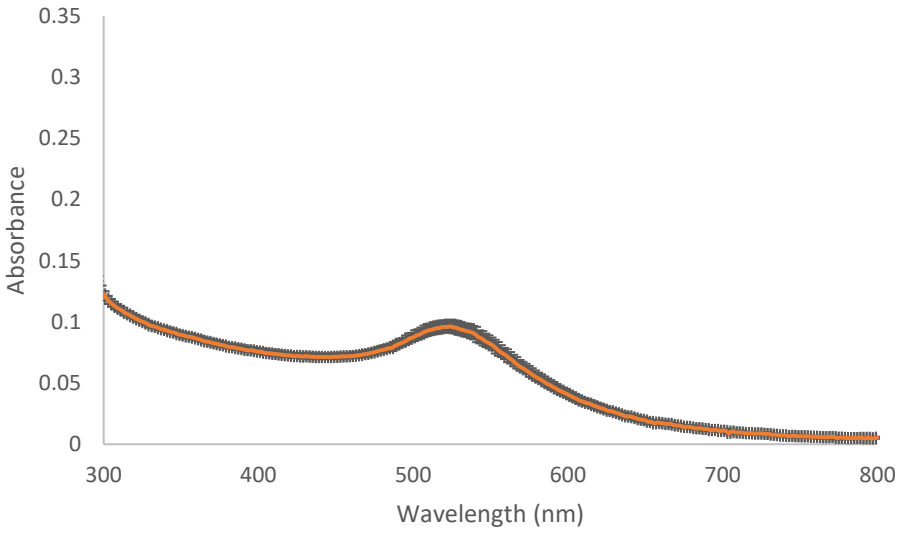

Figure 4-39. UV-Vis spectra of the reaction mixture triplicates for the 5:1 IL-1B:$HAuCl_4$ heated study syntheses. The concentrations used were 3.81 mM IL-1B, 0.762 mM $HAuCl_4$, 0.381 mM $NaBH_4$.

The 5:1 IL-1B:$HAuCl_4$ molar ratio triplicate gold nanoparticle syntheses with prior heating, see Figure 4-39, showed good reproducibility and a more pronounced SPR peak at 524 nm than the syntheses without prior heating (see Figures 4-39 and 4-33).

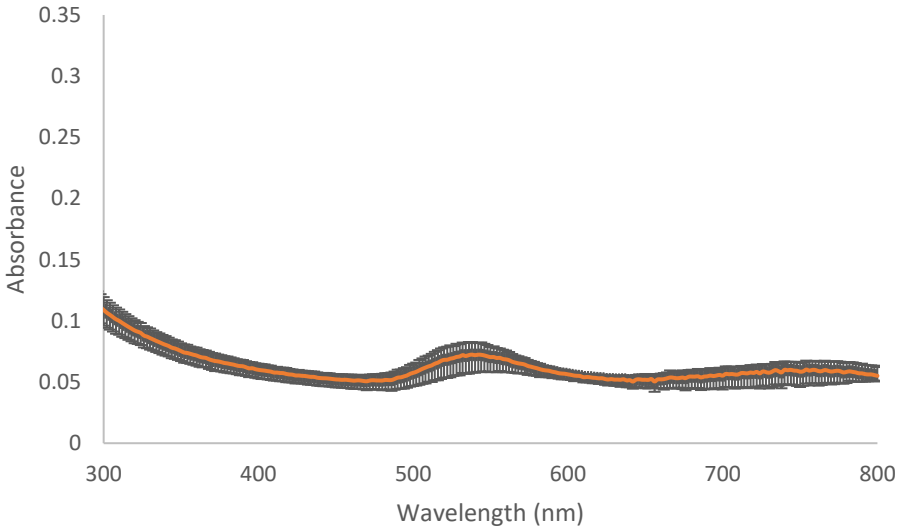

Figure 4-40. UV-Vis spectra of the reaction mixture triplicates for the 1:1 IL-1B:$HAuCl_4$ heated study syntheses. The concentrations used were 0.762 mM IL-1B, 0.762 mM $HAuCl_4$, 0.381 mM $NaBH_4$.

The 1:1 IL-1B:$HAuCl_4$ molar ratio triplicate gold nanoparticle syntheses with prior heating, see Figure 4-40, showed more variation between the replicates than for syntheses without prior heating (see Figures 4-40 and 4-34), which could be indicative of a change in the Au-IL-1B mixture upon heating. The average SPR absorbance maximum was 538 nm.

4.4 Gold Nanoparticles Synthesis with 2-(Ethylmercapto) Ethyl-Tributylphosphonium Chloride

In view of the solubility issue with IL-1A, 2-(ethylmercapto)ethyl-tributylphosphonium chloride (IL-2) was used in gold nanoparticle syntheses, in which the bulky phenyl group (IL-1A) was replaced by an ethyl group (IL-2). This modification did improve the solubility as the Au-IL mixture was homogenous prior to the addition of $NaBH_4$, without any heating. The syntheses were completed in triplicate with 10:1, 5:1, and 1:1 IL-2:$HAuCl_4$ molar ratios and a 1:2 $HAuCl_4$:$NaBH_4$ molar ratio. UV-Vis spectra of the reaction mixture were taken at the completion of each synthesis. The triplicates were averaged, and reproducibility was assessed. The triplicate UV-Vis spectra are shown below in Figures 4-41 to 4-43.

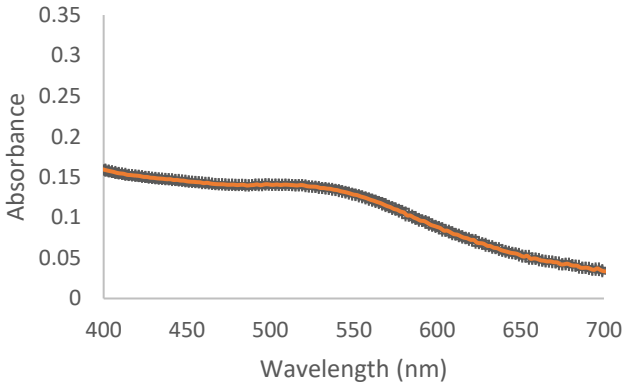

Figure 4-41. UV-Vis spectra of the reaction mixture triplicates for the 10:1 IL-2:$HAuCl_4$ syntheses. The concentrations used were 7.62 mM IL-2, 0.762 mM $HAuCl_4$, 0.381 mM $NaBH_4$.

The 10:1 IL-2:$HAuCl_4$ molar ratio gold nanoparticle synthesis triplicates showed improved reproducibility for the gold nanoparticles SPR absorbance (see Figures 4-41 and 4-24). The ionic liquid absorbance in the UV region lead to a shoulder rather than a defined peak in the SPR region, see Figure 4-24. Here, an SPR absorbance maximum could not be determined.

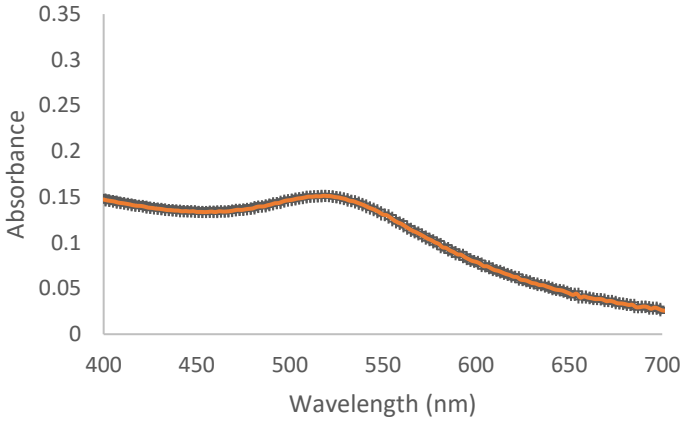

Figure 4-42. UV-Vis spectra of the reaction mixture triplicates for the 5:1 IL-2:$HAuCl_4$ syntheses. The concentrations used were 3.81 mM IL-2, 0.762 mM $HAuCl_4$, 0.381 mM $NaBH_4$.

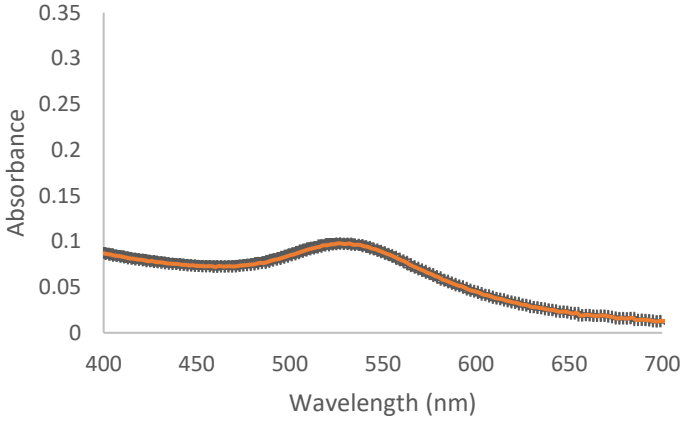

Figure 4-43. UV-Vis spectra of the reaction mixture triplicates for the 1:1 IL-2:$HAuCl_4$ syntheses. The concentrations used were 0.762 mM IL-2, 0.762 mM $HAuCl_4$, 0.381 mM $NaBH_4$.

The 5:1 and 1:1 IL-2:$HAuCl_4$ molar ratios gold nanoparticle syntheses showed increased reproducibility for the gold nanoparticles SPR absorbance as well (see Figures 4-42 and 4-25, and 4-43 and 4-26, respectively), likely due to the better solubility of the Au-IL-2 mixture. The average SPR absorbance maxima are shown in Table 4-4.

Table 4-4. Absorbance maxima of the reaction mixture triplicates for optimized syntheses with 2-(ethylmercapto)ethyl-tributylphosphonium chloride

	1	***2***	***3***	***Average λ_{max}***
5:1	518 nm	518 nm	520 nm	519(±1) nm
1:1	532 nm	532 nm	532 nm	532(±0) nm

4.4.1. SEM Characterization of Gold Nanoparticles Syntheses with IL-2

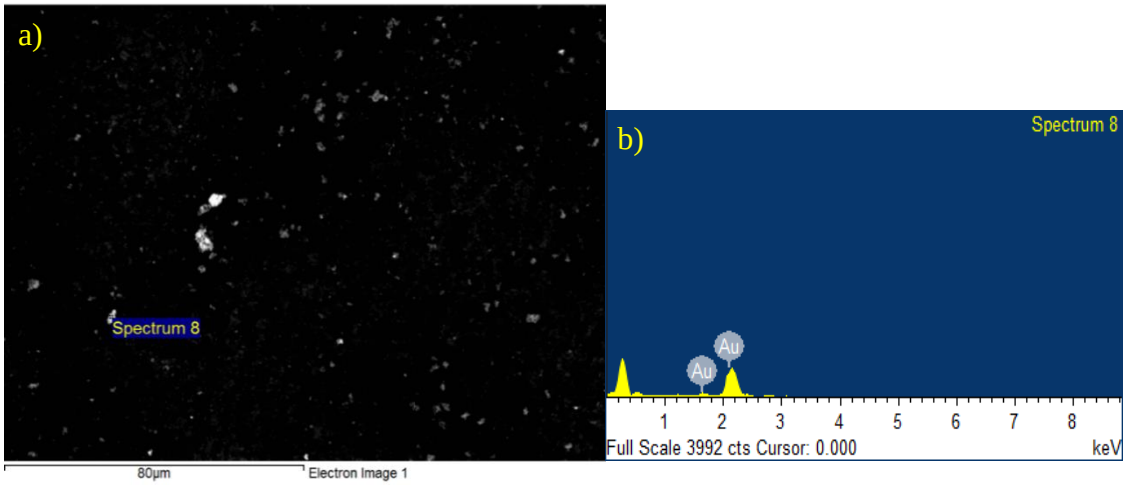

Figure 4-44. SEM-EDX of optimized 10:1 IL-2:$HAuCl_4$ molar ratio synthesis. The concentrations used in these syntheses were 7.62 mM IL-2, 0.762 mM $HAuCl_4$, 0.381 mM $NaBH_4$. a) SEM image b) EDX

The 10:1 IL-2:$HAuCl_4$ molar ratio gold nanoparticles synthesis sample shown in Figure 4-44(a) displays a reasonable dispersion of the nanoparticles, along with a mixture of aggregates (100 nm – 1.5 µm) amongst the nanoparticles (80 -100 nm). The elemental composition was found to be 100 (w)% gold, as shown by Figure 4-44(b).

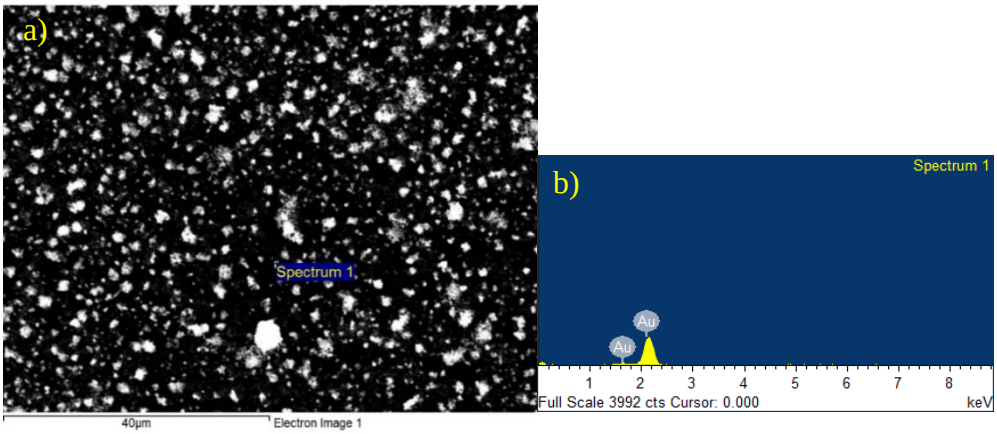

Figure 4-45. SEM-EDX of optimized 5:1 IL-2:Au molar ratio synthesis. The concentrations used in these syntheses were 3.81 mM IL-2, 0.762 mM $HAuCl_4$, 0.381 mM $NaBH_4$. a) SEM image b) EDX

The 5:1 IL-2:$HAuCl_4$ molar ratio gold nanoparticles synthesis sample dried in a ring, thus concentrating the nanoparticles. A high population of aggregates and nanoparticles can be thus be observed in Figure 4-45. The size estimates vary highly, from under 100 nm to 4 µm, likely due to the way the sample dried. The elemental composition was found to be 100 (w)% gold, as shown in Figure 4-45(b).

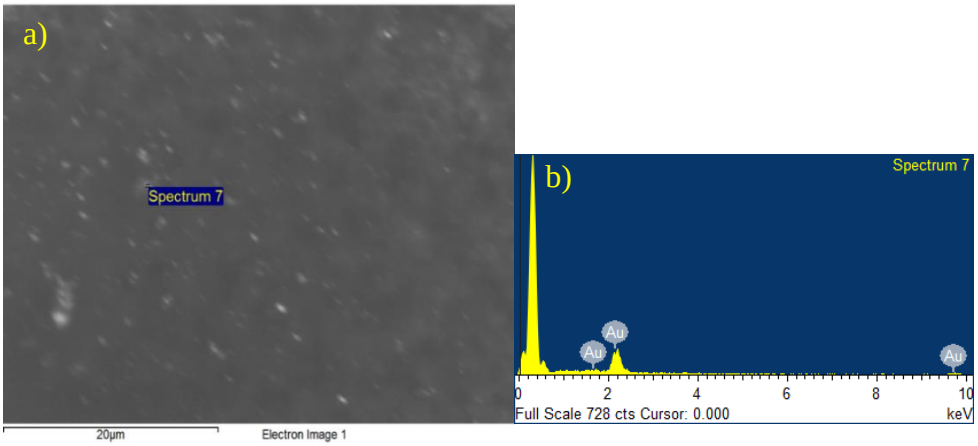

Figure 4-46. SEM-EDX of optimized 1:1 IL-2:Au molar ratio synthesis. The concentrations used in these syntheses were 0.762 mM IL-2, 0.762 mM $HAuCl_4$, 0.381 mM $NaBH_4$. a) SEM image b) EDX

The 1:1 IL-2:$HAuCl_4$ molar ratio gold nanoparticles synthesis sample showed good nanoparticle dispersion, as seen in Figure 4-46(a). Due to poor resolution and

blurred imaging of the particles, it was difficult to get accurate size data for the smaller nanoparticles, but aggregates over 500 nm were found. The elemental composition was found to be 89.14 (w)% gold and 10.86 (w)% oxygen, see Figure 4-46(b). This could be due to the formation of a gold oxide layer, as the sample sat for 13 days before analysis.

4.4.2. Attempted Atomic Force Microscopy Characterization of Gold Nanoparticles Syntheses with IL-2

AFM images of the 10:1 IL-2:$HAuCl_4$ molar ratio gold nanoparticles synthesis were obtained. During this AFM analysis, technical issues arose during which streaking and shadowing artifacts appeared. A change in the cantilever tip did not fix the issue. At this point, AFM analysis was not continued for the project. An example of this issue is shown below.

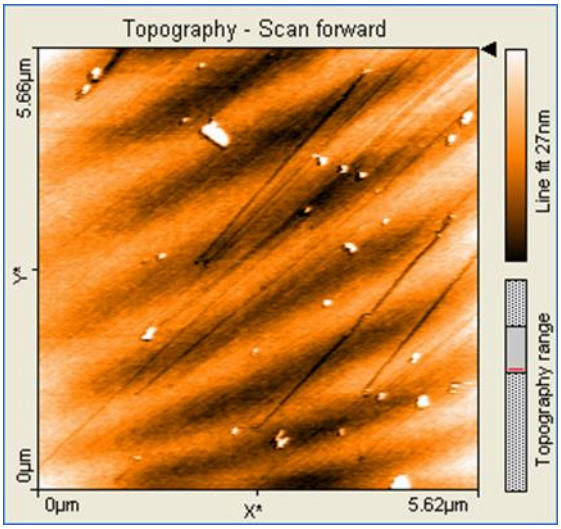

Figure 4-47. AFM image of 10:1 IL-2:$HAuCl_4$ molar ratio synthesis. The concentrations used were 3.81 mM IL-2, 0.762 mM $HAuCl_4$, and 0.381 mM $NaBH_4$.

4.4.3. Heating Studies of 2-(Ethylmercapto) Ethyl-Tributylphoshonium Chloride

The IL-2 syntheses showed to have increased reproducibility without heating. However, the Au-IL-2 mixture was heated to observe whether a change in reproducibility or results would occur. The mixture was heated for 35 minutes with a hot plate setting of 103 ºC , then cooled before addition of the $NaBH_4$ reducing agent, in a procedure similar to the optimized gold nanoparticles synthesis with IL-1A. The UV-Vis spectra of the reaction mixtures are shown below in Figures 4-48 to 4-50.

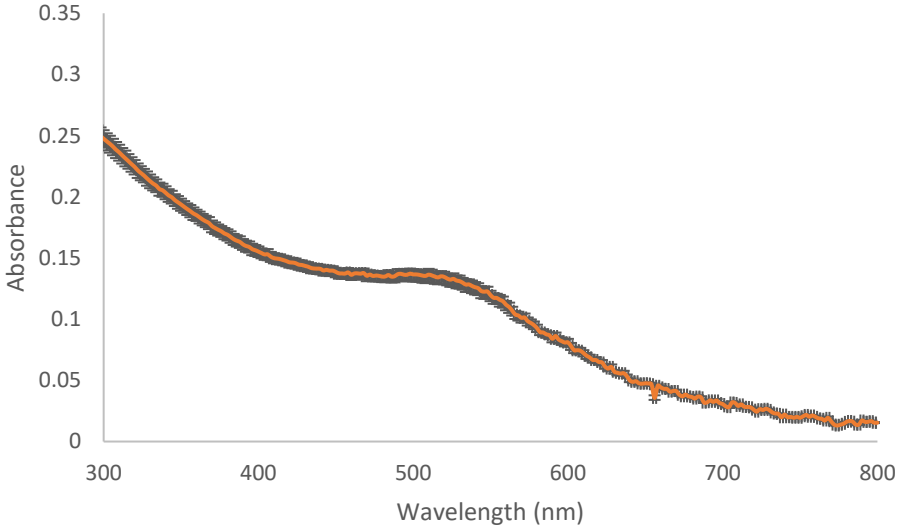

Figure 4-48. UV-Vis spectra of the reaction mixture triplicates for the 10:1 IL-2:$HAuCl_4$ heated study syntheses. The concentrations used were 7.62 mM IL-2, 0.762 mM $HAuCl_4$, 0.381 mM $NaBH_4$.

The 10:1 IL-2:$HAuCl_4$ molar ratio gold nanoparticles syntheses with prior heating showed a good reproducibility between replicates, and similar spectra as the syntheses without heating (see Figures 4-48 and 4-41), with a pronounced shoulder for the SPR peak.

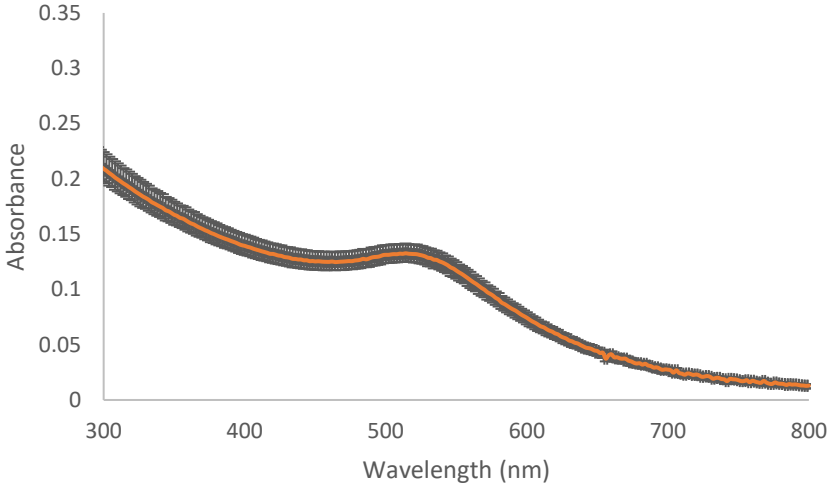

Figure 4-49. UV-Vis spectra of the reaction mixture triplicates for the 5:1 IL-2:$HAuCl_4$ heated study syntheses. The concentrations used were 3.81 mM IL-2, 0.762 mM $HAuCl_4$, 0.381 mM $NaBH_4$.

The 5:1 IL-2:$HAuCl_4$ molar ratio gold nanoparticles syntheses with prior heating showed slightly less reproducibility between replicates as the syntheses without heating (see Figures 4-49 and 4-42), with an average SPR peak absorbance maximum at 514 nm.

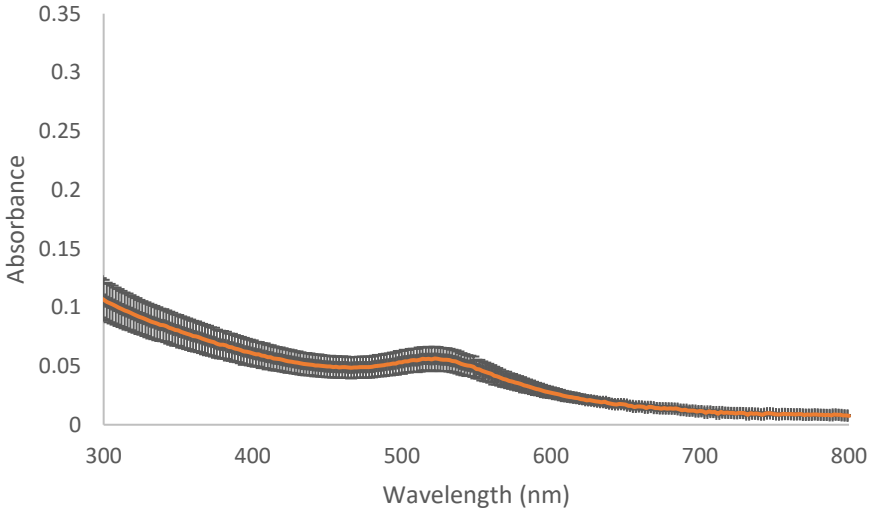

Figure 4-50. UV-Vis spectra of the reaction mixture triplicates for the 1:1 IL-2:$HAuCl_4$ heated study syntheses. The concentrations used were 0.762 mM IL-2, 0.762 mM $HAuCl_4$, 0.381 mM $NaBH_4$.

The 1:1 IL-2:$HAuCl_4$ molar ratio gold nanoparticles syntheses with prior heating showed less reproducibility between replicates as the syntheses without heating (see Figures 4-50 and 4-43), with an average SPR peak absorbance maximum at 522 nm.

4.5 Nanoparticle Purification Study

For a better SEM analysis of the gold metal nanoparticles, it should be ensured that the nanoparticles are rid of organic contaminants—such as here, excess ionic liquid. In previous analyzes, the nanoparticles were washed twice with ethanol. In some SEM-EDX samples, sulfur, likely from excess thioether-ionic liquid, could be detected with the nanoparticles, but inconsistently. A wash study was conducted to better ensure that the nanoparticles are rid of organic contaminants. Here, syntheses with 5:1 IL:$HAuCl_4$ molar ratios (for IL-1A, IL-2, and IL-1B) and a 1:2 $NaBH_4$:$HAuCl_4$ molar ratio were tested. Three wash solvents were studied (100% ethanol, 99.5% acetone, and nanopure water). The pellet isolate and supernatant were analyzed via UV-Vis spectroscopy. These results are shown below in Figures 4.51-4.69.

4.5.1 Gold Nanoparticles Prepared with a 5:1 IL-1A:$HAuCl_4$ Molar Ratio

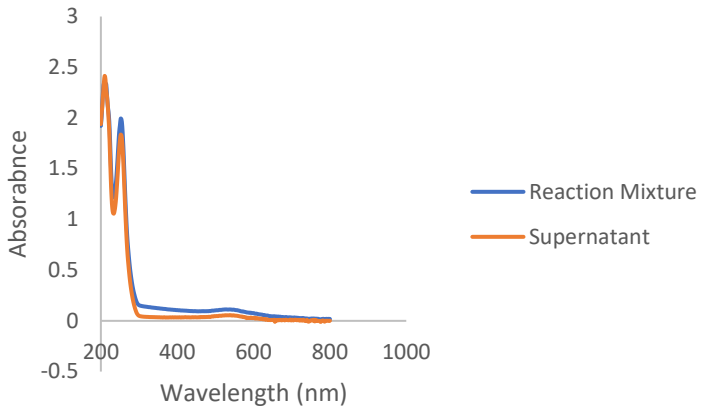

Figure 4-51. UV-Vis spectra of the reaction mixture and the initial supernatant (after the first centrifugation) for the 5:1 IL-1A:$HAuCl_4$ molar ratio gold nanoparticles synthesis. The concentrations used were 3.81 mM IL-1A, 0.762 mM $HAuCl_4$, 1.524 mM $NaBH_4$.

Figure 4-51 shows UV-Vis spectra of the reaction mixture and of the supernatant after the first centrifugation. The IL organic moieties absorbance range is found in the 200-300 nm range, while the gold nanoparticles SPR absorbance, still observed in the supernatant, is seen in the 500 – 600 nm range.

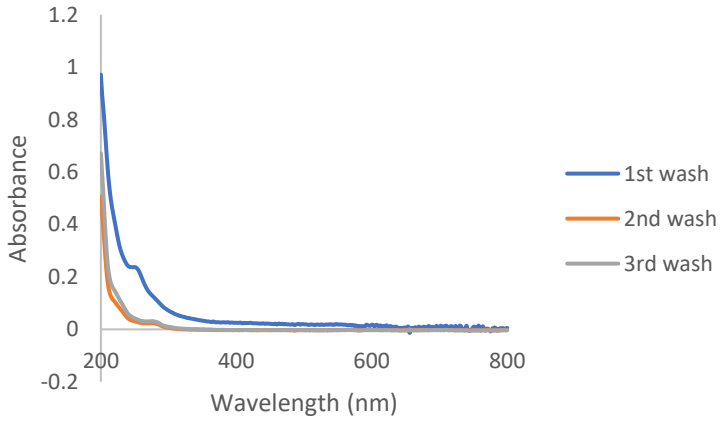

Figure 4-52. UV-Vis spectra of the supernatant for 3 consecutive ethanol washes of the gold nanoparticles isolates for the 5:1 IL-1A:$HAuCl_4$ molar ratio gold nanoparticles synthesis.

Figure 4-52 shows the UV-Vis spectra of the supernatants for 3 subsequent ethanol washes of the nanoparticles isolates. While absorbance from organic moieties in the 200-300 nm range is significantly reduced after the first ethanol wash, the presence of ethanol in the supernatant likely contributes to the remaining absorbance in that region.

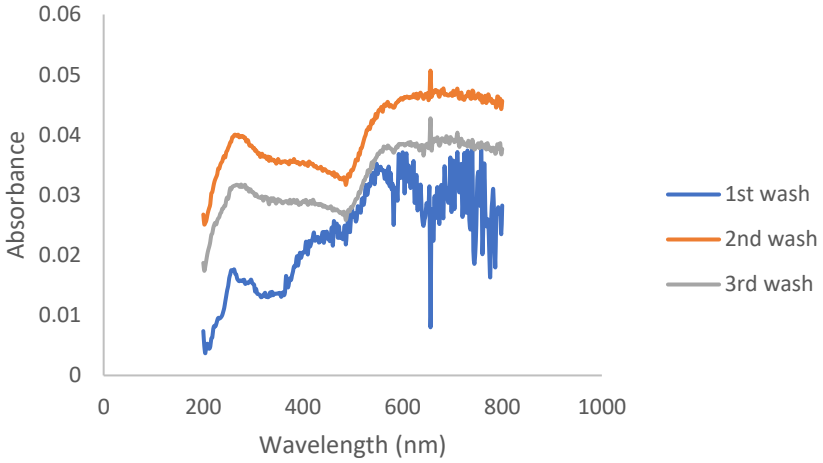

Figure 4-53. UV-Vis spectra of the nanoparticles isolates for 3 consecutive ethanol washes for the 5:1 IL-1A:$HAuCl_4$ molar ratio gold nanoparticles synthesis.

Figure 4-53 shows the UV-Vis spectra of the redispersed nanoparticles isolates (pellets) after 3 subsequent ethanol washes. The UV-Vis spectra show very low absorbances, indicating a low concentration of nanoparticles in these samples.

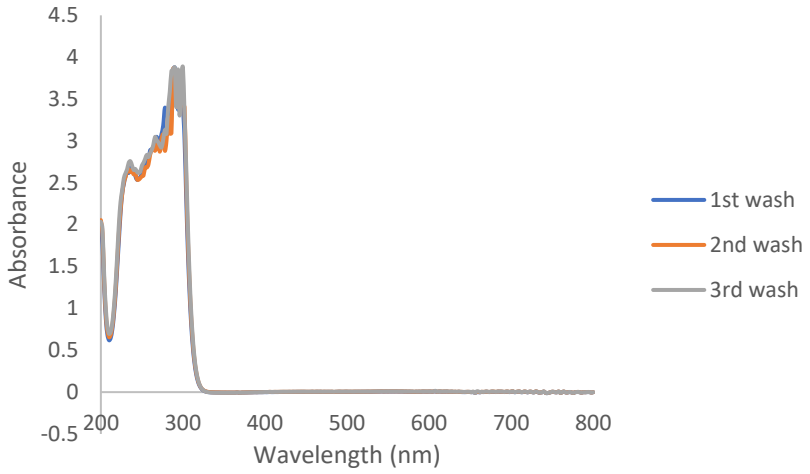

Figure 4-54. UV-Vis spectra of the supernatant for 3 consecutive acetone washes of the gold nanoparticles isolates for the 5:1 IL-1A:$HAuCl_4$ molar ratio gold nanoparticles synthesis.

Figure 4-54 shows the UV-Vis spectra of the supernatants for 3 subsequent acetone washes of the nanoparticles isolates. Here the strong absorbance of acetone from the supernatant obscures any absorbance from the ionic liquid in the 200-300 nm region.

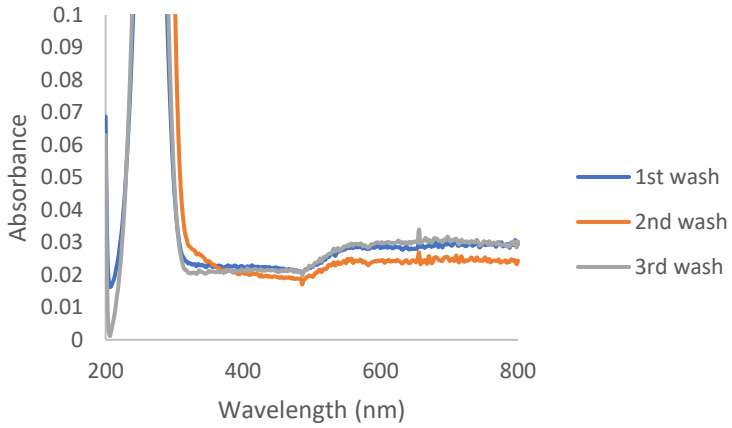

Figure 4-55. UV-Vis spectra of the nanoparticles isolates for 3 consecutive acetone washes for the 5:1 IL-1A:$HAuCl_4$ molar ratio gold nanoparticles synthesis.

Figure 4-55 shows the UV-Vis spectra of the redispersed nanoparticles isolates (pellets) after 3 subsequent acetone washes. The UV-Vis spectra show very low

absorbances in the 500-600 nm region, indicating a low concentration of nanoparticles in these samples. The absorbance peak around 270 nm is likely due to residual acetone.

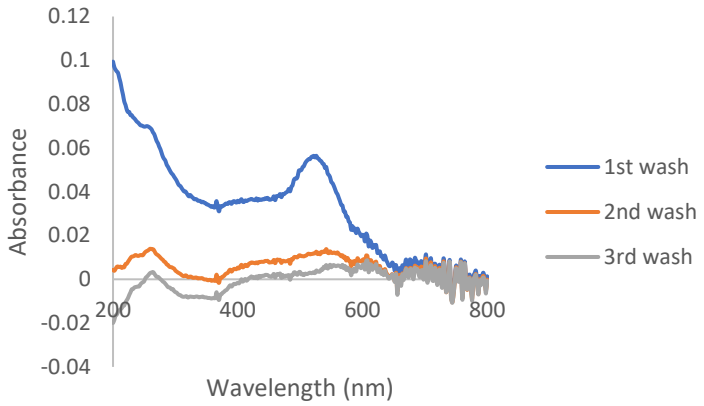

Figure 4-56. UV-Vis spectra of the supernatant for 3 consecutive washes of the gold nanoparticles isolates with water for the 5:1 IL-1A:$HAuCl_4$ molar ratio gold nanoparticles synthesis.

Figure 4-56 shows the UV-Vis spectra of the supernatants for 3 subsequent washes of the nanoparticles isolates with water. The supernatant of the first wash still contained gold nanoparticles, as indicated by the peak in the 500- 600 nm range. The second and third washes did not show significant absorbance in the organic region.

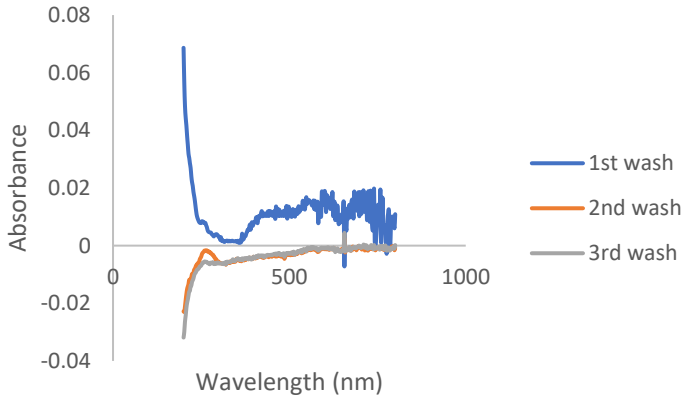

Figure 4-57. UV-Vis spectra of the nanoparticles isolates for 3 consecutive washes with water for the 5:1 IL-1A:$HAuCl_4$ molar ratio gold nanoparticles synthesis.

Figure 4-57 shows the UV-Vis spectra of the redispersed nanoparticles isolates (pellets) after 3 subsequent washes with water. The UV-Vis spectra show extremely low absorbances, indicating a very low concentration of nanoparticles in these samples.

4.5.2 Gold Nanoparticles Prepared with a 5:1 IL-1B:$HAuCl_4$ Molar Ratio

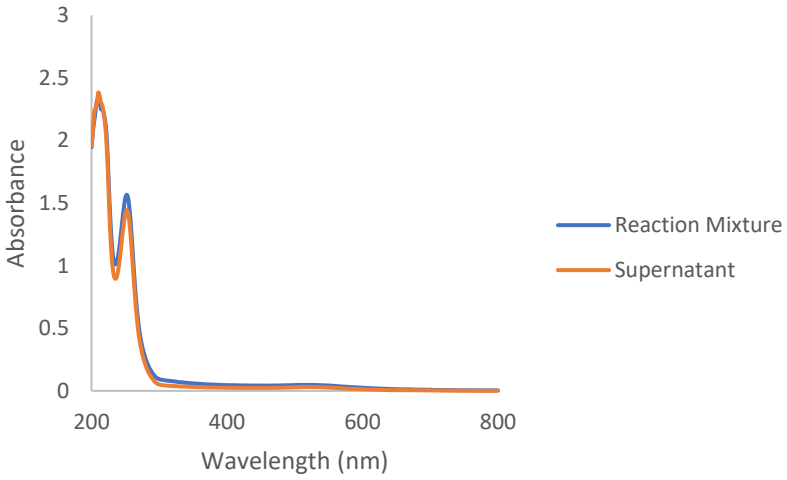

Figure 4-58. UV-Vis spectra of the reaction mixture and the initial supernatant (after the first centrifugation) for the 5:1 IL-1B:$HAuCl_4$ molar ratio gold nanoparticles synthesis. The concentrations used were 3.81 mM IL-1B, 0.762 mM $HAuCl_4$, 1.524 mM $NaBH_4$.

Figure 4-58 shows UV-Vis spectra of the reaction mixture and of the supernatant after the first centrifugation. The IL organic moieties absorbance range occurs in the 200-300 nm range, while the gold nanoparticles SPR absorbance, still observed in the supernatant, is seen in the 500 – 600 nm range. The gold nanoparticles pellets isolated from centrifugation were found to be quite soluble in ethanol, so that ethanol washes could not be performed here.

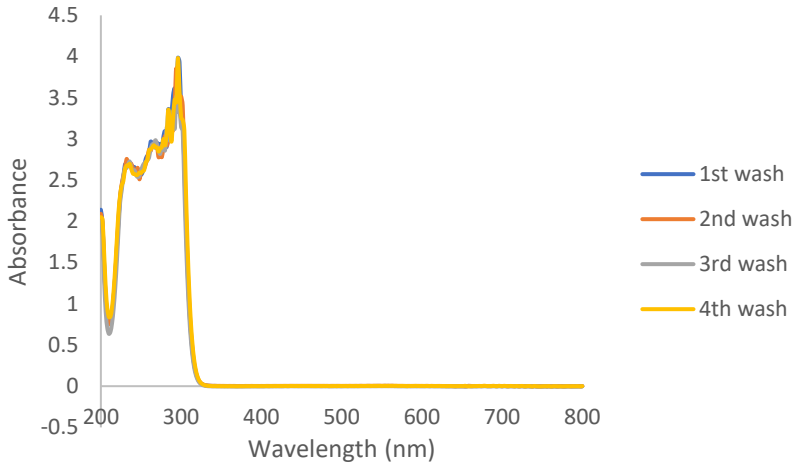

Figure 4-59. UV-Vis spectra of the supernatant for 3 consecutive acetone washes of the gold nanoparticles isolates for the 5:1 IL-1B:$HAuCl_4$ molar ratio gold nanoparticles synthesis.

Figure 4-59 shows UV-Vis spectra of the supernatants for 3 subsequent acetone washes of the nanoparticles isolates. Here the strong absorbance of acetone from the supernatant obscures any absorbance from the ionic liquid in the 200-300 nm region.

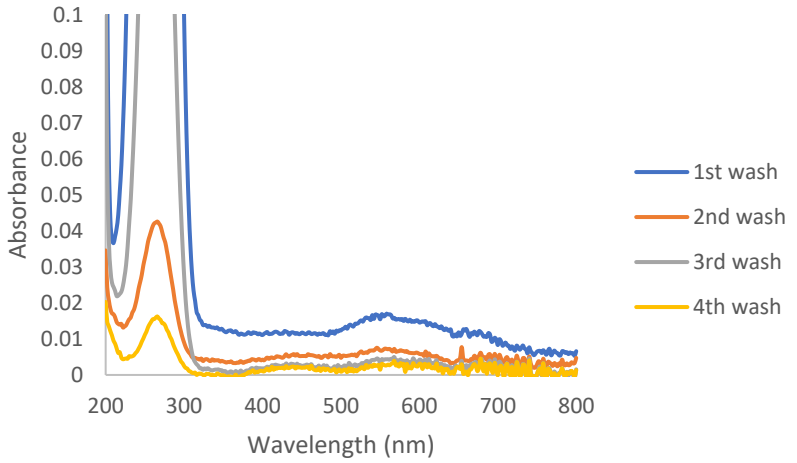

Figure 4-60. UV-Vis spectra of the nanoparticles isolates for 3 consecutive acetone washes for the 5:1 IL-1B:$HAuCl_4$ molar ratio gold nanoparticles synthesis.

Figure 4-60 shows UV-Vis spectra of the redispersed nanoparticles isolates (pellets) after 3 subsequent acetone washes. The UV-Vis spectra show a weak shoulder in the 500-600 nm region, indicating a weak presence of gold nanoparticles. The absorbance peak around 270 nm is likely due to residual acetone.

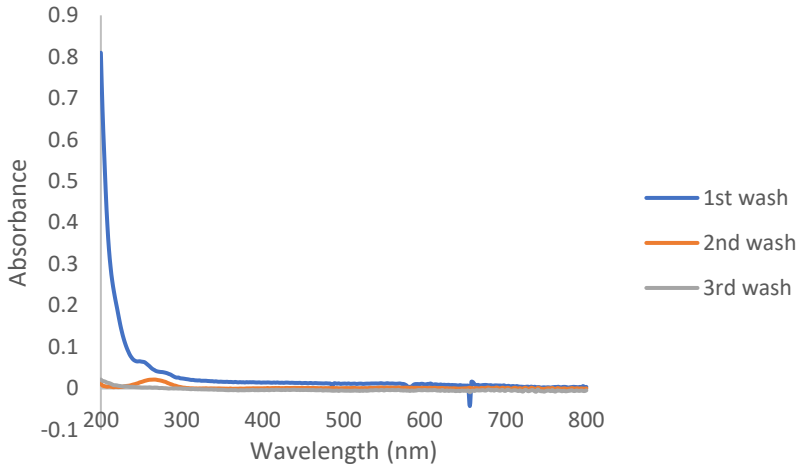

Figure 4-61. UV-Vis spectra of the supernatant for 3 consecutive washes of the gold nanoparticles isolates with water for the 5:1 IL-1B:$HAuCl_4$ molar ratio gold nanoparticles synthesis.

Figure 4-61 shows UV-Vis spectra of the supernatants for 3 subsequent washes of the nanoparticles isolates with water. The supernatant of the first wash still contained residual ionic liquid, as indicated by the peak around 200 nm. None of the supernatants showed the presence gold nanoparticles.

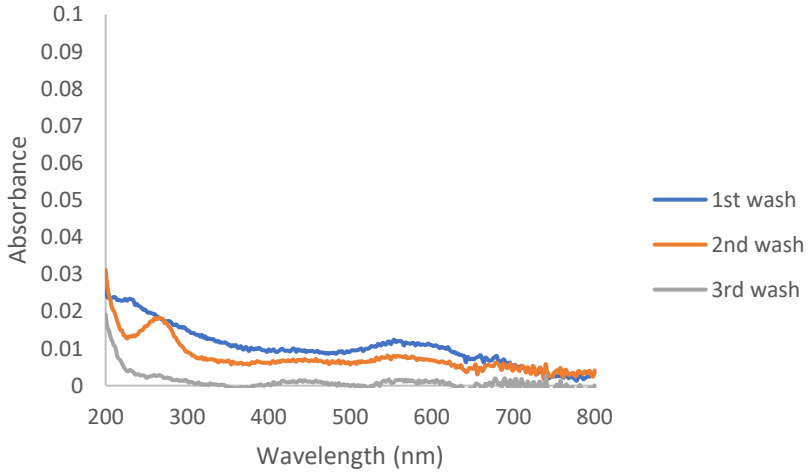

Figure 4-62. UV-Vis spectra of the nanoparticles synthesized with IL-2 washed with nanopure water after 3 washes. UV-Vis spectrum of the nanoparticles isolates for 3 consecutive washes with water for the 5:1 IL-1B:$HAuCl_4$ molar ratio gold nanoparticles synthesis.

Figure 4-62 shows UV-Vis spectra of the redispersed nanoparticles isolates (pellets) after 3 subsequent washes with water. The shoulder in the 500-600 nm region of the UV-Vis spectra is very weak, indicating a very low presence of gold nanoparticles.

4.5.3 Gold Nanoparticles Prepared with a 5:1 IL-2:$HAuCl_4$ Molar Ratio

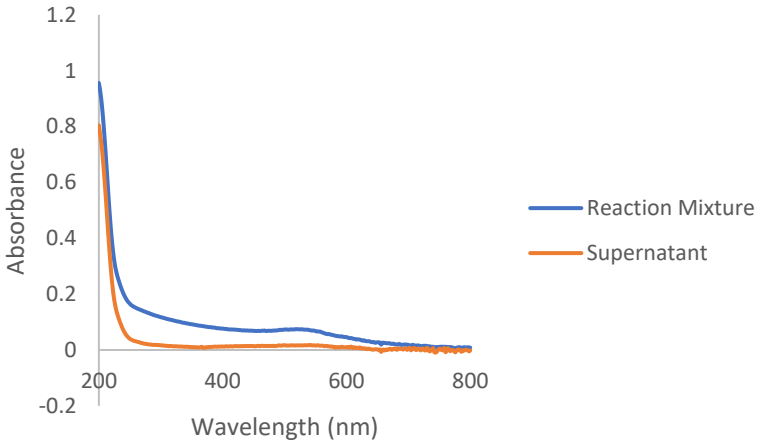

Figure 4-63. UV-Vis spectra of the initial supernatant for the 5:1 IL-2:$HAuCl_4$ molar ratio gold nanoparticles synthesis after the first centrifugation. The concentrations used were 3.81 mM IL-2, 0.762 mM $HAuCl_4$, 1.524 mM $NaBH_4$.

Figure 4-63 shows the UV-Vis spectrum of the supernatant after the first centrifugation. There may be a small amount of ionic liquid present; most of the nanoparticles seemed to have been removed.

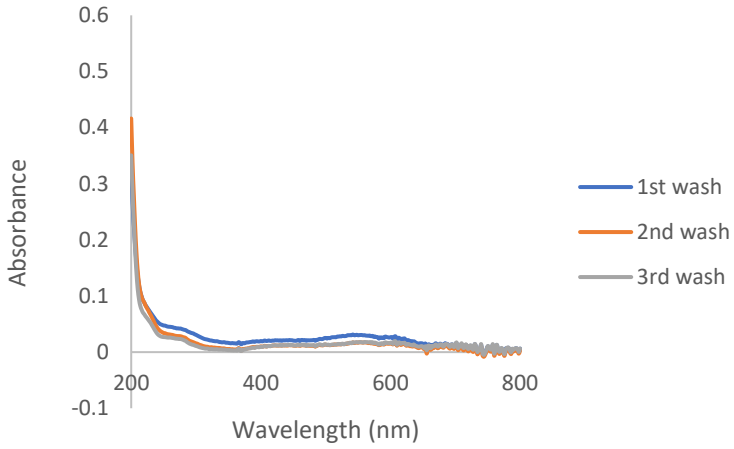

Figure 4-64. UV-Vis spectra of the supernatant for 3 consecutive ethanol washes of the gold nanoparticles isolates for the 5:1 IL-2:$HAuCl_4$ molar ratio gold nanoparticles synthesis.

Figure 4-64 shows UV-Vis spectra of the supernatants for 3 subsequent ethanol washes of the nanoparticles isolates. The presence of ethanol in the supernatant likely contributes to the absorbance in the 200-300 nm region.

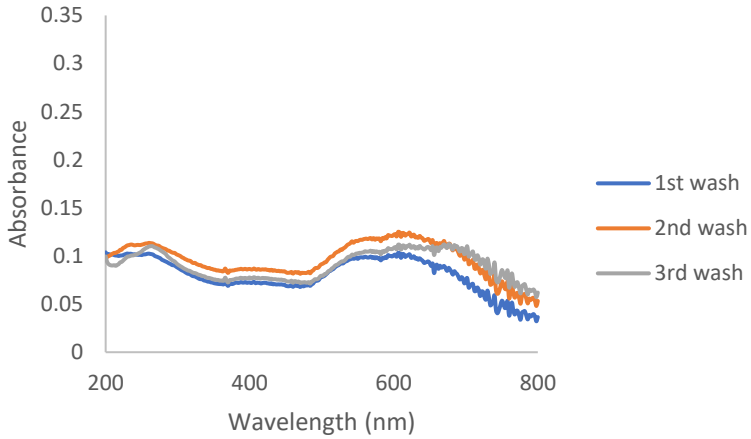

Figure 4-65. UV-Vis spectra of the nanoparticles isolates for 3 consecutive ethanol washes for the 5:1 IL-2:$HAuCl_4$ molar ratio gold nanoparticles synthesis.

Figure 4-65 shows UV-Vis spectra of the redispersed nanoparticles isolates (pellets) after 3 subsequent ethanol washes. The absorbance in the organic region of the spectrum is greatly decreased, and there is evidence of gold nanoparticles being present.

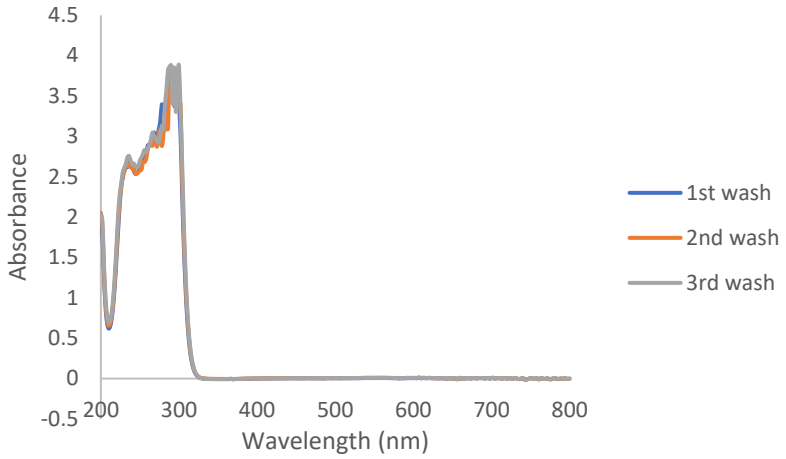

Figure 4-66. UV-Vis spectra of the supernatant for 3 consecutive acetone washes of the gold nanoparticles isolates for the 5:1 IL-2:$HAuCl_4$ molar ratio gold nanoparticles synthesis.

Figure 4-66 shows UV-Vis spectra of the supernatants for 3 subsequent acetone washes of the nanoparticles isolates. Here the strong absorbance of acetone from the supernatant obscures any absorbance from the ionic liquid in the 200-300 nm region.

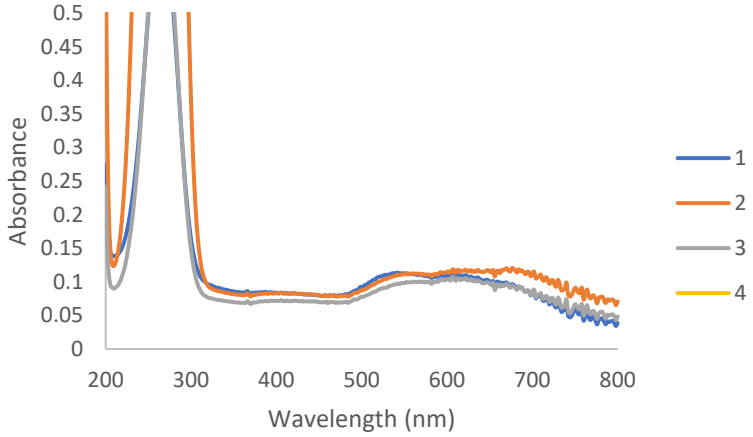

Figure 4-67. UV-Vis spectra of the nanoparticles isolates for 3 consecutive acetone washes for the 5:1 IL-2:$HAuCl_4$ molar ratio gold nanoparticles synthesis.

Figure 4-67 shows UV-Vis spectra of the redispersed nanoparticles isolates (pellets) after 3 subsequent acetone washes. The UV-Vis spectra show a shoulder in the

500-600 nm region, indicating the presence of gold nanoparticles. The absorbance peak around 270 nm is likely due to residual acetone.

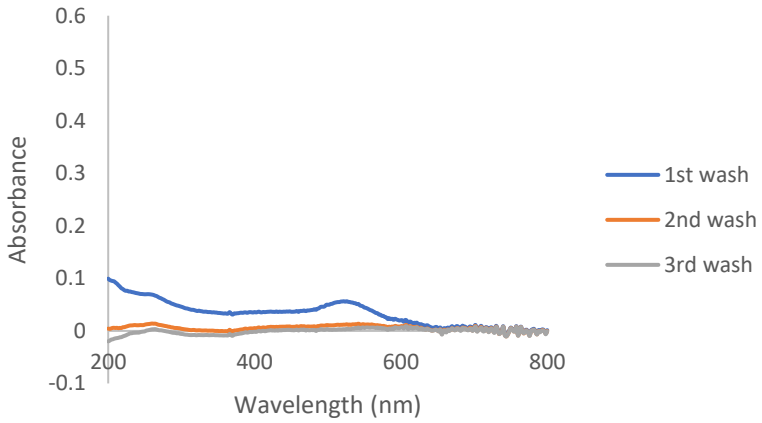

Figure 4-68. UV-Vis spectra of the supernatant for 3 consecutive washes of the gold nanoparticles isolates with water for the 5:1 IL-2:$HAuCl_4$ molar ratio gold nanoparticles synthesis.

Figure 4-68 shows UV-Vis spectra of the supernatants for 3 subsequent washes of the nanoparticles isolates with water. The supernatant of the first wash still contained gold nanoparticles, as indicated by the peak in the 500- 600 nm range. Subsequent washes did not show the presence of ionic liquid nor gold nanoparticles.

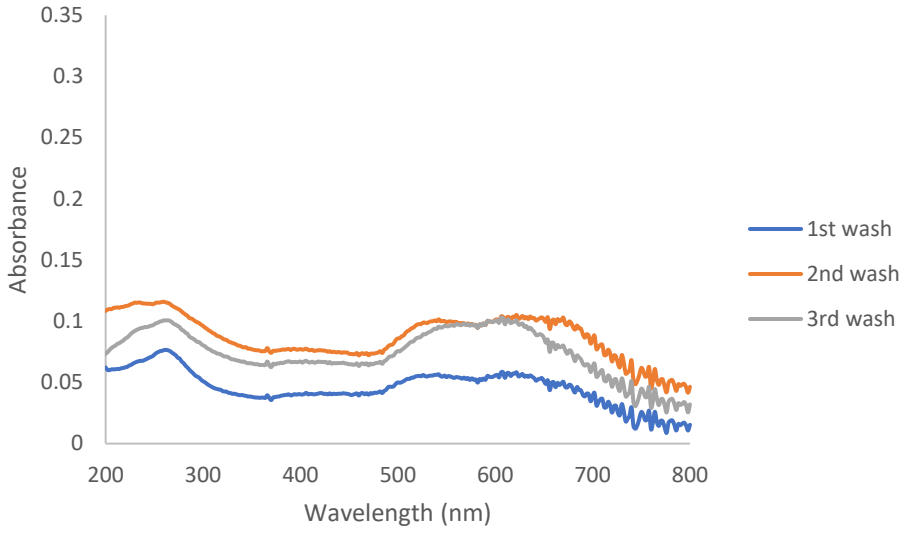

Figure 4-69. UV-Vis spectra of the nanoparticles isolates for 3 consecutive washes with water for the 5:1 IL-2:$HAuCl_4$ molar ratio gold nanoparticles synthesis.

Figure 4-69 shows UV-Vis spectra of the redispersed nanoparticles isolates (pellets) after 3 subsequent washes with water. The UV-Vis spectra have a shoulder in the 500-600 nm region indicating the presence of gold nanoparticles.

4.6 SEM-EDX Analysis of Gold Nanoparticles Purified with the New Washing Protocol

After the nanoparticle purification study, it was decided that acetone could be an optimal solvent, and that one wash should suffice to remove the excess ionic liquid. Gold nanoparticles syntheses were run with each IL using a 5:1 IL:$HAuCl_4$ molar ratio, and a 2:1 $NaBH_4$:$HAuCl_4$ molar ratio. A 1:2 $NaBH_4$:$HAuCl_4$ molar ratio had been used in previous syntheses; however this ratio was based on the stoichiometry of $NaBH_4$ oxidation in more basic conditions, see Equation (4.1) below. Here, the pH of the Au-IL solution mixtures was found to be between 4 and 5 (as measured with pH paper), due to the presence of acidic $HAuCl_4$. $NaBH_4$ is known to undergo spontaneous hydrolysis in acidic conditions, see Equation (4.2) below.[93]

$$BH_4^-(aq) + 8\,OH^-(aq) \rightarrow BO_2^-(aq) + 6\,H_2O(l) + 8\,e^- \quad (4.1)$$

$$BH_4^-(aq) + H_3O^+(aq) \rightarrow BH_3(aq) + H_2O(l) + H_2(g) \quad (4.2)$$

For the SEM/EDX samples, acetone-washed nanoparticle pellets were left to dry for residual acetone to evaporate, and were refrigerated for one week or less. The pellets were then redispersed in both water and ethanol as separate samples. SEM-EDX samples of the reaction mixture for gold nanoparticles syntheses with IL-1B and IL-2 were prepared as well. A selection of images to represent each sample is shown below.

4.6.1 Gold Nanoparticles Prepared with a 5:1 IL-1A:$HAuCl_4$ Molar Ratio

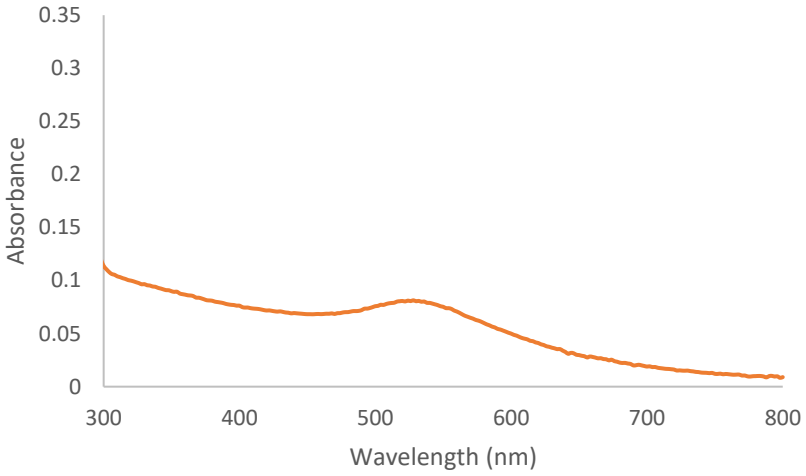

Figure 4-70. UV-Vis spectrum of the reaction mixture of the 5:1 IL-1A:$HAuCl_4$ molar ratio synthesis. The concentrations used were 3.81 mM IL-1A, 0.762 mM $HAuCl_4$, 1.524 mM $NaBH_4$.

The UV-Vis spectrum of the reaction mixture for gold nanoparticle synthesis with IL-1A is shown in Figure 4-70. The SPR absorbance maximum was 524 nm.

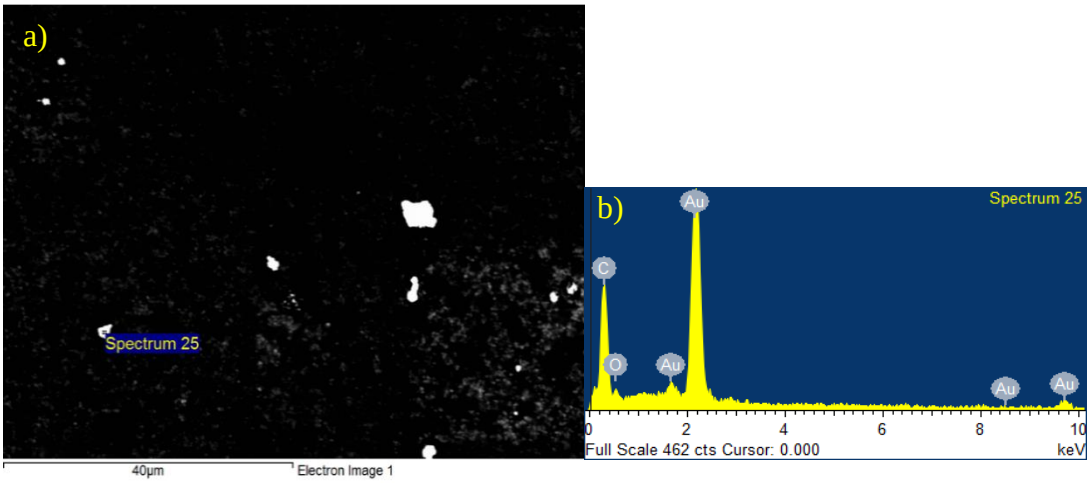

Figure 4-71. SEM-EDX of acetone-washed 5:1 IL-1A:$HAuCl_4$ molar ratio nanoparticles redispersed in nanopure water. The concentrations used were 3.81 mM IL-1A, 0.762 mM $HAuCl_4$, 1.524 mM $NaBH_4$. a) SEM image b) EDX

The 5:1 IL-1A:$HAuCl_4$ molar ratio gold nanoparticle synthesis sample redispersed in water showed dispersion, see Figure 4-71(a). The sample contained mostly aggregates ranging from 1-6 µm. Elemental analysis gave 19.28 (w)% carbon, 26.15 (w)% gold, and 54.56 (w)% oxygen see Figure 4-71(b). The oxygen is most likely due to a gold oxide layer forming as the pellets were refrigerated for a week.

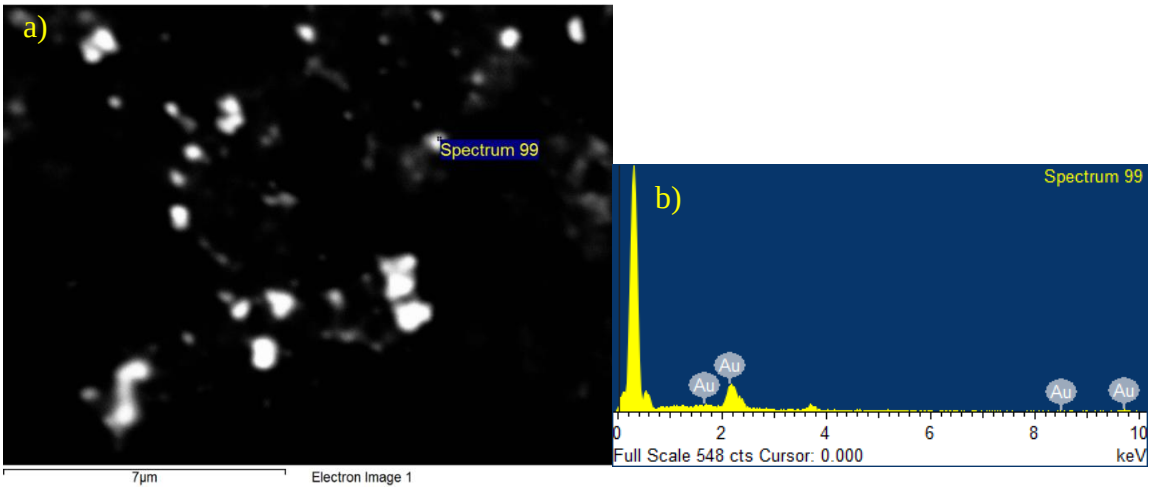

Figure 4-72. SEM-EDX of acetone-washed 5:1 IL-1A:$HAuCl_4$ molar ratio nanoparticles redispersed in ethanol. The concentrations used were 3.81 mM IL-1A, 0.762 mM $HAuCl_4$, 1.524 mM $NaBH_4$. a) SEM image b) EDX

The 5:1 IL-1A:$HAuCl_4$ molar ratio gold nanoparticle synthesis sample redispersed in ethanol showed dispersion, see Figure 4-72(a). Mostly aggregates ranging from 100 nm to 875 nm were present, with some nanoparticles ranging from 70 to 100 nm. Elemental analysis gave 89.14 (w)% gold, and 10.86 (w)% oxygen, see Figure 4-72(b). The oxygen is most likely due to a gold oxide layer forming as the pellets were refrigerated for a week.

4.6.2 Gold Nanoparticles Prepared with a 5:1 IL-1B:$HAuCl_4$ Molar Ratio

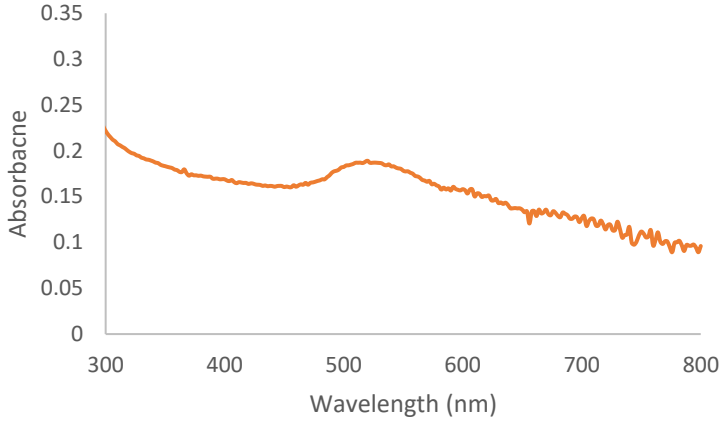

Figure 4-73. UV-Vis spectrum of the reaction mixture of the 5:1 IL-1B:$HAuCl_4$ molar ratio synthesis. The concentrations used were 3.81 mM IL-1B, 0.762 mM $HAuCl_4$, 1.524 mM $NaBH_4$.

The UV-Vis spectrum of the reaction mixture for gold nanoparticle synthesis with IL-1B is shown in Figure 4-73. The SPR absorbance maximum was 524 nm.

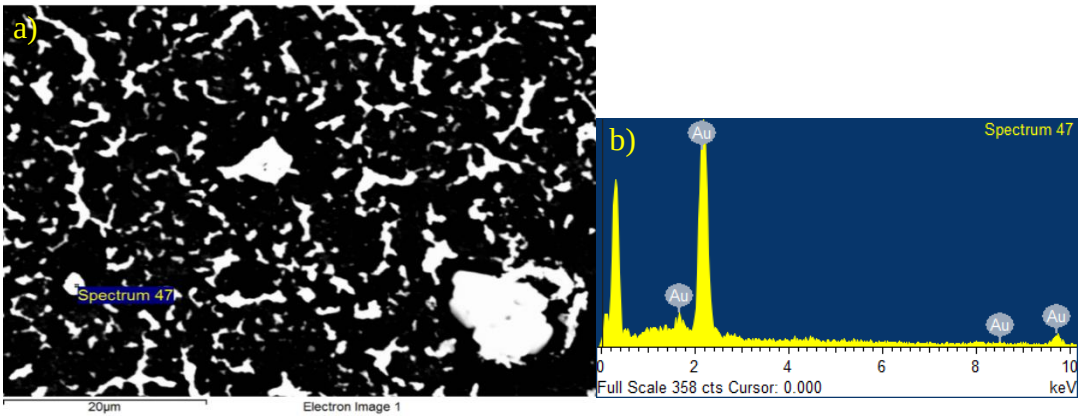

Figure 4-74. SEM-EDX of the reaction mixture of 5:1 IL-1B:$HAuCl_4$ molar ratio. The concentrations used were 3.81 mM IL-1B, 0.762 mM $HAuCl_4$, 1.524 mM $NaBH_4$. a) SEM image b) EDX

An SEM image for the 5:1 Il-1B:$HAuCl_4$ molar ratio gold nanoparticles synthesis reaction mixture is shown in Figure 4-74(a). Elemental analysis gave 89.14 (w)% gold and 10.86 (w)% oxygen, see Figure 4-74(b).

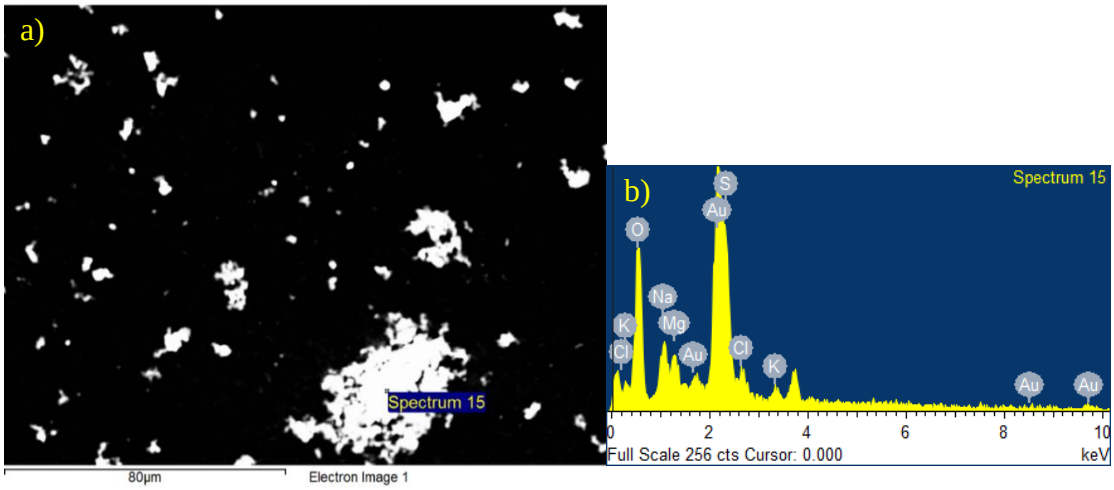

Figure 4-75. SEM-EDX of acetone-washed 5:1 IL-1B:$HAuCl_4$ molar ratio nanoparticles redispersed in nanopure water. The concentrations used were 3.81 mM IL-1B, 0.762 mM $HAuCl_4$, 1.524 mM $NaBH_4$. a) SEM image b) EDX

The 5:1 IL-1B:$HAuCl_4$ molar ratio gold nanoparticle synthesis sample redispersed in water showed dispersion, see Figure 4-75(a). The large structure seen is about 50 µm in diameter. Other structures ranging from 100 nm to 1 µm were found. Elemental analysis gave 4.46 (w)% sodium, 2.62 (w)% magnesium, 13.56 (w)% sulfur, 3.12 (w)%

chlorine, 2.09 (w)% potassium, and 44.71 (w)% gold, see Figure 4-75(b), indicating that organic contaminants were present.

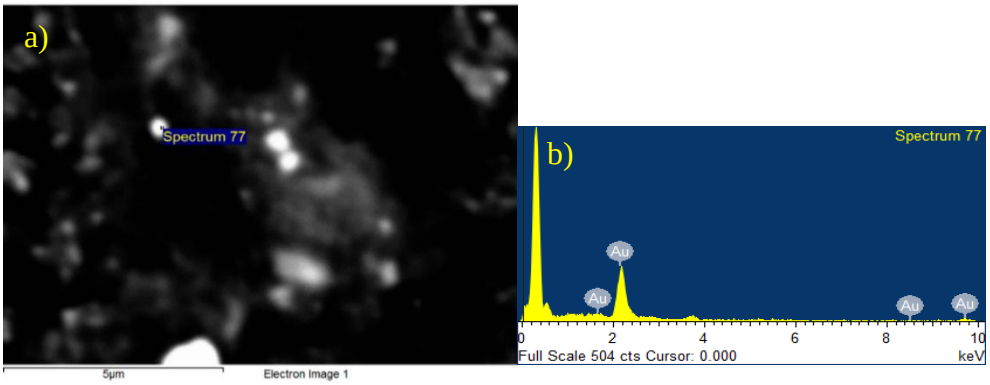

Figure 4-76. SEM-EDX of acetone-washed 5:1 IL-1B:$HAuCl_4$ molar ratio nanoparticles redispersed in ethanol. The concentrations used were 3.81 mM IL-1B, 0.762 mM $HAuCl_4$, 1.524 mM $NaBH_4$. a) SEM image b) EDX

The 5:1 IL-1B:$HAuCl_4$ molar ratio gold nanoparticle synthesis sample redispersed in ethanol showed mostly aggregates, ranging from 100 nm to 1.3 µm, see Figure 4-76(a). Elemental analysis gave 89.14 (w)% gold and 10.86 (w)% oxygen, see Figure 4-76(b), indicating the presence of a gold oxide layer.

4.6.3 Gold Nanoparticles Prepared with a 5:1 IL-2:$HAuCl_4$ Molar Ratio

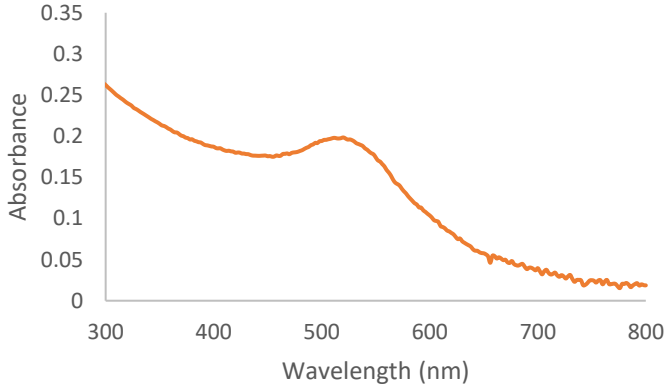

Figure 4-77. UV-Vis spectrum of the reaction mixture of the 5:1 IL-2:$HAuCl_4$ molar ratio synthesis. The concentrations used were 3.81 mM IL-2, 0.762 mM $HAuCl_4$, 1.524 mM $NaBH_4$.

The UV-Vis spectrum of the reaction mixture for gold nanoparticle synthesis with IL-2 is shown in Figure 4-77. The SPR absorbance maximum was 524 nm.

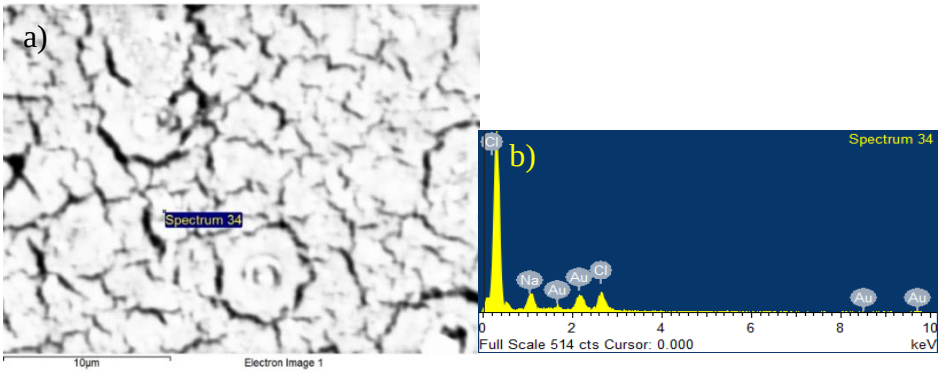

Figure 4-78. SEM-EDX of the reaction mixture of the 5:1 IL-2:$HAuCl_4$ molar ratio synthesis. The concentrations used were 3.81 mM IL-2, 0.762 mM $HAuCl_4$, 1.524 mM $NaBH_4$. a) SEM image b) EDX

An SEM image of the 5:1 IL-2:$HAuCl_4$ molar ratio gold nanoparticle synthesis reaction mixture sample is shown in Figure 4-78(a). The presence of excess ionic liquid is seen dried in a salt-like surface. The elemental analysis gave 18.72 (w)% sodium, 27.78 (w)% chlorine, 41.89 (w)% gold, 11.62 (w)% oxygen, see Figure 4-78(b).

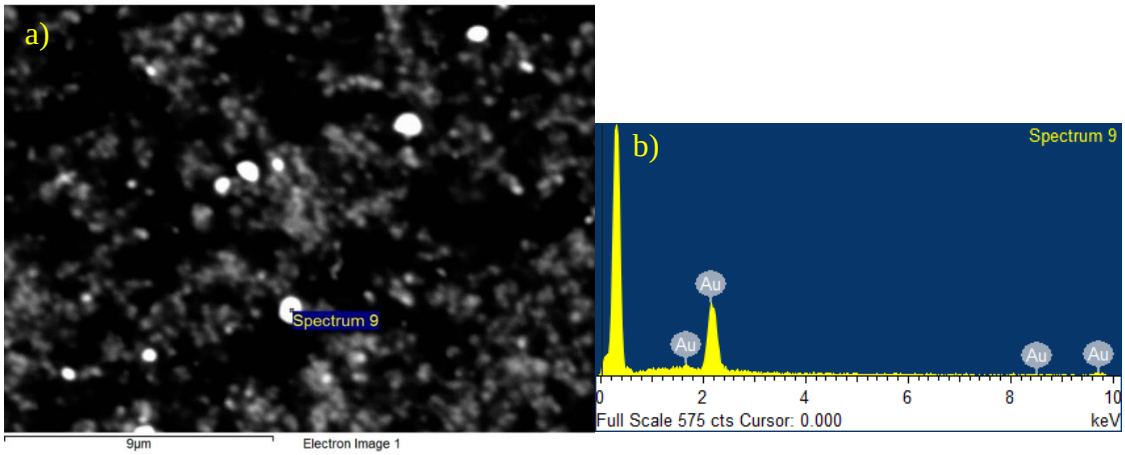

Figure 4-79. SEM-EDX of acetone-washed 5:1 IL-2:$HAuCl_4$ molar ratio nanoparticles redispersed in nanopure water. The concentrations used were 3.81 mM IL-2, 0.762 mM $HAuCl_4$, 1.524 mM $NaBH_4$. a) SEM image b) EDX

The 5:1 IL-1B:$HAuCl_4$ molar ratio gold nanoparticle synthesis sample redispersed in in water showed dispersion, see Figure 4-79(a). Aggregates ranging from 100 nm to 1 µm were found, with nanoparticles around 80 nm seen in this sample. Elemental analysis gave 89.14 (w)% gold and 10.86 (w)% oxygen, see Figure 4-79(b), indicating the likely presence of a gold oxide layer.

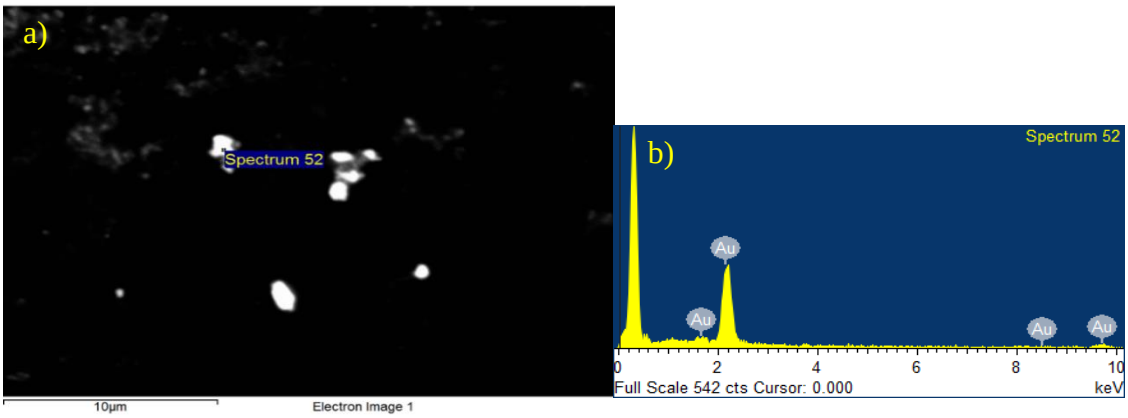

Figure 4-80. SEM-EDX of acetone-washed 5:1 IL-2:$HAuCl_4$ molar ratio nanoparticles redispersed in ethanol. The concentrations used were 3.81 mM IL-2, 0.762 mM $HAuCl_4$, 1.524 mM $NaBH_4$. a) SEM image b) EDX

The 5:1 IL-1B:$HAuCl_4$ molar ratio gold nanoparticle synthesis sample redispersed in ethanol had a lower nanoparticle population density, see Figure 4-80(a). Aggregates ranging from 100 nm to 2.7 µm were found. Elemental analysis gave 89.14 (w)% gold and 10.86 (w)% oxygen, see Figure 4-80(b), indicating the likely presence of a gold oxide layer.

4.7 Tabulated Summary of Gold Nanoparticle Syntheses

A summary of the UV-visible and imaging data is tabulated in Table 4-5. The size estimates are of nanoparticles with sizes <100 nm, and do not include possible aggregate sizes. When mostly aggregates were present, they are indicated as >100 nm. The average absorbance maxima (λ_{max}) and their calculated relative standard deviation (RSD) are

shown for replicates. Spectra without a prominent peak, or experiments with fewer than 3 replicates, do not show average λ_{max} nor RSD values.

Table 4-5. Tabulated summary of synthesized gold nanoparticle characterization

	Molar Ratio (IL:$HAuCl_4$)	**Average $\lambda_{max\ (nm)}$**	**RSD (%)**	**SEM Sizes (nm)**	**AFM Sizes (nm)**
IL-1A (preliminary)	10:1	-	-	<100	50-100
	5:1	-	-	>100	30-50
	1:1	-	-	>100	30-100
IL-1A (optimized)	10:1	526	0.31	50-100	-
	5:1	527	0.18	80-100	30-100
	1:1	547	0.46	>100	50-100
IL-1B	5:1	521	0.36	90-100	-
	1:1	539	0.70	90-100	-
IL-2	10:1	-	-	80-100	-
	5:1	519	0.18	80-100	-
	1:1	532	0.00	80-100	-
Wash Studies					
IL-1A (H_2O)	5:1	524	-	>100	-
IL-1A (EtOH)	5:1	524	-	70-100	-
IL-1B (H_2O)	5:1	524	-	>100	-
IL-1B (EtOH)	5:1	524	-	>100	-
IL-2 (H_2O)	5:1	524	-	80-100	-
IL-2 (EtOH)	5:1	524	-	>100	-

CHAPTER V

CONCLUSIONS AND FUTURE WORK

The goal of this project was to synthesize gold nanoparticles stabilized with novel thioether-functionalized ionic liquids via an aqueous bottom-up method. Ionic liquids, 2-(phenylmercapto)ethyl-tributylphosphonium chloride (IL-1A) and 2-(ethylmercapto)ethyl-tributylphosphonium chloride (IL-2), were prepared with the assistance of Dr. Hua Zhao's research group at the University of Northern Colorado, and were chosen for this project because of the potential of strong gold-sulfur interactions for increased nanoparticle stabilization. The ionic liquid 2-(phenylmercapto)ethyl-methylimidazolium chloride (IL-1B) was prepared during the course of this project. The ionic liquids were characterized and confirmed by ^{1}H-NMR and ^{13}C-NMR, see Figures 4-1 to 4-3 in Section 4.1 and Figures A.1-A.3 in Appendix A. The attempted synthesis of 1,8-bis(tri(*n*-butyl)phosphonium bromide)-3,6-dithiaoctane was performed to investigate whether dithioether ionic liquids could further take advantage of strong gold-sulfur interactions and is described in Section 4.14.

Syntheses of thioether-stabilized gold nanoparticles were first attempted with 2-(phenylmercapto)ethyl-tributylphosphonium chloride (IL-1A). It was observed that the $HAuCl_4$ and IL-1A aqueous mixture remained cloudy prior to the addition of $NaBH_4$ reducing agent, see Figure 4-14(a). Also, preliminary syntheses showed inconsistencies between replicates for the gold nanoparticles SPR absorbance spectrum, which is sensitive to nanoparticle size and nanoparticle dielectric environment, with variations up

to 20 nm for the SPR absorbance maximum of the reaction mixture, see Figures 4-5 to 4-7 and Table 4.1. The SEM/EDX and AFM characterization of these nanoparticles, prepared under different Au: IL-1A molar ratios, showed evidence of the formation of gold nanoparticles, see Sections 4.2.2 and 4.2.3. AFM images indicated that nanoparticles with sizes 30 – 100 nm could be observed, see Figures 4-11 to 4-13.

The lack of reproducibility in the gold nanoparticles syntheses above was attributed to the non-homogeneous medium present prior addition of the reducing agent. Particulate matter that is present in solution can act as potential nucleation site(s) for the formation of nanoparticles. Also, growing nanoparticles would be subject to different dielectric environments, affecting their final particle size, see Figure 5-1.[94]

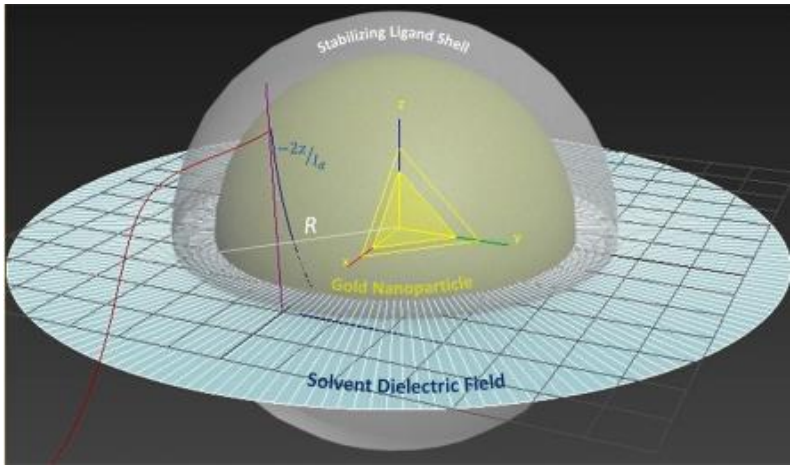

Figure 5-1. Depiction of the surrounding dielectric environment of a gold nanoparticle.[95]

In order to improve the reproducibility of the gold nanoparticles syntheses, efforts were made to ensure the $HAuCl_4$ and IL-1A aqueous mixture could be homogeneous prior to the addition of $NaBH_4$ as reducing agent. The Au-IL-1A mixture was thus heated until it formed a homogenous, colorless solution, see Figure 4-14(b). The homogenous, colorless solution formed upon heating was then used after subsequent cooling for gold nanoparticles syntheses with all three Au:IL-1A molar ratio, *vide infra*.

It was observed that the homogenous, colorless Au-IL-1A mixture would undergo a color change if it was further heated. The 10:1 Au:IL-1A molar ratio mixture gave a more brown solution, the 5:1 Au:IL-1A gave a brownish-pink solution, and the 1:1 Au:IL-1A gave a more pink solution, see Figure 4-16. This color change was monitored using UV-Vis for all three Au:IL-1A molar ratios. The 10:1 Au:IL-1A molar ratio mixture grew a shoulder in the 500-600 nm range, see Figure 4-15; the 5:1 and 1:1 Au:IL-1A both showed an absorbance peak around 560 nm, see Figures 4-17 to 4-18. It should be noted that this absorbance maximum falls into the range of SPR absorbance for gold nanoparticles, although no reducing agent was added.

Next, we examined whether this color change could be attributed to Au-IL-1A complex formation, as this ionic liquid could be acting as a ligand. Here we used fast scan cyclic voltammetry (FSCV) available in Dr. Aaron Apawu's research laboratory at the University of Northern Colorado; the FSCV experiments were performed by graduate student Patrick Wilson. As the redox potential of Au is expected to vary with its ligand environment, we looked for potential differences in the Au oxidation peak for insight into potential changes in Au complexation. The 10:1 Au-IL-1A molar ratio mixture was used in the initial study, with a 400 V/s scan rate. There, fouling of the working carbon electrode was found to occur, as the observed Au oxidation peaks were not reproducible between scans. Also, the voltammograms showed a lack of reversibility between oxidation and reduction, see Figure 4-19. Next, the 5:1 Au-IL-1A molar ratio mixture was used instead based on its more defined absorbance peak upon heating, see Figure 4-17. The FSCV scan rate was also lowered to 100 V/s to try to improve reversibility, and a less concentrated phosphate buffer was used, in better agreement with the literature.[96]

Here the working electrode was also conditioned between scans (at 60 Hz for 2-3 minutes). The resulting voltammograms are shown in Figure 4-20. The Au oxidation peaks now appear to be more aligned between samples. The reduction peaks can now be observed and do not appear to align. However, there are inconsistencies in reversibility between the samples. There is also fine structure observed with some of the Au oxidation and reduction peaks that could correspond to different redox couples (Au(III)/Au(I)/Au).

The $NaBH_4$:$HAuCl_4$ molar ratio was investigated in a preliminary attempt, see Section 4.2.6, before being finalized in the last syntheses, see Section 4.6. A 1:2 $NaBH_4$:$HAuCl_4$ molar ratio was initially chosen to match the reaction stoichiometry, see Equation 4.1.[97] However, $NaBH_4$ will undergo hydrolysis under acidic conditions, see Equation 4.2.[93] The pH of Au-IL mixtures was found to be between 4 and 5, due to the presence of $HAuCl_4$. Thus, a 2:1 $NaBH_4$:$HAuCl_4$ molar ratio was used for the final syntheses, see Section 4.6. A better reaction completion is thus expected with a higher $NaBH_4$:$HAuCl_4$ molar ratio. This could be seen with a higher SPR absorbance for the gold nanoparticles prepared with a 5:1 Au:IL-1B molar ratio, see Figures 4-33 and 4-73, and with a 5:1 Au:IL-2 molar ratio, see Figures 4-39 and 4-77. However, the gold nanoparticles prepared with a 5:1 Au:IL-1A molar ratio did not show a significant change in SPR absorbance, see Figures 4-25 and 4-70. The concentration of $NaBH_4$ is also expected to affect the rate of nanoparticle nucleation and thus final nanoparticle size, see Figure 2-4, although this could not be observed with this work.

The initially optimized syntheses were conducted with 7.62 (10:1 IL:Au) , 3.81 (5:1 IL:Au) , or 0.762 (1:1 IL:Au) mM IL, 0.762 mM $HAuCl_4$, and 0.381 mM $NaBH_4$ (1:2 $NaBH_4$:Au) with all three ionic liquids (IL-1A, IL-1B, and IL-2).

The irreproducibility between gold nanoparticle synthesis replicates with IL-1A was reduced upon first heating the Au-IL-1A mixture to a homogenous and colorless solution, see Section 4.2.7. The variation in SPR absorbance maximum decreased from 10-20 nm, see Figures 4-5 to 4-6 and Table 4-1, to 2-6 nm, see Figures 4-24 to 4-26 and Table 4-2. SEM/EDX analysis, see Section 4.2.8, confirmed that gold nanoparticles were formed. AFM analysis, see Section 4.2.9, showed that nanoparticles between 30-100 nm were obtained. EDX analysis of a 1:1 IL-1A:$HAuCl_4$ molar ratio sample showed the detectable presence of sulfur, indicating that excess ionic liquid residues could be present in the sample. A nanoparticle purification (wash) study was performed and reported in Section 4.5.

Gold nanoparticle syntheses with IL-1B were conducted without any prior heating of the Au-IL-1B mixture, as the mixture was already homogeneous at room temperature. This is most likely due to improved solubility upon changing the bulky tributylphosphonium group to a methylimidazolium group. The reproducibility between gold nanoparticle synthesis replicates was improved with IL-1B as well. The variation in SPR absorption maximum was reduced to 4-8 nm, see Figures 4-32 to 4-34 and Table 4-3. Samples for SEM/EDX and AFM analysis were prepared for syntheses with a 5:1 and 1:1 IL-1B:Au molar ratio; the 10:1 IL-1B:Au molar ratio sample could not be isolated from the first ethanol wash. SEM/EDX confirmed the presence of gold nanoparticles, with size estimates of 90-100 nm, see Section 4.3.1.

Gold nanoparticle syntheses with IL-2 were conducted without any prior heating of the Au-IL-2 mixture, as the mixture was already homogeneous at room temperature. This is most likely due to improved solubility upon changing the bulky phenyl group to

an ethyl group. The reproducibility between gold nanoparticle synthesis replicates was improved with IL-2 as well. The variation in SPR absorption maximum was reduced to 0-2 nm, see Figures 4-41 to 4-43 and Table 4-4. SEM/EDX, see Section 4.4.1, and AFM, see Section 4.4.2, confirmed the presence of gold nanoparticles with sizes in the 50-100 nm range. AFM characterization could not continue after the 10:1 IL-2: Au molar ratio sample, due to streaking and artifacts. The cantilever was changed, but the same artifacts appeared. This could be due to the cantilever picking up nanoparticles from the surface of the mica and dragging them across the sample surface.

Gold nanoparticle syntheses with IL-1B and IL-2 were also conducted *with* prior heating of the Au-IL-1B and Au-IL-2 mixture, for better comparison with the syntheses performed with IL-1A. However, the results were inconclusive. Overall, the variation in SPR absorbance spectra for the reaction mixtures seemed to increase, but not consistently, see Figures 4-38 to 4-40 for IL-1B, and Figures 4-48 to 4-50 for IL-2. These could indicate a change in the Au-IL-1B and Au-IL-2 mixtures upon heating.

Following the detection of organic contaminants in SEM samples by EDX analysis, the purification of isolated nanoparticles was studied, see section 4.5. Gold nanoparticle syntheses were performed with a 5:1 IL:Au molar ratio (IL-1A, IL-2, and IL-1B) and 1:2 $NaBH_4$:Au molar ratio; three wash solvents were used, 100% ethanol, 99.5% acetone, and nanopure water. The nanoparticles were found to be too soluble in water for proper isolation between washes. We also had difficulty isolating nanoparticles prepared with IL- 1B from ethanol. Acetone was thus chosen as the wash solvent. It was determined to the consecutive washes should be limited to one round only, due to the loss

of nanoparticles between washes, possible nanoparticle aggregation, and lack of evidence of further IL removal (see Figure 4-60).

For the final round of gold nanoparticles syntheses and purification for SEM/EDX analysis, syntheses were performed with a 5:1 IL:Au molar ratio (IL-1A, IL-2, and IL-1B) and 2:1 $NaBH_4$:Au molar ratio. The isolated nanoparticles were washed with acetone, and the samples were refrigerated for no more than one week. This last step is different from previous analyses, where SEM/EDX samples would be prepared on the same day as when the synthesis was completed. Here nanoparticles were redispersed in both water and ethanol. SEM/EDX analysis of samples taken directly from the reaction mixture was performed as well for syntheses with IL-1B (Figure 4-74) and IL-2 (Figure 4-78). The reaction mixture samples showed the presence of gold and of other contaminants. Some of the water-redispersed samples showed evidence of contamination, see Figure 4-75, while the ethanol-redispersed samples did not. Overall, the gold nanoparticles all showed the presence of a gold oxide (Au_2O_3) shell, likely due to having the nanoparticles held for under one week in the refrigerator (SEM/EDX analysis was performed the day after the samples were prepared). A lot of nanoparticle aggregation was observed among the samples, see Section 4.6, although it is not clear whether this was due to differences in SEM/EDX sample preparation, nanoparticle purification, and/or nanoparticle synthesis.

Future work for this project includes (i) further optimization of the gold nanoparticles synthesis conditions ($NaBH_4$:$HAuCl_4$ molar ratio, dropwise or batch addition of $NaBH_4$ to the $HAuCl_4$-IL mixture); (ii) further optimization of the isolation and purification of nanoparticles in order to remove organic contaminants without

compromising the stability of nanoparticles; (iii) scanning transmission electron microscopy – high angle annular dark field (STEM-HAADF) analysis at Colorado State University to obtain average particle size and size distribution for samples of interest; (iv) further (FS)CV studies to look for the formation of potential Au-IL intermediates; (v) kinetic studies of the formation (nucleation and growth) of gold nanoparticles by following the change in SPR absorbance, with a focus on the role of thioether ILs as a ligand. Dynamic light scattering (DLS) soon available at the University of Northern Colorado will allow us to perform routine size measurements (average hydrodynamic radius) on reaction samples.

REFERENCES

(1) Masson, J. Surface Plasmon Resonance Clinical Biosensors for Medical Diagnostics. *ACS Sensors* **2017**, *2* (1), 16–30.

(2) Willets, K. A.; Duyne, R. P. Van. Localized Surface Plasmon Resonance Spectroscopy and Sensing. *Annu. Rev. Phys. Chem.* **2007**, *58*, 267–297.

(3) Wang, Y.; Xia, Y. Bottom-Up and Top-Down Approaches to the Synthesis of Monodispersed Spherical Colloids of Low Melting-Point Metals. *Nano Lett.* **2004**, *4* (10), 1–4.

(4) Kim, K.; Demberelnyamba, D.; Lee, H. Size-Selective Synthesis of Gold and Platinum Nanoparticles Using Novel Thiol-Functionalized Ionic Liquids. *Langmuir* **2004**, *20* (3), 556–560.

(5) Yang, Y. W.; Fan, L. J. High-Resolution XPS Study of Decanethiol on Au (111): Single Sulfur-Gold Bonding Interaction. *Langmuir* **2002**, *18* (4), 1157–1164.

(6) Leonhardt, U. Invisibility Cup. *Nano Photonics* **2007**, *1* (April), 207–209.

(7) West, J. L.; Halas, N. J. Engineered Nanomaterials for Biophotonics Applications : Improving Sensing , Imaging , and Therapeutics. *Annu. Rev. Biomed. Eng.* **2003**, *5*, 285–292.

(8) Duyne, R. P. Van; Haes, A. J.; Mcfarland, A. D. Nanoparticle Optics: Sensing with Nanoparticle Arrays and Single Nanoparticles. *Proc. SPIE - Int. Soc. Opt. Eng.* **2003**, *5223*, 197–207.

(9) Xu, X. H. N.; Chen, J.; Jeffers, R.; Kyriacou, S. Direct Measurement of Sizes and Dynamics of Single Living Membrane Transporters Using Nanooptics. *Nano Lett.* **2002**, *2* (3), 175–182.

(10) Anker, J. N.; Hall, W. P.; Lyandres, O.; Shah, N. C.; Zhao, J.; Duyne, R. P. Van. Biosensing with Plasmonic Nanosensors. *Nat. Mater.* **2008**, *7*, 8–10.

(11) Ríos, A. P. D. L.; Irabien, A.; Hollmann, F.; José, F.; Fernández, H. Ionic Liquids: Green Solvents for Chemical Processing. *J. Chem.* **2013**, *2013*, 2–4.

(12) Harfouch, Y. El; Benichou, E.; Bertorelle, F. Effect of a Thioalkane Capping Layer on the First Hyperpolarizabilities of Gold and Silver Nanoparticles. *J. Phys. Condens. Matter* **2012**, *24* (12), 1–7.

(13) Khan, I.; Saeed, K.; Khan, I. Nanoparticles: Properties , Applications and Toxicities. *Arab. J. Chem.* **2019**, *12* (7), 908–931.

(14) Hurtado, R.; Cortez-Valadez, M.; Arizpe-Chavez, H.; S Flores Lopez, N.; Alvarez, R. A. .; Flores-Acosta, M. Nanowire Networks and Hollow Nanospheres of Ag–Au Bimetallic Alloys at Room Temperature. *Nanotechnology* **2017**, *28* (11), 115606.

(15) Shinde, S. T.; Takle, S. P.; Shinde, M. D.; Amalnerkar, P. ZnCl2 Loaded TiO2 Nanomaterial: An Efficient Green Catalyst to One-Pot Solvent-Free Synthesis of Propargylamines. *RSC Adv.* **2019**, *9*, 32735–32743.

(16) Zhuge, F.; Zheng, Z.; Luo, P.; Lv, L.; Huang, Y.; Li, H.; Zhai, T. Nanostructured Materials and Architectures for Advanced Infrared Photodetection. *Adv. Mater. Technol.* **2017**, *2* (8), 1–26.

(17) Shi, D.; Gu, H. Nanostructured Materials for Biomedical Applications. *J. Nanomater.* **2008**, *2008*, 2–4.

(18) Kongkanand, A.; Tvrdy, K.; Takechi, K.; Kuno, M.; Kamat, P. V; Dame, N. Quantum Dot Solar Cells. Tuning Photoresponse through Size and Shape Control of CdSe - TiO2 Architecture. *J. Am. Chem. Soc.* **2008**, *130* (12), 4007–4015.

(19) Zeng, S.; Baillargeat, D.; Ho, H.-P.; Yong, K.-T. Nanomaterials Enhanced Surface Plasmon Resonance for Biological and Chemical Sensing Applications. *Chem. Soc. Rev.* **2014**, *43* (10), 3426–3452.

(20) Haes, A. J.; Haynes, C. L.; Mcfarland, A. D.; Schatz, G. C. Plasmonic Materials for Surface-Enhanced Sensing and Spectroscopy. *MRS Bull.* **2005**, *30* (5), 368–375.

(21) Zeng, S.; Yu, X.; Law, W.; Zhang, Y.; Hu, R.; Dinh, X. Size Dependence of Au

NP-Enhanced Surface Plasmon Resonance Based on Differential Phase Measurement. *Sensors Actuators B Chem.* **2013**, *176*, 1128–1133.

(22) Golden, M. S.; Bjonnes, A. C.; Georgiadis, R. M. Distance- and Wavelength-Dependent Dielectric Function of Au Nanoparticles by Angle-Resolved Surface Plasmon Resonance Imaging. *J. Phys. Chem. C* **2010**, *114* (19), 8837–8843.

(23) Pelton, M.; Aizpurua, J.; Bryant, G. Metal-Nanoparticle Plasmonics. *Laser Photonics Rev.* **2008**, *2* (3), 136–159.

(24) Moores, A.; Goettmann, F. The Plasmon Band in Noble Metal Nanoparticles: An Introduction to Theory and Applications. *New J. Chem.* **2006**, *30* (8), 1121–1132.

(25) Mulvaney, P. Surface Plasmon Spectroscopy of Nanosized Metal Particles. *Langmuir* **1996**, *12* (3), 788–800.

(26) Kelly, K. L.; Coronado, E.; Zhao, L. L.; Schatz, G. C. The Optical Properties of Metal Nanoparticles: The Influence of Size, Shape, and Dielectric Environment. *J. Phys. Chem. B* **2003**, *107* (3), 668–677.

(27) Hamad-Schifferli, K. Exploiting the Novel Properties of Protein Coronas: Emerging Applications in Nanomedicine. *Nanomedicine* **2015**, *10* (10), 1663–1674.

(28) Jain, P. K.; El-Sayed, I. H.; El-Sayed, M. A. Au Nanoparticles Target Cancer. *Nano Today* **2007**, *2* (1), 18–29.

(29) Hirsch, L.; Stafford, R.; Bankson, J.; Sershen, S.; Rivera, B.; Price, R.; Hazle, J.; Halas, N.; West, J. Nanoshell-Mediated near-Infrared Thermal Therapy of Tumors under Magnetic Resonance Guidance. *Proc. Natl. Acad. Sci. U.S.A.* **2003**, *100* (23), 13549–13554.

(30) Aili, D.; Selegard, R.; Baltzer, L.; Enander, K.; Liedberg, B. Colorimetric Protein Sensing by Controlled Assembly of Gold Nanoparticles Functionalized with Synthetic Receptors. *Small* **2009**, *5* (21), 2445–2452.

(31) Alivisatos, P. The Use of Nanocrystals in Biological Detection. *Nat. Biotechnol.* **2004**, *22* (1), 47–52.

(32) Howes, P. D.; Chandrawati, R.; Stevens, M. M. Colloidal Nanoparticles as Advanced Biological Sensors. *Science.* **2014**, *346* (6205), 1247390.

(33) Petryayeva, E.; Krull, U. J. Localized Surface Plasmon Resonance: Nanostructures, Bioassays and Biosensing-A Review. *Anal. Chim. Acta* **2011**, *706* (1), 8–24.

(34) Amendola, V.; Pilot, R.; Fransconi, M.; Marago, O. M.; Iati, M. A. Surface Plasmon Resonance in Gold Nanoparticles. *J. Phys. Condens. Matter* **2017**, *29* (20), 203002.

(35) Ghosh, S. K.; Pal, T. Interparticle Coupling Effect on the Surface Plasmon Resonance of Gold Nanoparticles: From Theory to Applications. *Chem. Rev.* **2007**, *107* (11), 4797–4862.

(36) Wang, Q.; Li, Q.; Yang, X.; Wang, K.; Du, S.; Zhang, H.; Nie, Y. Graphene Oxide–Gold Nanoparticles Hybrids-Based Surface Plasmon Resonance for Sensitive Detection of MicroRNA. *Biosens. Bioelectron.* **2016**, *77*, 1001–1007.

(37) He, L.; Hannon, G. J. MicroRNAs: Small RNAs Witha Big Role in Gene Regulation. *Nat. Rev.* **2004**, *5* (7), 522–531.

(38) Shekhar, S.; Kumar, R.; Rai, N.; Kumar, V.; Singh, K. Estimation of Tau and Phosphorylated Tau 181 in Serum of Alzheimer ' s Disease and Mild Cognitive Impairment Patients. *PLoS One* **2016**, *11* (7), 1–10.

(39) Kim, J.; Kim, S.; Nguyen, T. T.; Lee, R.; Li, T.; Yun, C.; Ham, Y. Label-Free Quantitative Immunoassay of Fibrinogen in Alzheimer Disease Patient Plasma Using Fiber Optical Surface Plasmon Resonance. *J. Electron. Mater.* **2016**, *45* (5), 2354–2360.

(40) Frasconi, M.; Tortolini, C.; Botre, F.; Mazzei, F. Multifunctional Au Nanoparticle Dendrimer-Based Surface Plasmon Resonance Biosensor and Its Application for Improved Insulin Detection. *Anal. Chem.* **2010**, *82* (17), 7335–7342.

(41) Nakamoto, K.; Kurita, R.; Niwa, O. One-Chip Biosensor for Simultaneous Disease Marker/Calibration Substance Measurement in Human Urine by Electrochemical Surface Plasmon Resonance Method. *Biosens. Bioelectron.* **2010**, *26* (4), 1536–1542.

(42) Grzywa, R.; Gorodkiewicz, E.; Burchacka, E.; Lesner, A.; Laudanski, P.; Lukaszewski, Z.; Sienczyk, M. Determination of Cathepsin G in Endometrial Tissue Using a Surface Plasmon Resonance Imaging Biosensor with Tailored Phosphonic Inhibitor. *Eur. J. Obstet. Gynecol. Reprod. Biol.* **2014**, *182C*, 38–42.

(43) Domènech, B.; Bastos - Arrieta, J.; Alonso, A.; Macanás, J.; Muñoz, M.; Muraviev, D. Bifunctional Polymer-Metal Nanocomposite Ion Exchange Materials. In *Ion Exchange Technologies*; 2012; pp 35–72.

(44) Kumar, M.; Ando, Y. Chemical Vapor Deposition of Carbon Nanotubes: A Review on Growth Mechanism and Mass Production. *J. Nanosci. Nanotechnol.* **2010**, *10* (6), 3739–3758.

(45) Niederberger, M.; Garnweitner, G.; Krumeich, F.; Nesper, R.; Co, H. Tailoring the Surface and Solubility Properties of Nanocrystalline Titania by a Nonaqueous In Situ Functionalization Process. *Chem. Mater.* **2004**, *16* (13), 1202–1208.

(46) Yeh, Y.-C.; Creran, B.; Rotello, V. M. Gold Nanoparticles: Preparation, Properties, and Applications in Bionanotechnology. *Nanoscale* **2012**, *4* (6), 1871–1880.

(47) Niu, Z.; Li, Y. Removal and Utilization of Capping Agents in Nanocatalysis. *Chem. Mater.* **2014**, *26* (1), 72–83.

(48) Polte, J.; Kraehnert, R.; Radtke, M.; Reinholz, U.; Riesemeier, H.; Thunemann, A. F.; Emmerling, F. New Insights of the Nucleation and Growth Process of Gold Nanoparticles via in Situ Coupling of SAXS and XANES. *J. Phys. Conf. Ser.* **2010**, *247* (1), 1–10.

(49) Khan, Z.; Singh, T.; Hussain, J. I.; Hashmi, A. A. Biointerfaces Au(III)-CTAB Reduction by Ascorbic Acid: Preparation and Characterization of Gold Nanoparticles. *Colloids Surfaces B Biointerfaces* **2013**, *104*, 11–17.

(50) Camargo, P. H. C.; Rodrigues, T. S.; Silva, A. G. M.; Wang, J. Controlled Synthesis: Nucleation and Growth in Solution. In *Metallic Nanostructures: From Controlled Synthesis to Applications*; 2015; pp 49–58.

(51) Wuithschick, M.; Birnbaum, A.; Witte, S.; Sztucki, M.; Vainio, U.; Pinna, N.; Rademann, K.; Emmerling, F.; Kraehnert, R. Turkevich in New Robes : Key Questions Answered for the Most Common Gold Nanoparticle Synthesis. *ACS*

Nano **2015**, *9* (7), 7052–7071.

(52) Shevchenko, E. V; Talapin, D. V; Schnablegger, H.; Kornowski, A.; Svedlindh, P.; Haase, M.; Weller, H. Study of Nucleation and Growth in the Organometallic Synthesis of Magnetic Alloy Nanocrystals : The Role of Nucleation Rate in Size Control of CoPt 3 Nanocrystals. *J. Am. Chem. Soc.* **2003**, *125* (30), 9090–9101.

(53) Turkevich, J.; Stevenson, P. C.; Hillier, J. A Study of the Nucleation and Growth Processes in the Synthesis of Colloidal Gold. *Discuss. Faraday Soc.* **1951**, *11*, 55–75.

(54) Polte, J. Fundamental Growth Principles of Colloidal Metal Nanoparticles – a New Perspective. *CrystEngComm* **2015**, *17* (36), 6809–6830.

(55) Antonio, M.; Nogueira, J.; Vitorino, R.; Daniel-da-Silva, A. L. Functionalized Gold Nanoparticles for the Detection of C-Reactive Protein. *Nanomaterials* **2018**, *8* (4), 200.

(56) Schulz, F.; Homolka, T.; Bastu, N. G.; Puntes, V.; Weller, H.; Vossmeyer, T. Little Adjustments Significantly Improve the Turkevich Synthesis of Gold Nanoparticles. *Langmuir* **2014**, *30* (35), 10779–10784.

(57) Hostetler, M. J.; Wingate, J. E.; Zhong, C.; Harris, J. E.; Vachet, R. W.; Clark, M. R.; Londono, J. D.; Green, S. J.; Stokes, J. J.; Wignall, G. D.; et al. Alkanethiolate Gold Cluster Molecules with Core Diameters from 1.5 to 5.2 Nm: Core and Monolayer Properties as a Function of Core Size. *Langmuir* **1998**, *14* (1), 17–30.

(58) Brust, M.; Kiely, C. J. Some Recent Advances in Nanostructure Preparation from Gold and Silver Particles: A Short Topical Review. *Colloids Surfaces A Physicochem. Eng. Asp.* **2002**, *202* (2–3), 175–186.

(59) Yee, C. K.; Jordan, R.; Ulman, A.; White, H.; King, A.; Rafailovich, M.; Sokolov, J.; Brook, S.; York, N. Novel One-Phase Synthesis of Thiol-Functionalized Gold, Palladium, and Iridium Nanoparticles Using Superhydride. *Langmuir* **1999**, *15* (10), 3486–3491.

(60) Clare, B.; Sirwardana, A.; MacFarlane, D. R. Synthesis, Purification and Characterization of Ionic Liquids. In *Topics in Current Chemistry*; 2009; pp 1–6.

(61) Moosavi, F. The Structure of Supported Ionic Liquids at the Interface. In *Ionic Liquids - New Aspects for the Future Ionic*; 2013; pp 195–230.

(62) Li, W.; Chang, W.; Yang, X.; Qian, S.; Dong, L.; Zhang, P.; Yi, Y.; Li, B.; Zhang, S. Synthesis of Cyclic Carbonate Catalyzed by DBU Derived Basic Ionic Liquids. *Chinese J. Chem.* **2018**, *36* (4), 293–298.

(63) Luo, S.; Mi, X.; Zhang, L.; Liu, S.; Cheng, J. Functionalized Ionic Liquids Catalyzed Direct Aldol Reactions. *Tetrahedron* **2007**, *63* (9), 1923–1930.

(64) Li, J.; Yang, S.; Wu, W.; Jiang, H. Recent Advances in Pd-Catalyzed Cross-Coupling Reaction in Ionic Liquids. *European J. Org. Chem.* **2018**, *2018* (11), 1284–1306.

(65) Zhang, H.; Cui, H. Synthesis and Characterization of Functionalized Ionic Liquid-Stabilized Metal (Gold and Platinum) Nanoparticles and Metal Nanoparticle/Carbon Nanotube Hybrids. *Langmuir* **2009**, *25* (5), 2604–2612.

(66) Janiak, C. Ionic Liquids for the Synthesis and Stabilization of Metal Nanoparticles Ionic Liquids for the Synthesis and Stabilization of Metal Nanoparticles. *Zeitschrift für Naturforsch. B* **2013**, *68* (10), 1059–1089.

(67) Ostwald, W. Blocking of Ostwald Ripening Allowing Long-Term Stabilization. *Phys. Chem* **1901**, *37*, 385.

(68) Dupont, J.; Suarez, P. A. Z. Physico-Chemical Processes in Imidazolium Ionic Liquids. *Phys. Chem. Chem. Phys.* **2006**, *8* (21), 2441–2452.

(69) Love, J. C.; Estroff, L. A.; Kriebel, J. K.; Nuzzo, R. G.; Whitesides, G. M. Self-Assembled Monolayers of Thiolates on Metals as a Form of Nanotechnology. *Chem. Rev.* **2005**, *105* (4), 1103–1170.

(70) Xue, Y.; Li, X.; Li, H.; Zhang, W. Quantifying Thiol-Gold Interactions towards the Efficient Strength Control. *Nat. Commun.* **2014**, *5* (4348), 1–9.

(71) Abbott, A. P.; Capper, G.; Davies, D. L.; Rasheed, R. K.; Tambyrajah, V. Novel Solvent Properties of Choline Chloride/Urea Mixtures. *Chem. Commun.* **2003**, No. 1, 70–71.

(72) Abbott, A. P.; Boothby, D.; Capper, G.; Davies, D. L.; Rasheed, R. K. Deep Eutectic Solvents Formed between Choline Chloride and Carboxylic Acids: Versatile Alternatives to Ionic Liquids. *J. Am. Chem. Soc.* **2004**, *126* (29), 9142–9147.

(73) Vanda, H.; Dai, Y.; Wilson, E. G.; Verpoorte, R.; Hae, Y. Green Solvents from Ionic Liquids and Deep Eutectic Solvents to Natural Deep Eutectic Solvents. *Comptes Rendus Chim.* **2018**, *21* (6), 628–638.

(74) Borato, C. E.; Leite, F. L. Efficient Taste Sensors Made of Bare Metal Electrodes. *Sens. Lett.* **2006**, *4* (2), 155–159.

(75) Santos, N.; Castanho, M. An Overview of the Biophysical Applications of Atomic Force Microscopy. *Biophys. Chem.* **2004**, *107* (2), 133–149.

(76) de Souza, N.; Silva, J.; Pereira-da-Silvia, M.; Raposa, M.; Faria, R.; Giacometti, J.; Oliveira, O. Dynamic Scale Theory for Characterizing Surface Morphology of Layer-by-Layer Films of Poly(o-Methoxyaniline). *J. Nanosci. Nanotechnol.* **2004**, *4* (5), 548–552.

(77) Leite, F. L.; Riul, A.; Herrmann, P. S. P. Mapping of Adhesion Forces on Soil Minerals in Air and Water by Atomic Force Spectroscopy (AFS). *J. Adhes. Sci. Technol.* **2003**, *17* (16), 2141–2156.

(78) Meyer, G.; Amer, N. Novel Optical Approach to Atomic Force Microscopy. *Appl. Phys. Lett.* **1988**, *53* (12), 1045–1047.

(79) Voigtländer, B. Cantilevers and Detection Methods in Atomic Force Microscopy. In *Atomic Force Microscopy*; Springer International Publishing: Cham, 2019; pp 177–197.

(80) Alexander, S.; Hellemans, L.; Marti, O.; Schneir, J.; Elings, V.; K. Hansma, P.; Longmire, M.; Gurley, J. An Atomic-Resolution Atomic Force Microscope Implemented Using an Optical Lever. *J. Appl. Phys.* **1989**, *65* (1), 164–167.

(81) Zeng, G.; Duan, Y.; Besenbacher, F.; Dong, M. Nanomechanics of Amyloid Materials Studied by Atomic Force Microscopy. In *Atomic Force Microscopy Investigations into Biolgy - From Cell to Protein*; 2012; p 155.

(82) Meyer, E.; Hug, H.; Bennewitz, R. *Scanning Probe Microscopy: The Lab on a Tip*; Berlin: Springer-Verlag, 2004.

(83) Schmid, G. *Nanoparticles: From Theory to Application*; Weinheim: Wiley-VCH, 2003.

(84) Jillavenkatesa, A.; Dapkunas, S.; Lum, L. *Particle Size Characterization, NIST Recommended Practice Guide*, Special Pu.; National Institute of Standards and Technology, U.S. Department of Commerce, 2001.

(85) Goldstein, J. I.; Newbury, D. E.; Michael, J. R.; Ritchie, N. W. M.; Scott, J. H. J.; Joy, D. C. Scanning Electron Microscope (SEM) Instrumentation. In *Scanning Electron Microscopy and X-Ray Microanalysis*; Goldstein, J. I., Newbury, D. E., Michael, J. R., Ritchie, N. W. M., Scott, J. H. J., Joy, D. C., Eds.; Springer New York: New York, NY, 2018; pp 65–91.

(86) Gardinalli, P.; Singhal, R. K.; Ferreira, B.; Pe, S.; Mozeto, A. A. Analytical Chemistry of Metallic Nanoparticles in Natural Environments. *Trends Anal. Chem.* **2011**, *30* (3), 528–540.

(87) Inkson, B. J. Scanning Electron Microscopy (SEM) and Transmission Electron Microscopy (TEM) for Materials Characterization. In *Materials Characterization Using Nondestructive Evaluation (NDE) Methods*; Elsevier Ltd, 2016; p 26.

(88) Elgrishi, N.; Rountree, K. J.; Mccarthy, B. D.; Rountree, E. S.; Eisenhart, T. T.; Dempsey, J. L. A Practical Beginner's Guide to Cyclic Voltammetry. *J. Chem. Educ.* **2018**, *95* (2), 197–206.

(89) Gutierrez, C. On the Use of Cyclic Voltammetry for the Screening of Oxide Catalysts for NO Decomposition and Reduction. *Electrochim. Acta* **2006**, *51* (20), 4324–4325.

(90) Gomes, J. F.; Garcia, A. C.; Gasparotto, L. H. S.; Souza, N. E. De; Ferreira, E. B.; Pires, C. Influence of Silver on the Glycerol Electro-Oxidation over AuAg/C Catalysts in Alkaline Medium: A Cyclic Voltammetry and in Situ FTIR Spectroscopy Study. *Electrochim. Acta* **2014**, *144*, 361–368.

(91) Zhou, W.; Li, M.; Zhang, L.; Hwa, S. Supported PtAu Catalysts with Different Nano-Structures for Ethanol Electrooxidation. *Electrochim. Acta* **2014**, *123*, 233–239.

(92) Roy, F.; Et, A.; Lallemand, F.; Heintz, O.; Moutarlier, V.; Hihn, J. Alkanethiol Self-Assembling on Gold: Influence of High Frequency Ultrasound on Adsorption Kinetics and Electrochemical Blocking. *Ultrason. Sonochem.* **2018**, *40* (Pt B), 9–16.

(93) Bilge, U.; Hannauer, J.; Gervais, C.; Goutaudier, C.; Miele, P.; Multimate, L. Spontaneous Hydrolysis of Sodium Borohydride in Harsh Conditions. *Int. J. Hydrogen Energy* **2010**, *36* (1), 224–233.

(94) Huang, X.; El-sayed, M. A. Gold Nanoparticles: Optical Properties and Implementations in Cancer Diagnosis and Photothermal Therapy. *J. Adv. Res.* **2010**, *1* (1), 13–28.

(95) Chatterjee, H.; Ghosh, S. K. Cumulative Effect of Solvent and Ligand Dielectric around the Nanoparticles: Merging Past Century Theories into a Singular Scaling Equation. *J. Phys. Chem. C* **2017**, *121* (40), 22310–22325.

(96) Messori, L.; Abbate, F.; Marcon, G.; Orioli, P.; Fontani, M.; Mini, E.; Mazzei, T.; Carotti, S.; Connell, T. O.; Zanello, P. Gold (III) Complexes as Potential Antitumor Agents : Solution Chemistry and Cytotoxic Properties of Some Selected Gold (III) Compounds. *J. Med. Chem.* **2000**, *43* (19), 3541–3548.

(97) Pierre-Yves Olu, Antoine Bonnefont, Guillaume Braesch, Vincent Martin, Elena R. Savinova, M. C. Influence of the Concentration of Borohydride towards Hydrogen Production and Escape for Borohydride Oxidation Reaction on Pt and Au Electrodes – Experimental and Modelling Insights. *J. Power Sources* **2018**, *375*, 300–309.

APPENDIX A

ADDITIONAL ^{13}C-NMR OF NOVEL THIOETHER IONIC LIQUIDS

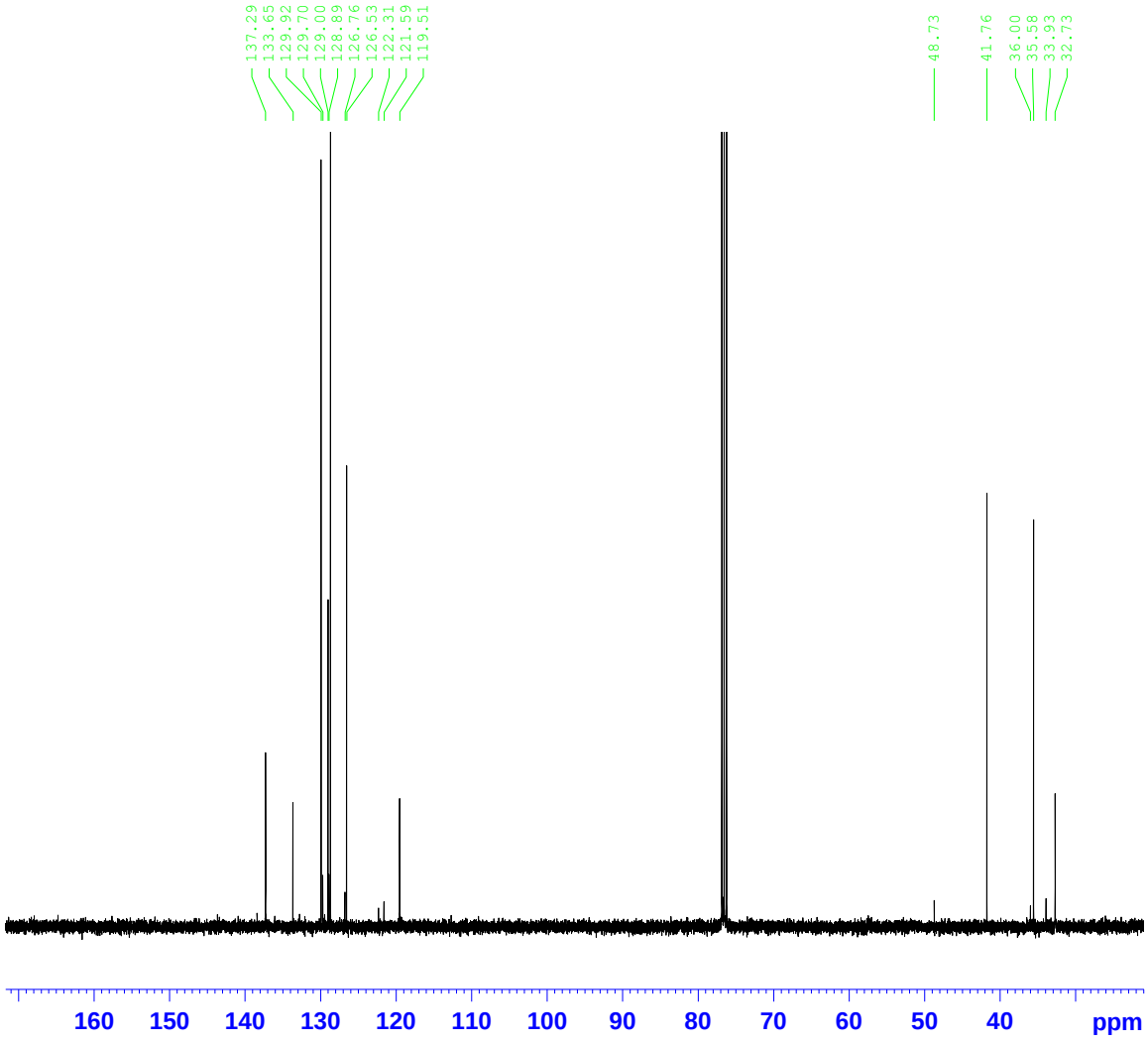

Figure A1. ^{13}C-NMR of 2-(phenylmercapto)ethyl-tributylphosphonium chloride**.**

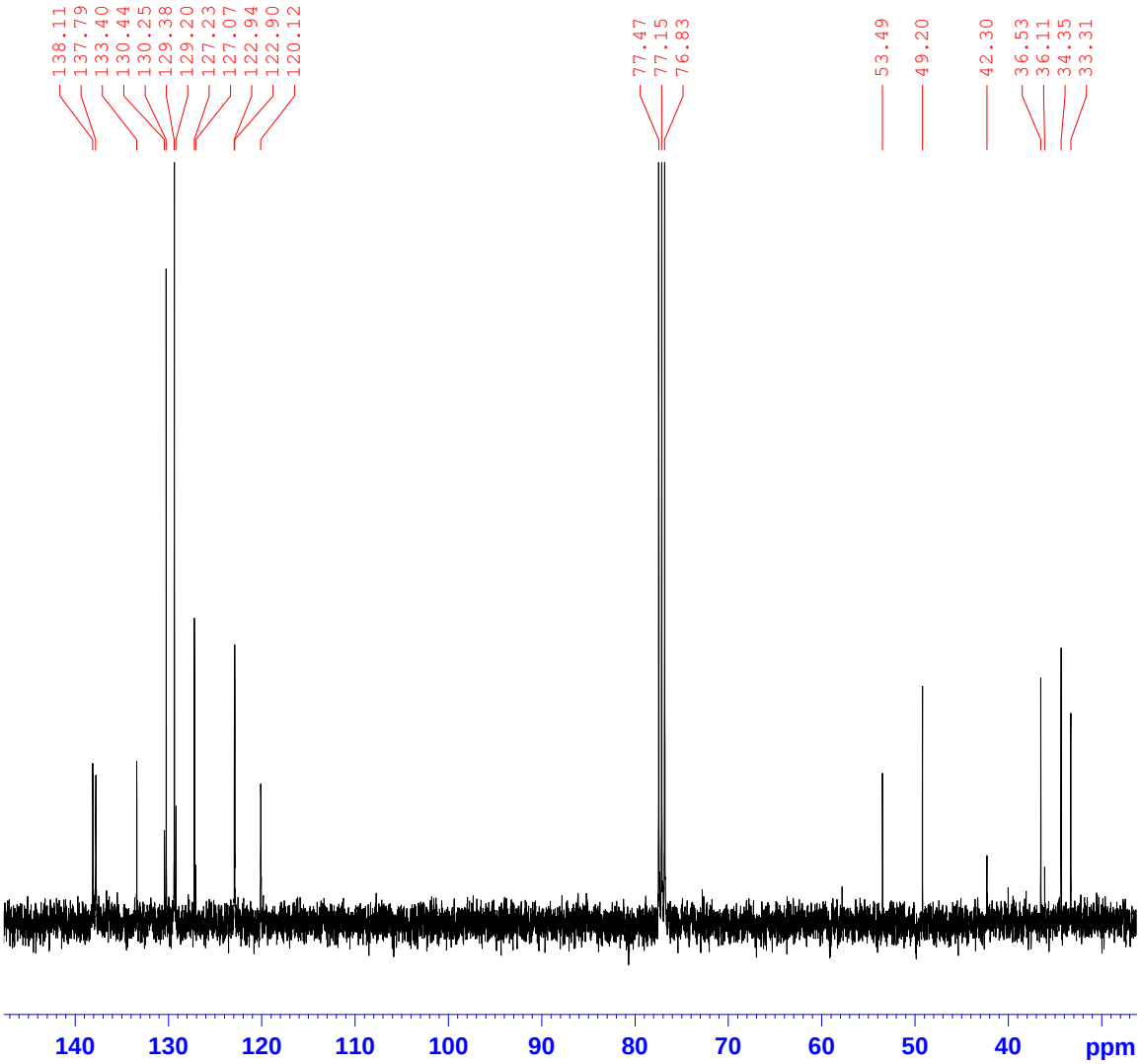

Figure A2. ^{13}C-NMR of 2-(phenylmercapto)ethyl-methylimidazolium chloride.

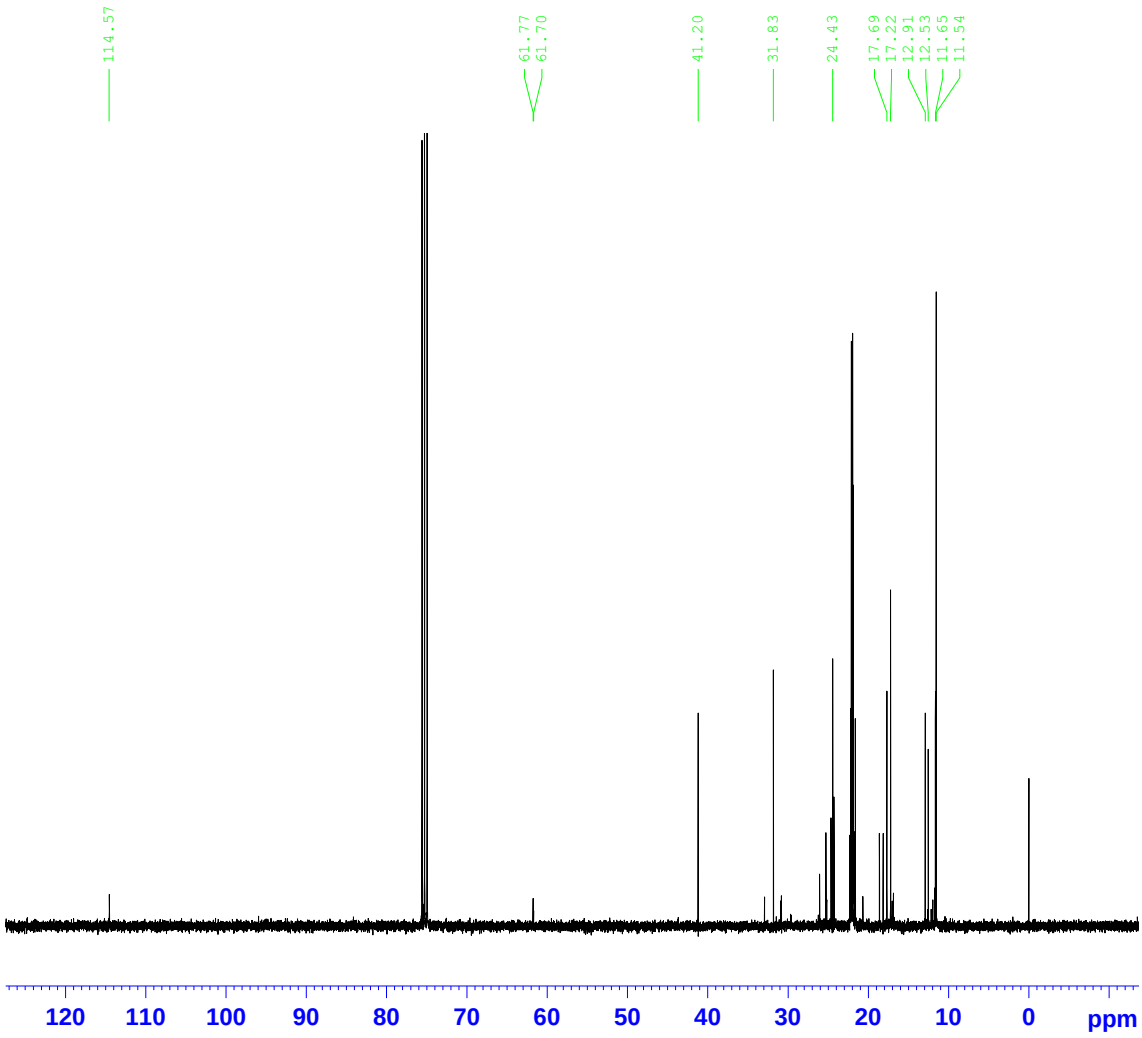

Figure A3. ^{13}C-NMR of 2-(ethylmercapto)ethyl-tributylphosphonium chloride.

APPENDIX B

ADDITIONAL SEM/EDX OF OPTIMIZED GOLD NANOPARTICLE SYNTHESES WITH IL-1A

The following are additional SEM/EDX of the optimized gold nanoparticle syntheses with IL-1A.

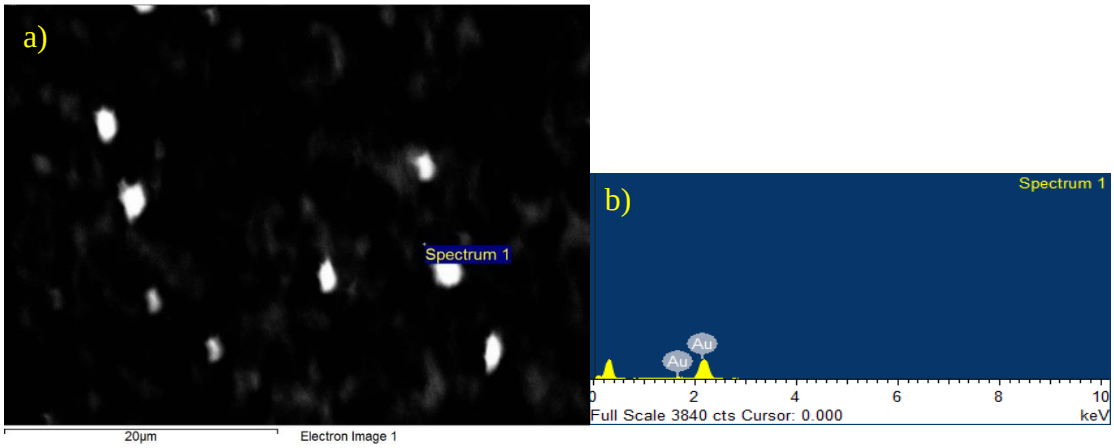

Figure B1. SEM-EDX of optimized 10:1 IL-1A:Au molar ratio synthesis. The concentrations used in these syntheses were 7.62 mM IL-1A, 0.762 mM $HAuCl_4$, 0.381 mM $NaBH_4$. Elemental analysis gave 100 (w)% gold. a) SEM image b) EDX

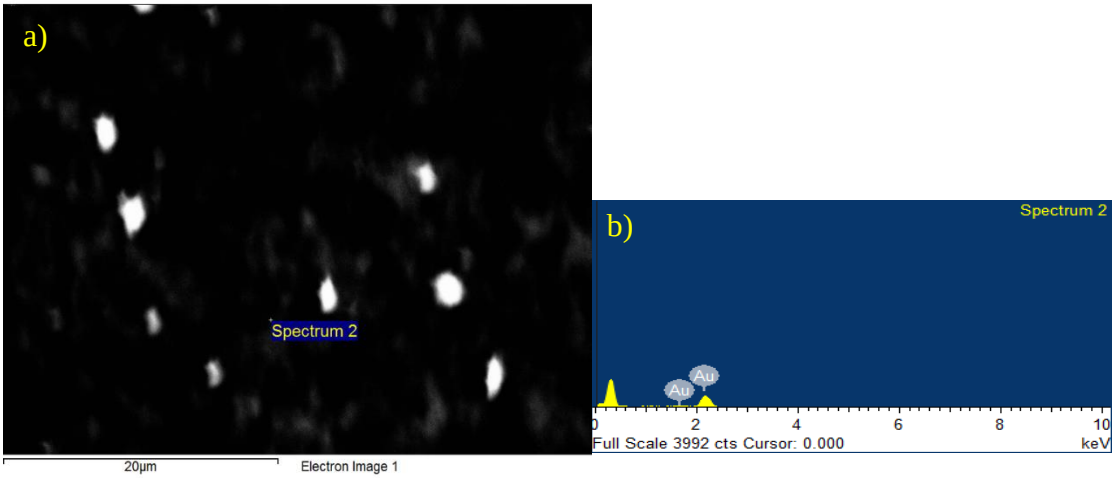

Figure B2. SEM-EDX of optimized 10:1 IL-1A:Au molar ratio synthesis. The concentrations used in these syntheses were 7.62 mM IL-1A, 0.762 mM $HAuCl_4$, 0.381 mM $NaBH_4$. Elemental analysis gave 100 (w)% gold. a) SEM image b) EDX

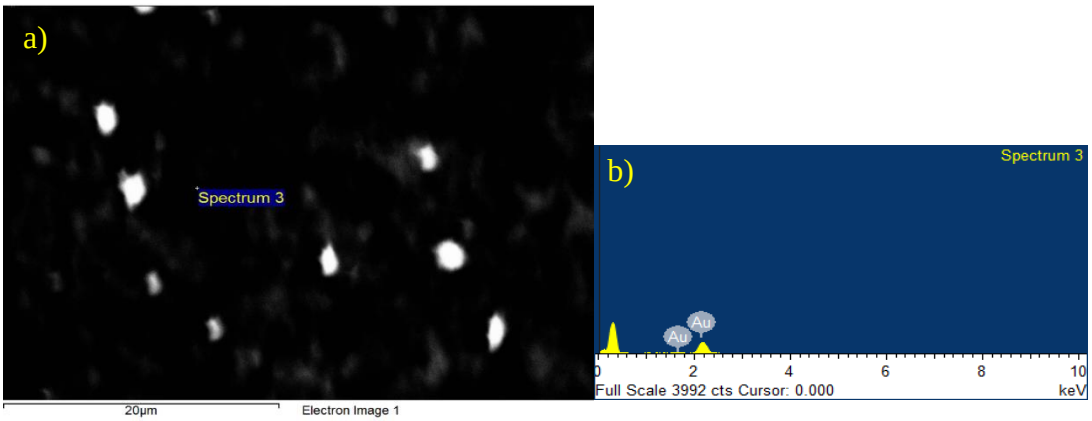

Figure B3. SEM-EDX of optimized 10:1 IL-1A:Au molar ratio synthesis. The concentrations used in these syntheses were 7.62 mM IL-1A, 0.762 mM $HAuCl_4$, 0.381 mM $NaBH_4$. Elemental analysis gave 100 (w)% gold. a) SEM image b) EDX

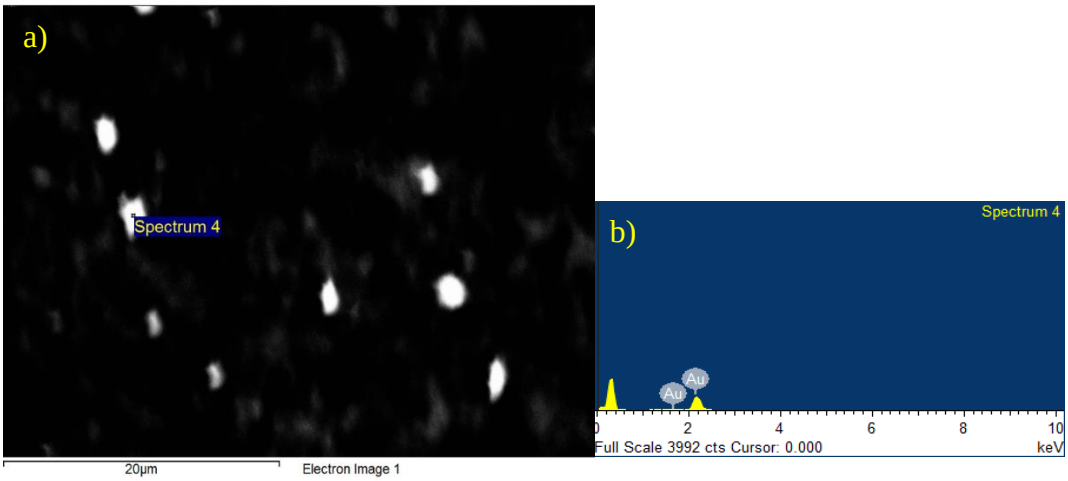

Figure B4. SEM-EDX of optimized 10:1 IL-1A:Au molar ratio synthesis. The concentrations used in these syntheses were 7.62 mM IL-1A, 0.762 mM $HAuCl_4$, 0.381 mM $NaBH_4$. Elemental analysis gave 100 (w)% gold. a) SEM image b) EDX

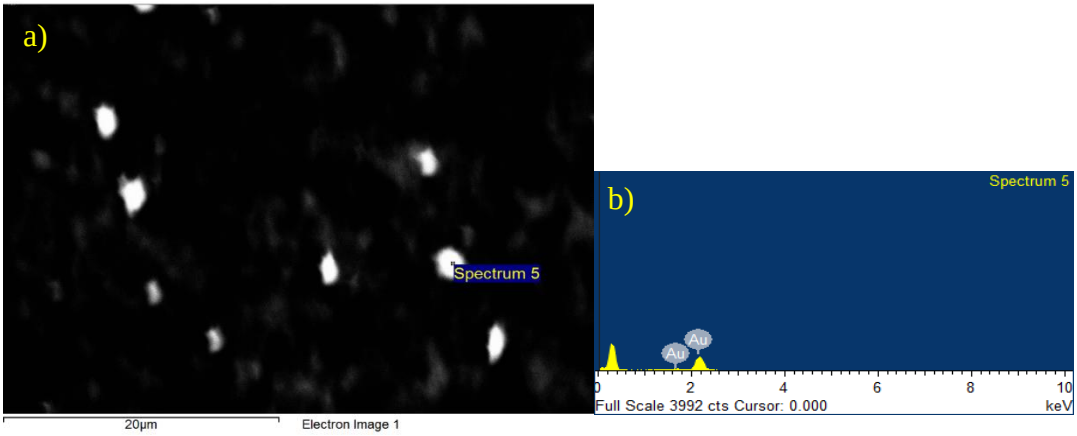

Figure B5. SEM-EDX of optimized 10:1 IL-1A:Au molar ratio synthesis. The concentrations used in these syntheses were 7.62 mM IL-1A, 0.762 mM $HAuCl_4$, 0.381 mM $NaBH_4$. Elemental analysis gave 100 (w)% gold. a) SEM image b) EDX

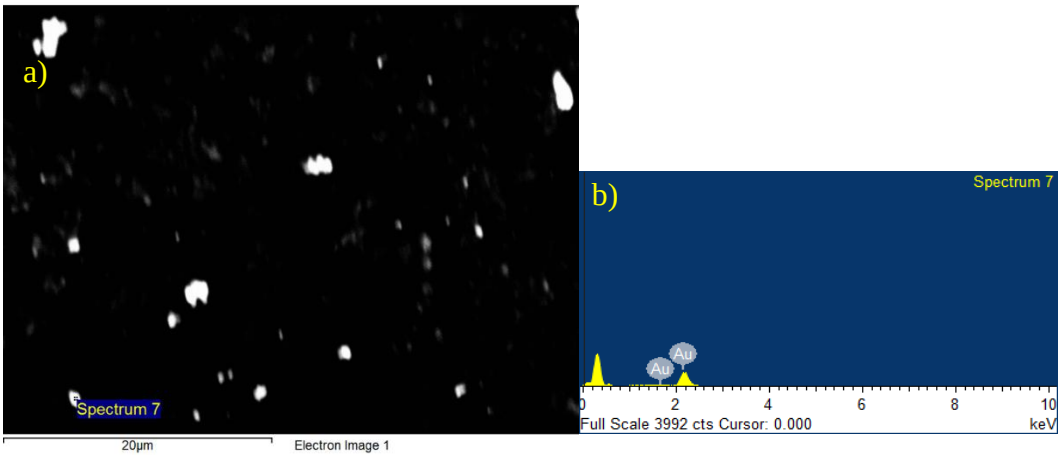

Figure B6. SEM-EDX of optimized 10:1 IL-1A:Au molar ratio synthesis. The concentrations used in these syntheses were 7.62 mM IL-1A, 0.762 mM $HAuCl_4$, 0.381 mM $NaBH_4$. Elemental analysis gave 100 (w)% gold. a) SEM image b) EDX

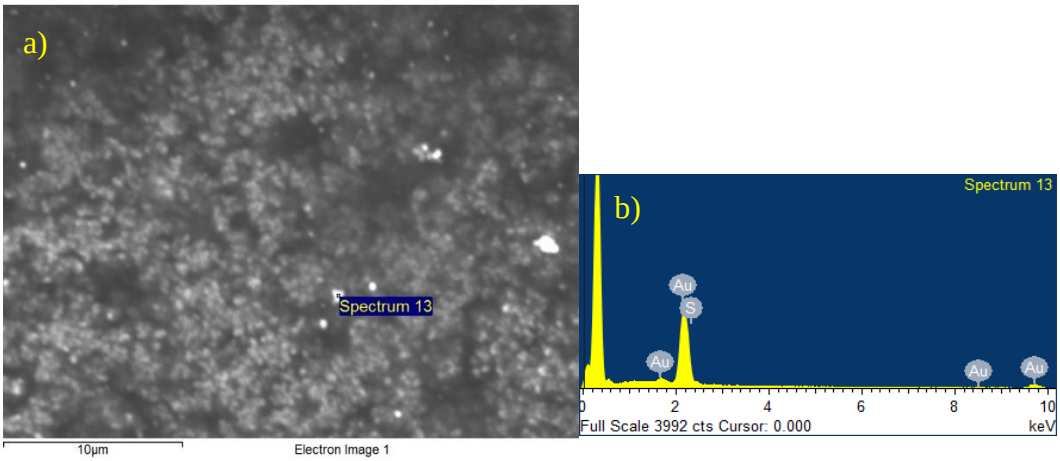

Figure B7. SEM-EDX of optimized 5:1 IL-1A:$HAuCl_4$ molar ratio synthesis. The concentrations used in these syntheses were 3.81 mM IL-1A, 0.762 mM $HAuCl_4$, 0.381 mM $NaBH_4$. Elemental analysis gave 100 (w)% gold and -0.11 (w)% sulfur. a) SEM image b) EDX

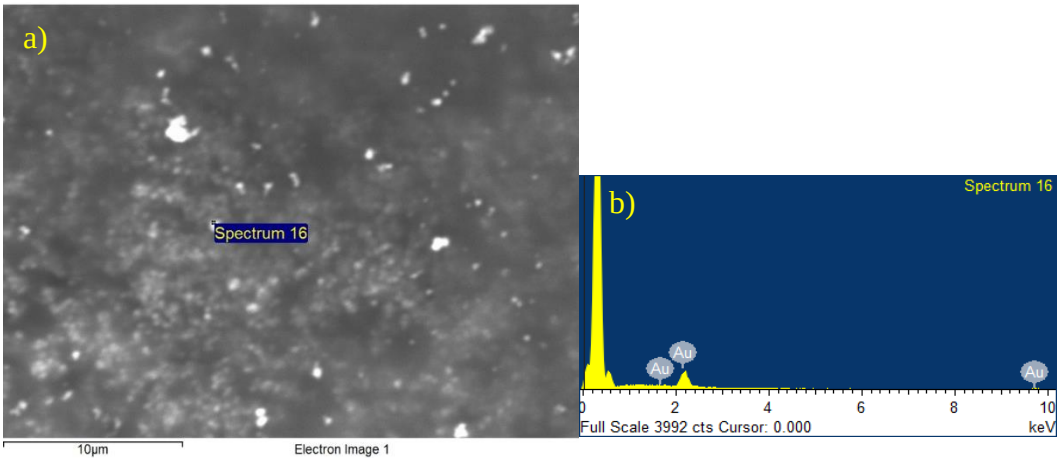

Figure B8. SEM-EDX of optimized 1:1 IL-1A:$HAuCl_4$ molar ratio synthesis. The concentrations used in these syntheses were 0.762 mM IL-1A, 0.762 mM $HAuCl_4$, 0.381 mM $NaBH_4$. Elemental analysis gave 100 (w)% gold. a) SEM image b) EDX

APPENDIX C

ADDITIONAL SEM/EDX OF OPTIMIZED GOLD NANOPARTICLE SYNTHESES WITH IL-1B

The following are additional SEM/EDX of the optimized gold nanoparticle syntheses with IL-1B.

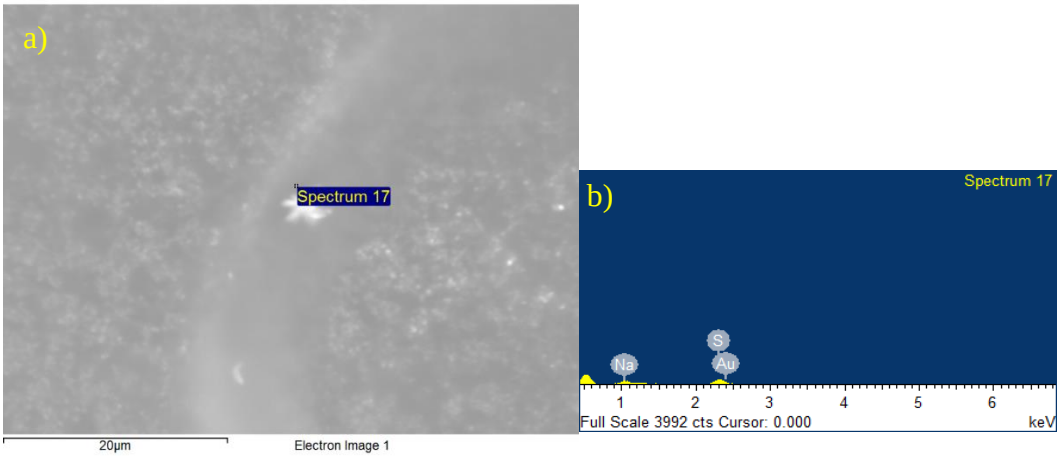

Figure C1. SEM-EDX of optimized 10:1 IL-1B:Au molar ratio synthesis. The concentrations used in these syntheses were 7.62 mM IL-1B, 0.762 mM $HAuCl_4$, 0.381 mM $NaBH_4$. Elemental analysis of the salt-like structure gave 93.23 (w)% carbon, 2.58 (w)% sodium, -0.85 (w)% gold , and 5.05 (w)% sulfur. a) SEM image b) EDX

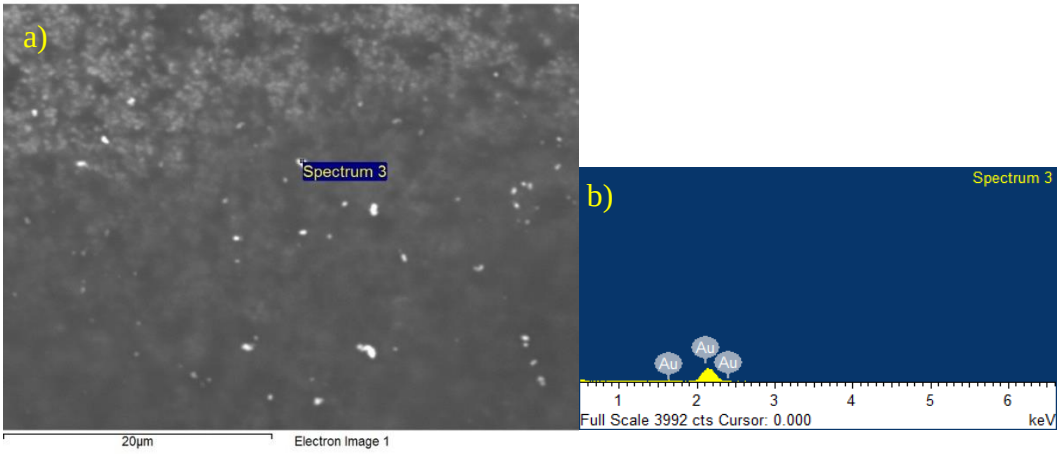

Figure C2. SEM-EDX of optimized 1:1 IL-1B:Au molar ratio synthesis. The concentrations used in these syntheses were 0.762 mM IL-1B, 0.762 mM $HAuCl_4$, 0.381 mM $NaBH_4$. Elemental analysis gave 100 (w)%. a) SEM image b) EDX

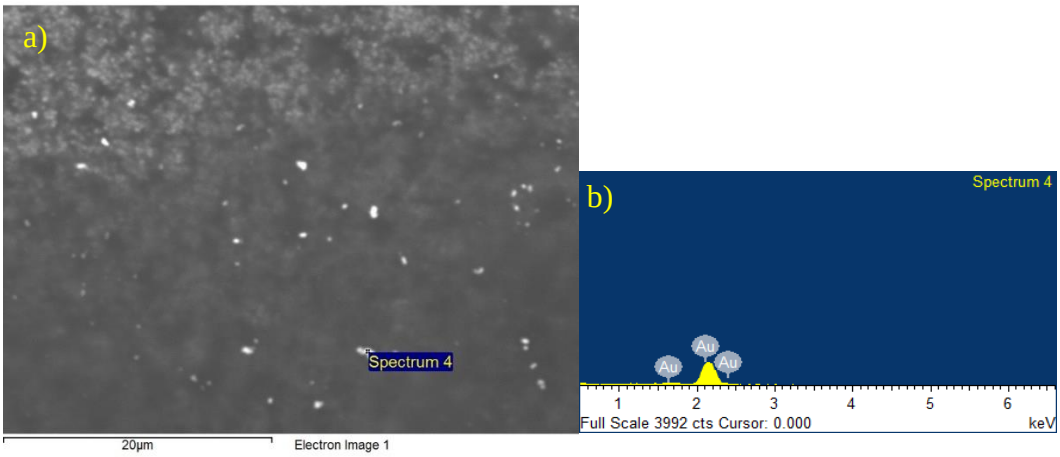

Figure C3. SEM-EDX of optimized 1:1 IL-1B:Au molar ratio synthesis. The concentrations used in these syntheses were 0.762 mM IL-1B, 0.762 mM $HAuCl_4$, 0.381 mM $NaBH_4$. Elemental analysis gave 100 (w)%. a) SEM image b) EDX

APPENDIX D

ADDITIONAL SEM/EDX OF OPTIMIZED GOLD NANOPARTICLE SYNTHESES WITH IL-2

The following are additional SEM/EDX of the optimized gold nanoparticle syntheses with IL-2.

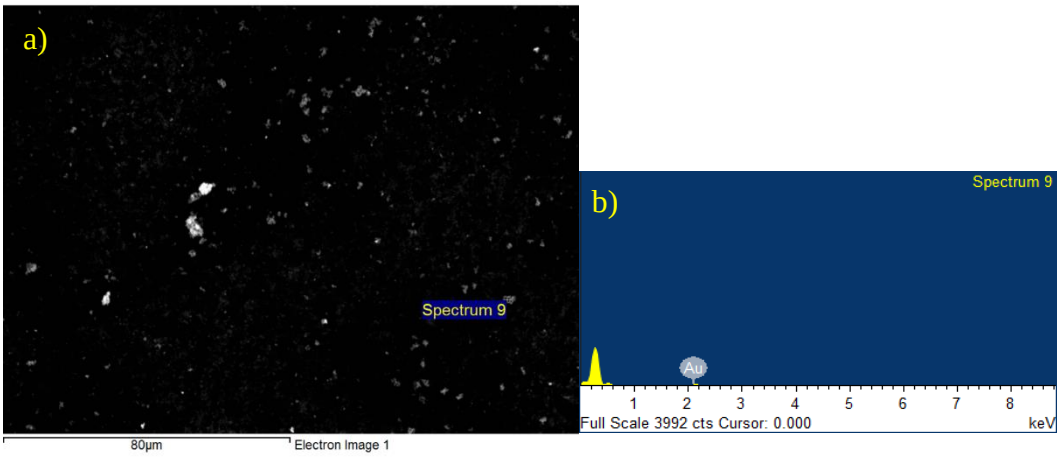

Figure D1. SEM-EDX of optimized 10:1 IL-2:$HAuCl_4$ molar ratio synthesis. The concentrations used in these syntheses were 7.62 mM IL-2, 0.762 mM $HAuCl_4$, 0.381 mM $NaBH_4$. Elemental analysis gave 100 (w) % gold. a) SEM image b) EDX

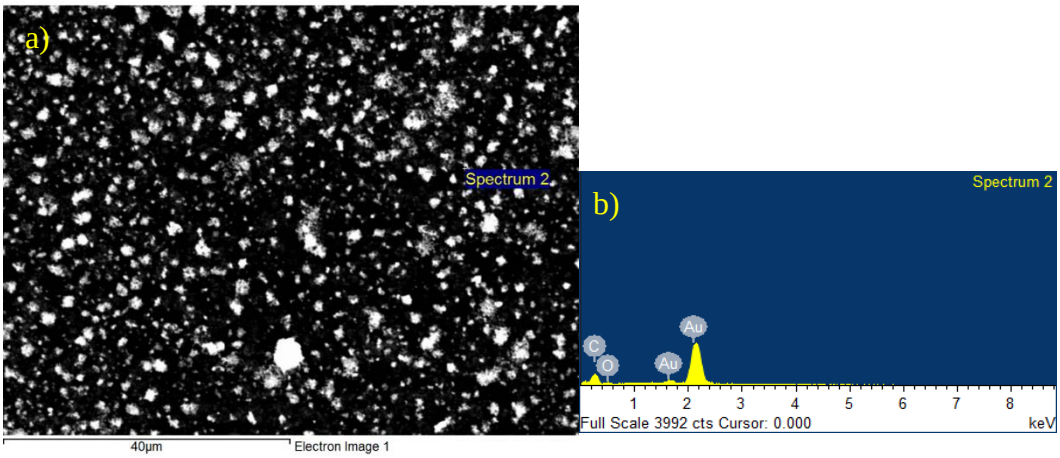

Figure D2. SEM-EDX of optimized 5:1 IL-2:$HAuCl_4$ molar ratio synthesis. The concentrations used in these syntheses were 3.81 mM IL-2, 0.762 mM $HAuCl_4$, 0.381 mM $NaBH_4$. Elemental analysis gave 67.25 (w)% gold, 30.25 (w)% carbon, and 2.50 (w)% . a) SEM image b) EDX

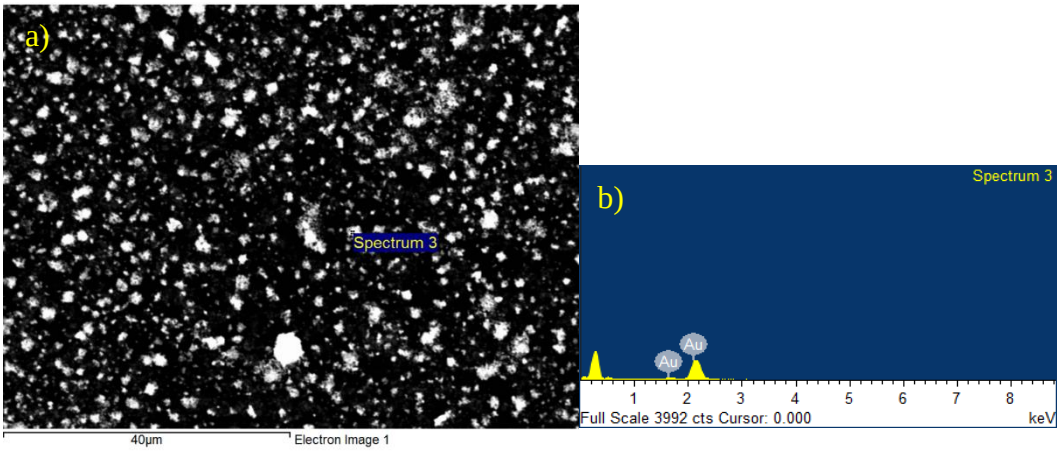

Figure D3. SEM-EDX of optimized 5:1 IL-2:$HAuCl_4$ molar ratio synthesis. The concentrations used in these syntheses were 3.81 mM IL-2, 0.762 mM $HAuCl_4$, 0.381 mM $NaBH_4$. Elemental analysis gave 100 (w)% gold. a) SEM image b) EDX

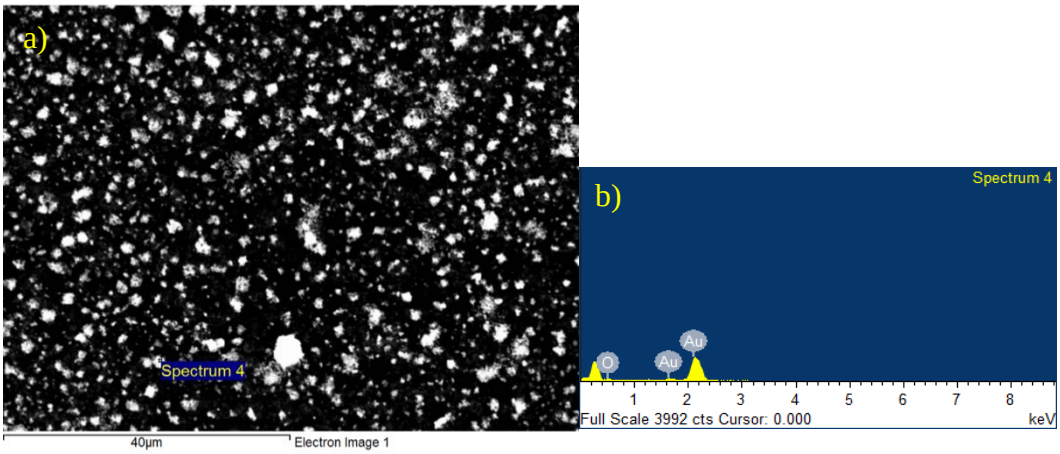

Figure D4. SEM-EDX of optimized 5:1 IL-2:$HAuCl_4$ molar ratio synthesis. The concentrations used in these syntheses were 3.81 mM IL-2, 0.762 mM $HAuCl_4$, 0.381 mM $NaBH_4$. Elemental analysis gave 93.21 (w)% gold and 6.79 (w)% oxygen. a) SEM image b) EDX

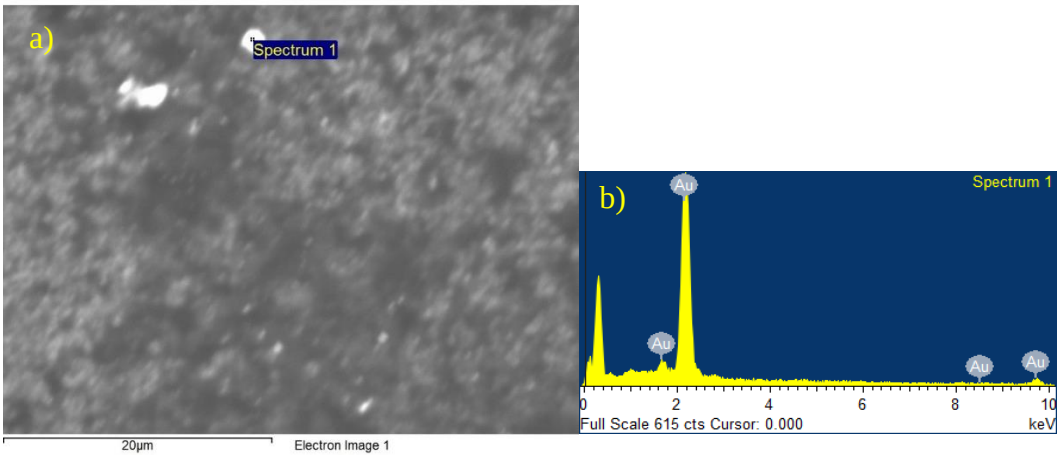

Figure D5. SEM-EDX of optimized 1:1 IL-2:$HAuCl_4$ molar ratio synthesis. The concentrations used in these syntheses were 0.762 mM IL-2, 0.762 mM $HAuCl_4$, 0.381 mM $NaBH_4$. Elemental analysis gave 89.14 (w)% gold and 10.86 (w)% oxygen. a) SEM image b) EDX

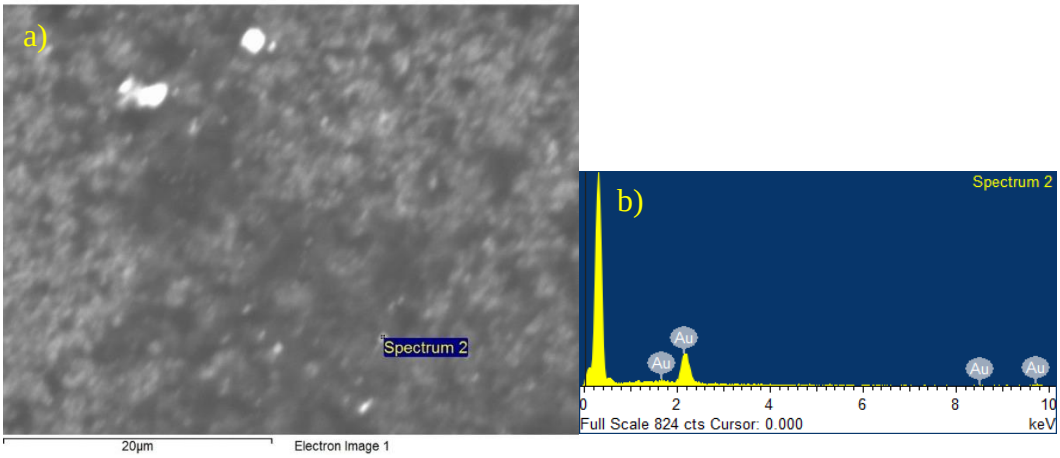

Figure D6. SEM-EDX of optimized 1:1 IL-2:$HAuCl_4$ molar ratio synthesis. The concentrations used in these syntheses were 0.762 mM IL-2, 0.762 mM $HAuCl_4$, 0.381 mM $NaBH_4$. Elemental analysis gave 89.14 (w)% gold and 10.86 (w)% oxygen. a) SEM image b) EDX

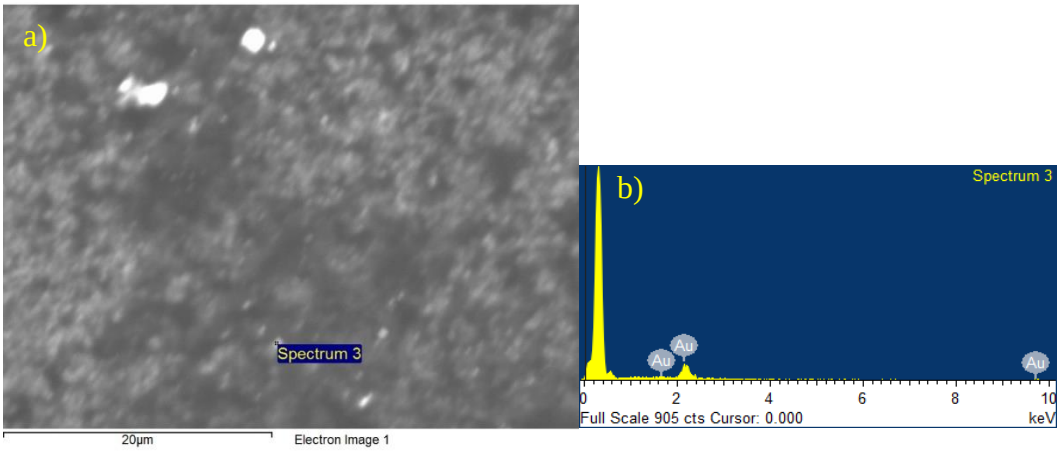

Figure D7. SEM-EDX of optimized 1:1 IL-2:$HAuCl_4$ molar ratio synthesis. The concentrations used in these syntheses were 0.762 mM IL-2, 0.762 mM $HAuCl_4$, 0.381 mM $NaBH_4$. Elemental analysis gave 89.14 (w)% gold and 10.86 (w)% oxygen. a) SEM image b) EDX

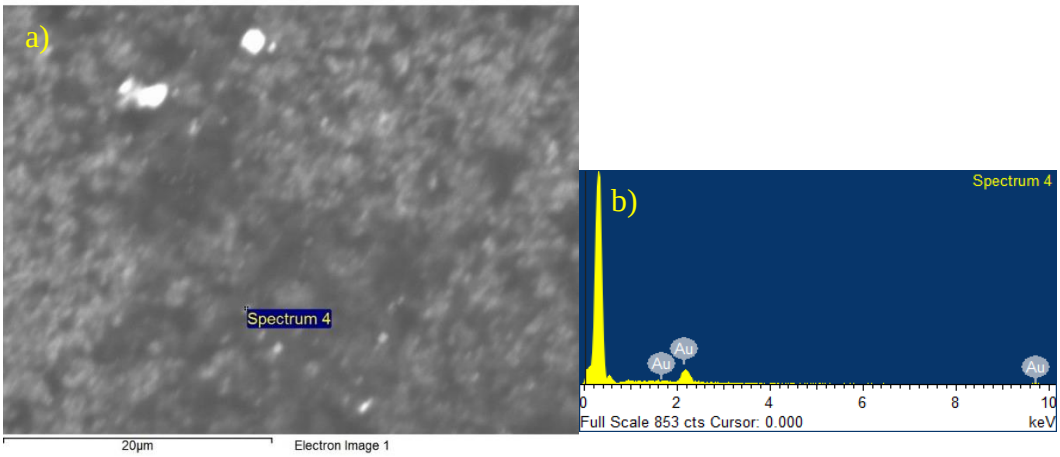

Figure D8. SEM-EDX of optimized 1:1 IL-2:$HAuCl_4$ molar ratio synthesis. The concentrations used in these syntheses were 0.762 mM IL-2, 0.762 mM $HAuCl_4$, 0.381 mM $NaBH_4$. Elemental analysis gave 89.14 (w)% gold and 10.86 (w)% oxygen. a) SEM image b) EDX

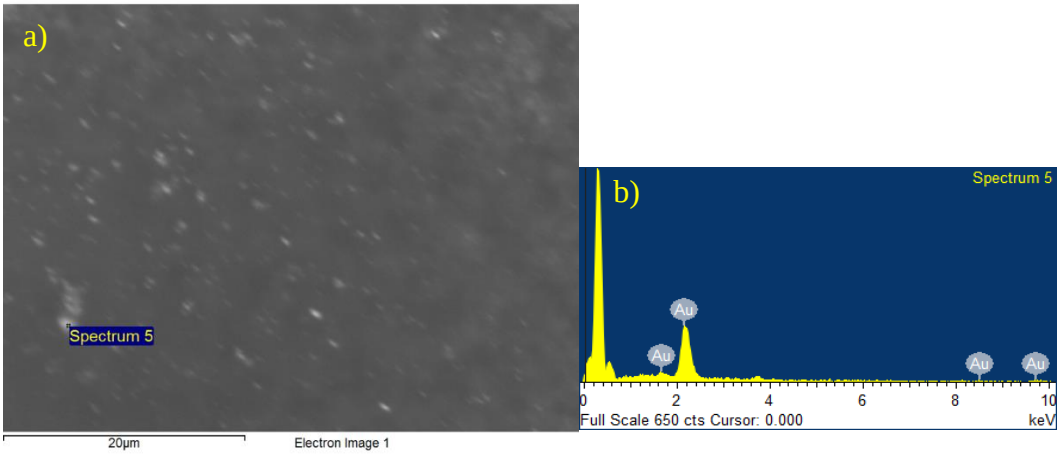

Figure D9. SEM-EDX of optimized 1:1 IL-2:$HAuCl_4$ molar ratio synthesis. The concentrations used in these syntheses were 0.762 mM IL-2, 0.762 mM $HAuCl_4$, 0.381 mM $NaBH_4$. Elemental analysis gave 89.14 (w)% gold and 10.86 (w)% oxygen. a) SEM image b) EDX

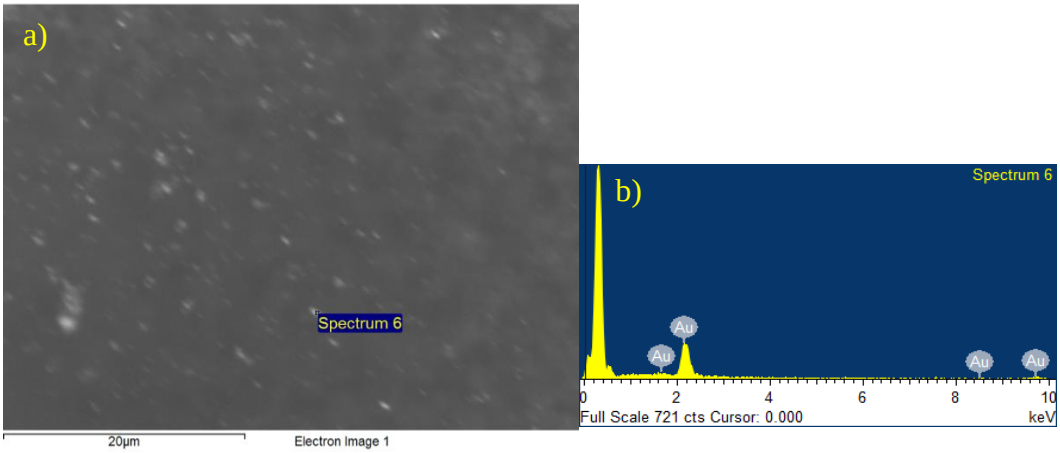

Figure D10. SEM-EDX of optimized 1:1 IL-2:$HAuCl_4$ molar ratio synthesis. The concentrations used in these syntheses were 0.762 mM IL-2, 0.762 mM $HAuCl_4$, 0.381 mM $NaBH_4$. Elemental analysis gave 89.14 (w)% gold and 10.86 (w)% oxygen. a) SEM image b) EDX

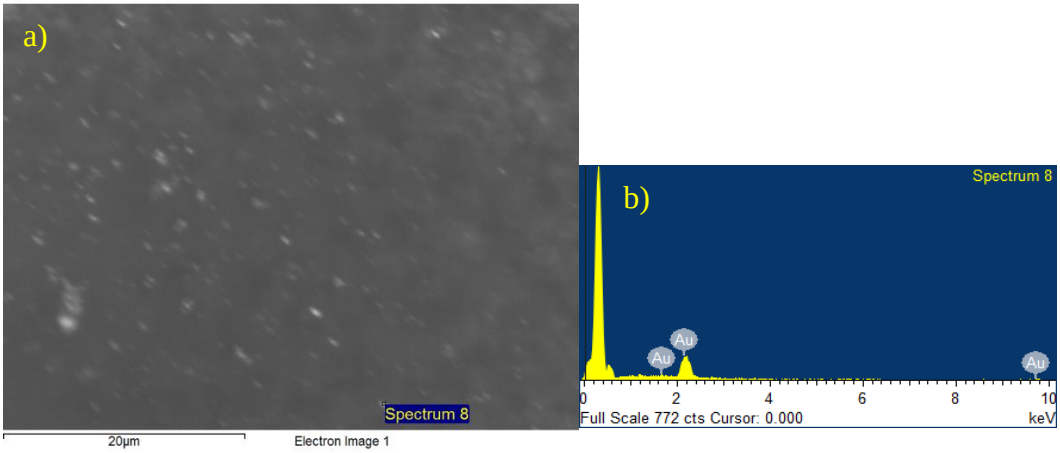

Figure D11. SEM-EDX of optimized 1:1 IL-2:$HAuCl_4$ molar ratio synthesis. The concentrations used in these syntheses were 0.762 mM IL-2, 0.762 mM $HAuCl_4$, 0.381 mM $NaBH_4$. Elemental analysis gave 89.14 (w)% gold and 10.86 (w)% oxygen. a) SEM image b) EDX

APPENDIX E

ADDITIONAL SEM/EDX OF GOLD NANOPARTICLE SYNTHESES WITH IL-1A PURIFIED WITH THE NEW WASHING PROTOCOL

The following are additional SEM/EDX of gold nanoparticle syntheses with IL-1A purified with the new washing protocol.

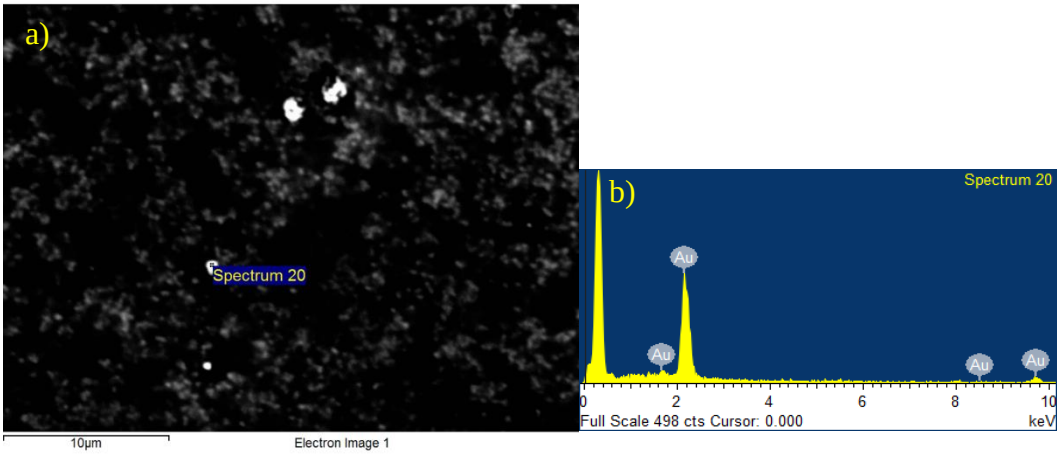

Figure E1. SEM-EDX of acetone-washed 5:1 IL-1A:$HAuCl_4$ molar ratio nanoparticles redispersed in nanopure water. The concentrations used were 3.81 mM IL-1A, 0.762 mM $HAuCl_4$, 1.524 mM $NaBH_4$. Elemental analysis gave 89.14 (w)% gold and 10.86 (w)% oxygen. a) SEM image b) EDX

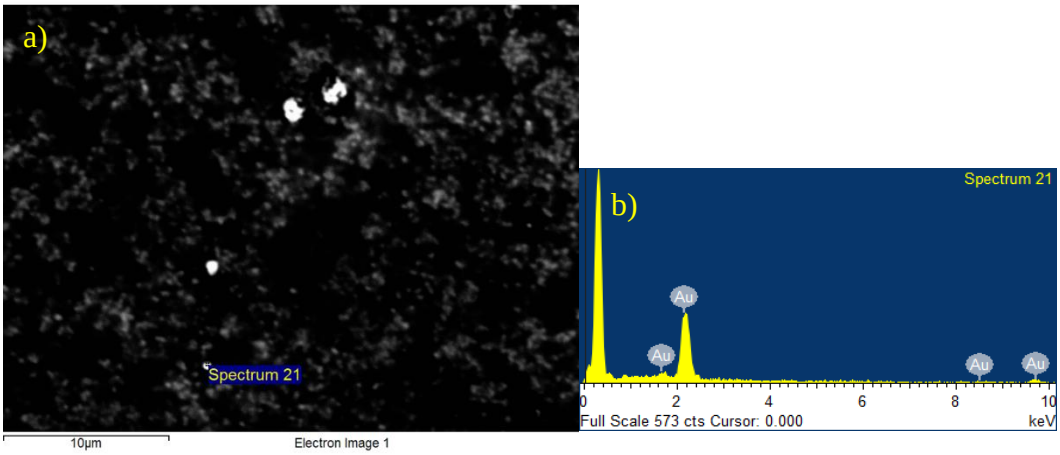

Figure E2. SEM-EDX of acetone-washed 5:1 IL-1A:$HAuCl_4$ molar ratio nanoparticles redispersed in nanopure water. The concentrations used were 3.81 mM IL-1A, 0.762 mM $HAuCl_4$, 1.524 mM $NaBH_4$. Elemental analysis gave 89.14 (w)% gold and 10.86 (w)% oxygen. a) SEM image b) EDX

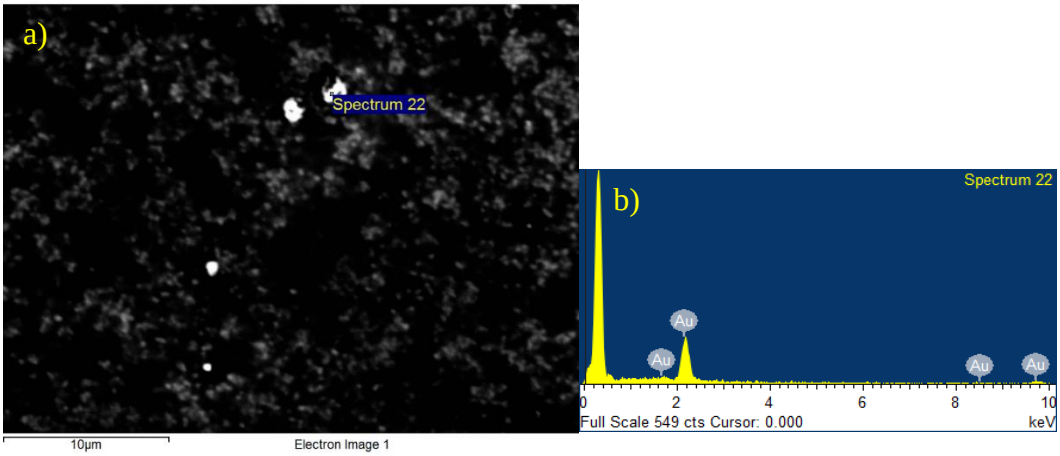

Figure E3. SEM-EDX of acetone-washed 5:1 IL-1A:$HAuCl_4$ molar ratio nanoparticles redispersed in nanopure water. The concentrations used were 3.81 mM IL-1A, 0.762 mM $HAuCl_4$, 1.524 mM $NaBH_4$. Elemental analysis gave 89.14 (w)% gold and 10.86 (w)% oxygen. a) SEM image b) EDX

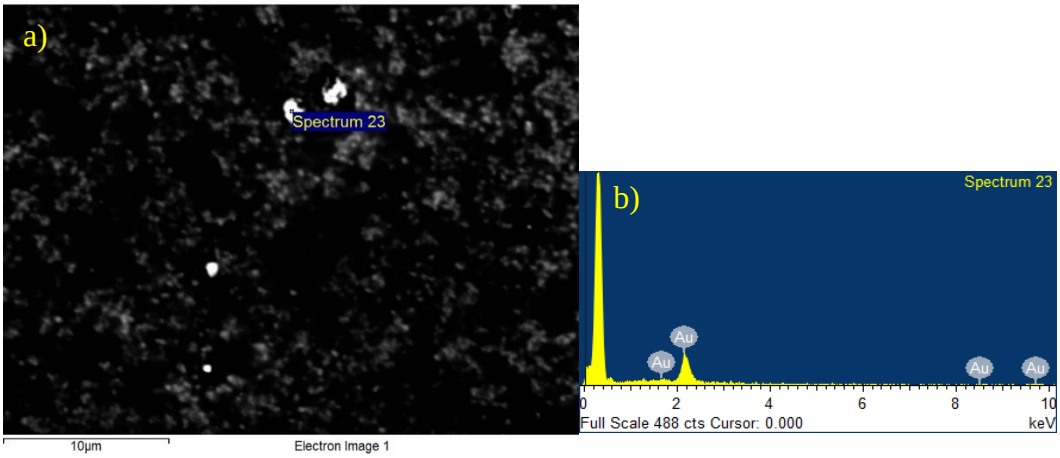

Figure E4. SEM-EDX of acetone-washed 5:1 IL-1A:$HAuCl_4$ molar ratio nanoparticles redispersed in nanopure water. The concentrations used were 3.81 mM IL-1A, 0.762 mM $HAuCl_4$, 1.524 mM $NaBH_4$. Elemental analysis gave 89.14 (w)% gold and 10.86 (w)% oxygen. a) SEM image b) EDX

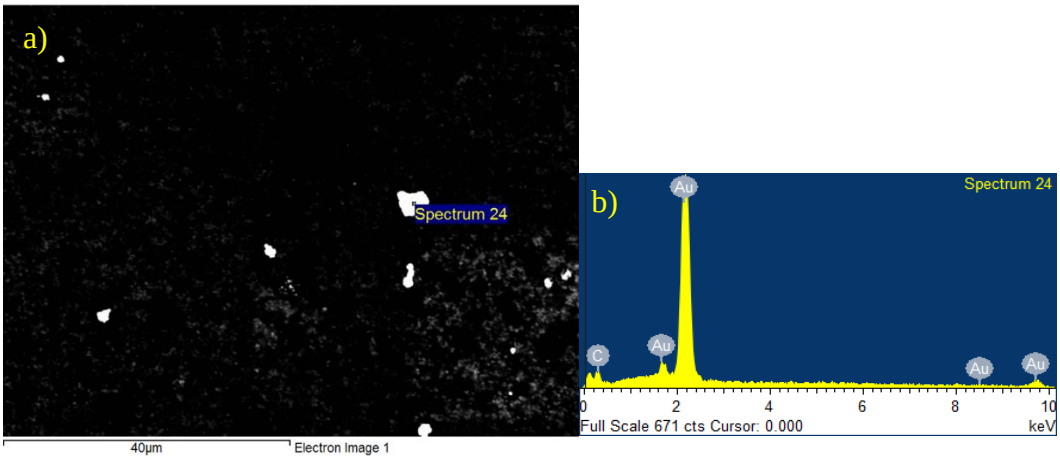

Figure E5. SEM-EDX of acetone-washed 5:1 IL-1A:$HAuCl_4$ molar ratio nanoparticles redispersed in nanopure water. The concentrations used were 3.81 mM IL-1A, 0.762 mM $HAuCl_4$, 1.524 mM $NaBH_4$. Elemental analysis gave 66.32 (w)% gold, 6.99 (w)% carbon, and 26.69 (w)% oxygen. a) SEM image b) EDX

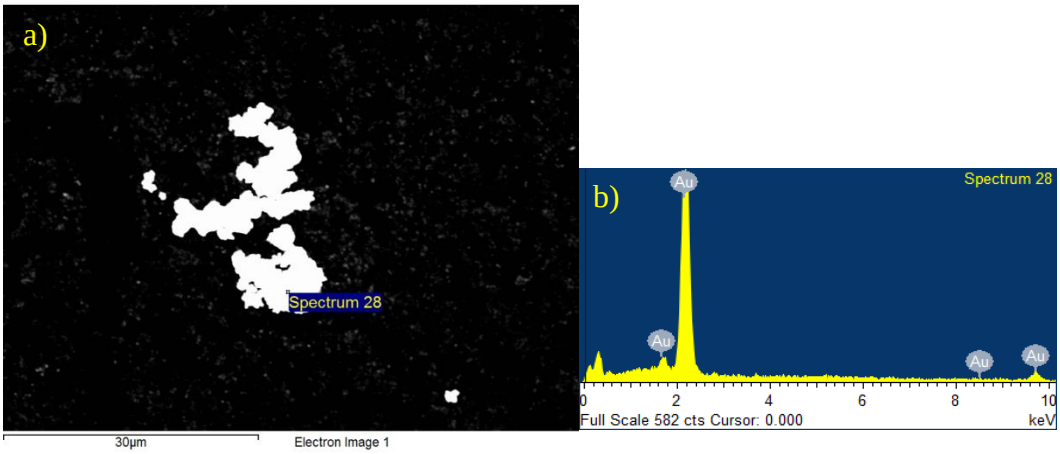

Figure E6. SEM-EDX of acetone-washed 5:1 IL-1A:$HAuCl_4$ molar ratio nanoparticles redispersed in nanopure water. The concentrations used were 3.81 mM IL-1A, 0.762 mM $HAuCl_4$, 1.524 mM $NaBH_4$. Elemental analysis gave 89.14 (w)% gold and 10.86 (w)% oxygen. a) SEM image b) EDX

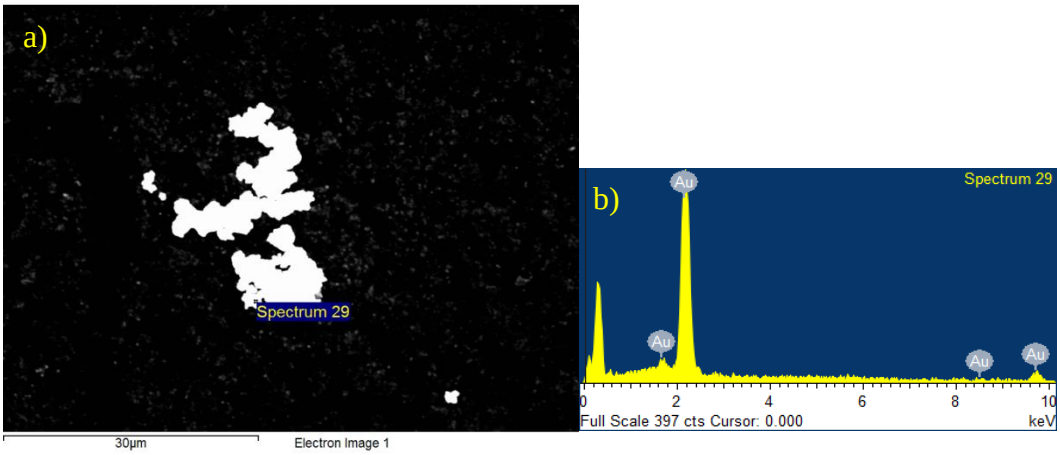

Figure E7. SEM-EDX of acetone-washed 5:1 IL-1A:$HAuCl_4$ molar ratio nanoparticles redispersed in nanopure water. The concentrations used were 3.81 mM IL-1A, 0.762 mM $HAuCl_4$, 1.524 mM $NaBH_4$. Elemental analysis gave 89.14 (w)% gold and 10.86 (w)% oxygen. a) SEM image b) EDX

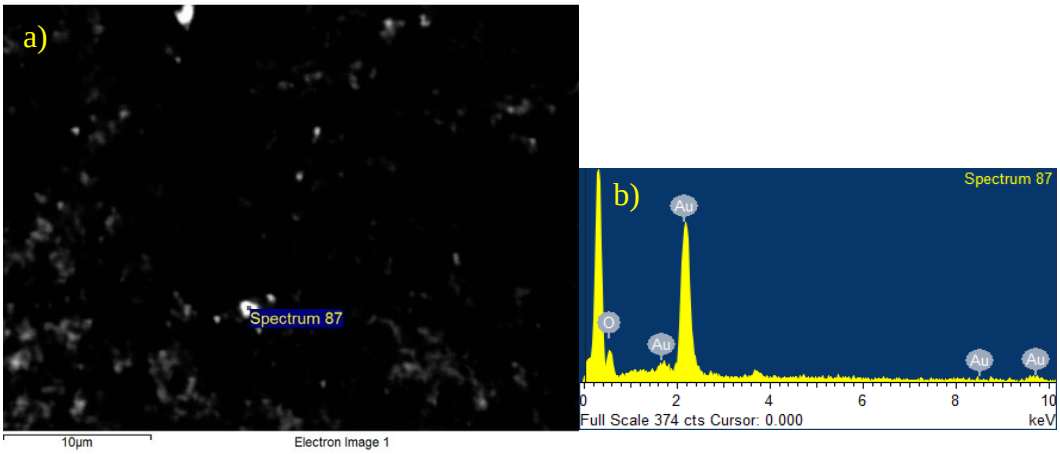

Figure E8. SEM-EDX of acetone-washed 5:1 IL-1A:$HAuCl_4$ molar ratio nanoparticles redispersed in ethanol. The concentrations used were 3.81 mM IL-1A, 0.762 mM $HAuCl_4$, 1.524 mM $NaBH_4$. Elemental analysis gave 89.14 (w)% gold and 10.86 (w)% oxygen. a) SEM image b) EDX

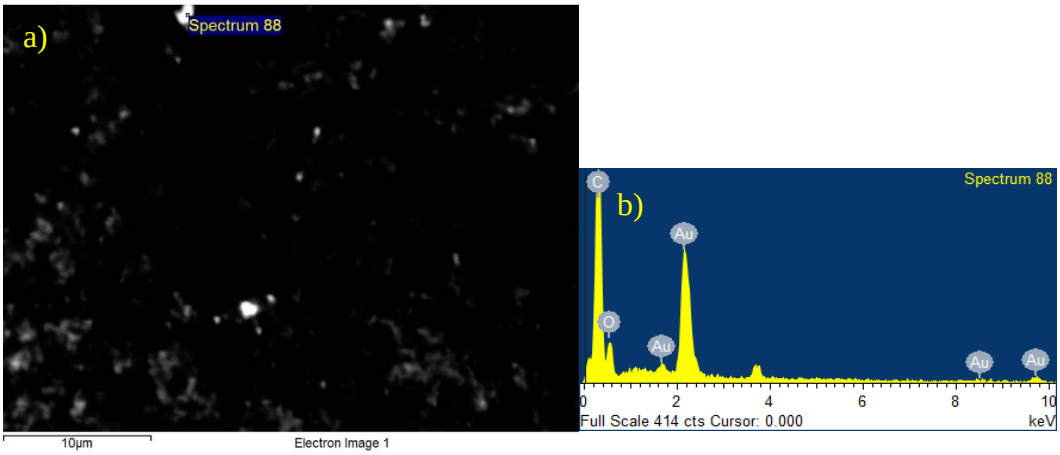

Figure E9. SEM-EDX of acetone-washed 5:1 IL-1A:$HAuCl_4$ molar ratio nanoparticles redispersed in ethanol. The concentrations used were 3.81 mM IL-1A, 0.762 mM $HAuCl_4$, 1.524 mM $NaBH_4$. Elemental analysis gave 11.11 (w)% gold, 23.89 (w)% carbon and 10.86 (w)% oxygen. a) SEM image b) EDX

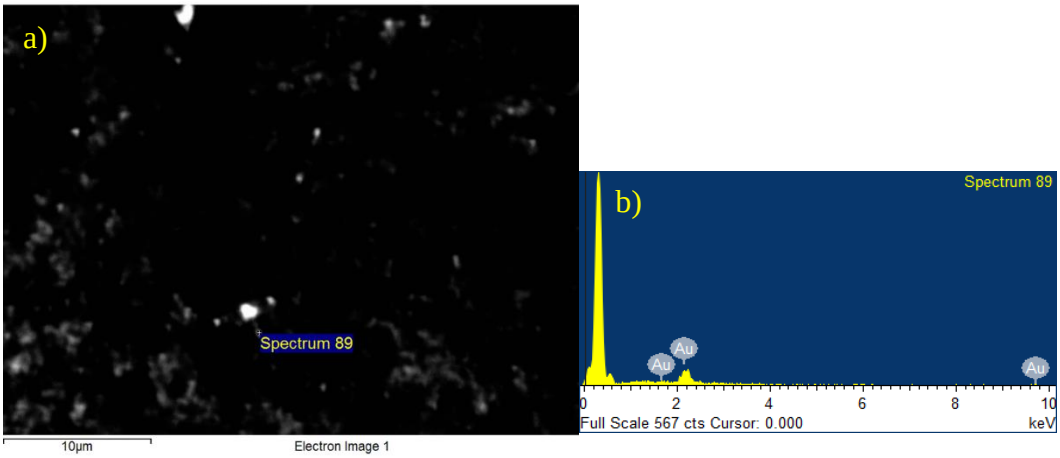

Figure E10. SEM-EDX of acetone-washed 5:1 IL-1A:$HAuCl_4$ molar ratio nanoparticles redispersed in ethanol. The concentrations used were 3.81 mM IL-1A, 0.762 mM $HAuCl_4$, 1.524 mM $NaBH_4$. Elemental analysis gave 89.14 (w)% gold and 10.86 (w)% oxygen. a) SEM image b) EDX

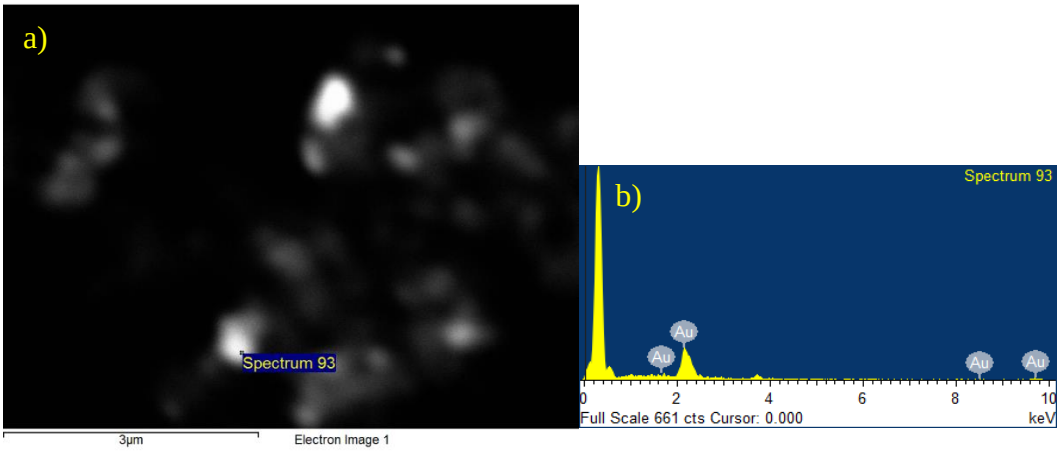

Figure E11. SEM-EDX of acetone-washed 5:1 IL-1A:$HAuCl_4$ molar ratio nanoparticles redispersed in ethanol. The concentrations used were 3.81 mM IL-1A, 0.762 mM $HAuCl_4$, 1.524 mM $NaBH_4$. Elemental analysis gave 89.14 (w)% gold and 10.86 (w)% oxygen. a) SEM image b) EDX

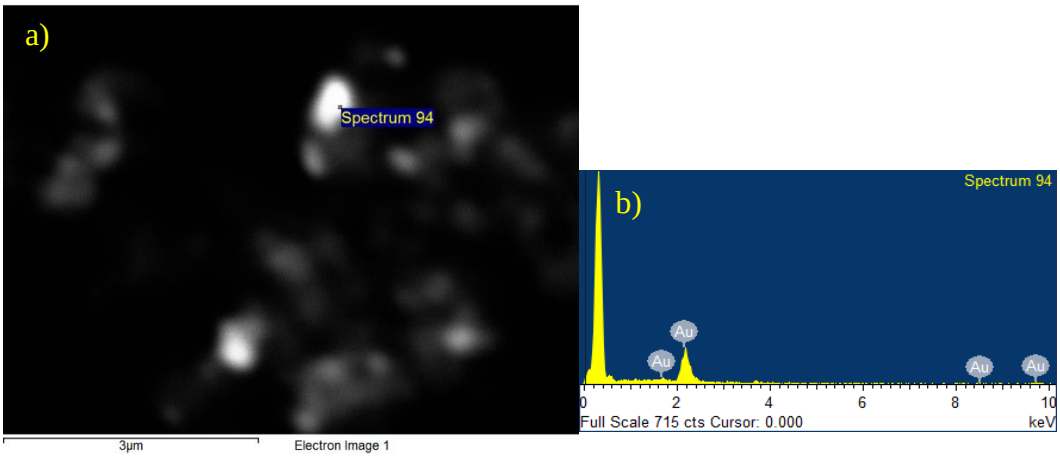

Figure E12. SEM-EDX of acetone-washed 5:1 IL-1A:$HAuCl_4$ molar ratio nanoparticles redispersed in ethanol. The concentrations used were 3.81 mM IL-1A, 0.762 mM $HAuCl_4$, 1.524 mM $NaBH_4$. Elemental analysis gave 89.14 (w)% gold and 10.86 (w)% oxygen. a) SEM image b) EDX

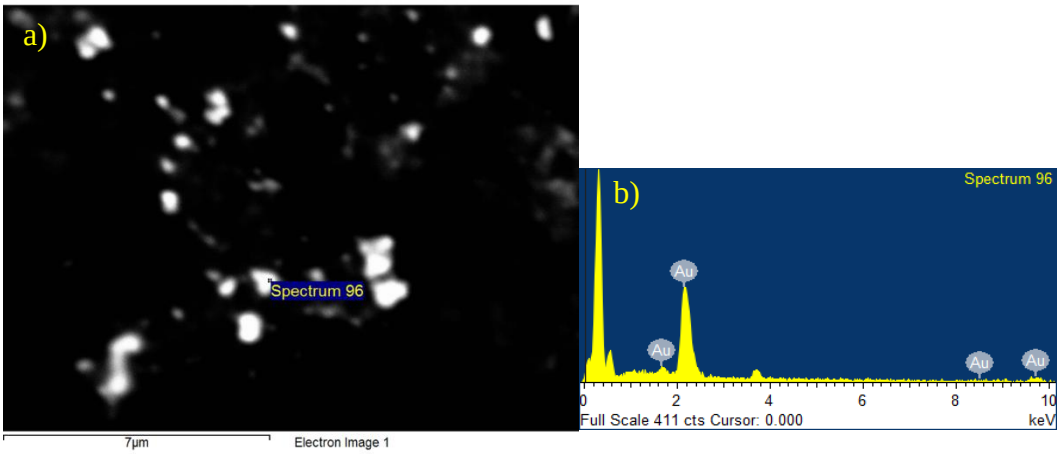

Figure E13. SEM-EDX of acetone-washed 5:1 IL-1A:$HAuCl_4$ molar ratio nanoparticles redispersed in ethanol. The concentrations used were 3.81 mM IL-1A, 0.762 mM $HAuCl_4$, 1.524 mM $NaBH_4$. Elemental analysis gave 89.14 (w)% gold and 10.86 (w)% oxygen. a) SEM image b) EDX

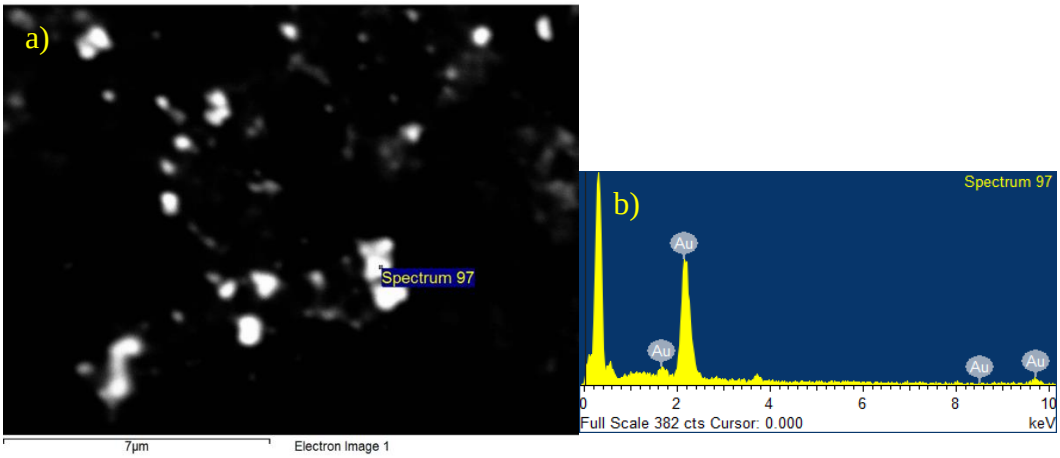

Figure E14. SEM-EDX of acetone-washed 5:1 IL-1A:$HAuCl_4$ molar ratio nanoparticles redispersed in ethanol. The concentrations used were 3.81 mM IL-1A, 0.762 mM $HAuCl_4$, 1.524 mM $NaBH_4$. Elemental analysis gave 89.14 (w)% gold and 10.86 (w)% oxygen. a) SEM image b) EDX

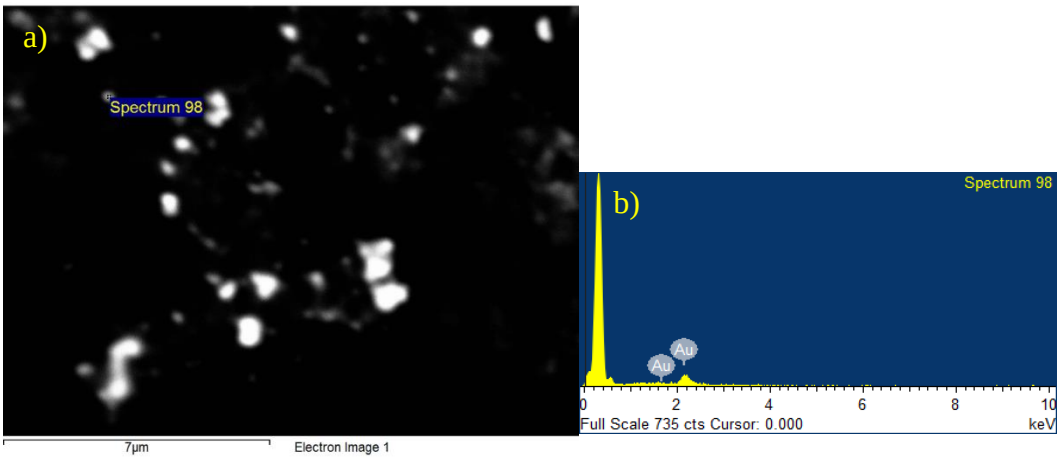

Figure E15. SEM-EDX of acetone-washed 5:1 IL-1A:$HAuCl_4$ molar ratio nanoparticles redispersed in ethanol. The concentrations used were 3.81 mM IL-1A, 0.762 mM $HAuCl_4$, 1.524 mM $NaBH_4$. Elemental analysis gave 89.14 (w)% gold and 10.86 (w)% oxygen. a) SEM image b) EDX

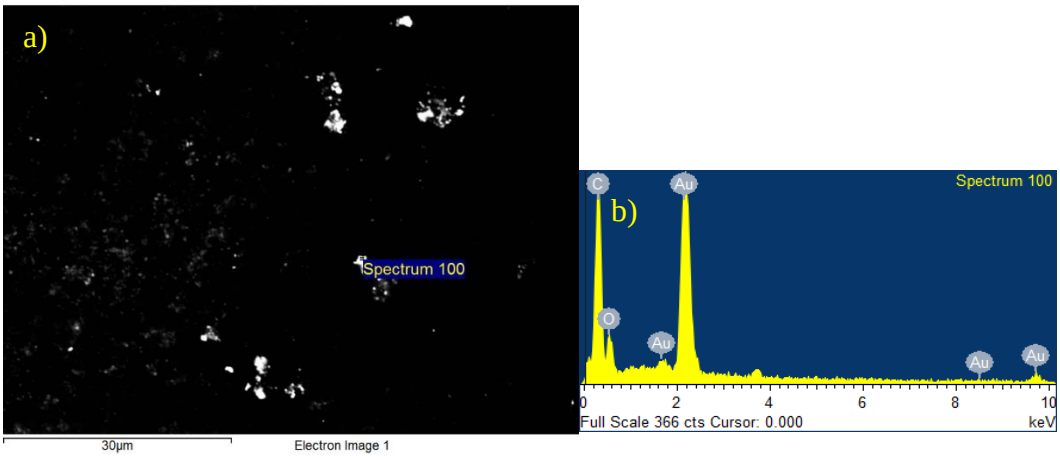

Figure E16. SEM-EDX of acetone-washed 5:1 IL-1A:$HAuCl_4$ molar ratio nanoparticles redispersed in ethanol. The concentrations used were 3.81 mM IL-1A, 0.762 mM $HAuCl_4$, 1.524 mM $NaBH_4$. Elemental analysis gave 18.08 (w)% gold, 21.76 (w)% carbon and 10.86 (w)% oxygen. a) SEM image b) EDX

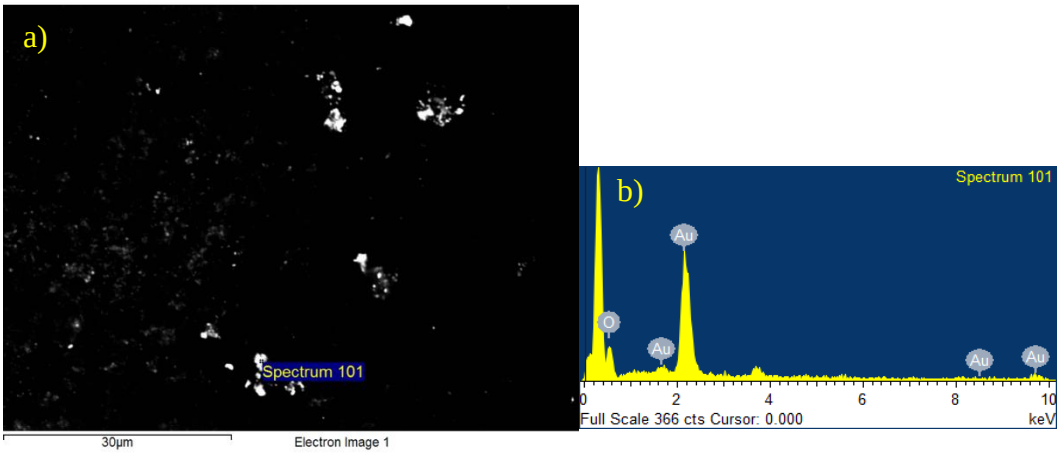

Figure E17. SEM-EDX of acetone-washed 5:1 IL-1A:$HAuCl_4$ molar ratio nanoparticles redispersed in ethanol. The concentrations used were 3.81 mM IL-1A, 0.762 mM $HAuCl_4$, 1.524 mM $NaBH_4$. Elemental analysis gave 89.14 (w)% gold and 10.86 (w)% oxygen. a) SEM image b) EDX

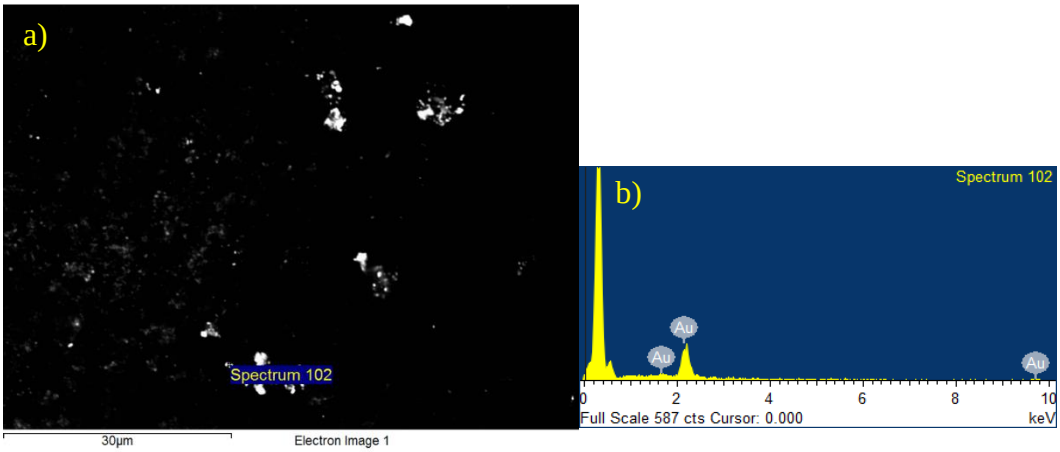

Figure E18. SEM-EDX of acetone-washed 5:1 IL-1A:$HAuCl_4$ molar ratio nanoparticles redispersed in ethanol. The concentrations used were 3.81 mM IL-1A, 0.762 mM $HAuCl_4$, 1.524 mM $NaBH_4$. Elemental analysis gave 89.14 (w)% gold and 10.86 (w)% oxygen. a) SEM image b) EDX

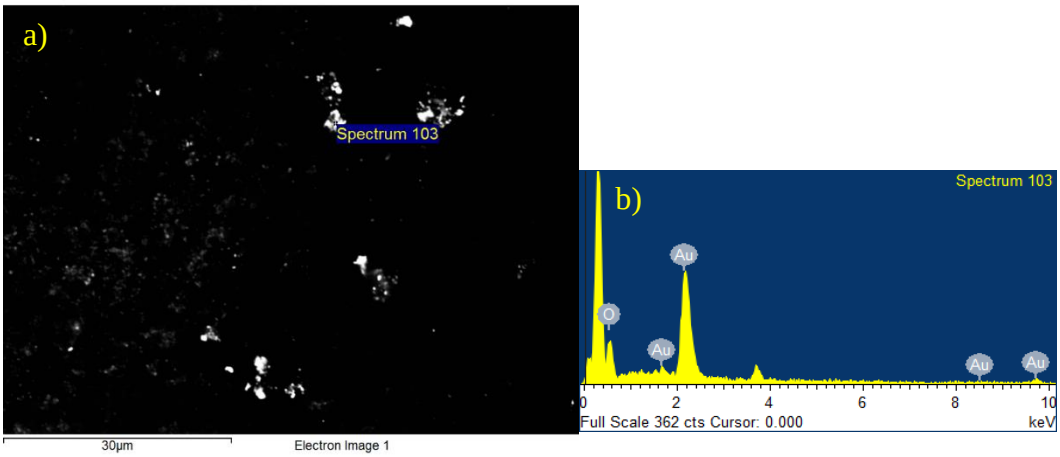

Figure E19. SEM-EDX of acetone-washed 5:1 IL-1A:$HAuCl_4$ molar ratio nanoparticles redispersed in ethanol. The concentrations used were 3.81 mM IL-1A, 0.762 mM $HAuCl_4$, 1.524 mM $NaBH_4$. Elemental analysis gave 89.14 (w)% gold and 10.86 (w)% oxygen. a) SEM image b) EDX

APPENDIX F

ADDITIONAL SEM/EDX OF GOLD NANOPARTICLE SYNTHESES WITH IL-1B PURIFIED WITH THE NEW WASHING PROTOCOL

The following are additional SEM/EDX of gold nanoparticle syntheses with IL-1B purified with the new washing protocol.

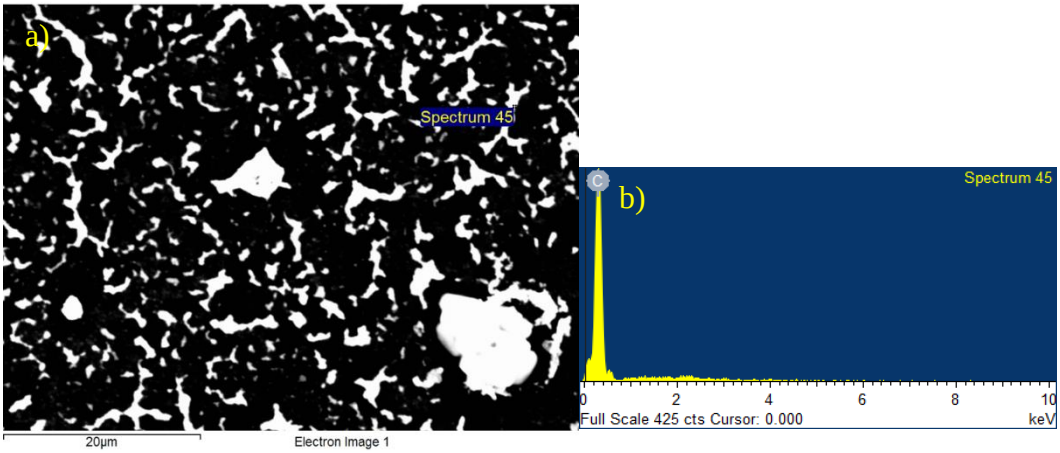

Figure F1. SEM-EDX of the reaction mixture of 5:1 IL-1B:$HAuCl_4$ molar ratio. The concentrations used were 3.81 mM IL-1B, 0.762 mM $HAuCl_4$, 1.524 mM $NaBH_4$. Elemental analysis gave 27.29 (w)% carbon and 72.71 (w)% oxygen. a) SEM image b) EDX

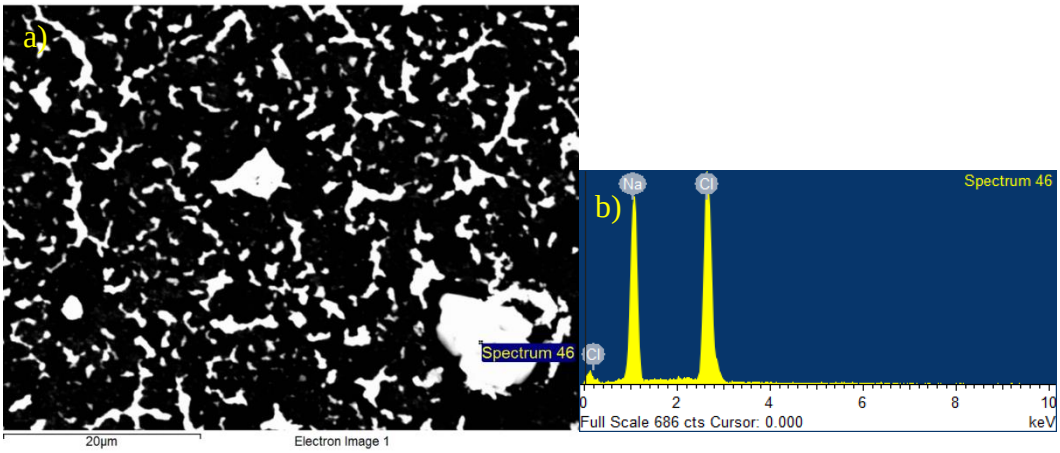

Figure F2. SEM-EDX of the reaction mixture of 5:1 IL-1B:$HAuCl_4$ molar ratio. The concentrations used were 3.81 mM IL-1B, 0.762 mM $HAuCl_4$, 1.524 mM $NaBH_4$. Elemental analysis gave 34.43 (w)% sodium, 53.58 (w)% chlorine, and 11.98 (w)% oxygen. a) SEM image b) EDX

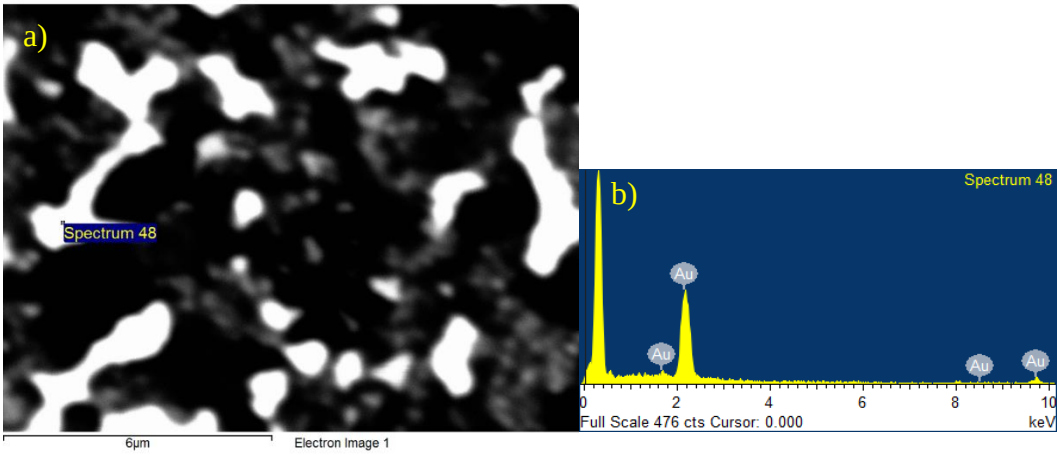

Figure F3. SEM-EDX of the reaction mixture of 5:1 IL-1B:$HAuCl_4$ molar ratio. The concentrations used were 3.81 mM IL-1B, 0.762 mM $HAuCl_4$, 1.524 mM $NaBH_4$. Elemental analysis gave 89.14 (w)% gold and 10.86 (w)% oxygen. a) SEM image b) EDX

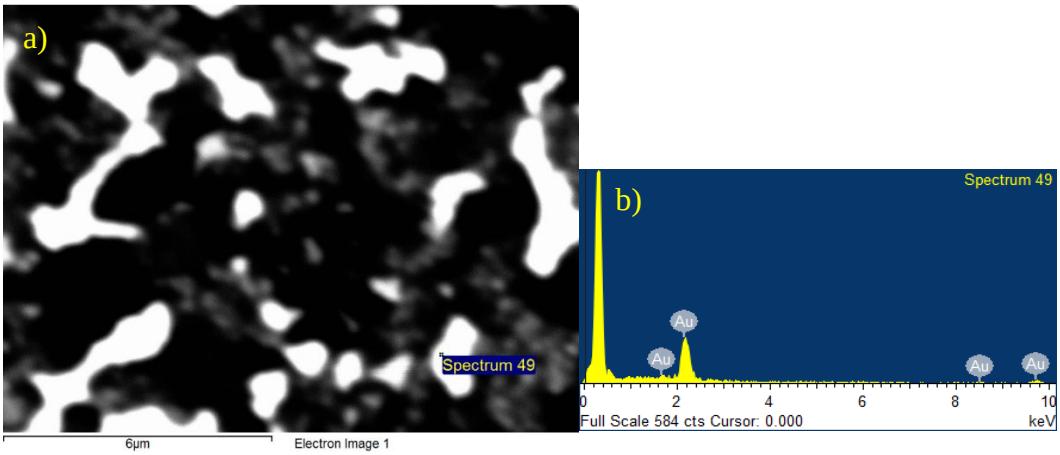

Figure F4. SEM-EDX of the reaction mixture of 5:1 IL-1B:$HAuCl_4$ molar ratio. The concentrations used were 3.81 mM IL-1B, 0.762 mM $HAuCl_4$, 1.524 mM $NaBH_4$. Elemental analysis gave 89.14 (w)% gold and 10.86 (w)% oxygen. a) SEM image b) EDX

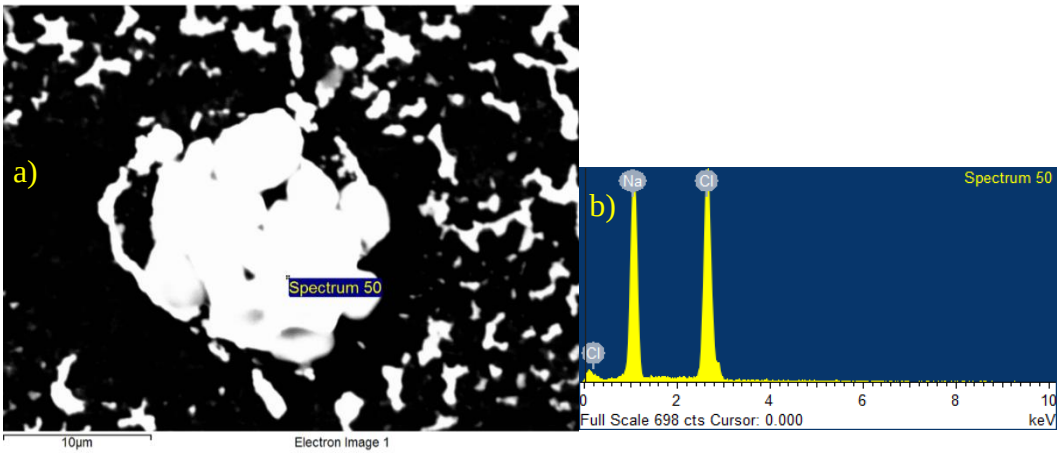

Figure F5. SEM-EDX of the reaction mixture of 5:1 IL-1B:$HAuCl_4$ molar ratio. The concentrations used were 3.81 mM IL-1B, 0.762 mM $HAuCl_4$, 1.524 mM $NaBH_4$. Elemental analysis gave 36.13 (w)% sodium, 51.30 (w)% chlorine and 10.86 (w)% oxygen. a) SEM image b) EDX

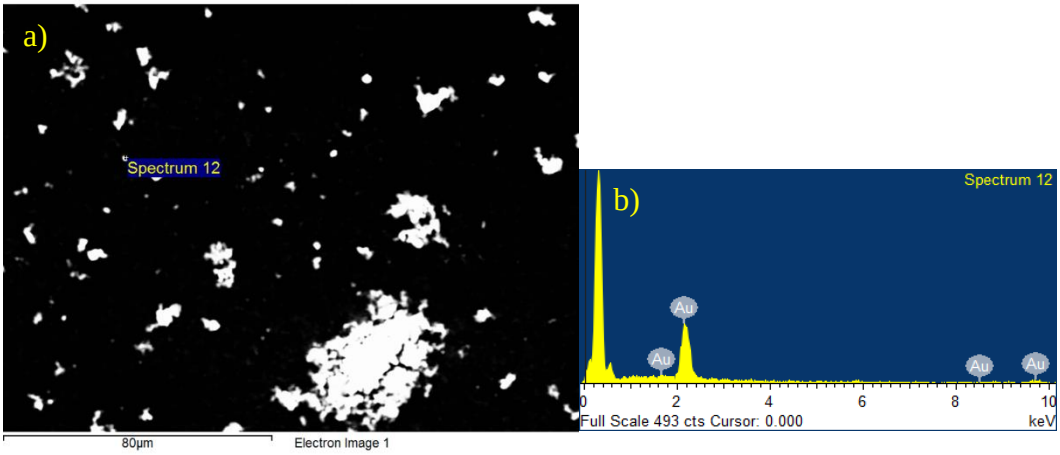

Figure F6. SEM-EDX of acetone-washed 5:1 IL-1B:$HAuCl_4$ molar ratio nanoparticles redispersed in nanopure water. The concentrations used were 3.81 mM IL-1B, 0.762 mM $HAuCl_4$, 1.524 mM $NaBH_4$. Elemental analysis gave 89.14 (w)% gold and 10.86 (w)% oxygen. a) SEM image b) EDX

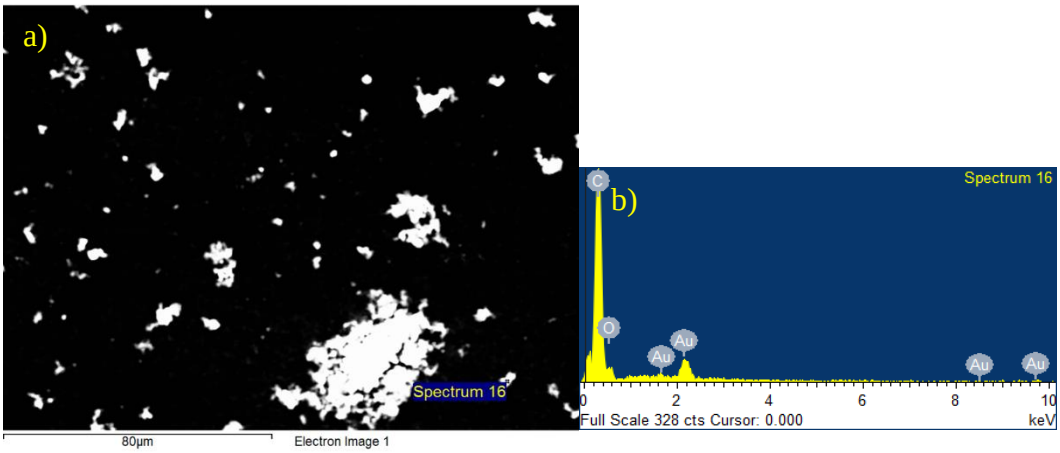

Figure F7. SEM-EDX of acetone-washed 5:1 IL-1B:$HAuCl_4$ molar ratio nanoparticles redispersed in nanopure water. The concentrations used were 3.81 mM IL-1B, 0.762 mM $HAuCl_4$, 1.524 mM $NaBH_4$. Elemental analysis gave 2.41 (w)% gold, 26.55 (w)% carbon and 71.04 (w)% oxygen. a) SEM image b) EDX

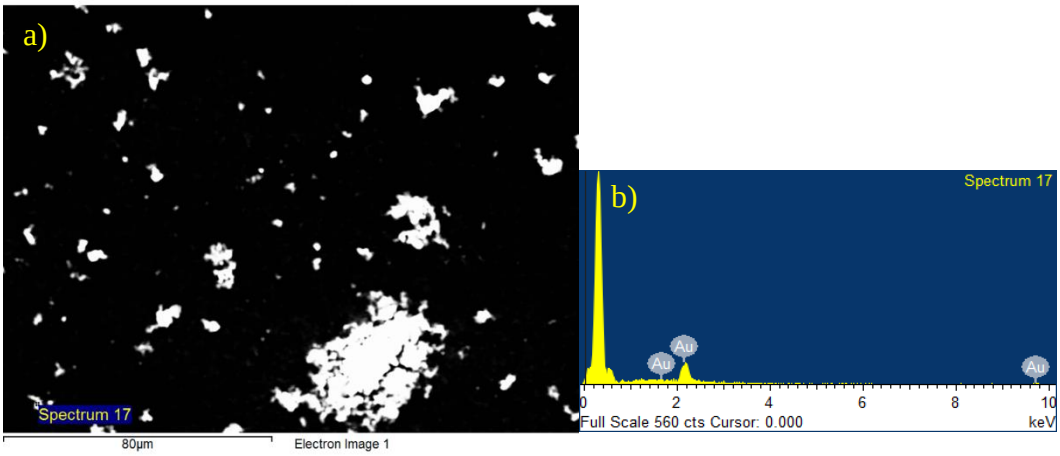

Figure F8. SEM-EDX of acetone-washed 5:1 IL-1B:$HAuCl_4$ molar ratio nanoparticles redispersed in nanopure water. The concentrations used were 3.81 mM IL-1B, 0.762 mM $HAuCl_4$, 1.524 mM $NaBH_4$. Elemental analysis gave 89.14 (w)% gold and 10.86 (w)% oxygen. a) SEM image b) EDX

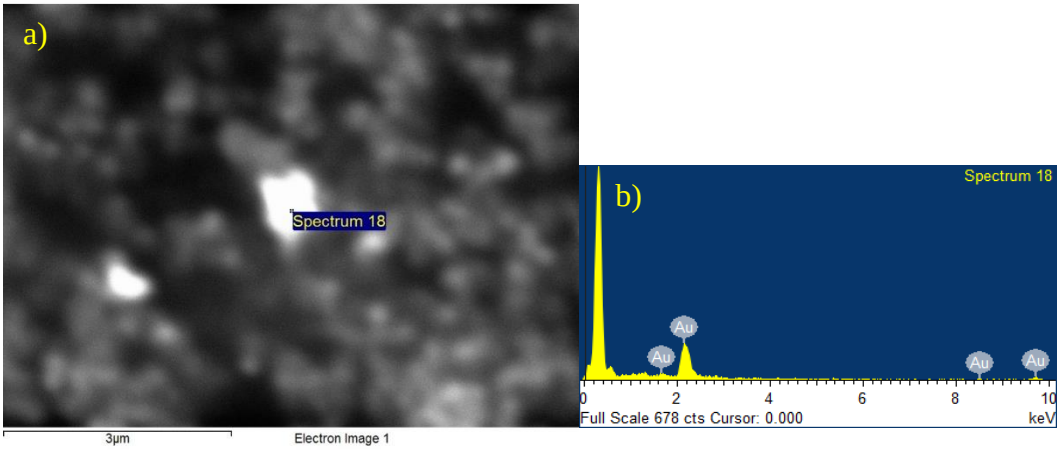

Figure F9. SEM-EDX of acetone-washed 5:1 IL-1B:$HAuCl_4$ molar ratio nanoparticles redispersed in nanopure water. The concentrations used were 3.81 mM IL-1B, 0.762 mM $HAuCl_4$, 1.524 mM $NaBH_4$. Elemental analysis gave 89.14 (w)% gold and 10.86 (w)% oxygen. a) SEM image b) EDX

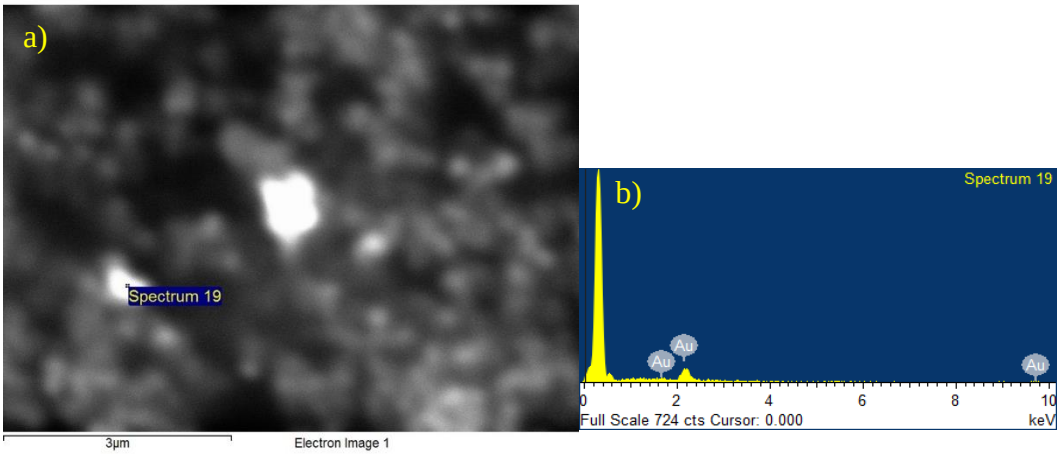

Figure F10. SEM-EDX of acetone-washed 5:1 IL-1B:$HAuCl_4$ molar ratio nanoparticles redispersed in nanopure water. The concentrations used were 3.81 mM IL-1B, 0.762 mM $HAuCl_4$, 1.524 mM $NaBH_4$. Elemental analysis gave 89.14 (w)% gold and 10.86 (w)% oxygen. a) SEM image b) EDX

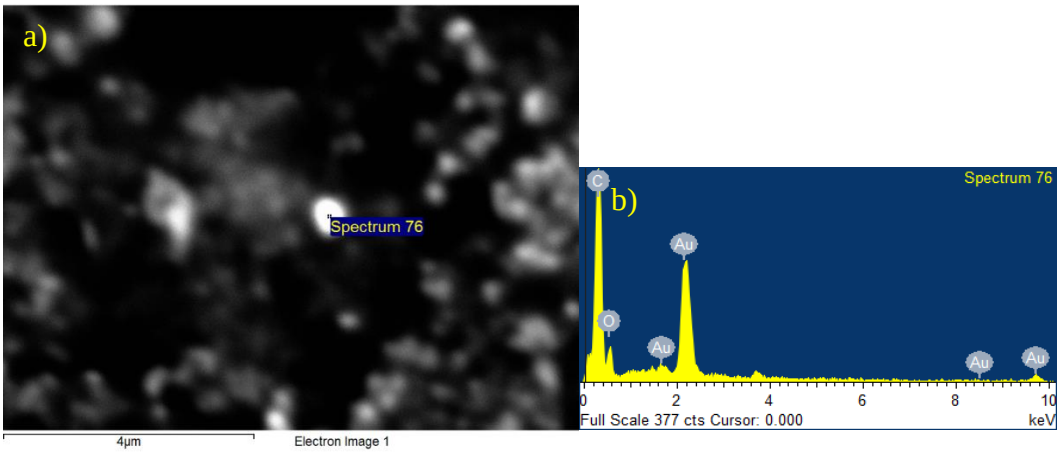

Figure F11. SEM-EDX of acetone-washed 5:1 IL-1B:$HAuCl_4$ molar ratio nanoparticles redispersed in ethanol. The concentrations used were 3.81 mM IL-1B, 0.762 mM $HAuCl_4$, 1.524 mM $NaBH_4$. Elemental analysis gave 11.09 (w)% gold, 23.90 (w)% carbon, and 65.01 (w)% oxygen. a) SEM image b) EDX

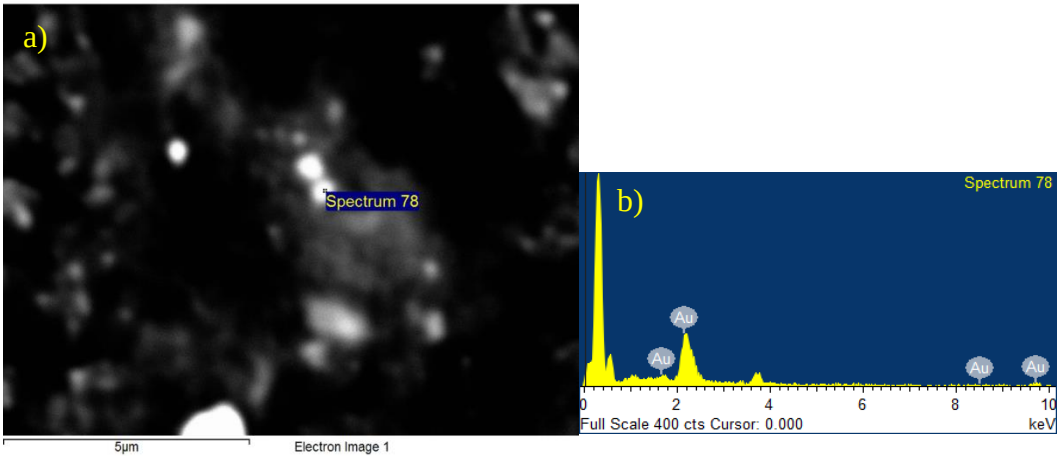

Figure F12. SEM-EDX of acetone-washed 5:1 IL-1B:$HAuCl_4$ molar ratio nanoparticles redispersed in ethanol. The concentrations used were 3.81 mM IL-1B, 0.762 mM $HAuCl_4$, 1.524 mM $NaBH_4$. Elemental analysis gave 89.14 (w)% gold and 10.86 (w)% oxygen. a) SEM image b) EDX

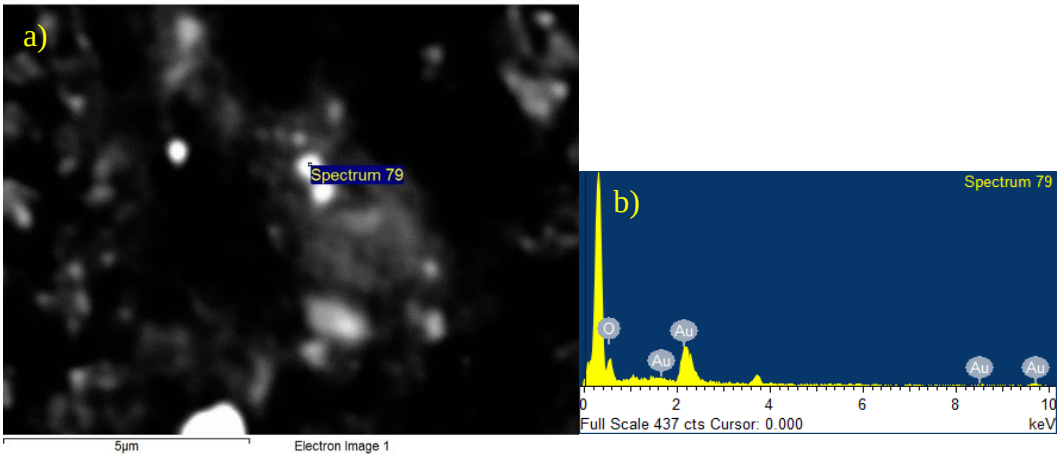

Figure F13. SEM-EDX of acetone-washed 5:1 IL-1B:$HAuCl_4$ molar ratio nanoparticles redispersed in ethanol. The concentrations used were 3.81 mM IL-1B, 0.762 mM $HAuCl_4$, 1.524 mM $NaBH_4$. Elemental analysis gave 89.14 (w)% gold and 10.86 (w)% oxygen. a) SEM image b) EDX

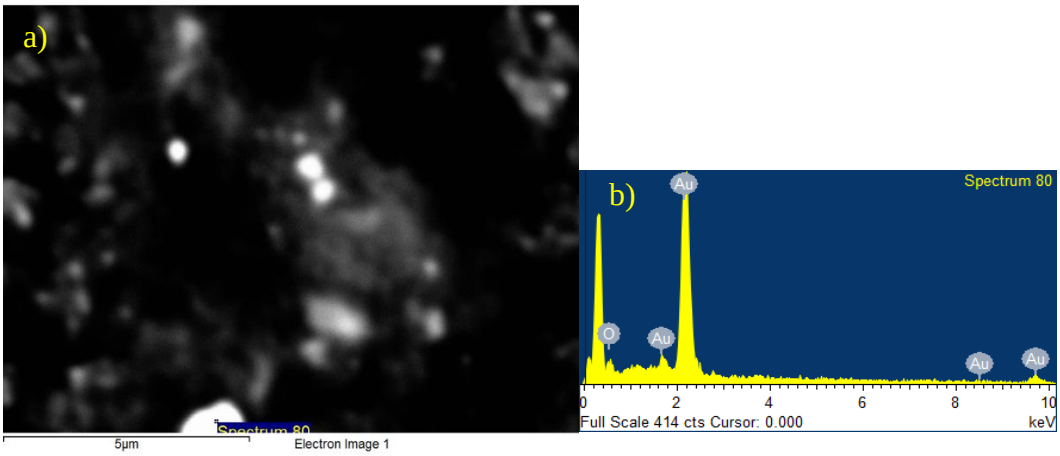

Figure F14. SEM-EDX of acetone-washed 5:1 IL-1B:$HAuCl_4$ molar ratio nanoparticles redispersed in ethanol. The concentrations used were 3.81 mM IL-1B, 0.762 mM $HAuCl_4$, 1.524 mM $NaBH_4$. Elemental analysis gave 89.14 (w)% gold and 10.86 (w)% oxygen. a) SEM image b) EDX

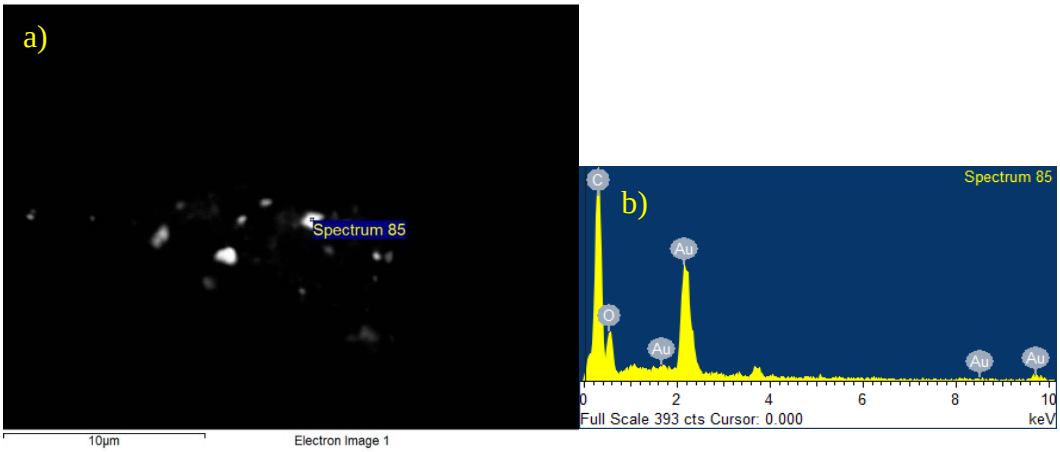

Figure F15. SEM-EDX of acetone-washed 5:1 IL-1B:$HAuCl_4$ molar ratio nanoparticles redispersed in ethanol. The concentrations used were 3.81 mM IL-1B, 0.762 mM $HAuCl_4$, 1.524 mM $NaBH_4$. Elemental analysis gave 10.66 (w)% gold, 24.03 (w)% carbon, and 65.31 (w)% oxygen. a) SEM image b) EDX

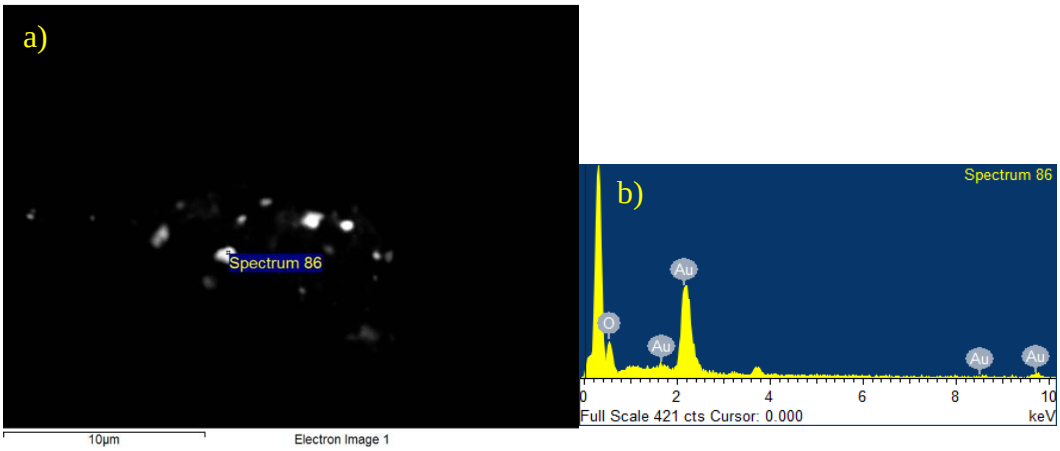

Figure F16. SEM-EDX of acetone-washed 5:1 IL-1B:$HAuCl_4$ molar ratio nanoparticles redispersed in ethanol. The concentrations used were 3.81 mM IL-1B, 0.762 mM $HAuCl_4$, 1.524 mM $NaBH_4$. Elemental analysis gave 89.14 (w)% gold and 10.86 (w)% oxygen. a) SEM image b) EDX

APPENDIX G

Additional SEM/EDX of Gold Nanoparticle Syntheses with IL-2 Purified with the New Washing Protocol

The following are additional SEM/EDX of gold nanoparticle syntheses with IL-2 purified with the new washing protocol.

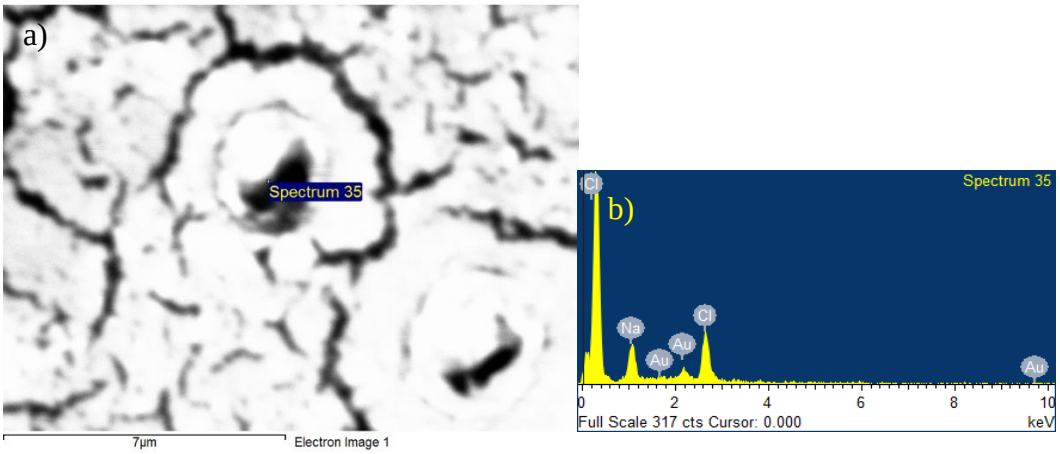

Figure G1. SEM-EDX of the reaction mixture of 5:1 IL-2:$HAuCl_4$ molar ratio. The concentrations used were 3.81 mM IL-2, 0.762 mM $HAuCl_4$, 1.524 mM $NaBH_4$. Elemental analysis gave 25.80 (w)% sodium, 45.87 (w)% chlorine, 17.25 (w)% gold and 11.08 (w)% oxygen. a) SEM image b) EDX

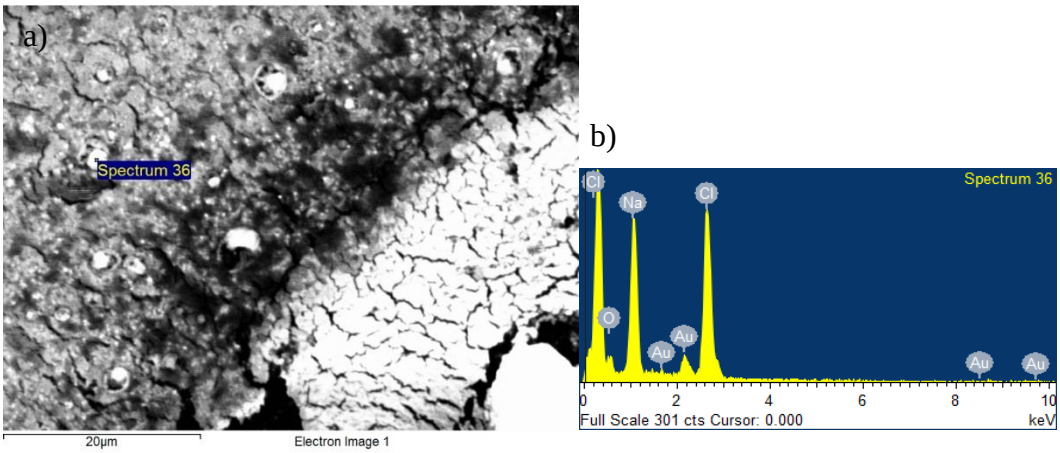

Figure G2. SEM-EDX of the reaction mixture of 5:1 IL-2:$HAuCl_4$ molar ratio. The concentrations used were 3.81 mM IL-2, 0.762 mM $HAuCl_4$, 1.524 mM $NaBH_4$. Elemental analysis gave 31.51 (w)% sodium, 46.00 (w)% chlorine, 10.27 (w)% gold and 12.22 (w)% oxygen. a) SEM image b) EDX

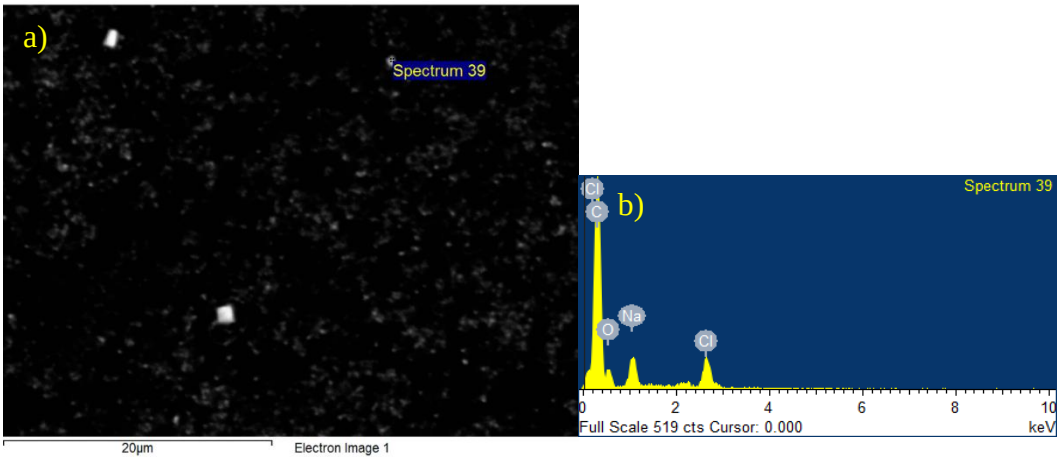

Figure G3. SEM-EDX of the reaction mixture of 5:1 IL-2:$HAuCl_4$ molar ratio. The concentrations used were 3.81 mM IL-2, 0.762 mM $HAuCl_4$, 1.524 mM $NaBH_4$. Elemental analysis gave 1.37 (w)% sodium, 1.25 (w)% chlorine, 26.45 (w)% carbon and 70.94 (w)% oxygen. a) SEM image b) EDX

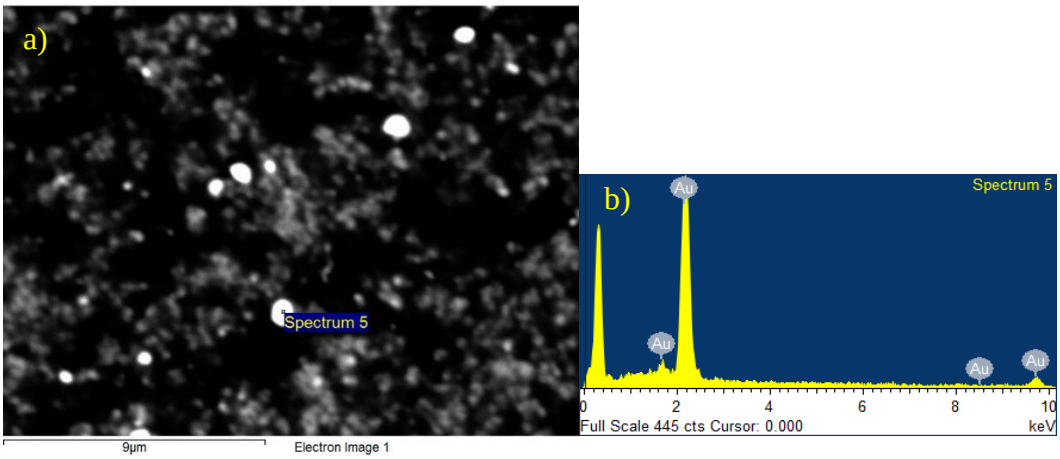

Figure G4. SEM-EDX of acetone-washed 5:1 IL-2:$HAuCl_4$ molar ratio nanoparticles redispersed in nanopure water. The concentrations used were 3.81 mM IL-2, 0.762 mM $HAuCl_4$, 1.524 mM $NaBH_4$. Elemental analysis gave 89.14 (w)% gold and 10.86 (w)% oxygen. a) SEM image b) EDX

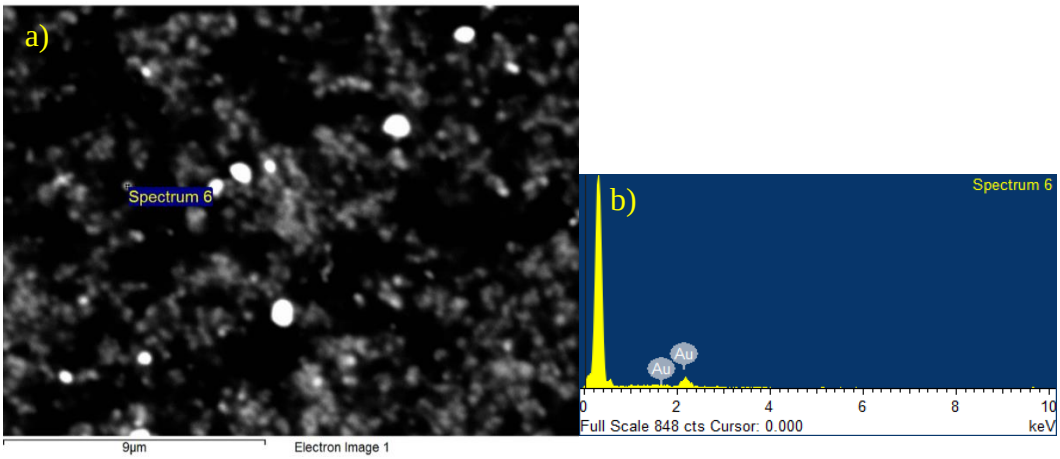

Figure G5. SEM-EDX of acetone-washed 5:1 IL-2:$HAuCl_4$ molar ratio nanoparticles redispersed in nanopure water. The concentrations used were 3.81 mM IL-2, 0.762 mM $HAuCl_4$, 1.524 mM $NaBH_4$. Elemental analysis gave 89.14 (w)% gold and 10.86 (w)% oxygen. a) SEM image b) EDX

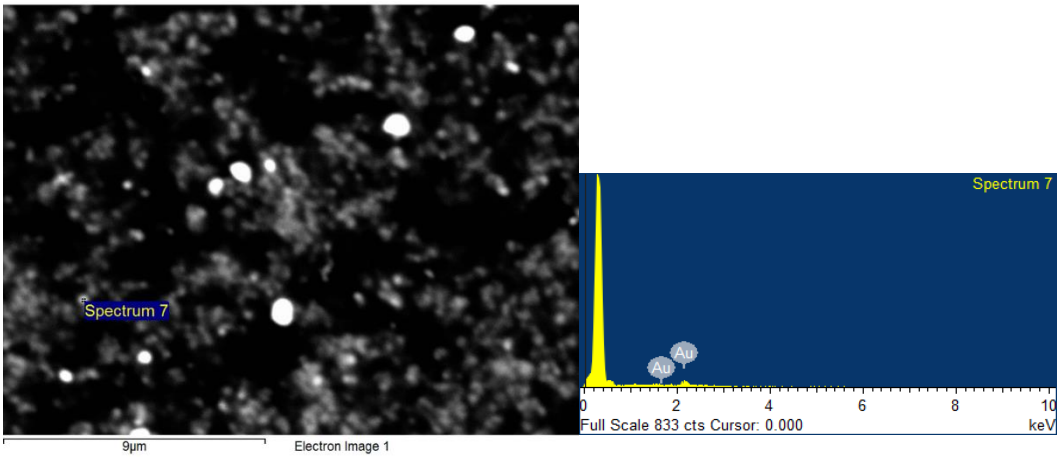

Figure G6. SEM-EDX of acetone-washed 5:1 IL-2:$HAuCl_4$ molar ratio nanoparticles redispersed in nanopure water. The concentrations used were 3.81 mM IL-2, 0.762 mM $HAuCl_4$, 1.524 mM $NaBH_4$. Elemental analysis gave 89.14 (w)% gold and 10.86 (w)% oxygen. a) SEM image b) EDX

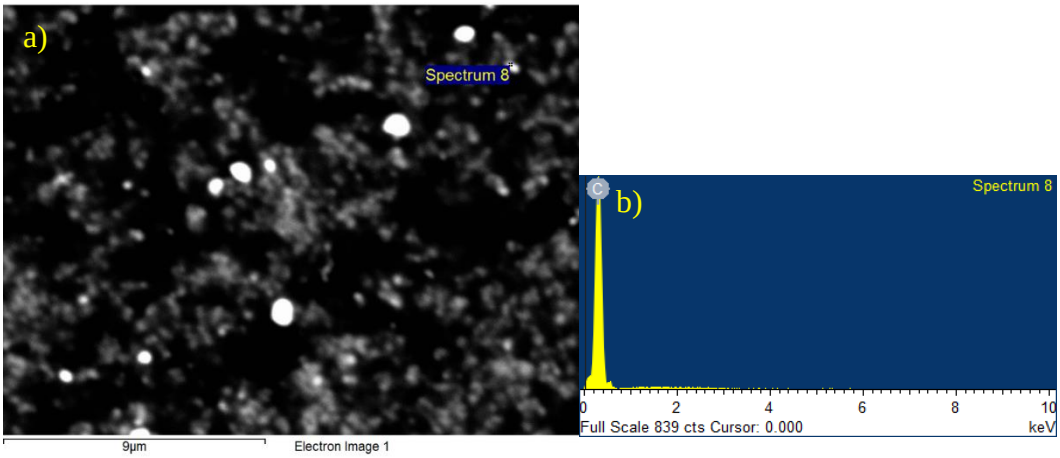

Figure G7. SEM-EDX of acetone-washed 5:1 IL-2:$HAuCl_4$ molar ratio nanoparticles redispersed in nanopure water. The concentrations used were 3.81 mM IL-2, 0.762 mM $HAuCl_4$, 1.524 mM $NaBH_4$. Elemental analysis gave 27.29 (w)% carbon and 72.71 (w)% oxygen. a) SEM image b) EDX

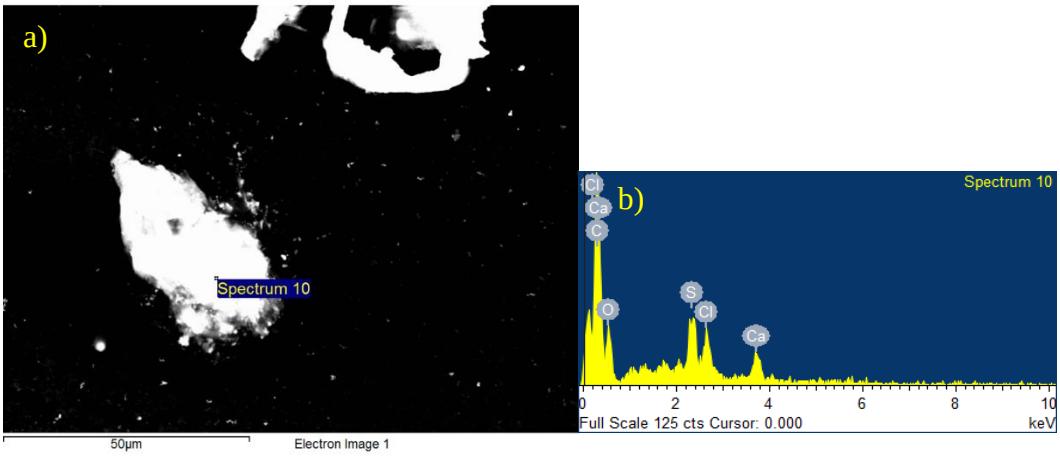

Figure G8. SEM-EDX of acetone-washed 5:1 IL-2:$HAuCl_4$ molar ratio nanoparticles redispersed in nanopure water. The concentrations used were 3.81 mM IL-2, 0.762 mM $HAuCl_4$, 1.524 mM $NaBH_4$. Elemental analysis gave 24.31 (w)% carbon, 2.44 (w)% sulfur, 2.09 (w)% chlorine, 1.96 (w)% calcium and 69.20 (w)% oxygen. a) SEM image b) EDX

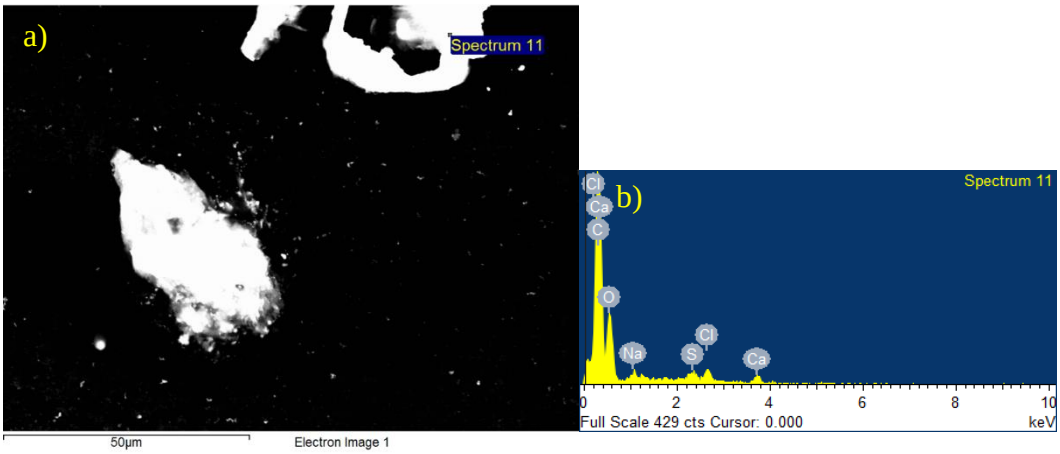

Figure G9. SEM-EDX of acetone-washed 5:1 IL-2:$HAuCl_4$ molar ratio nanoparticles redispersed in nanopure water. The concentrations used were 3.81 mM IL-2, 0.762 mM $HAuCl_4$, 1.524 mM $NaBH_4$. Elemental analysis gave 26.44 (w)% carbon, 0.32 (w)% sodium, 0.44 (w)% sulfur, 0.8 (w)% chlorine, 0.58 (w)% calcium and 71.43 (w)% oxygen. a) SEM image b) EDX

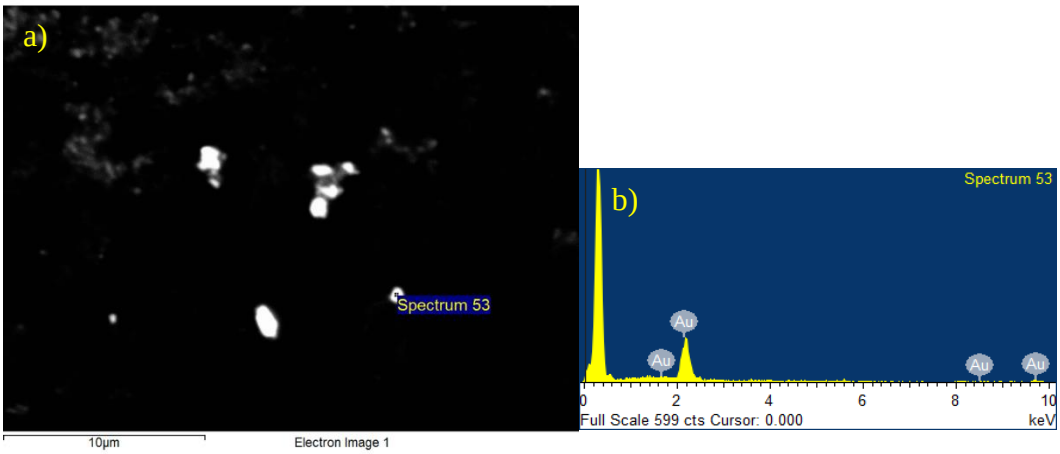

Figure G10. SEM-EDX of acetone-washed 5:1 IL-2:$HAuCl_4$ molar ratio nanoparticles redispersed in ethanol. The concentrations used were 3.81 mM IL-2, 0.762 mM $HAuCl_4$, 1.524 mM $NaBH_4$. Elemental analysis gave 89.14 (w)% gold and 10.86 (w)% oxygen. a) SEM image b) EDX

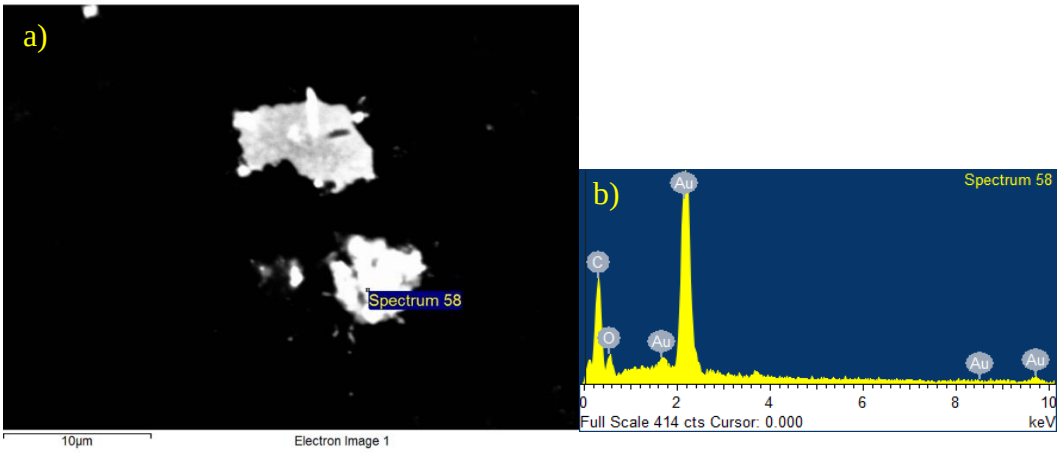

Figure G11. SEM-EDX of acetone-washed 5:1 IL-2:$HAuCl_4$ molar ratio nanoparticles redispersed in ethanol. The concentrations used were 3.81 mM IL-2, 0.762 mM $HAuCl_4$, 1.524 mM $NaBH_4$. Elemental analysis gave 28.39 (w)% gold, 18.60 (w)% carbon and 53.01 (w)% oxygen. a) SEM image b) EDX

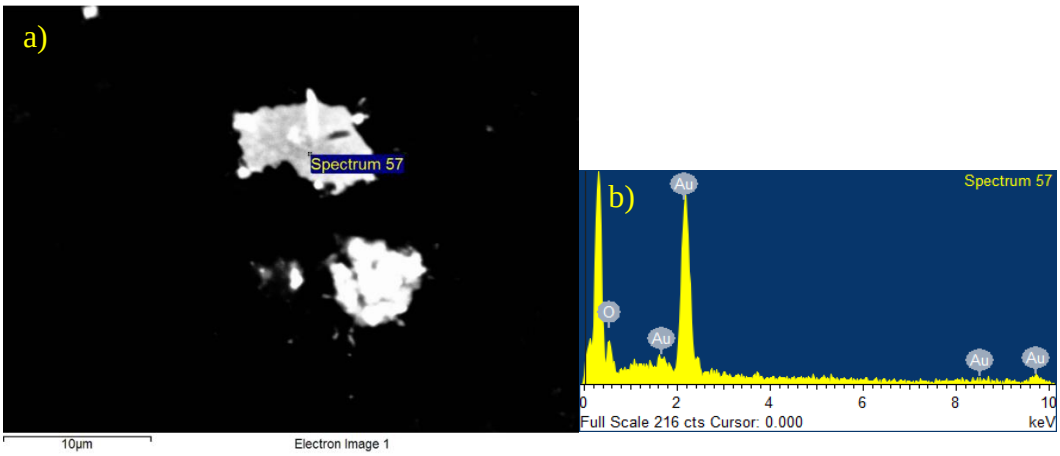

Figure G12. SEM-EDX of acetone-washed 5:1 IL-2:$HAuCl_4$ molar ratio nanoparticles redispersed in ethanol. The concentrations used were 3.81 mM IL-2, 0.762 mM $HAuCl_4$, 1.524 mM $NaBH_4$. Elemental analysis gave 89.14 (w)% gold and 10.86 (w)% oxygen. a) SEM image b) EDX

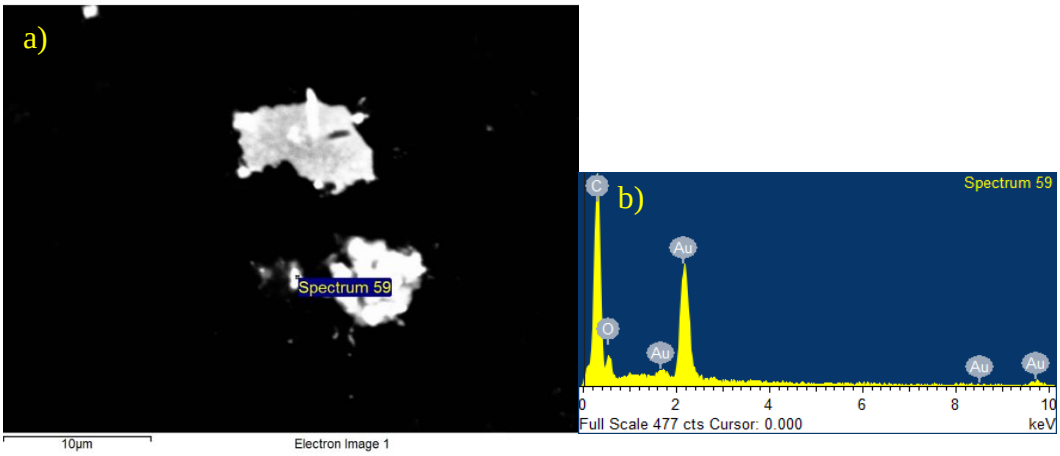

Figure G13. SEM-EDX of acetone-washed 5:1 IL-2:$HAuCl_4$ molar ratio nanoparticles redispersed in ethanol. The concentrations used were 3.81 mM IL-2, 0.762 mM $HAuCl_4$, 1.524 mM $NaBH_4$. Elemental analysis gave 11.67 (w)% gold, 23.72 (w)% carbon and 64.61 (w)% oxygen. a) SEM image b) EDX

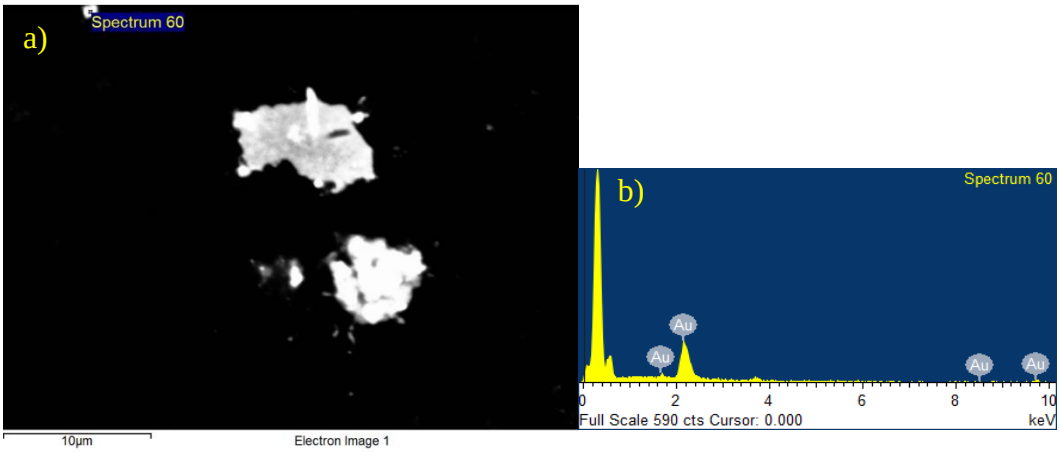

Figure G14. SEM-EDX of acetone-washed 5:1 IL-2:$HAuCl_4$ molar ratio nanoparticles redispersed in ethanol. The concentrations used were 3.81 mM IL-2, 0.762 mM $HAuCl_4$, 1.524 mM $NaBH_4$. Elemental analysis gave 89.14 (w)% gold and 10.86 (w)% oxygen. a) SEM image b) EDX

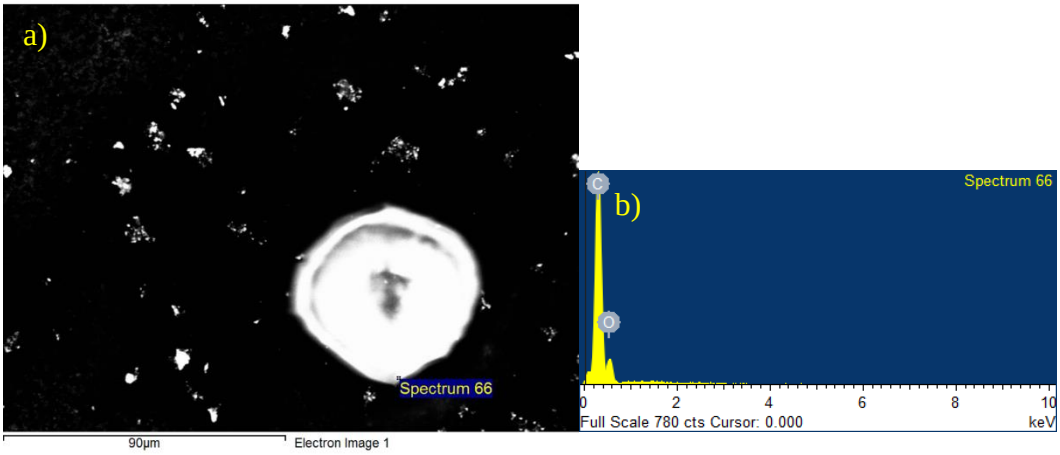

Figure G15. SEM-EDX of acetone-washed 5:1 IL-2:$HAuCl_4$ molar ratio nanoparticles redispersed in ethanol. The concentrations used were 3.81 mM IL-2, 0.762 mM $HAuCl_4$, 1.524 mM $NaBH_4$. Elemental analysis gave 27.29 (w)% carbon and 72.71 (w)% oxygen. a) SEM image b) EDX

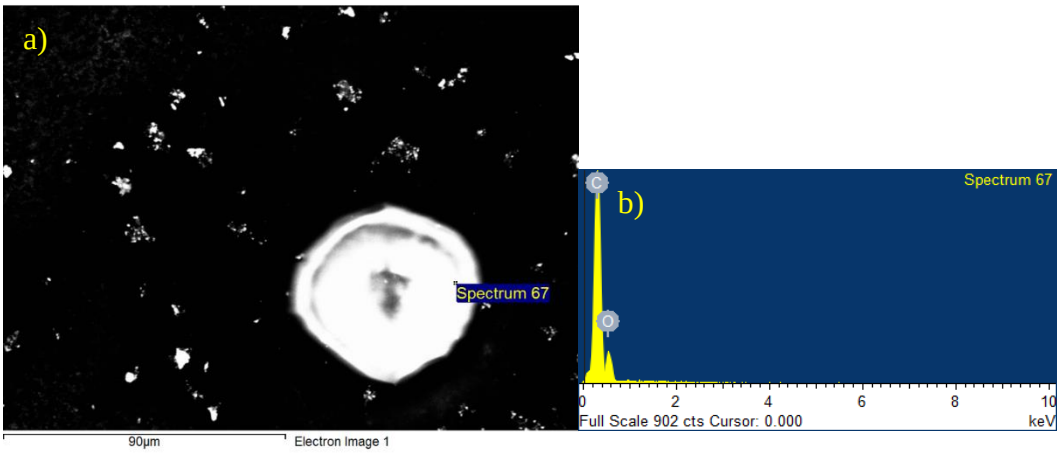

Figure G16. SEM-EDX of acetone-washed 5:1 IL-2:$HAuCl_4$ molar ratio nanoparticles redispersed in ethanol. The concentrations used were 3.81 mM IL-2, 0.762 mM $HAuCl_4$, 1.524 mM $NaBH_4$. Elemental analysis gave 27.29 (w)% carbon and 72.71 (w)% oxygen. a) SEM image b) EDX

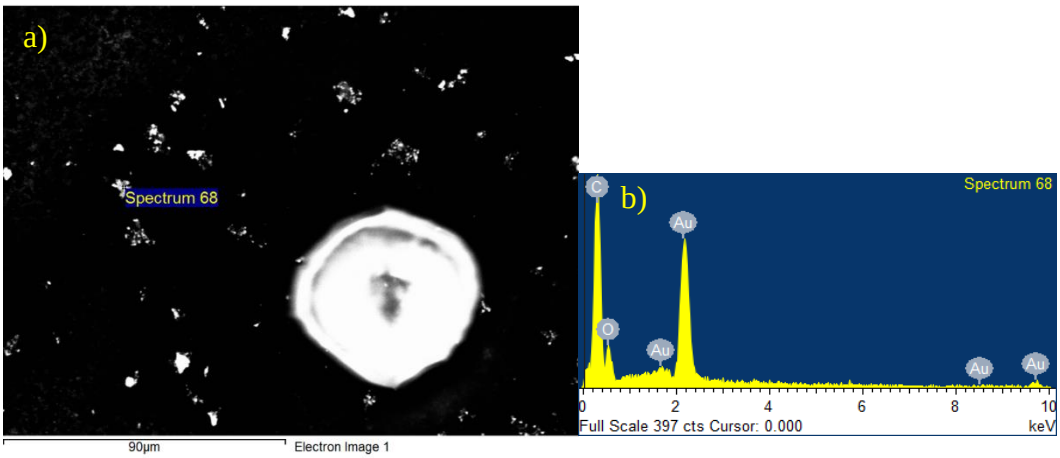

Figure G17. SEM-EDX of acetone-washed 5:1 IL-2:$HAuCl_4$ molar ratio nanoparticles redispersed in ethanol. The concentrations used were 3.81 mM IL-2, 0.762 mM $HAuCl_4$, 1.524 mM $NaBH_4$. Elemental analysis gave 23.05 (w)% carbon, 13.85 (w)% gold and 63.10 (w)% oxygen. a) SEM image b) EDX

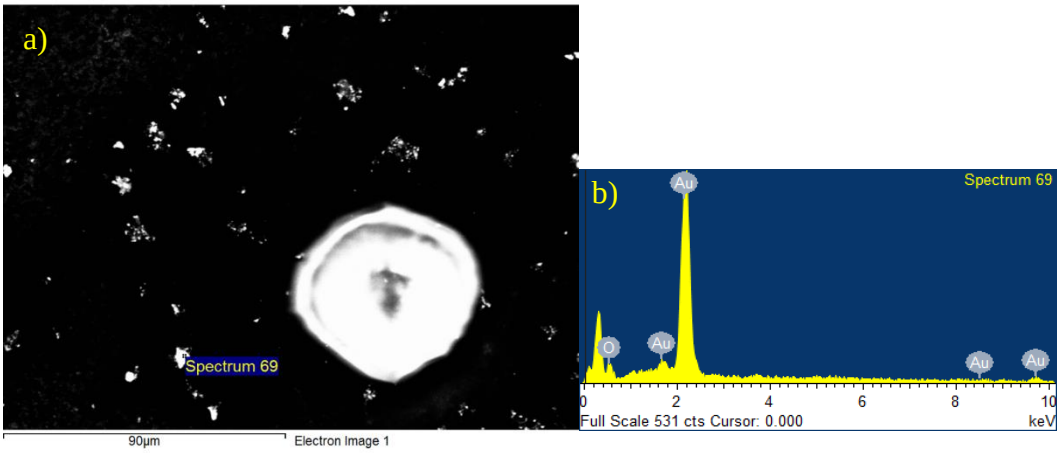

Figure G18. SEM-EDX of acetone-washed 5:1 IL-2:$HAuCl_4$ molar ratio nanoparticles redispersed in ethanol. The concentrations used were 3.81 mM IL-2, 0.762 mM $HAuCl_4$, 1.524 mM $NaBH_4$. Elemental analysis gave 89.14 (w)% gold and 10.86 (w)% oxygen. a) SEM image b) EDX

APPENDIX H

ADDITIONAL AFM OF GOLD NANOPARTICLE SYNTHESES WITH IL-1A

The following are additional AFM images of the optimized gold nanoparticle syntheses with IL-1A.

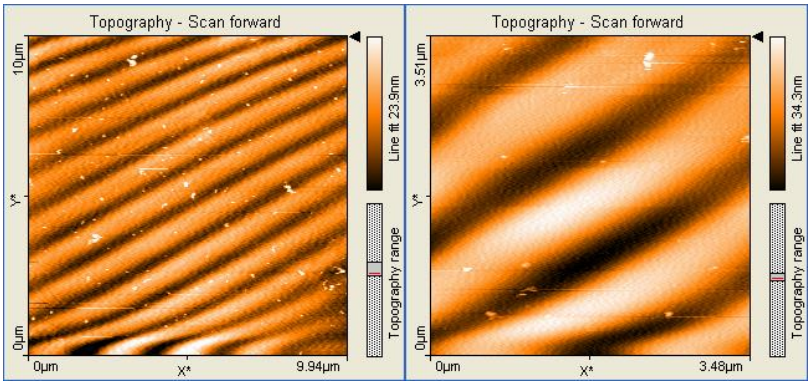

Figure H1. AFM images of the optimized 5:1 IL-1A:$HAuCl_4$ molar ratio synthesis. The first area of the sample starting with 9.94µm x 10µm(left) and zoomed into a 3.48µm x 3.51µm(right) images. The concentrations used were 3.81 mM IL-1A, 0.762 mM $HAuCl_4$, and 0.381 mM $NaBH_4$.

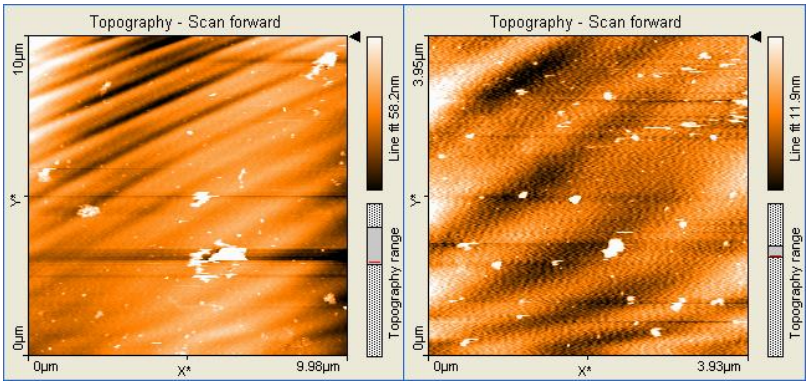

Figure H2. AFM images of the optimized 5:1 IL-1A:$HAuCl_4$ molar ratio synthesis. The second area of the sample starting with 9.98µm x 10µm(left) and zoomed into a 3.93µm x 3.95µm(right) images. The concentrations used were 3.81 mM IL-1A, 0.762 mM $HAuCl_4$, and 0.381 mM $NaBH_4$.

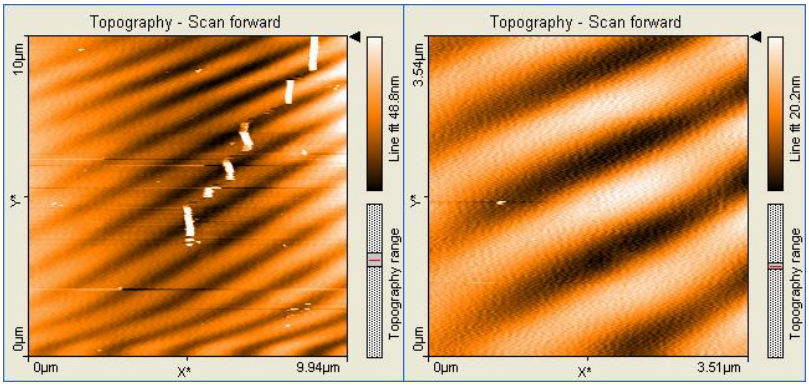

Figure H3. AFM images of the optimized 1:1 IL-1A:$HAuCl_4$ molar ratio synthesis. The first area of the sample starting with 9.94µm x 10µm(left) and zoomed into a 3.51µm x 3.54µm(right) images. The concentrations used were 0.762 mM IL-1A, 0.762 mM $HAuCl_4$, and 0.381 mM $NaBH_4$.

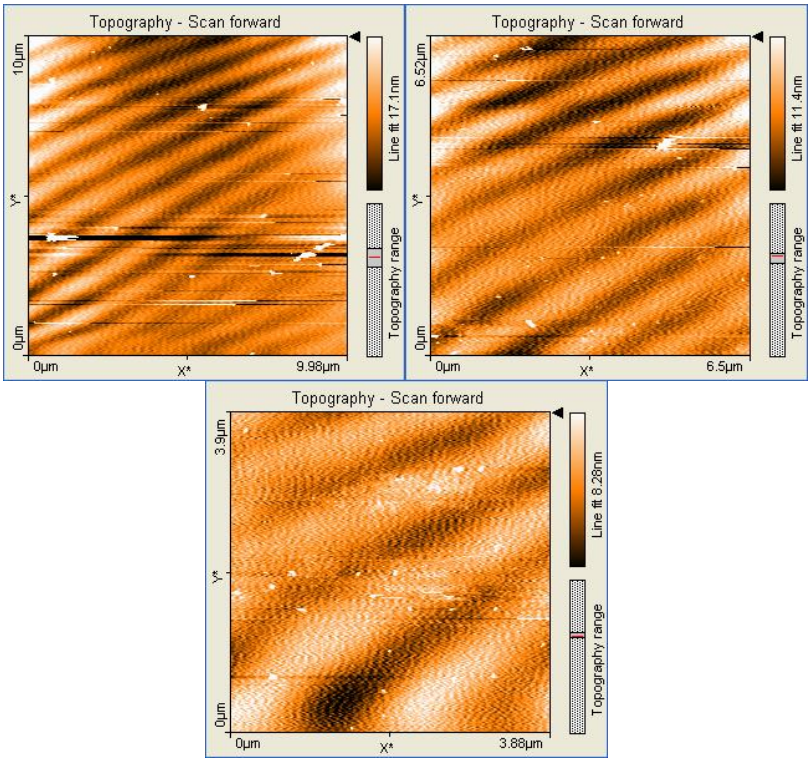

Figure H4. AFM images of the optimized 1:1 IL-1A:$HAuCl_4$ molar ratio synthesis. The second area of the sample starting with 9.94µm x 10µm(top left), zoomed into 6.5µm x 6.52µm(top right) and then into a 3.51µm x 3.54µm(bottom) images. The concentrations used were 0.762 mM IL-1A, 0.762 mM $HAuCl_4$, and 0.381 mM $NaBH_4$.